11-2014

Effects of Sodium/Glucose co-transporter inhibitors on contractility and Ca2+ signaling in Ventricular Myocytes from Streptozotocin-Induced diabetic rats

Norin Nabil Fathalla Hamouda

United Arab Emirates University

College of Medicine and Health Sciences

Department of Pharmacology and Toxicology

EFFECTS OF SODIUM/GLUCOSE CO-TRANSPORTER INHIBITORS ON CONTRACTILITY AND Ca^{2+} SIGNALING IN VENTRICULAR MYOCYTES FROM STREPTOZOTOCIN-INDUCED DIABETIC RATS

Norin Nabil Fathalla Hamouda

This thesis is submitted in partial fulfillment of the requirements for the degree of Master of Medical Sciences (Pharmacology and Toxicology)

Under the supervision of Professor Frank Christopher Howarth

November 2014

Declaration of Original Work

I, Norin Nabil Fathalla Hamouda, the undersigned, a graduate student at the United Arab Emirates University (UAEU), and the author of this thesis, entitled "*Effects of Sodium/Glucose Co-transporter Inhibitors on Contractility and* Ca^{2+} *Signaling in Ventricular Myocytes from Streptozotocin-Induced Diabetic Rats*" hereby solemnly declare that this thesis is an original research work that has been done and prepared by me under the supervision of Professor Frank Christopher Howarth, in the College of Medicine and Health Sciences at UAEU. This work has not been previously formed as the basis for the award of any academic degree, diploma or similar title at this or any other university. The materials borrowed from other sources and included in my thesis have been properly cited and acknowledged.

Student's Signature _____ Date _____

Approval of the Master Thesis

This Master Thesis is approved by the following Examining Committee Members:

1) Advisor (Committee Chair): Frank Christopher Howarth

   Title: Chairman and Professor

   Department of Physiology

   College of Medicine and Health Sciences

   Signature _____ Date_____

2) Member: Murat Ahmet Oz

   Title: Associate Professor

   Department of Pharmacology and Toxicology

   College of Medicine and Health Sciences

   Signature _____ Date_____

3) Member (External Examiner): Saadeh Suleiman

   Title: Professor

   Department of Cardiac Physiology

   Institution: University of Bristol, England, United Kingdom

   Signature _____ Date_____

This Master Thesis is accepted by:

Dean of the College of Medicine and Health Sciences: Prof. Dennis J. Templeton

Signature _____ Date_____

Dean of the College of Graduate Studies: Prof. Nagi T. Wakim

Signature _____ Date_____

Copy ___ of ___

Abstract

The prevalence of diabetes mellitus is increasing at an alarming rate worldwide. Cardiovascular (CV) disease is the major cause of morbidity and mortality in diabetic patients. The search for new treatments has led to developing alternative insulin-independent treatment strategies such as sodium/glucose co-transporter (SGLT) inhibitors. Inhibition of intestinal SGLT1 impairs dietary glucose absorption, while inhibition of renal SGLT2 promotes glucose excretion leading to calorie loss and improved glycemic control. In this study, we hypothesized that inhibiting cardiac SGLTs may alter Ca^{2+} mobilization in myocytes. The effects of Phlorizin (PHLOR) (non-selective SGLT1 and 2 inhibitor), Quercetin-3-O-glucoside (QUER-3-G) (selective SGLT1 inhibitor), Dapagliflozin (DAPA) (selective SGLT2 inhibitor) on ventricular myocyte shortening and intracellular Ca^{2+} have been investigated in streptozotocin (STZ)-induced diabetic rats and age-matched Controls. Experiments were performed at 35-36°C after 2 months of STZ treatment. Myocyte shortening, intracellular Ca^{2+} and L-type Ca^{2+} current were measured by video edge detection in electrically-stimulated (1Hz) myocytes, by fluorescence photometry in Fura-2 loaded myocytes and by whole-cell patch clamp, respectively before and after a 5 minute application of the SGLT inhibitor (10^{-6} M) tested. The amplitude (AMP) of shortening was significantly ($P<0.05$) reduced by PHLOR in STZ (84.76±2.91%, n=20) myocytes and Controls (83.72±2.65%, n=23), by QUER-3-G in STZ (79.12±2.28%, n=20) myocytes and Controls (76.69±1.92%, n=30) and by DAPA in STZ (76.58±1.89%, n=42) myocytes and Controls (76.68±2.28%, n=37). The AMP of the Ca^{2+} transient was significantly reduced by PHLOR in STZ (82.37±3.16%,

n=16) myocytes and Controls (73.94±5.22%, *n*=21) and by QUER-3-G in STZ (73.62±5.83%, *n*=18) myocytes and Controls (78.32±3.54%, *n*=41). DAPA reduced the AMP of the Ca^{2+} transient significantly in STZ (71.45±5.35%, *n*=16) myocytes and modestly in Controls (92.01±2.72%, *n*=17). The AMP of L-type Ca^{2+} current was significantly reduced in myocytes from STZ compared to Control rats across a range of test potentials and was additionally reduced by DAPA. Myofilament sensitivity to Ca^{2+} and SR Ca^{2+} were not significantly altered by PHLOR, QUER-3-G or DAPA. The reduction in L-type Ca^{2+} current in the presence of DAPA may partly underlie its negative inotropic effects. However, further studies are required to investigate the mechanism(s) behind the negative inotropic effects of PHLOR and QUER-3-G.

Keywords: Diabetes mellitus; SGLT inhibitors; Phlorizin; Quercetin-3-O-glucoside; Dapagliflozin; Ventricular myocytes

Title and Abstract (in Arabic)

تأثيرات موانع الناقل المشترك للصوديوم و الجلوكوز على الإنقباض و تأشير الكالسيوم في خلايا البطين القلبية المأخوذة من جرذان مصابة بداء السكري مستحث من الستربتوزوتوسين

الملخص

يزداد إنتشار داء السكري حول العالم بمعدل مثير للقلق. أمراض القلب والأوعية الدموية هي السبب الرئيسى للمرضية و الوفيات في مرضى داء السكري. لقد أدى البحث عن علاجات جديدة إلى تطوير استراتيجيات علاجية بديلة لا تعتمد على الأنسولين مثل موانع الناقل المشترك للصوديوم و الجلوكوز. يسبب منع الناقل المشترك للصوديوم و الجلوكوز رقم ١ فى الأمعاء إلى إضعاف إمتصاص الجلوكوز الغذائى. أما منع الناقل المشترك للصوديوم و الجلوكوز رقم ٢ في الكلي يسبب تعزيزالتخلص من الجلوكوز مما يؤدى إلى خسارة السعرات الحرارية و تحسين السيطرة على نسبة السكر في الدم. في هذه الدراسة قمنا بإفتراض أن تثبيط النواقل المشتركة للصوديوم و الجلوكوز فى القلب قد تغير تحريك الكالسيوم في الخلايا العضلية. تمت دراسة تأثيرات كلٍ من الفلوريزين (مانع غير انتقائي للناقلين المشتركين للصوديوم و الجلوكوز رقم ١ و٢)، و الكيرسيتين ٣-O- جلوكوسيدي (مانع انتقائي للناقل المشترك للصوديوم و الجلوكوز رقم ١)، و الداباجليفلوزين (مانع انتقائي للناقل المشترك للصوديوم و الجلوكوز رقم ٢) علي التقلص و الكالسيوم الداخلي في خلايا البطين القلبية المأخوذة من جرذان مصابة بداء السكري مستحث من الستربتوزوتوسين و جرذان ضابطة مطابقة فى العمر. أجريت التجارب في درجة حرارة ٣٥- ٣٦ درجة مئوية بعد إنقضاء شهرين علي العلاج بالستربتوزوتوسين. تم قياس تقلص (إنقباض) الخلايا، و الكالسيوم الداخلي، و تيار الكالسيوم طويل الأمد بإستخدام جهاز فيديو كاشف للحواف في خلايا محفزة كهربائياً على تردد ١ هرتز، و جهاز ضوئي للتألق في خلايا محملة بمؤشر الكالسيوم الفلورى فيورا-٢، وتقنية الالتقاط الرقعي لكامل الخلية على التوالي، قبل و بعد إضافة مانع الناقل المشترك للصوديوم و الجلوكوز (تركيز $^{-٦}$ ١٠ مول) تحت الإختبار بخمس دقائق. و تم قياس تأثيرات الداباجليفلوزين بإستخدام تقنية الالتقاط الرقعي. قام الفلوريزين بخفض سعة الإنقباض بشكل ملحوظ (قيمة أحتمالية أصغر من ٠،٠٥) في الخلايا المعالجة بالستربتوزوتوسين (٨٤،٧٦±٢،٩١%، عدد=٢٠) والخلايا الضابطة

(٧٢،٨٣±٢،٦٥%، عدد=٢٣). كما قام الكيرسيتين ٣-O- جلوكوسيدي بخفض سعة الإنقباض بشكل ملحوظفي الخلايا المعالجة بالستربتوزوتوسين (٧٩،١٢±٢،٢٨%، عدد=٢٠) والخلايا الضابطة (٧٦،٦٩±١،٩٢%، عدد=٣٠). و قام الداباجليفلوزين ايضاً بخفض سعة الإنقباض بشكل ملحوظ في الخلايا المعالجة بالستربتوزوتوسين (٧٦،٥٨ ± ١،٨٩%، عدد=٤٢) والخلايا الضابطة (٧٦،٦٨±٢،٢٨%، عدد=٣٧). تم خفض سعة بشكل ملحوظ بواسطة الفلوريزين في الخلايا المعالجة بالستربتوزوتوسين (٨٢،٣٧±٣،١٦%، عدد=١٦) والخلايا الضابطة (٧٣،٩٤±٥،٢٢%، عدد=٢١)، و بواسطة الكيرسيتين ٣-O- جلوكوسيدي في الخلايا المعالجة بالستربتوزوتوسين (٧٣،٦٢±٥،٨٣%، عدد=١٨) والخلايا الضابطة (٧٨،٣٢±٣،٥٤%، عدد=٤١). وكان إنخفاض سعة الكالسيوم الداخلي بواسطة الداباجليفلوزين ملحوظاً في الخلايا المعالجة بالستربتوزوتوسين (٧١،٤٥ ± ٥،٣٥%، عدد=١٦) و طفيفاً في الخلايا الضابطة (٩٢،٠١±٢،٧٢%، عدد=١٧). تم خفض سعة تيار الكالسيوم طويل الأمد في في الخلايا المعالجة بالستربتوزوتوسين مقارنة بالخلايا الضابطة في نطاق الإمكانات المختبرة، و قام الداباجليفلوزين بزيادة هذا الإنخفاض. لم يتأثر أى من حساسية الخيوط العضلية للكالسيوم، والكالسيوم داخل شبكة الهيولى العضلية بواسطة الفلوريزين ،أو الكيرسيتين ٣-O- جلوكوسيدي ،أو الداباجليفلوزين. قد يكمن إنخفاض سعة تيار الكالسيوم طويل الأمد جزئيا وراء التأثيرات السلبية للداباجليفلوزين فى التقلص العضلى. لكن يلزم إجراء مزيد من الدراسات للكشف عن آلية التأثيرات السلبية لكلٍ من الفلوريزين و الكيرسيتين ٣-O- جلوكوسيدي.

Acknowledgements

I would like to express my sincere and deep gratitude to my respected supervisor, Professor Frank Christopher Howarth, for being a greatly supportive mentor and teacher. I acknowledge his guidance, encouragement, patience and effort in order to make this project as good as it can be. It has been a great honor to work with him and I have learned a lot from his knowledge and experience that I will apply throughout my academic career.

From the bottom of my heart, I would love to cordially thank my beloved family: my father, mother, sister and brother for their ultimate support, both emotionally and financially. I am more than blessed to have them around me through the ups and downs of this journey providing me with infinite strength and motivation. May ALLAH bless and protect them all, and provide them with endless blessings, success, happiness and prosperity in life and the eternal afterlife.

I would like to thank the thesis advisory committee: Professor Haider Raza, Dr. Murat Oz and Dr. Jumaa Al-Kaabi, for their expertise and valuable time spent following my project step by step. I am grateful to them for providing me with suggestions and opinions during the progress of my project, thesis preparation and preparation of the defense.

I would like to thank the external examiner, Professor Saadeh Suleiman, for reviewing my thesis/dissertation and I highly appreciate him coming all the way from the United Kingdom for my examination.

I would like to thank the chairman of the pharmacology and toxicology department for providing me with the great opportunity to enroll in the department's Master's program. I would like to especially thank the program coordinator, Dr. Samir Attoub, for his continuous help and support since day one of my enrollment until the very end. He was more than generous with his advice and help. I owe a great deal of gratitude toward him.

I would like to thank Mr. Muhammed Anwar Qureshi for his valuable technical support and help in the laboratory throughout my experiments. He was very co-operative and supportive. And I also would like to thank Dr. Vadym Syderenko for his technical support and help with patch clamp experiments.

Dedication

This thesis is dedicated to my parents and siblings, the most precious people in my life.

Table of Contents

List of Tables

List of Figures

List of Abbreviations/Nomenclatures/Symbols

Abbreviation	Description
ACTH	Adrenocorticotrpin hormone
ADA	American Diabetes Association
AM	Acetoxy methyl
AMP	Amplitude
ANOVA	Analysis of variance
AP	Action potential
ATP	Adenosine triphosphate
AV node	Atrio-ventricular node
β-cells	Beta cells
BAPTA	1,2-bis-(2-aminophenoxy) ethane-NNN'N'-tetra-acetic acid
BGL	Blood glucose level
BSA	Bovine serum albumin
CAD	Coronary artery disease
CHT	Sodium/choline co-transporter
CICR	Calcium-induced calcium release
$\mathbf{C_{max}}$	Maximum plasma concentration
CS	Caffeine-stimulated
CV	Cardiovascular
DAPA	Dapagliflozin

DD	Double diabetes
DED	Double-edge detection
DKA	Diabetic ketoacidosis
DM	Diabetes Mellitus
DMSO	Dimethyl sulphoxide
DNA	Deoxyribonucleic acid
DPP 4	Dipeptidyl peptidase 4
EASD	European Association for the Study of Diabetes
ECC	Excitation-contraction coupling
EGTA	Ethylene glycol tetra-acetic acid
EMA	European Medicines Agency
ES	Electrically-stimulated
FDA	Food and Drug Administration,
FFA	Free fatty acids
FPG	Fasting plasma glucose
GΩ	Giga-Ohm
GAD 65	Glutamic acid decarboxylase 65
GLP 1	Glucagon-like peptide 1
GLUT	Facilitative glucose transporters
HbA_{1c}	Glycated (or glycosylated) hemoglobin
HDL-C	High-density lipoprotein-cholesterol
HEPES	4-(2-hydroxyethyl)-1-piperazine ethanesulfonic acid

HLA	Human leukocyte antigen
HMIT	Proton (H^+)-coupled myo-inositol symporter
H_2O_2	Hydrogen peroxide
HR	Heart rate
Hz	Hertz
IA-2	Insulinoma-associated antigen
ICA	Islet cell auto-antibodies
IDF	International Diabetes Federation
I_f	Pacemaker current
IFG	Impaired fasting glucose
IGT	Impaired glucose tolerance
i.p.	Intraperitonial
i.v.	Intravenous
KB solution	Kraft-Brühe solution
kHz	Kilo-hertz
LADA	Latent autoimmune diabetes in adults
LADY	Latent autoimmune diabetes in the young
LDL-C	Low-density lipoprotein-cholesterol
L-type Ca^{2+} channel	Long opening- type Ca^{2+} channel
M	Molar concentration
MΩ	Mega-Ohm
MENA region	Middle East and North Africa region

MFS	Major Facilitator Superfamily
MHLW	Ministry of Health, Labor and Welfare
MI	Myocardial infarction
MODY	Maturity onset diabetes of the young
µmol	Micro-mole
mmol	Milli-mole
ms	Milli-second
mV	Milli-volt
NA	Not applicable
NAD^+	Nicotinamide adenine dinucleotide
NCX	Na^+/Ca^{2+} exchanger
NEFA	Non-esterified fatty acid
NIS	Sodium/iodide symporter
NO	Nitric oxide
NT	Normal Tyrode
O_2^-	Superoxide anion
OGTT	Oral glucose tolerance test
OH^-	Hydroxyl radicals
ONOO	Peroxynitrate
pA	Pico-ampere
PARS	Poly-ADP-ribose synthase
PCR	Polymerase chain reaction

PCT	Proximal convoluted tubule
pF	Pico-farad
PHLOR	Phlorizin
PMT	Photomultiplier tube
QUER-3-G	Quercetin-3-O-Glucoside
RCL	Resting cell length
ROS	Reactive oxygen species
Rpm	Round per minute
RU	Fura-2 ratio unit
RyR	Ryanodine receptor
SA node	Sino-atrial node
s.c.	Subcutaneous
SED	Single-edge detection
SEM	Standard error of the mean
SERCA	Sarco-endoplasmic reticulum Ca^{2+}-ATPase pump
SGLT	Sodium/glucose co-transporter
SLC	Solute carrier
SMIT	Sodium/myo-inositol co-transporter
SMVT	Sodium/multivitamin co-transporter
SR	Sarcoplasmic reticulum
SSSF	Sodium/Substrate Symporter Family
STZ	Streptozotocin

SWEET	Sugar efflux transporter
T1DM	Type 1 diabetes mellitus
T1ADM	Type 1A diabetes mellitus
T1BDM	Type 1B diabetes mellitus
T2DM	Type 2 diabetes mellitus
TEA Cl	N,N,N,N-tetramethylammonium chloride
TGA	Therapeutic Goods Administration
THALF	Time to half
TPEN	N,N,N',N'-tetrakis (2-pyridylmethyl) ethylenediamine
TPK	Time to peak
T-type Ca^{2+} channel	Transient-type Ca^{2+} channel
T-tubules	Transverse tubules
VED	Video edge detection
WHO	World Health Organization

Chapter 1: Introduction

1.1. Diabetes Mellitus

Diabetes Mellitus (DM) is a chronic progressive metabolic disease characterized by impaired metabolism of carbohydrate, fat and protein accompanied by persistent hyperglycemia due to absolute or relative deficiency of insulin secretion and/or decreased sensitivity to insulin effect [10]. Several acute and chronic complications affect a variety of organs including the eyes, nerves, kidneys and the cardiovascular (CV) system, by damage, failure or dysfunction owing to chronic exposure to hyperglycemia [10; 43].

1.1.1. Types and Classification of Diabetes Mellitus

Despite the fact that DM is commonly classified into two etiopathogenic types: type 1 diabetes mellitus (T1DM) and type 2 diabetes mellitus (T2DM), this classification does not accurately reflect the range of DM [284]. Besides, categorizing the type of DM for some patients is not always simple [10]. Therefore, this classification has been expanded into further subdivisions based on pathogenesis (Fig. 1-1).

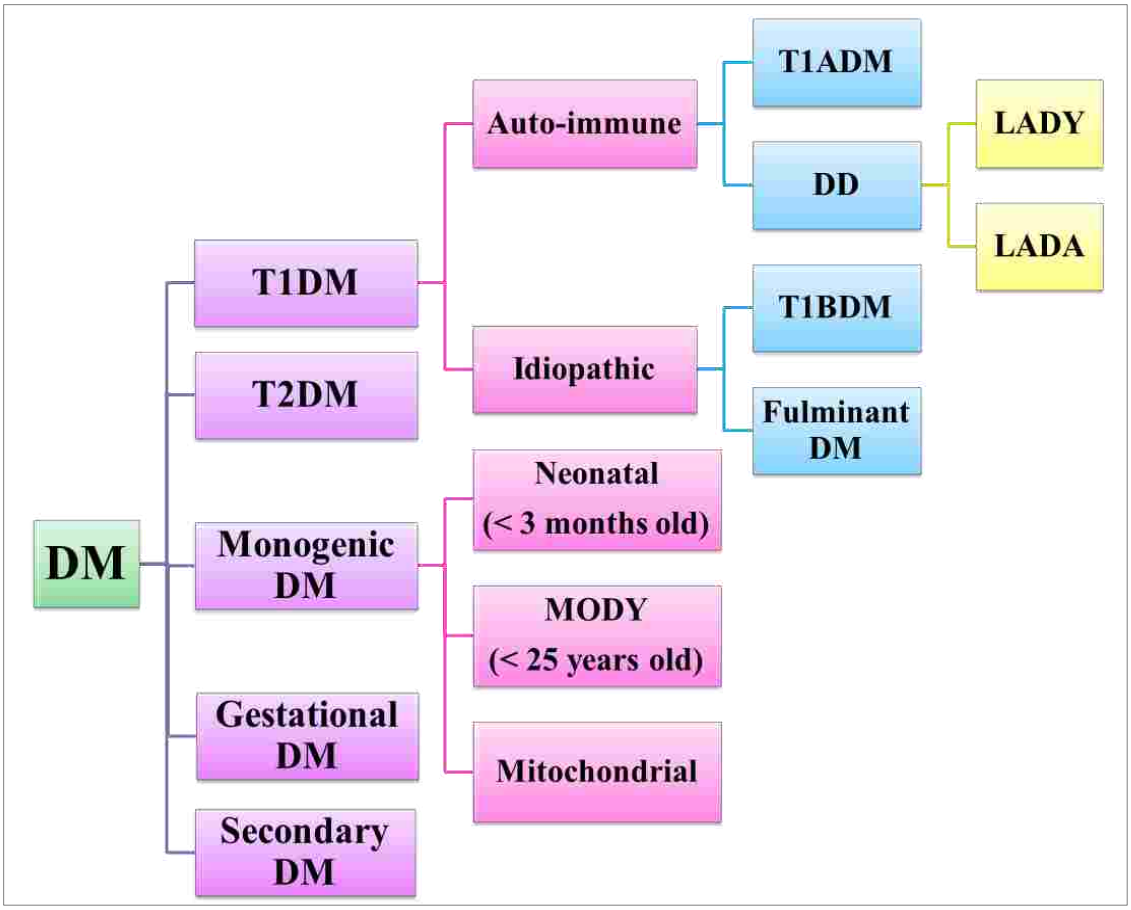

Figure 1-1: Classification of diabetes mellitus

T1DM: type 1 diabetes mellitus; **T2DM:** type 2 diabetes mellitus; **T1ADM:** type 1A diabetes mellitus; **T1BDM:** type 1B diabetes mellitus; **DD:** double diabetes; **LADY:** latent autoimmune diabetes in the young; **LADA:** latent autoimmune diabetes in adults **MODY:** maturity onset diabetes of the young

1.1.1.1. Type 1 Diabetes Mellitus

A. Autoimmune Diabetes Mellitus

A.1. Type 1A Diabetes Mellitus

It is believed that type 1A diabetes mellitus (T1ADM) occurs due to exposure of genetically susceptible individuals to an environmental trigger resulting in the development of humoral autoimmunity over a period of months or years [138]. T-

lymphocyte-mediated autoimmune responses destroy the pancreatic β-cells [290]. The rate of β-cell destruction differs according to age. It is fast in infants and children and it is slow in adults [10]. Autoimmune destruction can be detected by the presence of auto-antibodies to β-cell-specific antigens such as insulin and proinsulin, and neuroendocrine antigens such as glutamic acid decarboxylase 65 (GAD65) and insulinoma-associated protein-2 (IA-2) [138].

The detection of auto-antibodies can be done years before the disease is clinically diagnosed as shown in Figure 1-2 [102]. The late stage is characterized by the presence of hypoinsulinemia, which is indicated by low or undetectable C-peptide, and susceptiblity to developing diabetic ketoacidosis (DKA) [10].

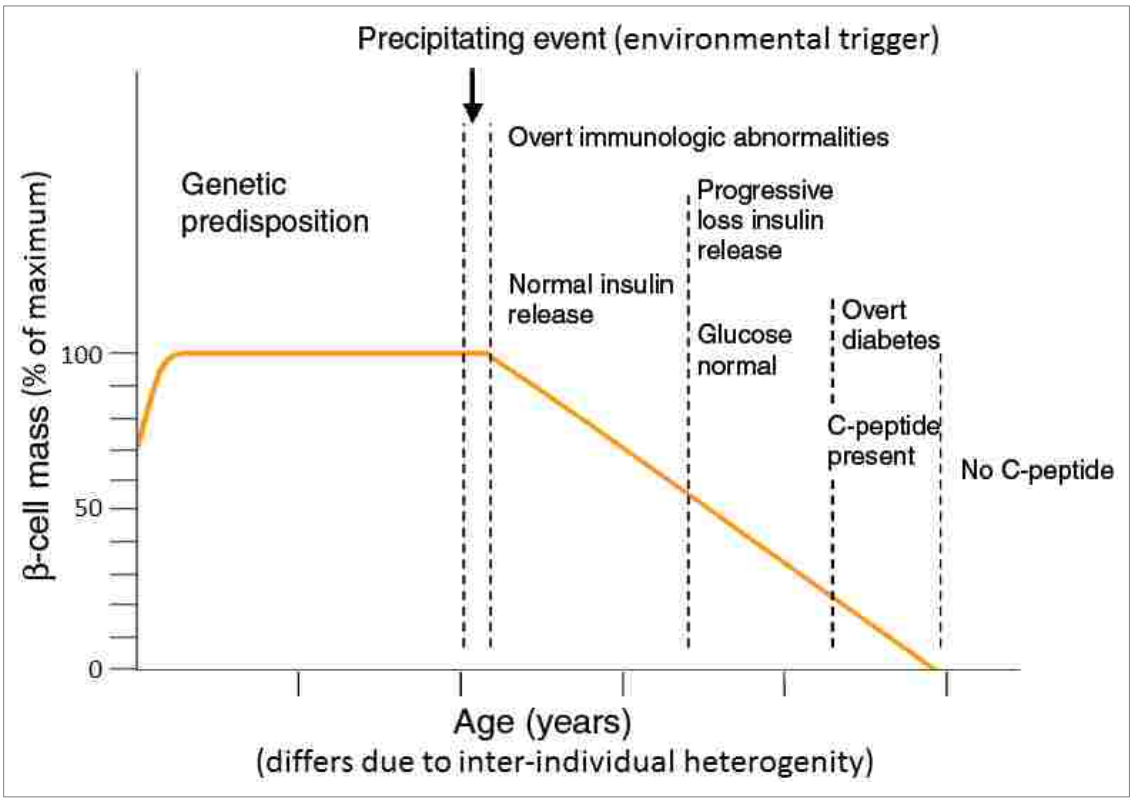

Figure 1-2: Model showing the stages of development of type 1A diabetes mellitus Adapted from [81; 102]

A.2. Double Diabetes Mellitus

The term double diabetes (DD) simply refers to the presence of both T1DM and T2DM characteristics in the patient. Other names used to describe DD include hybrid diabetes and type 1.5 DM. It has two versions: latent autoimmune diabetes in the young (LADY), affecting children, and latent autoimmune diabetes in adults (LADA), affecting adults [225].

A.2.1. Latent Autoimmune Diabetes in the Young

Children and youths affected are obese with insulin resistance (as T2DM) and have β-cell specific auto-antibodies in their sera (as T1DM) [225].

Reinehr and colleagues showed that 36% of the children used in this study, who were diagnosed with T2DM, had β-cell specific auto-antibodies indicating that they have DD and were misdiagnosed with T2DM [230]. Another study also reported that 33% of the children were also misdiagnosed with T2DM due to the presence of auto-antibodies [103]. Although, auto-antibodies were detected in children previously diagnosed with T2DM, they did not need insulin for more than a year [230]. It was also shown that, like LADA in adults, some children originally diagnosed with DD or initially misdiagnosed with T2DM switched from oral anti-diabetic medications to insulin [103]. The detection of single or more auto-antibodies including anti-insulin, anti-GAD, anti-IA-2 and islet cell auto-antibodies (ICA) indicates DD in children [103]. It is suggested that the progression of β-cell destruction in DD is slower than that in T1ADM which is indicated by the detection

of only a single auto-antibody [225]. Figure 1-3 shows the number of detected types of auto-antibodies types in T1DM and DD.

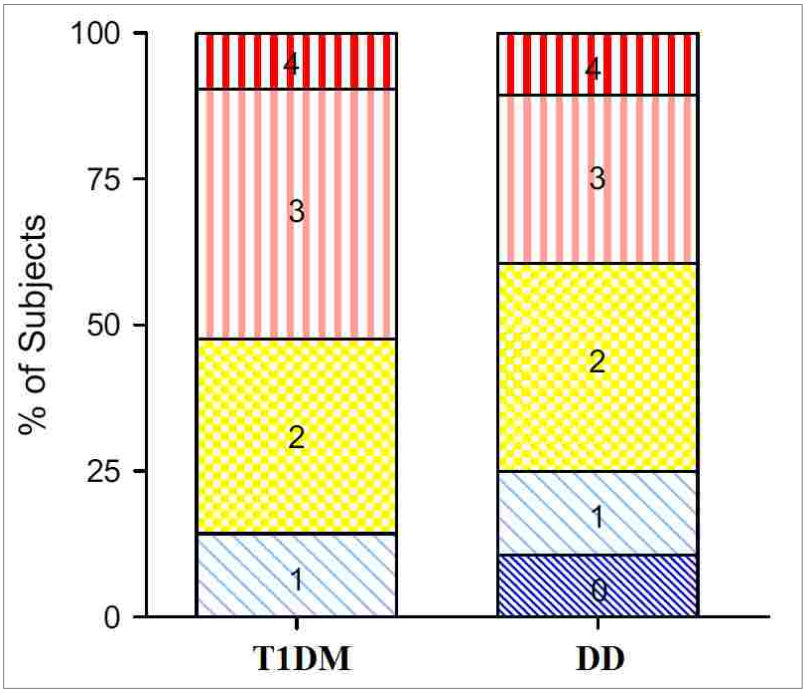

Figure 1-3: The percentage of subjects diagnosed with type 1 diabetes mellitus (T1DM) and double-diabetes (DD) according to the number of detected types of auto-antibodies

Adapted from [103]

Subjects include children aged between 8-18 years, from different ethnicities of the United States population, who were newly diagnosed with diabetes mellitus.

A.2.2. Latent Autoimmune Diabetes in Adults

LADA is a slowly progressive autoimmune disease [92]. During the early stages of the disease, patients with LADA are often misdiagnosed with T2DM because they are not dependent on insulin [92]. Some studies also reported the presence of T2DM insulin resistance in LADA patients [63], while others disagree [21]. However, LADA is characterized by the presence of auto-antibodies to insulin,

GAD, IA-2 and others [92]. As the disease progresses to its late stage, the patients experience weight loss, susceptibility to DKA, undetectable C-peptide levels and insulin dependence [209].

Diagnosis of LADA relies on three factors including the age of the patient (about 25-40 years), presence of auto-antibodies with anti-GAD and ICA being the most common antibodies, and lack of insulin dependence for at least 6 months after diagnosis [92; 209]. The treatment changes as the disease progresses starting with diet control, then oral anti-diabetic medications and eventually insulin [209].

B. Idiopathic Diabetes Mellitus

B.1. Type 1B Diabetes Mellitus

Being characterized as an idiopathic disease, the actual pathogenesis is still not clear. It occurs due to β-cell destruction resulting in hypoinsulinemia and DKA [10]. This disease does not show any signs of autoimmunity or genetic relation to human leukocyte antigen (HLA) genes [10]. It is believed to be an inherited disease as it only affects specific races (Africans and Asians) [10].

B.2. Fulminant Diabetes Mellitus

This is an idiopathic rapidly progressing DM that involves nearly total destruction of β-cells and consequently absolute insulin deficiency, hyperglycemia and DKA [129]. It was first reported in 2000 in Japan [130]. The population affected is mainly from east Asian countries like Japan, Korea, China, Taiwan, the Philippines and Malaysia [281]. Cases were also reported in the Caucasian population in France

[202] and the Hispanic population in the United States [192]. It also affects pregnant women, especially in the third trimester or right after delivery [117]. Unlike the autoimmune DM where progression takes years, fulminant DM progression only takes a few days and in rare cases may exceed one week (Fig. 1-4) [117].

The clinical features of fulminant DM include the abrupt onset of hyperglycemia accompanied by weight loss, polyuria and polydipsia, rapid development of DKA (one week after the onset of symptoms), almost normal levels of glycated (or glycosylated) hemoglobin (HbA_{1c}), undetectable or low C-peptide levels, elevated levels of serum pancreatic enzyme (such as amylase and lipase) and usually absence of auto-antibodies [129; 131]. However, it was reported that some patients diagnosed with fulminant DM were positive for anti-GAD but none were positive for anti-IA-2 [131]. Flu-like symptoms such as rhinorrhea, fever, sore throat were seen in about 71.7% of fulminant diabetics [131].

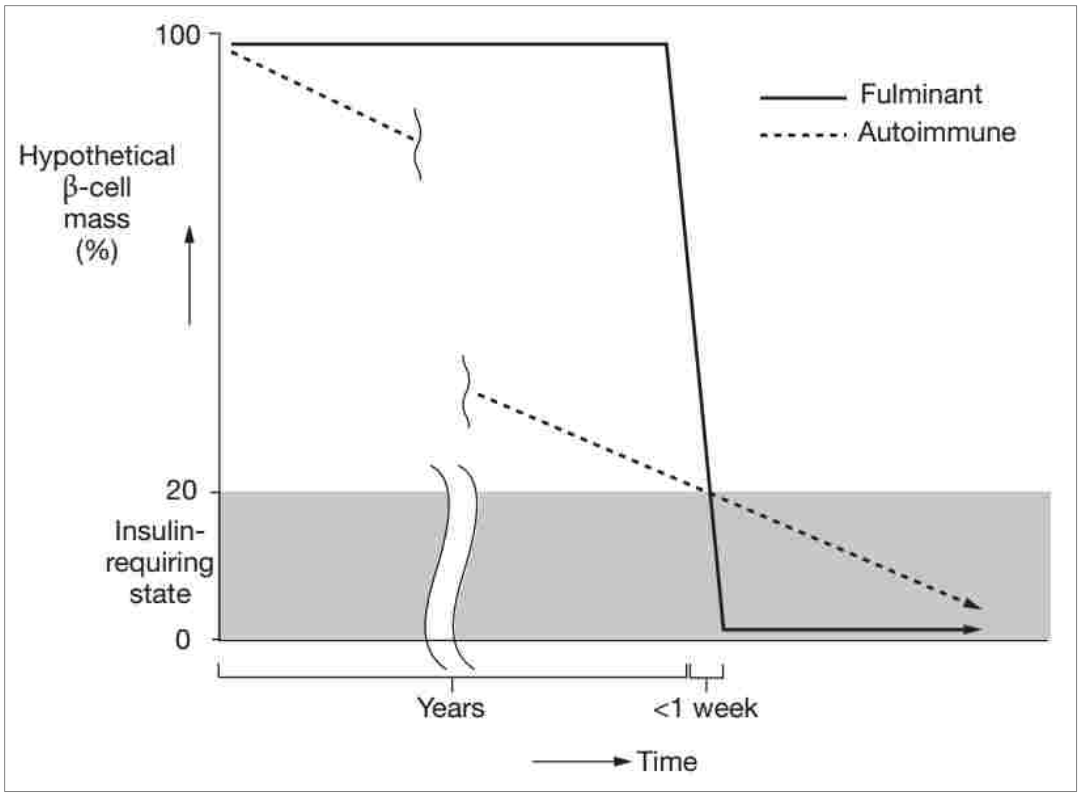

Figure 1-4: Duration of β-cell mass destruction in fulminant diabetes mellitus versus autoimmune diabetes mellitus

Retrieved from [117]

Pathogenesis is believed to be viral-mediated owing to the abrupt onset of the disease and the presence of flu-like symptoms [127]. A study reported high titers of immunoglobulin A antibodies to enterovirus in the sera of fulminant diabetics suggesting recurrence of enterovirus infection and high susceptibility of these patients to this virus [127]. Moreover, other studies showed a relationship between the disease and some genetic factors such as disease-susceptible HLA alleles [128; 154; 281]. Although it is classified as an idiopathic type of DM, some studies reported evidence for the involvement of autoimmunity in the pathogenesis of this disease [167; 208].

1.1.1.2. Type 2 Diabetes Mellitus

About 90-95% of diabetic patients have this type of DM which makes it the most common type of DM [10]. Unlike T1DM, T2DM is characterized by relative insulin deficiency that is sometimes accompanied by insulin resistance [10]. Therefore, patients with T2DM are not insulin dependent, and rarely develop DKA [10]. There are risk factors for T2DM, however, its exact etiology is still unclear [132]. The risk factors include environmental factors such as obesity or increased percentage of body fat especially abdominal fat, low physical inactivity and increased age, and genetic factors such as ethnicity and family history [10; 132].

1.1.1.3. Monogenic Diabetes Mellitus

This occurs as a result of spontaneous de novo mutation(s) or the inheritance of dominant or recessive mutation(s) in one single gene (thus, called monogenic) which is involved in maintaining glucose homeostasis [254]. Monogenic DM arises as a result of reduced β-cell functions or number, pancreatic transcription factors or insulin receptor sensitivity, depending on the gene involved [254]. Mutations affecting β-cell functions or number lead to defects in glucose sensing, or insulin synthesis, packaging or secretion [254]. Mutations affecting pancreatic transcription factors can also impair insulin synthesis, reduce pancreatic growth or cause agenesis [254]. Moreover, mutations affecting T-lymphocytes result in the generation of an autoimmune response against β-cells [254]. Since mutations can lead to the development of an autoimmune response, as well as, insulin sensitivity and resistance, monogenic DM can be neither classified under T1DM nor T2DM.

Monogenic DM can be further classified to neonatal DM, maturity onset diabetes of the young (MODY) and mitochondrial DM [118] (Fig. 1-1). Neonatal DM is generally defined as insulin-dependent hyperglycemia. It occurs during the first three months of age [68] and it has been extended to include six to nine months of age [238]. Insulin secretion mutations are more commonly the cause of neonatal DM compared to insulin sensitivity mutations [238]. MODY has been initially characterized by three criteria which include being considered as non-insulin dependent DM, affecting individuals below 25 years of age and showing autosomal dominant inheritance [99]. However, nowadays identifying MODY is based on its genetic etiology which clearly distinguishes between different genetic subgroups and differentiates it from T2DM in young individuals [68]. So far, mutations of nine genes have been found to produce different genetic subgroups of MODY (MODY1-MODY9) [99]. Mitochondrial DM involves the transmission of mutated mitochondrial deoxyribonucleic acid (DNA) from the mother to the fetus resulting in development of non-autoimmune β-cell dysfunction [68]. Organs having a high energy requirement, such as the brain, pancreatic β-cells, sensory organs and skeletal muscle, can also be impaired resulting in various syndromes such as deafness [68; 118].

Molecular studies involving genetic testing provide a highly sensitive and specific diagnostic tool for monogenic DM [238]. However, they are not widely applicable owing to the high cost and long time consumption [238].

1.1.1.4. Gestational Diabetes Mellitus

Gestational DM is the type of DM or glucose intolerance that is diagnosed for the first time during pregnancy (gestation) [10]. Gestational DM occurs approximately at the 24^{th} week of pregnancy where insulin resistance contributes to its occurrence [132]. Since the hyperglycemia can badly affect the health of the mother and fetus/neonate, diagnosis of DM by plasma glucose tests (See diagnosis section) should be done at the $24\text{-}28^{th}$ weeks of pregnancy. Fortunately, the hyperglycemia is usually reversed after delivery [10].

1.1.1.5. Secondary Diabetes Mellitus

Secondary DM is a disease that develops as a result of secondary factors such as pancreatic disease, autoimmune diseases, infections, genetic syndromes, drugs or chemicals [10; 305]. Impairment of either the exocrine or endocrine functions of the pancreas can cause DM. Exocrine dysfunction can result from pancreatitis, cancer, trauma/pancreatectomy and cystic fibrosis, however these factors, excluding cancer, must cause greatly pronounced pancreatic damage before DM can develop [305]. On the other hand, endocrine dysfunction may result from endocrine diseases such as Cushing's Syndrome, glucagonoma, acromegaly, hyperthyroidism and pheochromocytoma, that involve the secretion of insulin-antagonizing hormones including cortisol, glucagon, growth hormone, thyroid hormone and catecholamines [305]. In addition, autoimmune diseases such as lupus erythematosus and stiff-man syndrome can cause the generation of auto-antibodies against insulin receptors [10]. Viral infections such as congenital rubella and cytomegalovirus can also lead to DM.

Moreover, administration of some drugs such as nicotinic acid, thiazides and β-adrenergic agonists, or hormones such as glucocorticoids and thyroid hormone can disturb insulin function and induce DM [10]. Patients with genetic syndromes such as Down Syndrome, Klinefelter Syndrome and Turner Syndrome have a high susceptibility to DM and those with Wolfram Syndrome have no β-cells and consequently insulin deficiency [10].

1.1.2. Diagnosis of Diabetes Mellitus

It is estimated that about 46% of the patients with DM worldwide are undiagnosed and unaware of being diabetic [132]. Since DM is a progressive disease that can cause development of serious complications if left uncontrolled, a correct diagnosis is crucial.

DM has well-established clinical symptoms including polyuria, polydipsia, polyphagia, fatigue, unexplained weight loss, blurred vision, slow healing of wounds, and higher susceptability to infection [133]. Nevertheless, some diabetic patients can be asymptomatic [133]. Therefore, diagnosis does not solely rely on the existance of symptoms, rather there are tests for measuring plasma glucose levels as an indication for the presence of DM. Table 1-1 shows the latest updated diagnostic criteria used for DM according to the World Health Organization (WHO) and American Diabetes Association (ADA).

	Diabetes (WHO and ADA)*	IFG (WHO)*	IGT (WHO)*	Prediabetic (ADA)*
HbA_{1c} (%)	≥ 6.5% **§**	NA	NA	≥ 5.7% to 6.4%
Fasting plasma glucose (mmol/l)	≥ 7.0 (≥ 126 mg/dl) **§**	≥ 6.1 to 6.9 (≥ 110 mg/dl to 125 mg/dl)	< 7.0 (< 126 mg/dl)	≥ 5.6 to 6.9 (≥ 100 mg/dl to 125 mg/dl)
75 g OGTT post-load plasma glucose (mmol/l)	2h, ≥ 11.1 (≥ 200 mg/dl) **§**	2h, < 7.8 (< 140 mg/dl)	2h, ≥ 7.8 to 11.0 (≥ 140 mg/dl to 199 mg/dl)	2 h, ≥ 7.8 to 11.0 (≥ 140 mg/dl to 199 mg/dl)
Random glucose (mmol/l)	≥ 11.1 (≥ 200 mg/dl) with classic symptoms	NA	NA	NA

Table 1-1: Diagnostic criteria of diabetes mellitus

Adapted from [212; 306]

WHO: World Health Organization**; ADA:** American Diabetes Association; **IFG:** impaired fasting glucose; **IGT:** impaired glucose tolerance; **HbA_{1c}:** glycated haemoglobin A_{1c}; **NA:** not applicable; **OGTT:** oral glucose tolerance test

***** WHO and ADA have identical diagnostic criteria for diabetes, while they have different terms and approaches in defining and diagnosing intermediate hyperglycaemia or prediabetes.

§ If the results are equivocal, retesting should be done for confirmation.

The diagnosis of DM should be done using venous plasma as a universal standard. It has been stated that venous and capillary samples are identical when measuring fasting plasma glucose (FPG), however, capillary samples gives higher non-fasting glucose levels compared to venous ones [306]. In addition, glucose levels should be measured in plasma separated from blood samples rather than the whole blood because approximately 11% higher glucose is measured in plasma samples than that in whole blood samples [306].

Impaired fasting glucose (IFG) and impaired glucose tolerance (IGT) have the same definition. They represent the region that lies between the upper borderline of normal glucose and the lower borderline of diabetic glucose in the fasting and fed states, respectively [132; 306]. If a patient was diagnosed with IFG, this indicates impaired insulin secretion and impaired inhibition of hepatic glycolysis and gluconeogensis [306]. IGT provides evidence for an increased risk of developing DM, however, not all invdividuals with IGT will develop DM [306]. If IGT is detected, this indicates impaired insulin secretion and the presence of insulin resistance. Both IFG and IGT provide a predictive measure for DM development [306].

Measuring HbA_{1c} gives an indication of the average plasma glucose levels during the past 2-3 months (8-12 weeks) [307]. HbA_{1c} is considered as the gold standard for monitoring glycemic control during treatment of diabetic patients [306]. At least 3 days before the test, the patient should eat normally (an unrestricted carbohydrate diet that involves ingesting above 150 g carbohydrate) and maintain his usual physical activity [305]. FPG involves measuring the plasma glucose level after fasting overnight for 8-14 hours where drinking is permitted [305]. Then, oral glucose tolerance test (OGTT) requires ingestion of 75 g of anhydrous glucose (or any equivalent carhohydrate content) dissolved in 250-300 ml of water, where blood glucose is measured after 2 hours from the beginning of the glucose drink [305], or at 30 minute intervals for 2 hours. Random (casual) glucose involves measuring plasma glucose at any time of the day regardless the time of the last meal [68].

In 2009, diagnosis using the HbA_{1c} test was recommended by the ADA, the International Diabetes Federation (IDF), and the European Association for the Study of Diabetes (EASD) [11]. HbA_{1c} overcomes many disadvantages of FPG and OGTT because it is more convenient for the patient as it does not require fasting or any prior dietry preparations and it avoids the problem of day-to-day fluctauations of blood glucose levels (BGL) as a result of illness or stress [11; 307]. On the other hand, HbA_{1c} has some disadvantages including high cost, unavailabilty in some developing countries, lack of standardization in some countries and variation among races and ethnicities (it is higher in African-Americans) [11; 307]. In addition, it is influnenced by several factors such as genetic background and illness especially hemoglobinopathies such as certain anemias and malaria [307]. If a patient was shown to be diabetic according to the diagnostic results, the patient should confirm these results by repeating the test [11]. This is applicable especially for asymptomatic patients but not applicable for patients with DKA (hyperglycemic crisis) or random plasma glucose exceeding 200mg/dl, accompanying the known DM symptoms [11; 307]. Using the same test is recommended for a higher chance of consistent results [11]. Two different diagnostic tests (such as HbA_{1c} and FBG) can also be used in which the diagnosis of DM is confirmed if the results from both tests are above the diagnostic threshold. If one test only was above the threshold while the other was below it, the test above the threshold should be repeated [11].

After DM is confirmed in a patient, further tests and follow-ups should be performed to identify the type of DM. A simple schematic diagram on identification of different types of DM is shown in Figure 1-5.

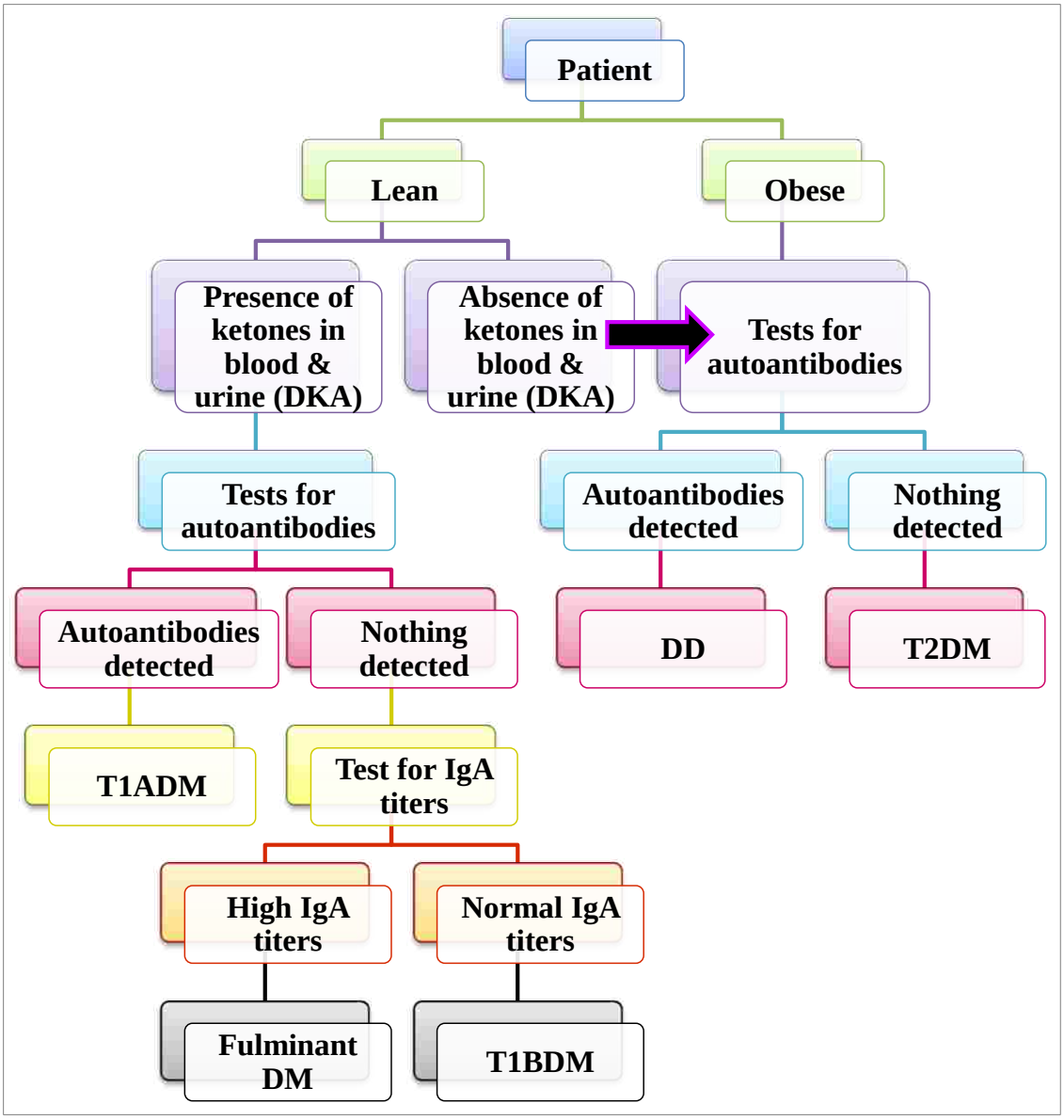

Figure 1-5: Simple schematic diagram for identifying the type of diabetes mellitus

T1ADM: type 1A diabetes mellitus; **T1BDM:** type 1B diabetes mellitus; **DD:** double-diabetes; **T2DM:** type 2 diabetes mellitus

1.1.3. Epidemiology of Diabetes Mellitus

1.1.3.1. Prevalence

DM is one of the non-communicable diseases which poses a global threat [308]. Worldwide, DM affected about 328 million individuals in 2013 and this is expected to increase by 55% to reach 592 million in 2035 (Fig. 1-6) [132]. In the Middle East and North Africa (MENA) region (Fig. 1-6), to which the United Arab Emirates (UAE) belongs, there are about 35 million diabetic patients [132]. The UAE was reported in 2013 to have one of the highest age-standardized comparative prevalences (18.98%) worldwide and a global comparative prevalence of 8.3%, with Abu-Dhabi having the most elevated rates of DM among the other emirates [37]. The prevalence of IGT in the UAE was also ranked among the top ten worldwide reaching 16.6% (3^{rd}) in 2013 and is expected to rise to 17.0% (4^{th}) by 2035 [132]. Among the UAE population in 2005, the prevalence was reported to be 25% below the age of 55 years and 40% above it [190]. Moreover, in 2007, a study in the UAE national citizens in Al-Ain, Abu Dhabi reported a prevalence of 10.5% for diagnosed diabetic patients, 6.6% for undiagnosed diabetic patients and 20.2% for pre-diabetic patients [239].

1.1.3.2. Regional Variation

According to the regional classification of the IDF (Fig. 1-6), the MENA region has the highest prevalence (10.9%) among other world regions [132]. The North America and Caribbean region has the second highest (9.6%) prevalence followed by the South and Central America region (8.2%) [132]. When comparing

urban and rural regions, it has been shown that urban populations have a higher prevalence of DM than rural populations [132].

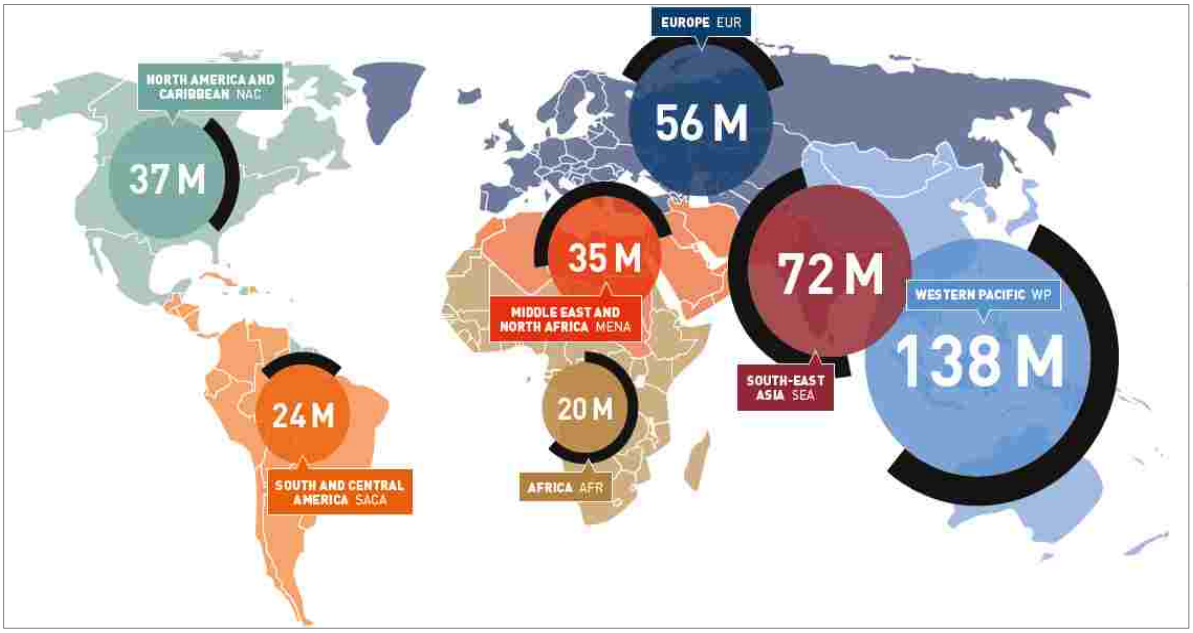

Figure 1-6: The world regional classification of the International Diabetes Federation showing the number of diabetic population in each region

Retrieved from [132]

1.1.3.3. Age at Onset

As mentioned earlier, DM can develop at any age from birth in neonates until senescence in adults. The age range to which 50% of adult diabetic patients belong is from 40 to 59 years [132]. Several studies showed a significant increase in the incidence of T1DM in children with age [150; 275]. Similarly in T2DM, there was a positive correlation between the prevalence of DM and age in Asian and European populations, but it was more pronounced in the Asian population [273; 274].

1.1.3.4. Male-to-Female Variation

Generally, there are more diabetic males than females worldwide, with a total difference of 14 million [132]. In children aged from 0-14 years, the incidence of T1DM was not shown to be different between males and females [275]. It was shown previously that ethnicities at high risk of T1DM incidence such as Caucasians (represented by Europeans) have a higher male-to-female ratio, while ethnicities at low risk such as Africans and Asians have higher female-to-male ratios [150]. Two large studies on T2DM prevalence in Asian and European populations showed a higher prevalence of IFG in males from China, Japan and Europe and in females from India. There was a higher prevalence of IGT in females from China, Japan and Europe and in males from India [273; 274]. Undiagnosed DM was more common in Asian females and European males [273; 274]. T2DM affects females more than males in the United States population and the same was seen among children with T2DM [8].

The global difference in DM-causing mortality between males and females is very little [132]. But if each region is considered individually, there are differences seen in all the world regions, except for MENA and Western Pacific regions, in which diabetic females have higher mortality rates than males [132].

1.1.3.5. Association with Pregnancy

During pregnancy, women are prone to two types of DM: fulminant DM and gestational DM. Fulminant DM was recently discovered in Japan and it is not specific to pregnant women as it can also affect males and non-pregnant females [130]. It can

affect pregnant women during the third trimester or after delivery leading to a poor prognosis for the fetus [117].

About 21.4 million women had gestational DM in 2013 [132]. As the age of a pregnant woman increases, she has a higher chance of getting gestational DM reaching its highest chance at the age of 45 years [132].

1.1.4. Pathophysiology of Diabetes Mellitus

In order to fully understand the pathophysiology of DM, it is important to understand normal glucose homeostasis (Fig. 1-7). During fasting, there is simultaneous endogenous glucose production and glucose utilization [212]. Endogenous glucose production is carried out by the liver via glycogenolysis and gluconeogenesis, whereas its utilization is done by insulin-independent tissues like the brain. Endogenous glucose production via glycogenolysis and gluconeogenesis is carried out by the liver (85%) and kidneys (15%) to match basal glucose utilization (≈ 2.0 mg/kg/min) [73]. The endogenous glucose produced is then mainly utilized by insulin-independent tissues including the brain (50%), and liver and gastrointestinal tissues (called splanchnic area) (25%) which are solely dependent on glucose, unlike insulin-sensitive tissues (25%) such as the heart, skeletal muscles and adipose tissue which can make use of other energy sources rather than glucose such as non-esterified fatty acids produced via adipose tissue lipolysis [73; 212]. The interaction between these two processes prevents hypoglycemia during fasting [212]. On the other hand after carbohydrate intake (fed state), dietary glucose is absorbed in the small intestine by the bloodstream thereby raising the BGL [212]. Elevated BGL

induces β-cells to secrete insulin and inhibits α-cells from secreting glucagon [212]. Glucagon-like peptide 1 (GLP 1) amplifies the effects of the elevated BGL on insulin secretion and glucagon suppression [212]. The secreted insulin then works on decreasing the BGL via three processes including promotion of glucose uptake in insulin-sensitive tissues (heart, skeletal muscles and adipose tissue) and in splanchnic areas, inhibition of endogenous glucose production by hepatocytes and inhibition of adipose tissue lipolysis [73; 212]. Decreasing postprandial BGL usually takes about 2 hours to reach fasting levels [212]. The uptake of dietary glucose in insulin-sensitive tissues is about 80-85% in muscles and about 4-5% in adipocytes [73].

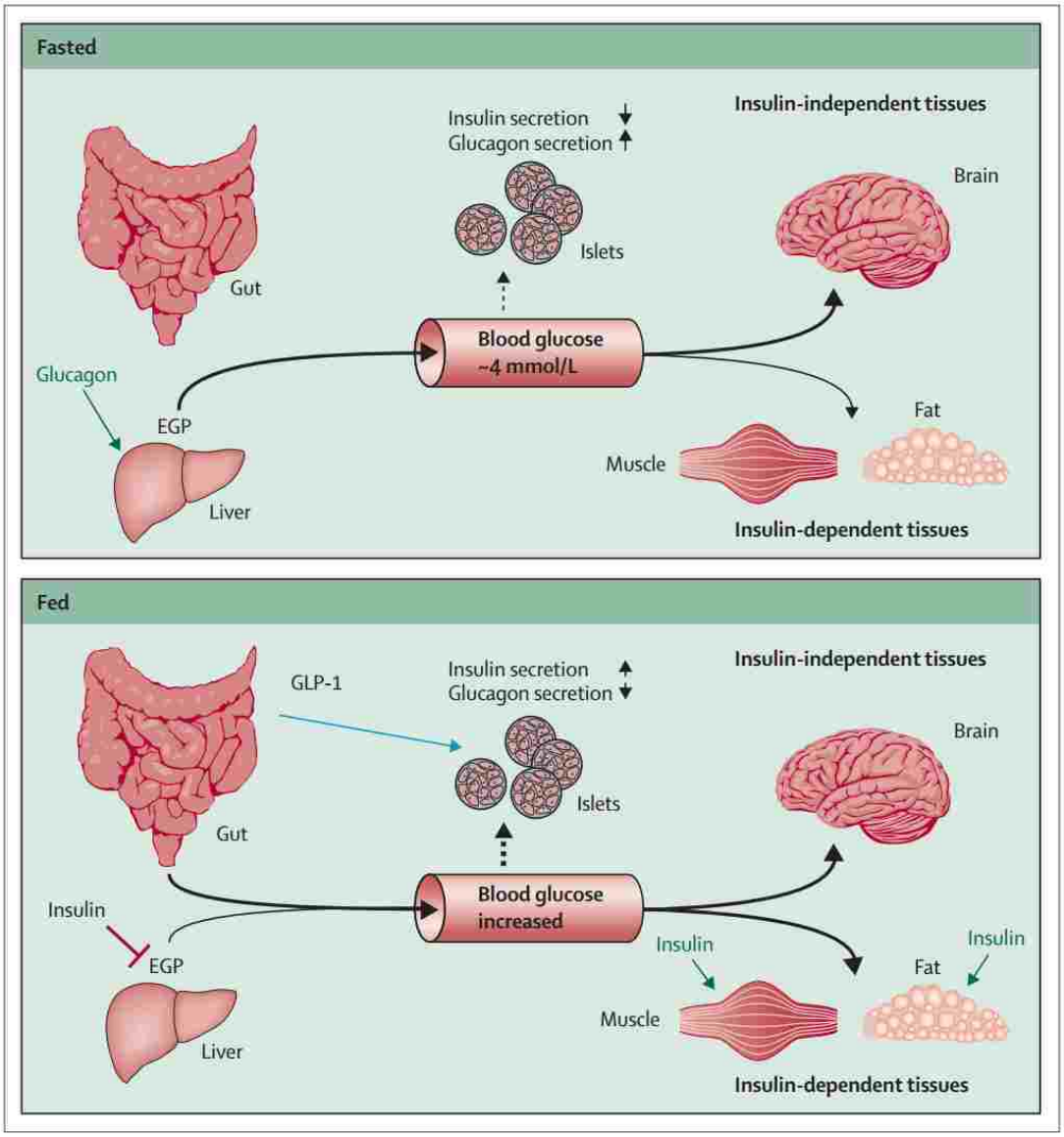

Figure 1-7: Normal glucose homeostasis in fasting (upper panel) and fed (lower panel) states

Retrieved from [212]

The pathophysiology of T1DM is characterized by complete insulin deficiency and consequent hyperglycemia and DKA. Deficiency of insulin secretion leads to a disturbance in the secretion of other hormones such as leptin whose secretion, from adipose tissue, is reduced [198]. Glucagon secretion, which is

normally controlled by insulin and leptin, is then increased [198]. It has been shown recently that leptin deficiency, in diabetic rats, increases the pituitary gland secretion of adrenocorticotrpin hormone (ACTH) [198]. ACTH increases the adrenal gland secretion of corticosterone which leads to increasing lipolysis, and production of free fatty acids (FFA) and glycerol from triglycerides [198]. Glycerol and FFA are then carried by the bloodstream to the liver where they are converted to glucose and ketone bodies, respectively [198]. Moreover, oxidation of FAA produces acetyl-CoA which leads to glucose production from pyruvate [198]. Collectively, these events result in hyperglycemia and DKA [198]. Figure 1-8 shows the pathophysiology of T1DM.

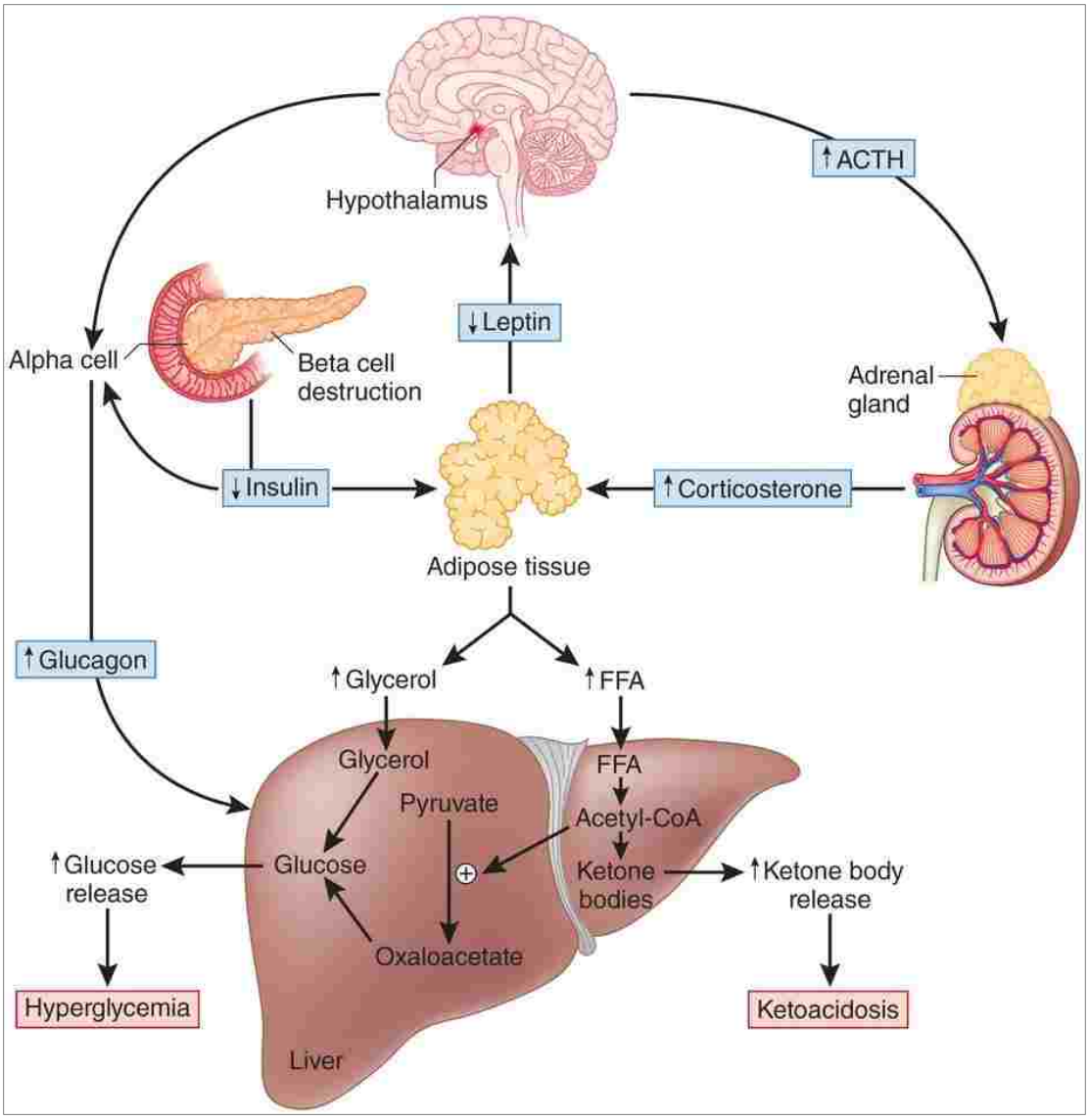

Figure 1-8: Pathophysiology of type 1 diabetes mellitus

Retrieved from [198]

ACTH: adrenocorticotropin hormone; **FFA:** free fatty acids

The pathophysiology of T2DM is shown in Figure 1-9. T2DM occurs due to lack of responsiveness of insulin-sensitive tissues to insulin effects (insulin resistance) resulting in β-cell dysfunction [115; 145]. Besides, it is associated with accelerated production of endogenous glucose [262]. A lack of response of target

tissues to insulin, due to insulin resistance, drives the β-cells to produce more insulin at early or intermediate stages of DM [145; 262]. Insulin resistance causes the β-cells to eventually become irresponsive to elevated BGL [145]. Moreover, insulin resistance eliminates insulin effects on target tissues including glucose uptake by insulin-sensitive tissues (heart, skeletal muscles and adipose tissue) and splanchnic area, inhibiting endogenous glucose production and inhibiting lipolysis in adipose tissue [262]. This results in the persistence of hyperglycemia and production of FFA via lipolysis (hyperlipidemia) in adipose tissue [262].

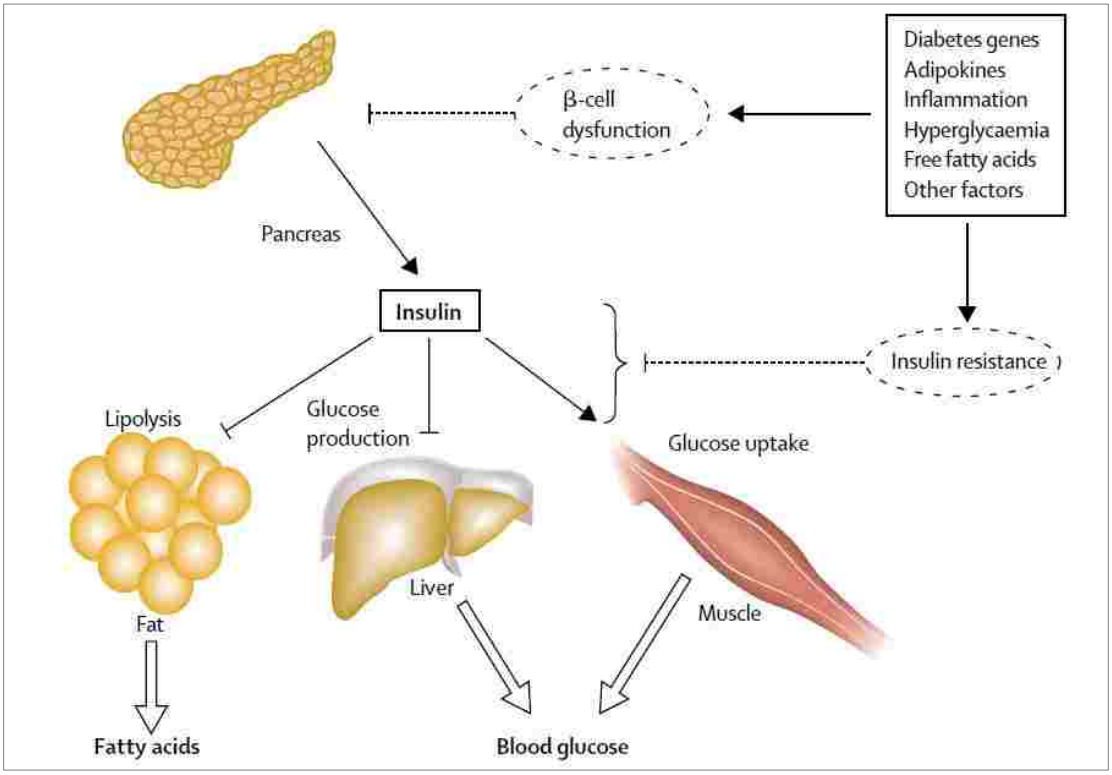

Figure 1-9: Pathophysiology of type 2 diabetes mellitus

Retrieved from [262]

1.1.5. Complications of Diabetes Mellitus

As stated by the IDF, "DM is the leading cause of CV disease, blindness, kidney failure, and lower-limb amputation" [132]. The persistent hyperglycemia of DM causes damage to blood vessels, known as angiopathy. In small blood vessels, including capillaries, this results in 'microvascular complications' and in large blood vessels, including arteries and veins, this results in 'macrovascular complications' [39; 91]. These complications are what make DM a dangerous progressive disease as they represent the main cause of morbidity and mortality in all types of DM [93]. Microvascular complications affect the eyes (retinopathy), neurons (neuropathy) and kidneys (nephropathy), while macrovascular complications affect the heart arteries (CV disease), brain arteries (cerebrovascular disease) and peripheral arteries (Fig.1-10) [91; 93]. The presence of more than one macrovascular complication can sometimes be called polyvascular disease [221]. Moreover, persistent hyperglycemia can lead to other chronic complications such as depression, dementia, impaired oral health (gingivitis and tooth loss), high susceptibility to infection, sleep apnea and sexual dysfunction [91; 132].

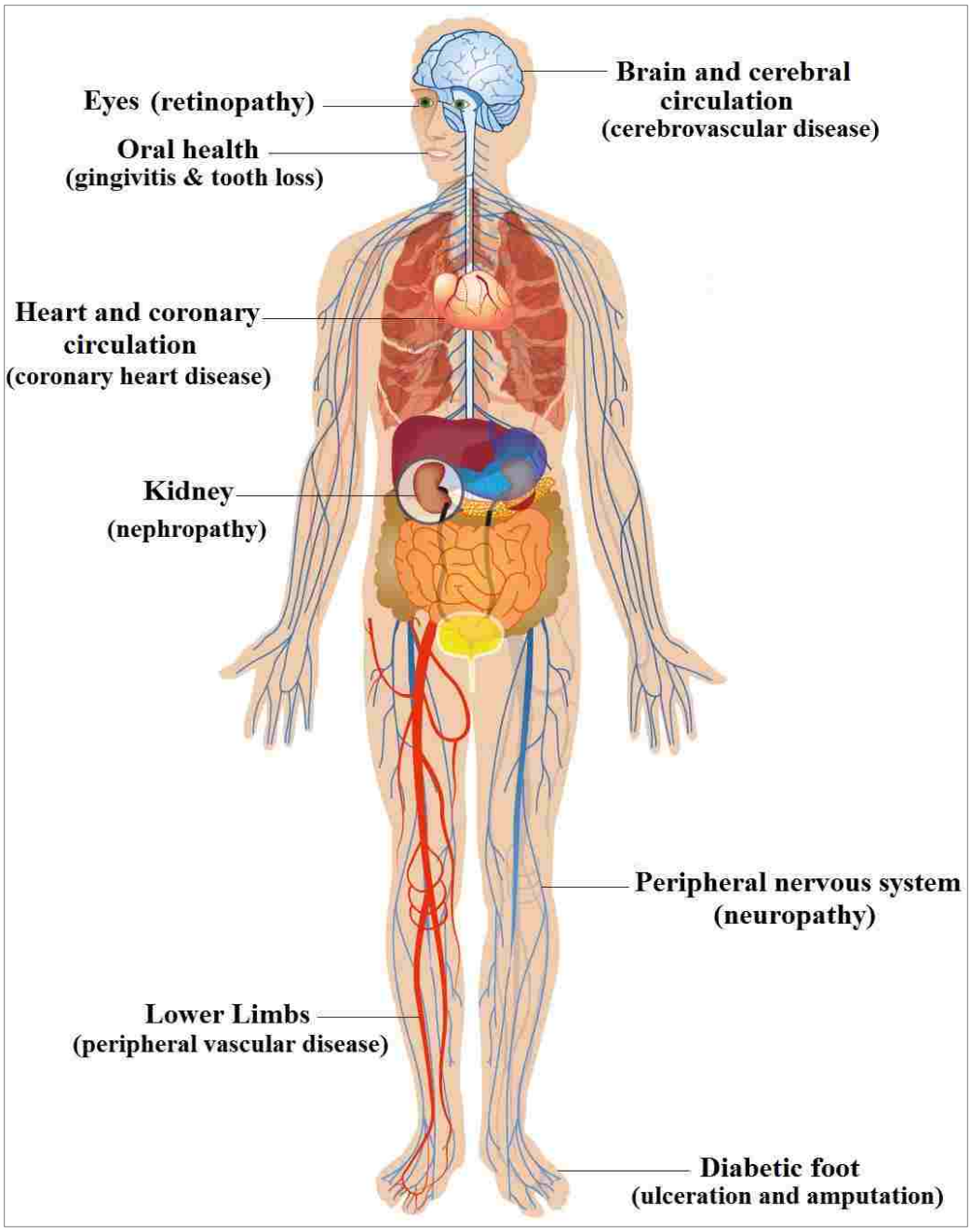

Figure 1-10: Complications of diabetes mellitus

Adapted from [132]

1.1.5.1. Microvascular Complications

The development of microvascular complications depends on the duration and severity of hyperglycemia [93].

A. Diabetic Retinopathy

Diabetic retinopathy involves impaired retinal blood flow, and blockage and damage of the retinal vessels which can lead to hypoxia and retinal damage [39]. Studies have shown that diabetic retinopathy is more prevalent in T1DM patients and less prevalent in T2DM patients diagnosed after the age of 30 [39]. After 20 years of being diagnosed with DM, nearly all T1DM patients and most of T2DM have some signs of retinopathy [91]. Development of retinopathy may begin 7 years before DM is diagnosed in type 2 patients [93]. The first sign of retinopathy is microaneurysms which are small retinal vascular dilatations and are clinically indicated by red dots (balloon-like sacs) during retinal examination (Fig. 1-l1) [39; 93]. Microaneurysms occur due to loss of pericytes which are elongated contractile cells surrounding the small vessels to control the vessel constriction and dilatation (tone), control vessel growth and provide protection against reactive oxygen species (ROS) [39]. There are five grades of diabetic retinopathy including (i) background retinopathy, (ii) background retinopathy with maculopathy, (iii) pre-proliferative retinopathy, (iv) proliferative retinopathy and (v) advanced diabetic eye disease which differ in the progression and prognosis of DM [78]. Background retinopathy is characterized by the presence of dot hemorrhages with marginal lipid deposition (hard exudates) in the middle retinal layers, microaneurysm and grayish retinal areas indicating retinal

edema [78; 93]. Background retinopathy with maculopathy exhibit hard exudates, capillary occlusion and leakage in the macular region accompanied by central visual loss (such as reading difficulty) [78]. Pre-proliferative retinopathy is characterized by the presence of white areas on the retina resembling ‘cotton wool spots’ and large hemorrhages. Proliferative retinopathy shows abnormal growth of new retinal vessels and may cause visual loss [78]. Advanced diabetic eye disease is the most dangerous and exhibits vitreous hemorrhage, retinal detachment and thrombotic glaucoma resulting in partial or total visual loss [39; 78].

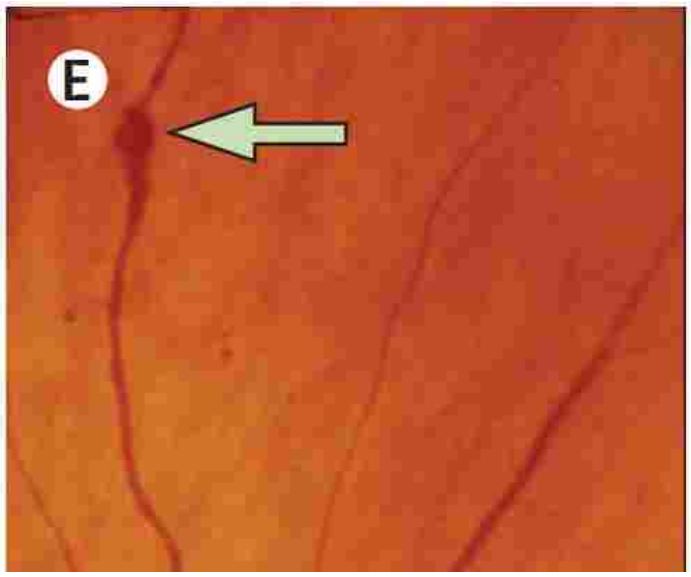

Figure 1-11: Microaneurysm manifested by balloon-like sacs (arrow) during retinal examination

Adapted from [62]

B. Diabetic Neuropathy

Diabetic neuropathy is the damage of peripheral nerves resulting from extreme hyperglycemia along with hypertension [132]. There are two types of diabetic

peripheral neuropathies: focal neuropathies (mononeuropathies) and sensorimotor polyneuropathy which is more common [76]. Peripheral polyneuropathies affect motor and sensory nerves especially in the feet causing pain, tingling and loss of sensation which can consequently lead to unnoticed injuries, infections, ulcerations and amputations [76; 132]. Foot ulceration or injury, associated with diabetic neuropathy, accounts for more than 80% of amputations [93]. Long nerve fibers are the first to be affected. Loss of nerve terminals and nerve conduction velocity are first manifested in the feet and then affect other areas, mainly the hands, giving a pattern of 'glove and stocking' (Fig. 1-12A) [91]. The systems affected by autonomic neuropathy include the CV, gastrointestinal, urogenital, sudomotor and pupillomotor systems (Fig. 1-12B) [95]. Cardiac autonomic neuropathy can be manifested as resting tachycardia, exercise intolerance, variable resting HR, slow HR recovery after exercise, orthostatic hypotension, prolonged QT intervals, 'silent' myocardial infarction (MI) and increased mortality [39; 76]. Other autonomic neuropathies include gastroparesis, vomiting, diarrhea, constipation, bladder paresis, sweating abnormalities (anhidrosis), impaired wound healing, impaired light reflex and erectile dysfunction [76; 91; 93]. Whereas in addition to sensorimotor neuropathy, sensory neuropathy (without motor neuropathy) can also be found in some diabetic patients but it is relatively rare [93]. Mononeuropathies commonly affect median, ulnar and radial nerves but can also affect any other nerves (Fig. 1-12C) [93]. They can also be manifested by severe pain, weakness and atrophy of large muscles (thigh muscles), a condition known as diabetic amyotrophy [93].

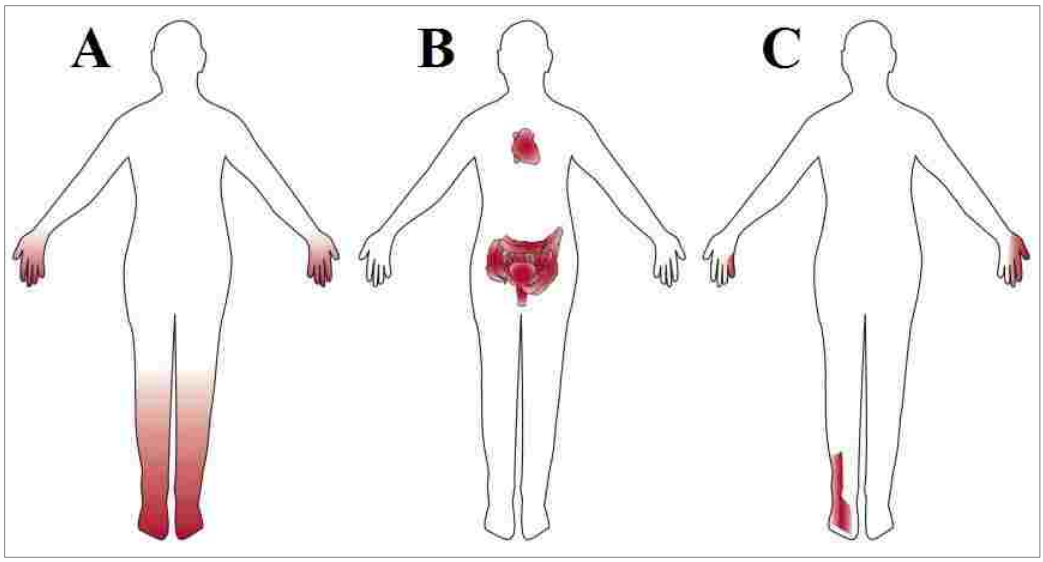

Figure 1-12: Different patterns of diabetic neuropathy distribution

Adapted from [41]

(A) Polyneuropathy (glove and stocking)
(B) Autonomic neuropathy
(C) Mononeuropathy

C. Diabetic Nephropathy

Diabetic nephropathy involves damage to small renal blood vessels resulting in kidney dysfunction or even failure [132]. The risk factors for diabetic nephropathy include hyperglycemia, hypertension, obesity, dyslipidemia and smoking tobacco [39]. Before development of the overt diabetic nephropathy, a stage called 'incipient nephropathy' occurs, which is characterized by microalbuminuria (20-200 µg/min or 20-300 mg/24h) [78]. Overt diabetic nephropathy develops, in the majority of cases, as a result of uncontrolled hyperglycemia and hypertension, however, it can also develop with good glycemic control and normal blood pressure [91]. It is manifested by proteinuria in which albumin is the main protein excreted, elevated blood pressure and progressive reduction of the glomerular filtration rate over a period of 10-20

years [78; 91]. During the early stages of DM, an increase in renal size takes place due to hyperplasia and hypertrophy and consequently the glomerular filtration rate increases leading to filtration of more glucose, proteins and fatty acids [91]. Proteinuria indicates alterations in the glomerular filtration barrier, vascular damage and subsequent end stage renal disease [78; 91]. The end stage renal disease is the most severe stage in which hemodialysis or a renal transplant is a necessity [78]. Diabetic nephropathy predisposes the development of macrovascular complications [91].

1.1.5.2. Macrovascular Complications

Macrovascular complications are the most dangerous and are the major cause of morbidity and mortality in diabetic patients [132]. The risk factors for macrovascular complications, aside from hyperglycemia, include hypertension and hypercholesterolemia [132]. Atherosclerosis is the principle pathological process that results in the development of macrovascular complications [93]. Chronic inflammation and injury to the coronary and peripheral arteries lead to accumulation of oxidized low-density lipoprotein-cholesterol (LDL-C), which may be oxidized by angiotensin II, in the arterial wall [93]. Oxidation of LDL-C particles changes their properties and makes them antigenic causing stimulation of the immune system [75]. The arterial wall is then infiltrated by macrophages (differentiated from monocytes), which together with oxidized LDL-C, result in the formation of foam cells due to engulfing LDL-C particles by the macrophages [75; 93]. Macrophages then proliferate and attract T-lymphocytes which stimulate proliferation of endothelial

cells and arterial smooth muscles, plus the accumulation of collagen [75; 93]. This series of events eventually result in the formation of atherosclerotic plaque. These plaques are lipid-rich in content and are covered with a fibrous cap [93]. When the plaque ruptures, acute vascular infarction occurs [93].

A. Cardiovascular Disease

Diabetic patients, particularly those with T2DM, have a 2 to 6-fold higher risk of developing CV disease compared to non-diabetic individuals [132]. CV disease is one of the most common causes of death in diabetic patients and is responsible for more than half of the deaths of these patients. Diabetic CV diseases include angina, MI and congestive heart failure (diabetic cardiomyopathy) [132]. Risk factors for diabetic CV diseases include uncontrolled hyperglycemia, dyslipidemia, nephropathy and hypertension [91]. The age-comparative mortality risk of coronary artery disease (CAD) is 3-fold in diabetic men and 2 to 5-fold in diabetic women compared to non-diabetic individuals [94].

A.1. Angina

Atherosclerotic CAD is the major cause of myocardial ischemia [94]. Angina is usually an indicative symptom for myocardial ischemia [268]. The type of angina mainly observed in diabetic patients is unstable angina [91]. Angina is associated with pressure, tightness, constricting or burning pain that is mainly felt near the sternum, but can also occur in other areas such as the epigastrium, lower jaw, shoulders and arms [94]. Other symptoms may also occur such as shortness of breath,

fatigue, nausea and restlessness [94]. Moreover, some patients exhibit silent myocardial ischemia which occurs without angina or any angina symptoms and can occur at rest or with minimal physical activity [268]. DM is a risk factor for silent myocardial ischemia and therefore, it is common among diabetic patients [111; 268].

A.2. Myocardial Infarction

MI takes place due to a rupture of atherosclerotic plaque deposited in the coronary arteries. This can result in coronary arterial occlusion, consequent myocardial ischemia and myocardial cell necrosis [278]. The risk of MI in diabetic patients is 3 times that of the general population and is almost equal to that of non-diabetic individuals with previous MI [91]. The size of the infarct size is an indicator for the prognosis of the disease [197]. Diabetic patients have a relatively poor prognosis and higher mortality due to ventricular dysfunction and hypertrophy as well as the abundance of atherosclerotic plaques [197]

A.3. Congestive Heart Failure (Diabetic Cardiomyopathy)

Diabetic cardiomyopathy is a myocardial disease that occurs as a result of the cardiac structural and functional changes induced by DM in the absence of other predisposing factors for CV diseases such hypertension and atherosclerosis [75]. These diabetic changes predispose the patient to congestive heart failure [75]. Congestive heart failure is a condition characterized by structural and functional impairment in which the ability of the heart to fill with blood and/or eject blood is impeded [75]. Congestive heart failure can involve diastolic dysfunction and/or

systolic dysfunction [256]. Systolic dysfunction is impaired cardiac contractility, associated with low left ventricular fraction (< 45%) [75]. On the other hand, diastolic dysfunction is impaired cardiac relaxation, which exhibits impaired cardiac ability to properly relax and fill with blood during diastole [75]. Diastolic dysfunction causes dyspnea upon exertion which prevents the patient from losing the extra weight necessary for the treatment regimen [91]. Diabetic patients have several risk factors for diabetic cardiomyopathy such as persistent hyperglycemia, atherosclerosis, chronic hypertension and microvascular complications, especially autonomic neuropathy [111]. Fortunately, controlling these risk factors by anti-diabetic, anti-hypertensive and cholesterol-lowering medications may prevent the development of diabetic cardiomyopathy [111].

B. Cerebrovascular Disease

DM increases the risk of atherosclerotic plaque formation in the cerebrovascular circulation including intracranial and extracranial (such as carotid artery) arteries [39]. Rupture of atherosclerotic plaque formed in cerebral arteries causes strokes. Following ischemic heart disease, strokes are ranked as the second most common cause of death [77]. Abnormalities that can be associated with DM such as hyperglycemia, hypertension, dyslipidemia, retinopathy, nephropathy, heart failure and atrial fibrillation predispose patients to strokes [39]. In addition, hyperinsulinemia is also a risk factor for strokes, but the reason behind this is still not clear [39]. There are two types of stroke: ischemic (arthrothrombic) and hemorrhagic [77]. Arthrothrombic strokes account for about 85% of acute strokes, while

hemorrhagic strokes account for the remaining 15% [78]. Diabetic patients are 2-3 times more prone to arthrothrombic strokes, and are equally prone to hemorrhagic strokes compared to the non-diabetic population [78]. Unfortunately, ischemic brain damage tends to be irreversible in diabetic patients leading to higher disability and mortality. The high rate of stroke recurrence also reduces the likelihood for long-term survival [78].

C. Peripheral Artery Disease

Peripheral artery disease involves the blockage of peripheral arteries (in lower extremities) as a result of atherosclerosis [9]. Intermittent claudication is the most common symptom, which involves pain, cramping, or aching in the leg (calves, thighs or buttocks) especially during physical activity which affects the patients' quality of life [9; 39]. This pain is usually relieved by stopping the physical activity. However, in severe cases of peripheral artery disease, the pain is also felt at rest and can be associated with tissue loss and gangrene; a condition called 'critical limb ischemia' [9]. Peripheral artery disease, together with peripheral neuropathy, can lead to a condition known as 'diabetic foot', which is characterized by foot infections and ulcerations and can result in amputation [132].

1.2. Heart and Cardiovascular System

The CV system is composed of a pump (heart) that pumps a fluid (blood containing cells and plasma) to a network of tubes (blood vessels) [251]. The CV system is responsible for three types of transportation processes in the body [251]. These include transporting oxygen, nutrients and water throughout the body, transporting carbon dioxide, metabolic wastes and heat to lungs, kidneys and skin, and transporting cellular materials from one cell to another [251].

1.2.1. Heart Anatomy and Structure

The heart, the central component of the CV system, is a hollow fibromuscular cone-shaped and fist-sized organ [188; 300]. It is located in the middle mediastinum in the thorax, where it lies on the diaphragm facing the sternum anteriorly and the 5^{th}-8^{th} thoracic vertebrae posteriorly [83; 300]. Two thirds of the heart are located in the left side of the midline, while the left one third is located in the right side of the midline [300]. The heart and origins of the large vessels are surrounded by a fibroserous sac called ‘the pericardium’ [83; 188]. The inferior part of the pericardium is firmly attached to the diaphragm and tied by a ligament to the sternum [83]. The pericardium acts as a protective layer for the heart and the origins of the large vessels coming out of the heart [188]. As shown in Figure 1-13, the heart is composed of four chambers including the upper right atrium, upper left atrium, lower right ventricle and lower left ventricle. There are also four valves in the heart including the tricuspid, mitral, pulmonary and aortic valves [188]. The anterior surface of the heart is mainly covered by the right ventricle, whereas the majority of

the posterior surface is covered by the left atrium and a small portion is covered by the right atrium and the inferior surface has both ventricles and some of the right atrium [83]. A fibrous skeleton having the shape of a figure eight provides support to the four chambers, which are attached to its central fibrous body, and to the four valves (cusps), which are attached to its extensions [300]. The right atrium has the openings for the superior vena cava on its top and the inferior vena cava at its base, where it receives the deoxygenated blood coming from the body [83]. It also has openings for the coronary sinus and the anterior cardiac vein, where it receives the deoxygenated blood coming from the heart [83]. Moreover, the atrio-ventricular (AV) and the sino-atrial (SA) nodes are located in the right atrium [188]. The left atrium is connected to the four valveless pulmonary veins posteriorly from which it receives the oxygenated blood coming from the lungs [188; 300]. The right ventricle receives the deoxygenated blood from the right atrium that passes through an opening guarded by the tricuspid valve [300]. The blood is then pumped by the right ventricle to the lungs through an opening guarded by the pulmonary valve [300]. The left ventricle receives the blood from the left atrium through the mitral opening, where the mitral valve is located, and pumps it to the aorta after passing through the aortic valve [300].

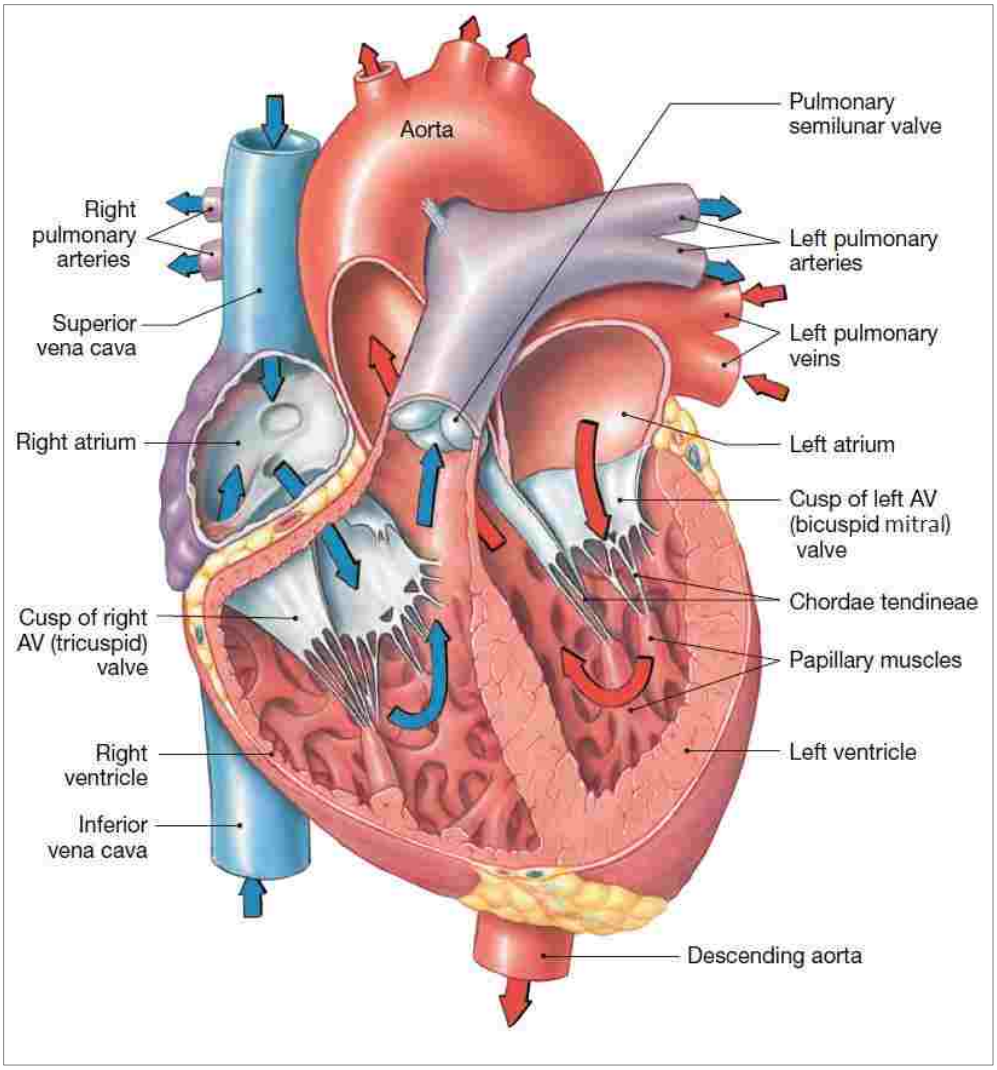

Figure 1-13: Structure of the heart and directions of blood flow

Blue arrows indicate deoxygenated blood and red arrows indicate oxygenated blood. Retrieved from [251]

1.2.1.1. Cardiac Blood Supply

The heart receives its share of the oxygenated blood and nutrients through the first two branches of the aorta; the right and left coronary arteries [188]. This occurs during cardiac muscle relaxation (diastole) [300]. Above each of the three cusps of the aortic valve, there is a dilatation (sinus) called the aortic sinus [188], making a

total of three sinuses: the right coronary aortic sinus (or anterior sinus), left coronary aortic sinus (or posterior sinus) and non-coronary sinus (or right posterior sinus) [300]. The right and left coronary arteries arise from the right and left coronary aortic sinuses, respectively [300]. The right coronary artery branches to several arteries which supply the right atrium, right ventricle and one third of the inter-ventricular septum. It also supplies the AV node in about 80% of individuals and the SA node in about 60% of individuals, while in the rest of individuals, the AV and SA nodes are supplied with blood through the circumflex artery, a branch of the left coronary artery [83; 188]. The left coronary artery branches to other arteries such as the circumflex artery and supplies the left atrium, left ventricle, inter-ventricular septum and the SA node (≈ 40% of individuals) and AV node (≈ 10% of individuals) [188]. Cardiac venous drainage goes from the different coronary veins to the coronary sinus vein which transmits the deoxygenated blood to the right atrium [188]. Trivial amounts (≈ 20-30%) of venous blood can drain into the four cardiac chambers through the Thebesian Veins [300].

1.2.1.2. Cardiac Nerve Supply

Sympathetic cardiac activity is supplied from nerve fibers coming out of the cervical and thoracic sympathetic ganglia, whereas parasympathetic cardiac activity originates from the vagus nerve [83]. Noradrenaline mediates sympathetic activities, during exercise for example, resulting in an increased cardiac contraction force (positive inotropism), contraction rate (positive chronotropism) and conduction rate of the electrical signal (positive dromotropism) from the AV node to the His-

Purkinjie System [301]. Sympathetic nerves are also responsible for cardiac pain conduction [83]. Vagal nerve effects predominate during rest resulting in decreased heart rate (HR) [301].

1.2.2. Heart Physiology

1.2.2.1. Cardiac Conduction System and the Cardiac Cycle

The heart, being the blood pump of the body, has two main characteristics: contractility and rhythmicity [301]. The cardiac conduction system is composed of specialized tissues that coordinate cardiac contraction resulting in synchronized contraction and relaxation. The tissues of the cardiac conduction system include the SA node, AV node, AV bundle of His, right and left branches of the AV bundle of His and Purkinjie fibers [188]. As shown in Figure 1-14, the cardiac action potential (AP) starts in the right atrium from the SA node, the cardiac pacemaker [33]. The electrical signal of the SA node propagates to both atria causing their contraction [301]. The signal propagation does not extend to the ventricles due to the presence of a fibrous tissue that acts as a barrier between the atria and ventricles [33]. Therefore, the AV node, at the base of the right atrium, conducts the electrical signal to the ventricles via the His-Purkinjie System [33]. There is a small time gap between the signal conduction in the atria and the bundle of His owing to the relatively slow conduction of the AV node [33; 301]. This gap provides enough time for the atria to eject the blood into the ventricles [33]. In some cases where the SA node fails to generate the AP or in atrial fibrillation where the atria are contracting very fast, the AV node acts as a back-up pacemaker generating and regulating the electrical signal

needed for the ventricular contraction [33]. After the signal reaches the bundle of His, in the inter-ventricular septum, from the AV node, it is transmitted to the right and left branches of the bundle of His and then to the Purkinjie fibers [188]. Purkinjie fibers then propagate the signal rapidly to both ventricles so that the ventricles contract simultaneously starting from the posterior side [33; 300].

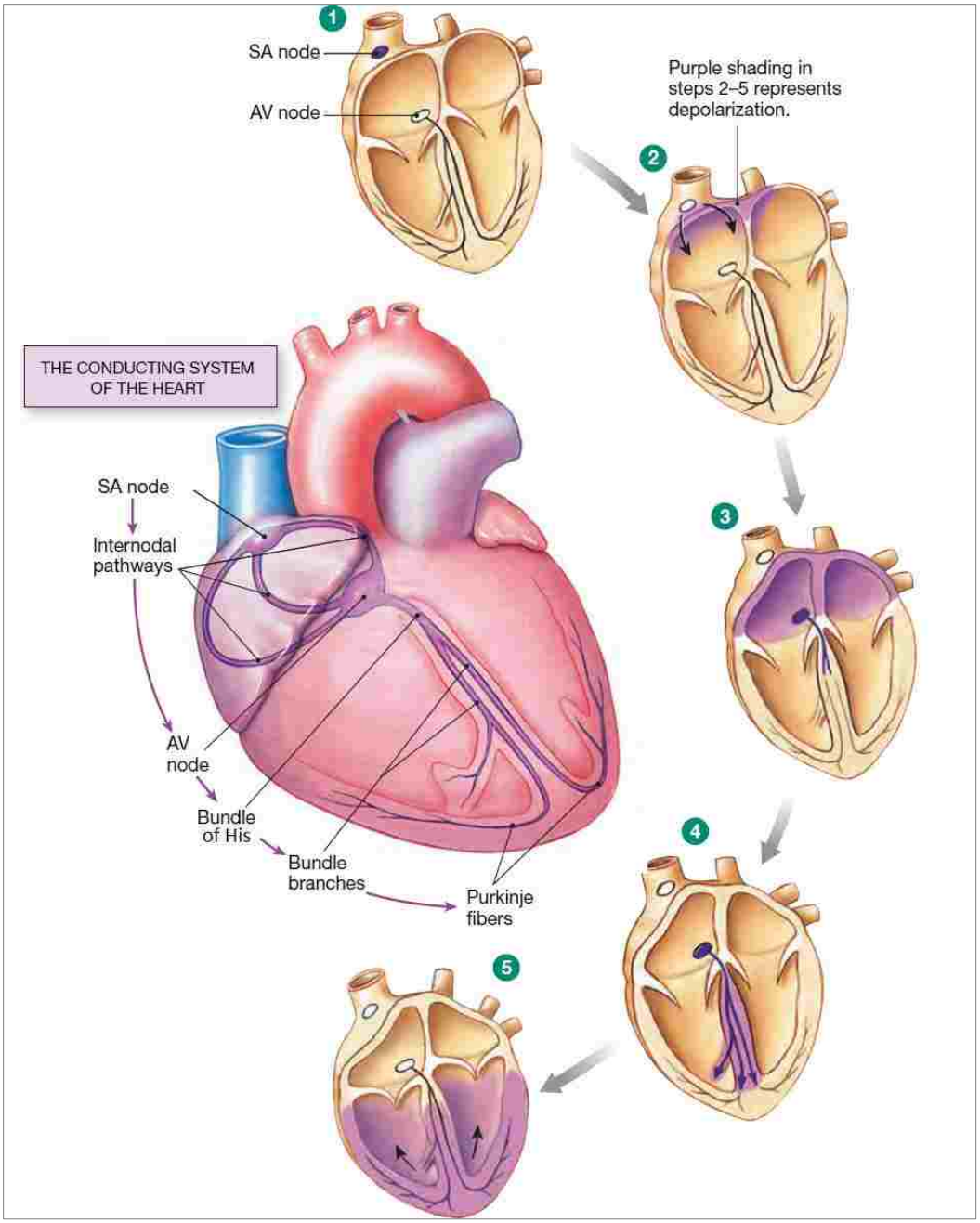

Figure 1-14: Cardiac conduction system and the spread of the electrical impulse

Adapted from [251]

1) The sino-atrial (SA) node depolarizes.
2) The atria contract and the depolarizing signal travels rapidly to the atrio-ventricular (AV) node.
3) The AV conducts the depolarizing signal slowly.
4) The signal propagates rapidly through the bundle of His and its branches.
5) Purkinjie fibers spread the signal to both of the ventricles.

1.2.2.2. Excitation-Contraction Coupling

Several cellular events take place during contraction and relaxation. The heart is a combination of different cell types including cardiomyocytes, fibroblasts, endocardial and endothelial cells and immune cells [207]. Although cardiomyocytes account for approximately 30% of cardiac cells, they compose the vast majority of the cardiac mass and volume [207]. Generation of the contractile force is the responsibility of cardiomyocytes pumping more than 7,000 liters of blood per day over a distance of 100,000 miles of blood vessels [248; 304]. There are two types of cardiomyocytes including pacemaker (cells of SA and AV nodes) and contractile (working) myocytes (Fig. 1-15) [223]. Each cardiomyocyte has intercalated disks at its blunted ends which connect it with neighboring myocytes (Fig. 1-15) [248]. The membranes of the intercalated disk are connected by three types of junctions: the gap junction, the fascia adherens and the desmosome [248]. The gap junctions are composed of a group of channels made up of a protein family called the connexins [207; 248]. Their function is to allow the rapid spread of AP between adjacent cells through ionic movement between the myocytes [207]. The fascia adherens and the desmosome connect the plasma membrane of adjacent cells [248].

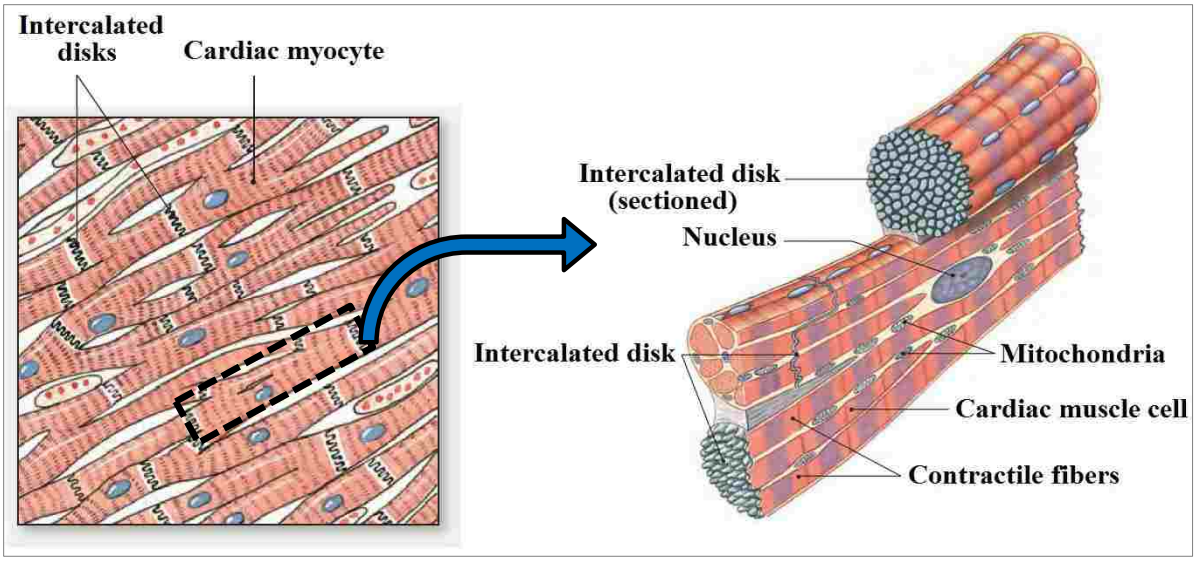

Figure 1-15: Structure of a contractile cardiomyocyte

Adapted from [251]

Cardiomyocytes are surrounded by the sacrolemmal membrane which has invaginations, called transverse tubules (T-tubules), extending deeply into the cell close to the sarcoplasmic reticulum (SR) (Fig. 1-16) [207; 248]. SR plays a pivotal role in cardiac contraction because it is the main Ca^{2+} store inside the cell [207]. Ca^{2+}, a ubiquitous second messenger ion, is the main regulator of contractility in the heart which directly activates myofilament contraction [26; 27]. The sarcomere, which is the fundamental contractile unit, is composed of contractile proteins, called myofibrils, and non-contractile proteins such as titin, myomesin and telethonin [207]. Contractile myofibrils consist of thin myofilaments called actin, thick myofilaments called myosin and regulatory proteins such as tropomyosin and troponins C, I and T [207]. Contractile myofibrils cause contraction in the presence of Ca^{2+} [207]. On the other hand, the non-contractile proteins play structural and signaling roles [207].

Excitation-contraction coupling (ECC) in contractile cardiomyocytes starts when an AP arrives causing activation and opening of the voltage-gated L-type Ca^{2+} channels, which allow Ca^{2+} to flow inside the myocyte [26]. In addition to the entry of Ca^{2+} through the L-type Ca^{2+} channels, Na^{+}/Ca^{2+} exchanger (NCX) contributes to Ca^{2+} entry but to a lesser extent [26]. The entered Ca^{2+} stimulates the release of Ca^{2+} from the intracellular stores in the SR through the ryanodine receptors (RyR) (ryanodine-sensitive intracellular Ca^{2+} channels), particularly type 2 RyR (RyR2) as they are the most abundant in cardiomyocytes [304]. The process of enhancing calcium release from the SR is termed calcium-induced calcium release (CICR) [304]. Entry and release of Ca^{2+} causes Ca^{2+} accumulation inside the myocyte resulting in elevation of the free intracellular Ca^{2+} concentration (Ca^{2+} sparks or spontaneous local Ca^{2+} transient) [27]. A Ca^{2+} spark indicates the synchronous release of Ca^{2+} from about 6-20 RyRs and Ca^{2+} sparks reach several thousand sparks during ECC in each cell [27; 44]. Ca^{2+} then binds to troponin C protein on the actin [207]. Without Ca^{2+}, troponin C prevents the interaction between actin and myosin but on binding to Ca^{2+}, the myosin projections interact with actin filaments producing contraction [207]. Myofilaments are stretched during the blood filling the heart, resulting in increased myofilament sensitivity to Ca^{2+} and stronger contraction [27]. Relaxation takes place due to the removal of the cytosolic Ca^{2+} resulting in dissociation of Ca^{2+} from troponin C, which then terminates the actin-myosin interaction to initiate relaxation [207]. Ca^{2+} is removed from the cytosol by four processes including sarco-endoplasmic reticulum Ca^{2+}-ATPase (SERCA) pump, which removes the majority of Ca^{2+}, followed by the NCX, while the minority ($\approx$ 1%)

is removed by the sarcolemmal Ca^{2+}-ATPase and mitochondrial uniporter (called the slow systems) [27; 301]. Under physiological conditions, the amount of Ca^{2+} entering the myocyte during contraction equals that leaving during relaxation [27]. A summary of the events taking place during ECC is shown in Figure 1-16.

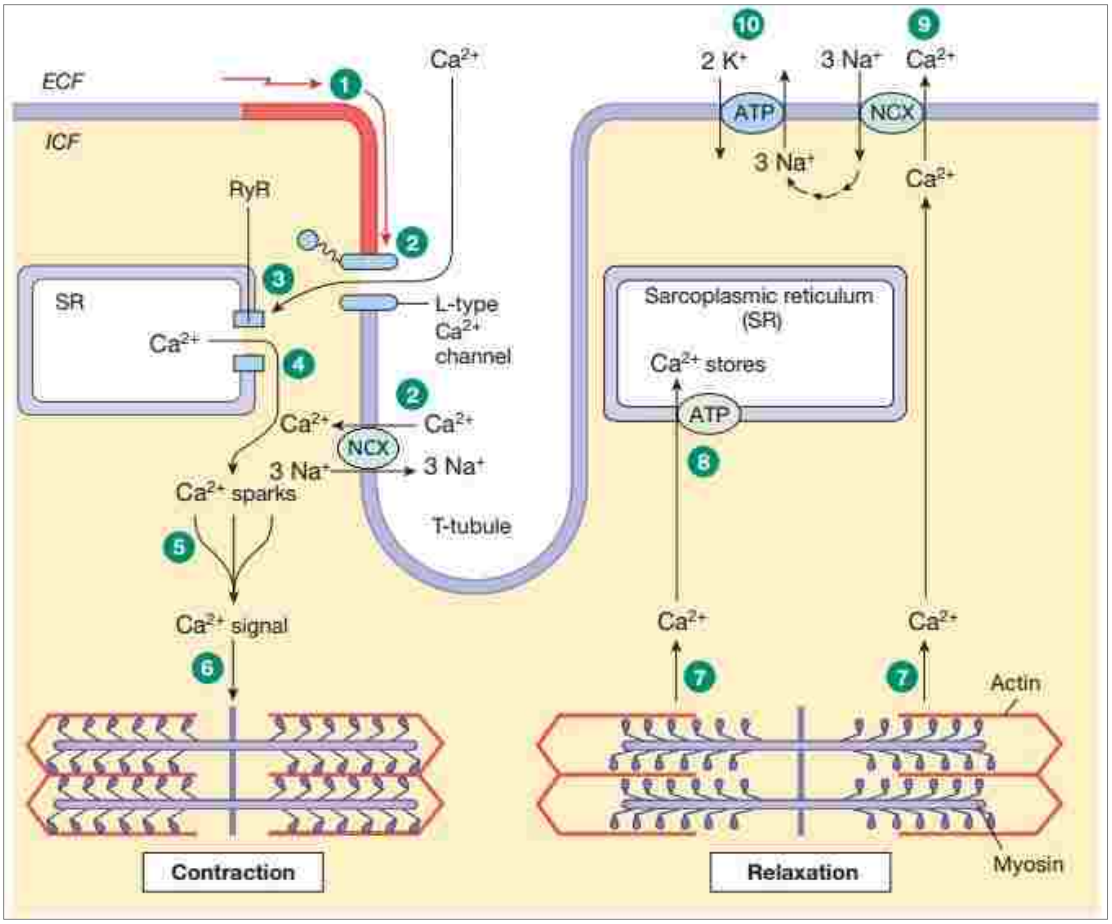

Figure 1-16: Excitation-contraction coupling (ECC) (left) and relaxation (right) in a cardiomyocyte

Adapted from [251]

1) Action potential arrives from an adjacent cell.
2) Ca^{2+} enters into the myocyte mainly through the voltage-gated L-type Ca^{2+} channels and to a smaller extent through Na^{+}/Ca^{2+} exchanger (NCX).
3) The small entry of Ca^{2+} triggers Ca^{2+} release from the sarcoplasmic reticulum (SR) through the ryanodine receptors (RyRs).
4) SR Ca^{2+} release causes Ca^{2+} sparks.
5) Ca^{2+} sparks create a Ca^{2+} signal.
6) Ca^{2+} ions associate with troponin proteins resulting in myocyte contraction.
7) Ca^{2+} ions dissociate from troponin proteins resulting in myocyte relaxation.
8) Some Ca^{2+} is taken up again by the SR.
9) Rest of the Ca^{2+} flows out of the myocyte by NCX in exchange for Na^{+}.
10) Na^{+}/K^{+} ATPase maintains the Na^{+} gradient.

1.2.2.3. Cardiac Action Potential and Ion Movement

Cardiac AP differs between contractile and pacemaker myocytes. Contractile myocytes have a relatively long AP with a plateau (Fig. 1-17A), while pacemaker myocytes have a shorter AP with no plateau (Fig. 1-17B) [223]. In a contractile myocyte, the AP is described by 5 phases (0, 1, 2, 3 and 4) that last for a duration of approximately 300 ms [223]. Phase 4 represents the resting potential which is ≈ -90 mV [108]. AP arrival begins a series of ionic movements in and out of the myocyte starting with phase 0 (rapid depolarization) which involves an influx of Na^+ through fast voltage-gated Na^+ channels causing generation of the AP upstroke by depolarizing the membrane from -90 mV to +10 mV [211; 223]. Phase 1 (rapid repolarization) involves inactivation of Na^+ influx and activation of K^+ efflux leading to partial repolarization [211; 223]. During phase 2 (plateau), Ca^{2+} enters the myocytes mainly through voltage-gated L-type Ca^{2+} (L stands for Long opening) channels maintaining depolarization causing a plateau in the AP [223]. Towards the end of phase 2, Ca^{2+} influx is reduced and Na^+ influx starts through NCX (3 Na^+: 1 Ca^{2+}) to maintain depolarization [223]. Phase 3 (rapid repolarization) starts after inactivation of Ca^{2+} channels in which K^+ efflux causes rapid repolarization and the membrane potential returns to phase 4 [223]. To summarize, the influx of Na^+ and Ca^{2+} (inward currents) results in depolarization, while the efflux of K^+ (outward current) results in repolarization [211]. In pacemaker myocytes, the resting membrane potential is ≈ -50 to -65 mV which is more positive than that of contractile myocytes [108]. The AP of pacemaker myocytes consists of only three phases equivalent to phases 0, 3 and 4, in which it starts with phase 4 with slow influx of Ca^{2+} through the

T-type Ca^{2+} (T stands for Transient) channels and influx of Na^{+} through NCX and I_f channels [223; 251]. I_f channels allow the flow of a current known as pacemaker or funny current [108; 251]. They permit the influx of Na^{+} and efflux of K^{+}, where at negative membrane potential, they open and the Na^{+} influx predominates over the K^{+} efflux and they gradually close as the membrane gets more positive [251]. Depolarization (phase 0) occurs, after the activation threshold is reached, through the L-type Ca^{2+} channels allowing influx of Ca^{2+} and repolarization (phase 3) occurs by K^{+} efflux [223].

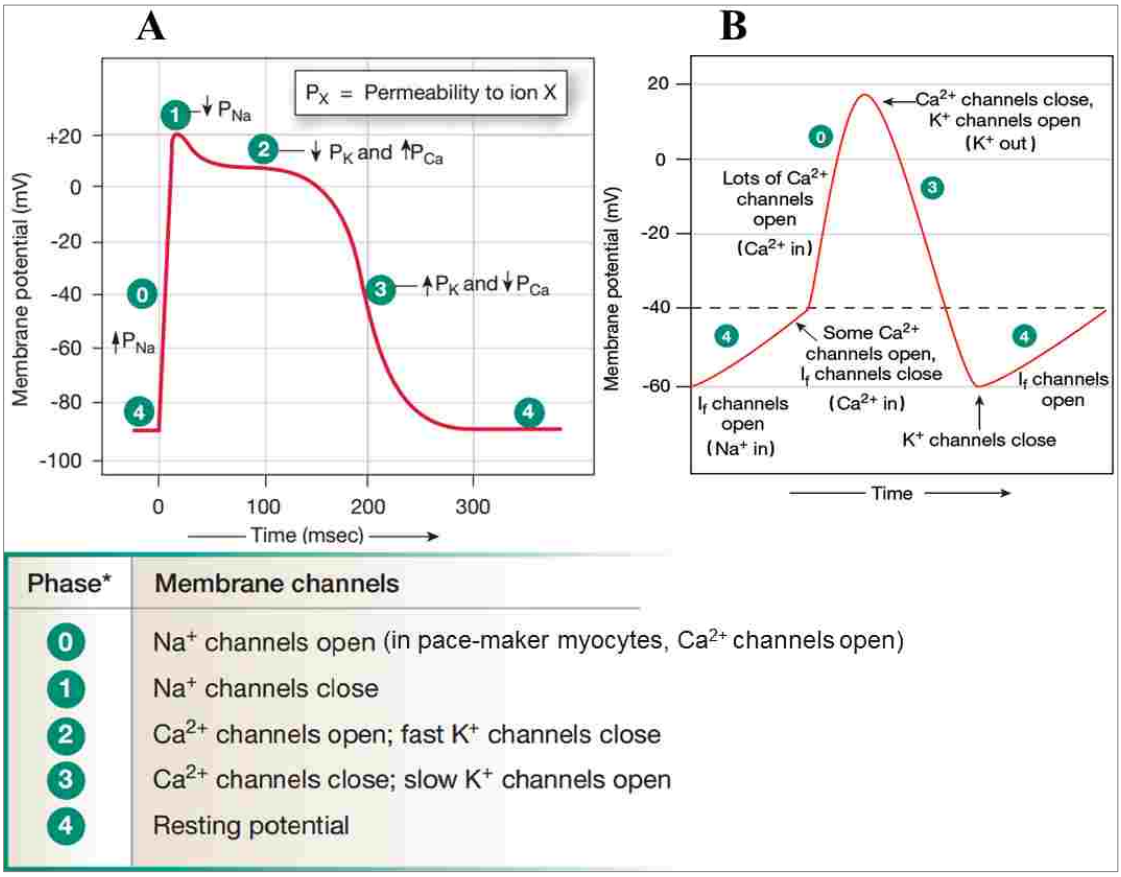

Phase*	Membrane channels
0	Na^{+} channels open (in pace-maker myocytes, Ca^{2+} channels open)
1	Na^{+} channels close
2	Ca^{2+} channels open; fast K^{+} channels close
3	Ca^{2+} channels close; slow K^{+} channels open
4	Resting potential

Figure 1-17: Cardiac action potential and ionic movement in **(A)** contractile and **(B)** pacemaker myocytes

Adapted from [251]

I_f: pacemaker current

1.3. Glucose Transporters

Glucose is the main fuel that supplies all eukaryotic cells with energy, however, glucose is a polar molecule that cannot cross the lipophilic cellular membrane to enter the cell [22]. Therefore, entry and exit of glucose and other sugars into and from the cell are mediated by specialized glucose transporters. Current evidence suggests that there are three glucose transporter families expressed in the eukaryotic cells, which are encoded by the solute carrier (SLC) genes [57; 245]. These include the SLC2A family encoding for facilitative glucose transporters (GLUTs), SLC5A family encoding for sodium/glucose co-transporters (SGLTs) and SLC50 family encoding for sugar efflux transporters (SWEETs) [57; 245].

1.3.1. Facilitative Glucose Transporters

The GLUT family is a part of the Major Facilitator Superfamily (MFS) [277]. To date, 14 protein members (isoforms), including GLUT1-12,14 and proton (H^+)-coupled myo-inositol symporter (HMIT also called GLUT13), and 4 pseudogenes have been discovered in the GLUT family [205]. GLUTs are transmembrane proteins predicted to have 12 spanning transmembrane domains [277]. They are classified according to the similarity of their amino acid sequence into three classes including class 1 comprising GLUT1-4,14, class 2 comprising GLUT5,7,9 and 11, and class 3 comprising GLUT6,8,10,12 and HMIT [205]. Their main function is to transfer glucose and other substrates, such as fructose, myo-inositol and urate, across the cell membrane either from the blood to the cell cytosol or vice versa [204; 277]. The GLUT isoforms differ in their affinities to glucose, substrates (other than glucose)

and tissue distribution (Table 1-2). The wide abundance of different isoforms for GLUTs is suggested to be due to the importance of glucose as a source of energy for the cells which requires the existence of several types of transporters exhibiting different kinetic and regulatory properties, and cell-type specific distribution [205].

GLUT Isoform	Substrate(s)	Tissue Distribution
GLUT1	Glucose, galactose, mannose, glucosamine	Erythrocytes, brain, blood–brain barrier, blood-tissue barrier, many fetal tissues
GLUT2	Glucose, fructose, galactose, mannose, glucosamine	Liver, islet of Langerhans, intestine, kidney, brain
GLUT3	Glucose, galactose, mannose, maltose, xylose, dehydroascorbic acid	Brain (neurons), testis
GLUT4	Glucose, galactose, glucosamaine, dehydroascorbic acid	Adipose tissue (white and brown), heart, skeletal muscle
GLUT5	Fructose	Small intestine, kidney
GLUT6	Glucose	Brain, spleen, leucocytes
GLUT7	Glucose, fructose	Small intestine, colon, testis, prostate
GLUT8	Glucose, fructose, galactose	Testis, brain, adrenal gland, liver, spleen, brown adipose tissue, lung
GLUT9	Urate	Kidney, liver, small intestine, placenta, lung, leucocytes
GLUT10	Glucose, galactose	Heart, lung, brain, liver, skeletal muscle, pancreas, placenta, Kidney
GLUT11	Glucose, fructose	Heart, skeletal muscle
GLUT12	Glucose	Heart, prostate, skeletal muscle, placenta
HMIT	Myo-inositol	Brain, adipose tissue
GLUT14		Testis

Table 1-2: Substrates and tissue distribution of facilitative glucose transporters

Adapted from [205; 323]

GLUT: facilitative glucose transporter; **HMIT:** proton (H^+)/myo-inositol co-transporter

1.3.1.1. Mechanism of Glucose Transport by Facilitative Glucose Transporters

Glucose is transported passively by GLUTs by facilitative diffusion and no energy is required. This process involves two steps starting when glucose binds to GLUT protein on the cell membrane forming a GLUT-glucose complex (Fig. 1-18) [55]. The second step involves inverting the direction of the GLUT-glucose complex with respect to the membrane allowing the glucose to be released on the other side of the membrane (Fig. 1-18) [55]. The inversion of GLUT protein is then reversed to start another transport cycle [55]. All GLUTs (GLUT1-12,14) are bidirectional facilitative glucose uniporters which transport glucose via an energy-independent facilitative diffusion along its concentration gradient across the cell membrane [205]. On the other hand, HMIT is a pH-dependent myo-inositol specific symporter which does not transport glucose [205; 323].

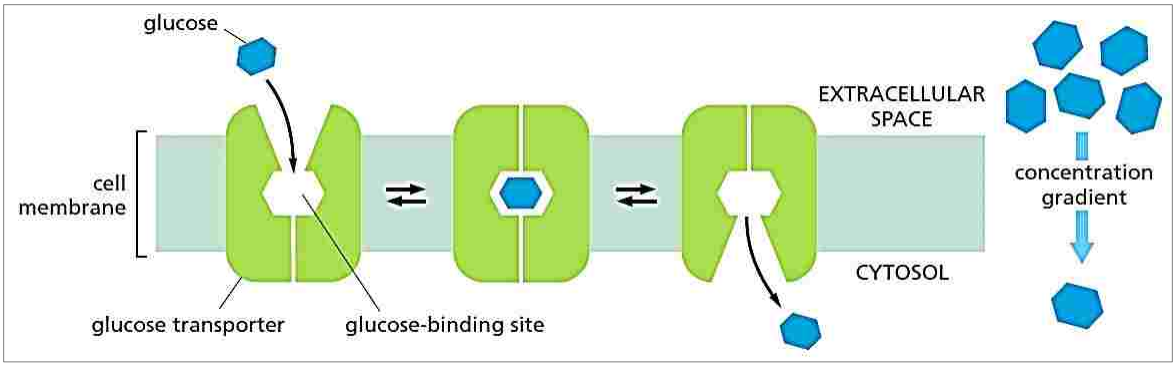

Figure 1-18: Mechanism of glucose transport by facilitative glucose transporters Retrieved from [7]

1.3.2. Sodium/Glucose Co-transporters

To date, 12 members (isoforms) of the SGLT family have been identified including SGLT1-5, SMIT1, 2 (sodium/myo-inositol co-transporters), SMCT1, 2 (sodium/monocarboxylate co-transporters), SMVT (sodium/multivitamin co-transporter), NIS (sodium/iodide symporter) and CHT (sodium/choline co-transporter) [310]. They belong to a superfamily known as the Sodium/Substrate Symporter Family (SSSF) [142]. Table 1-3 shows all the members of this family with their different substrates and tissue distributions. Since SGLT1 and SGLT2 are the most extensively studied members of this family, they are discussed in more detail in this section.

SGLT Isoform	Substrate(s)	Tissue Distribution
SGLT1	Glucose, galactose	Small Intestine, heart, trachea, kidney, brain, testes, prostrate
SGLT2	Glucose	Kidney, brain, liver, heart, thyroid gland, salivary glands
SMIT1	Myo-inositol	Brain, heart, kidney, lung, pancreas, placenta, skeletal muscle
SGLT3	Na^+	Small Intestine (cholinergic neurons), skeletal muscle, kidney, uterus, testis
NIS	I^-	Thyroid gland, lactating breast, colon, stomach, ovary
SMVT	Biotin, lipoate panthothenate, I^-	Brain, heart, kidney, lung, placenta
CHT	Choline	Spinal cord, medulla
SMCT1	Short chain fatty acids	Small Intestine, kidney, brain, retina, skeletal muscle
SGLT4	Mannose, fructose, glucose	Kidney, small intestine, brain, liver, heart, uterus, lung
SGLT5	Mannose, fructose, glucose	Kidney cortex
SMIT2	Myoinositol, chiro-inositol	Thyroid gland, brain, heart, skeletal muscle, spleen, liver, lung
SMCT2	Short chain fatty acids	Intestine, brain, retina, skeletal muscle

Table 1-3: Substrates and tissue distribution of sodium/glucose co-transporters

Adapted from [25; 310]

Isoforms are arranged according to the ascending order of the number given to their genes (not shown)

SGLT: sodium/glucose co-transporter; **SMIT:** sodium/myo-inositol co-transporter; **SMCT:** sodium/monocarboxylate co-transporter; **SMVT:** sodium/multivitamin co-transporter; **NIS:** sodium/iodide symporter; **CHT:** sodium/choline co-transporter

1.3.2.1. Sodium/Glucose Co-transporters 1 and 2

As shown in Figure 1-19, after a dietary intake of carbohydrates (glucose), glucose absorption in the small intestine to the bloodstream is carried out by SGLT1 [270]. Glucose then circulates in the blood and is distributed to different body tissues including the kidneys where the blood is filtered and glucose is reabsorbed [270]. Reabsorption is mediated by SGLT2, which is located mainly in S1 segment of the proximal convoluted tubule (PCT) and reabsorbs the majority of glucose (≈ 90%), and SGLT1, which is located in S2/S3 of the PCT and reabsorbs the remaining glucose [56]. As shown in Table 1-3, both SGLT1 and SGLT2 are expressed in different tissues such as the heart. However owing to their essential roles in glucose absorption and reabsorption, SGLT1 and SGLT2 have their highest expression levels in the small intestine and kidneys, respectively [327]. SGLT1 is a low-capacity high-affinity co-transporter, transporting Na^+ and glucose with a 2:1 stoichiometry, whereas SGLT2 is a high-capacity low-affinity co-transporter, transporting Na^+ and glucose with a 1:1 stoichiometry [270].

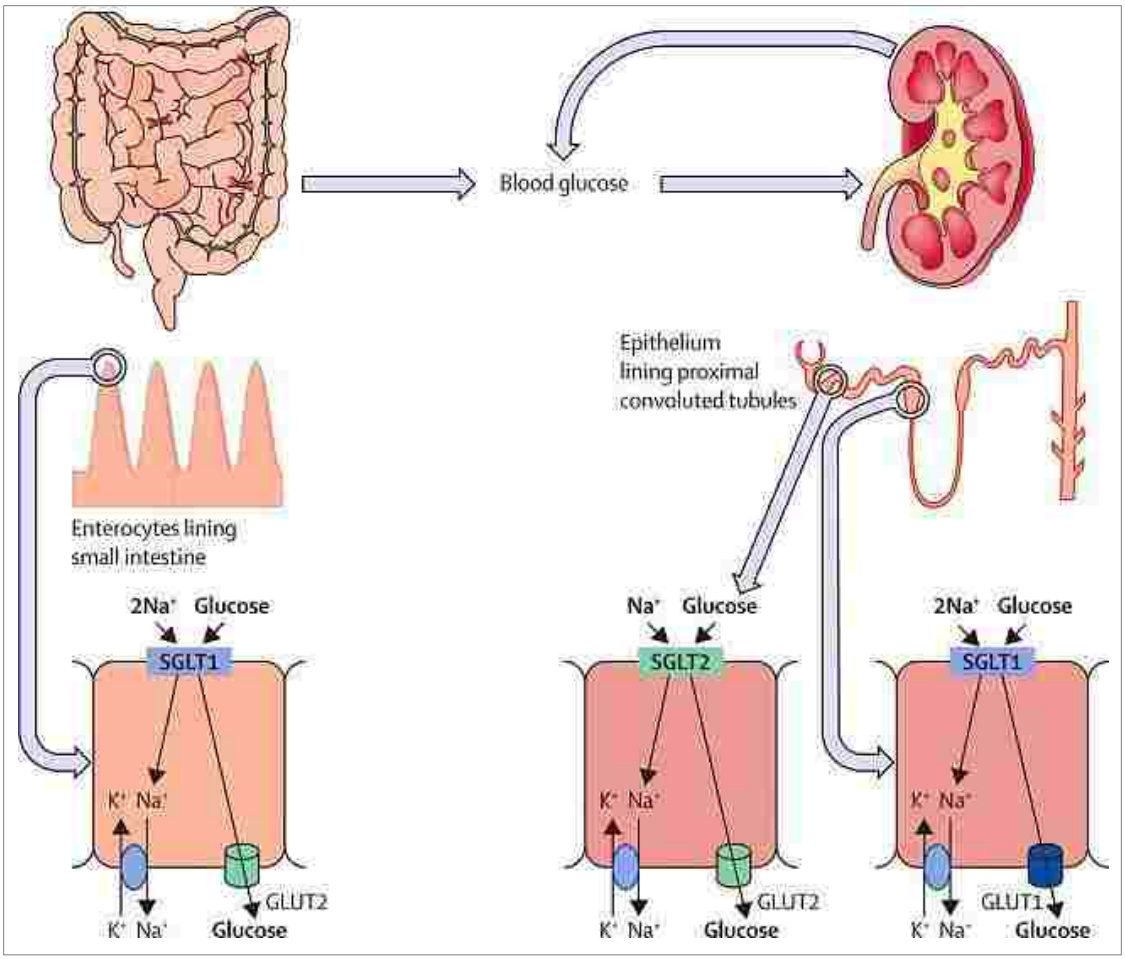

Figure 1-19: The role of sodium/glucose co-transporters 1 and 2 in glucose absorption (left) and reabsorption (right)

Retrieved from [270]

GLUT: facilitative glucose transporter; **SGLT:** sodium/glucose co-transporter

1.3.2.2. Mechanism of Transporting Glucose

SGLT-mediated glucose transport across the cell membrane against its concentration gradient is a process that requires energy (adenosine triphosphate; ATP) [240]. However, SGLTs do not directly consume ATP rather they depend on another transporter that directly consumes ATP which is Na^+/K^+ ATPase [240]. That is why glucose transport by SGLT is called secondary active transport [303], while

Na^+ transport by Na^+/K^+ ATPase is primary active transport. As shown in Figure 1-20, SGLT is located in the cell side facing the lumen of the organ (intestine or kidney) while, Na^+/K^+ ATPase is located on the other side of the cell facing the interstitial fluid and bloodstream. Na^+/K^+ ATPase constantly expels Na^+ into the bloodstream which makes the intracellular concentration of Na^+ relatively lower than in the lumen. On transporting glucose from the lumen to the cell, Na^+ moves along its electrochemical potential gradient driving glucose transport with it (against its concentration gradient) [240]. Then Na^+ is removed from the cell to the blood by Na^+/K^+ ATPase and glucose accumulation inside the cell allows it to passively move to the blood through GLUTs [51].

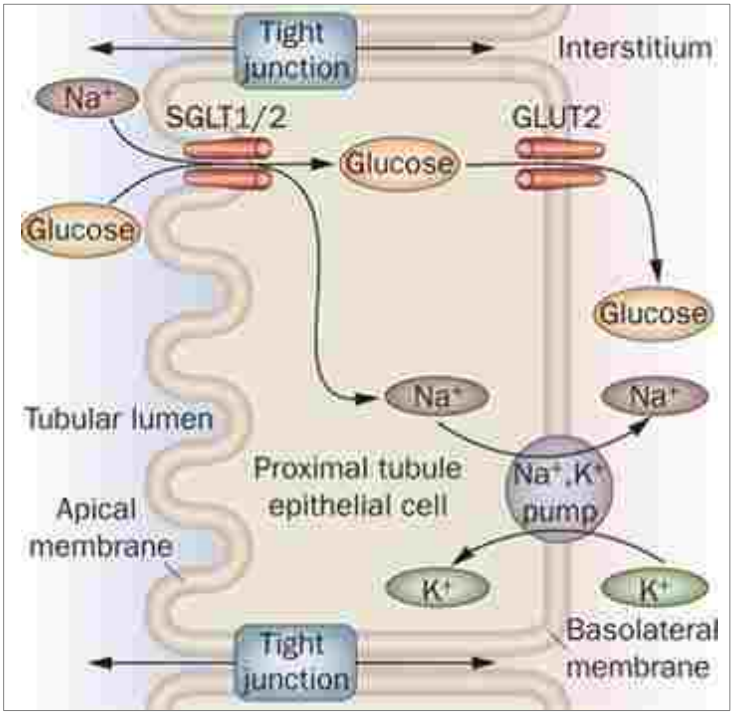

Figure 1-20: Mechanism of glucose transport by sodium/glucose co-transporters Retrieved from [191]

GLUT: facilitative glucose transporter; **SGLT:** sodium/glucose co-transporter

1.3.3. Sugar Efflux Transporters

SWEETs are sugar uniporters which direct glucose out of the cell (efflux) [57]. They were recently discovered in 2010 by Chen and colleagues in Arabidoposis plant genes [57]. SWEETs have been found to be expressed by humans, plants, fungi, bacteria and others [57; 311; 312]. Humans express only one SWEET protein (SWEET1), which is hypothesized to be responsible for glucose efflux in hepatocytes and enterocytes in pathophysiological conditions involving impaired function of GLUT2 such as Fanconi-Bickel Syndrome [57; 242; 261]. In plants, SWEETs have essential functions such as phloem loading and nectar secretion [58; 177]. Pathogenic bacteria and fungi were found to increase expression of SWEET genes in plants, which is thought to be the mechanism by which these organisms get nutrients from their host cells [57].

1.3.4. Glucose Transport in Cardiomyocytes

To maintain continuous contraction, the heart has to be constantly supplied with energy and oxygen. About 3.5-5 kg of ATP are produced and consumed by the human heart daily [28]. Cardiomyocytes are not only dependent on glucose for their energy source, but they can also acquire their fuel from FFA, lactate and ketone bodies [201]. At rest, under physiological conditions, glucose accounts for only about 25% of cardiac energy while FAA contribute the major share [200]. This is attributed to the fact that the process of FFA oxidation leads to inhibiting glucose uptake and catabolism [28]. However, during exercise and under some pathological conditions such as hyperthyroidism, ischemia, hypertrophy and congestive heart failure,

utilization of glucose by cardiomyocytes becomes more significant [1]. Under physiological conditions, glucose intracellular concentration is low, which facilitates the transport of glucose from outside into the myocyte along its concentration gradient [316]. The GLUT isoforms GLUT1 and GLUT4 play the major role in glucose absorption in cardiomyocytes [200]. Fetal and postnatal cardiomyocytes are mainly dependent on GLUT1 while, adult cardiomyocytes are mainly dependent on GLUT4 [200]. GLUT4 has a higher affinity to glucose and is insulin-sensitive, on the other hand, GLUT1 has a lower affinity to glucose and is insulin-insensitive [200; 303]. In adult cardiomyocytes, the predominance of GLUT4 function is shifted to GLUT1 in pathophysiological conditions such as post-ischemic reperfusion, post-infarction heart failure and pressure overload hypertrophy [200]. It has been shown previously that cardiac hypertrophy is associated with an increased glucose uptake due to the increased expression of GLUT1 [1]. Moreover, it has been found that cardiac GLUT4 knockout mice exhibited about a 3-fold increase in GLUT1 expression and glucose uptake as well as abolished insulin-dependent glucose uptake which is mediated by GLUT4 [1].

Under physiological conditions, GLUT4 is located in the intracellular compartments when no glucose is being transported into the cell [200]. Insulin stimulus, which indicates the presence of a relatively high BGL, triggers the translocation of GLUT4 from its intracellular compartments to the surface of the cell membrane to stimulate the uptake of glucose into the myocyte [200]. It should be noted that insulin presence swaps the energy substrate preference of the cardiomyocyte from FFA to glucose [28]. Obesity and accumulation of FFA and their

metabolites in the cardiomyocytes causes lipotoxicity as well as insulin resistance because FFA metabolites inhibit insulin signaling [104]. Studies in insulin-resistant and T2DM animal models have demonstrated increased expression and availability on the membrane surface of the FFA transporter protein leading to increased FFA transport, which exceeds the cellular capacity to oxidize, thus resulting in their accumulation [104]. The consequent abolished insulin signaling prevents stimulation of GLUT4 translocation and impaired cellular glucose uptake [104].

1.4. Sodium/Glucose Co-transporter Inhibitors

Owing to the central function of SGLT1 and SGLT2 in glucose homeostasis by controlling glucose absorption and reabsorption, respectively, studies were carried out to target them as a novel way to treat DM. The first SGLT inhibitor discovered was Phlorizin (PHLOR) which was isolated from apple tree bark by French chemists in 1835 [80]. In the late 1980s, experiments by Rossetti and colleagues, in partially pancreatectomized rats, showed normalized insulin sensitivity, increased urinary exertion and improved BGL in PHLOR-treated rats compared to untreated rats [236]. SGLT inhibitors can be subclassified into three subclasses, based on their SGLT isoform selectivity, including non-selective SGLT1 and 2, selective SGLT1 and selective SGLT2 inhibitors. To date, the subclass of non-selective SGLT1 and 2 inhibitors comprises two compounds including PHLOR [80] and LX4211 [319]. The subclass of selective SGLT1 inhibitors includes Quercetin-3-O-glucoside (QUER-3-G) [2; 54], KGA-2727 [250] and KGA-3235 [162]. The majority of the known SGLT inhibitors belong to the subclass of selective SGLT2 inhibitors, such as Dapagliflozin

(DAPA) [195], canagliflozin [213], empagliflozin [109], ipragliflozin [246], topogliflozin [265] and others.

1.4.1. Mechanism of Action of Sodium/Glucose Co-transporter Inhibitors

The mechanism of SGLT inhibitors is unique compared to the mechanisms of other anti-diabetic medications (Fig. 1-21) because it targets insulin-independent pathways to reduce BGL.

Since the brush-border membrane of the small intestine exhibits the highest expression of SGLT1 protein, it is the main site of action for SGLT1 inhibitors. Inhibiting SGLT1 protein would result in impairment of intestinal absorption of dietary glucose, which was shown to improve post-prandial hyperglycemia in STZ-induced diabetic rats after OGTT [250]. Mutations causing dysfunction of SGLT1 protein are associated with glucose-galactose malabsorption leading to severe diarrhea in neonates which might be fatal [309]. Despite the concerns about glucose-galactose malabsorption resulting from inhibiting SGLT1 protein by non-selective and selective SGLT1 inhibitors, it was found that, after gastric bypass surgery and after an intake of dietary-resistant starch, increased intestinal glucose can improve glucose tolerance without gastrointestinal side effects [319].

On the other hand, SGLT2 inhibitors obviously target SGLT2 protein in the renal PCT where it is highly expressed. This causes inhibition of glucose reabsorption causing glycosuria and decreased BGL. Mutations of SGLT2 protein result in familial renal glycosuria which is associated with glucose excretion despite the absence of DM as indicated by normal plasma glucose and plasma insulin levels [310].

Unlike other anti-diabetic drugs, SGLT inhibitors are unlikely to cause hypoglycemia for two reasons; they are insulin-independent meaning that they do not mediate insulin production, and they do not interfere with hypoglycemia-induced glucose production [288].

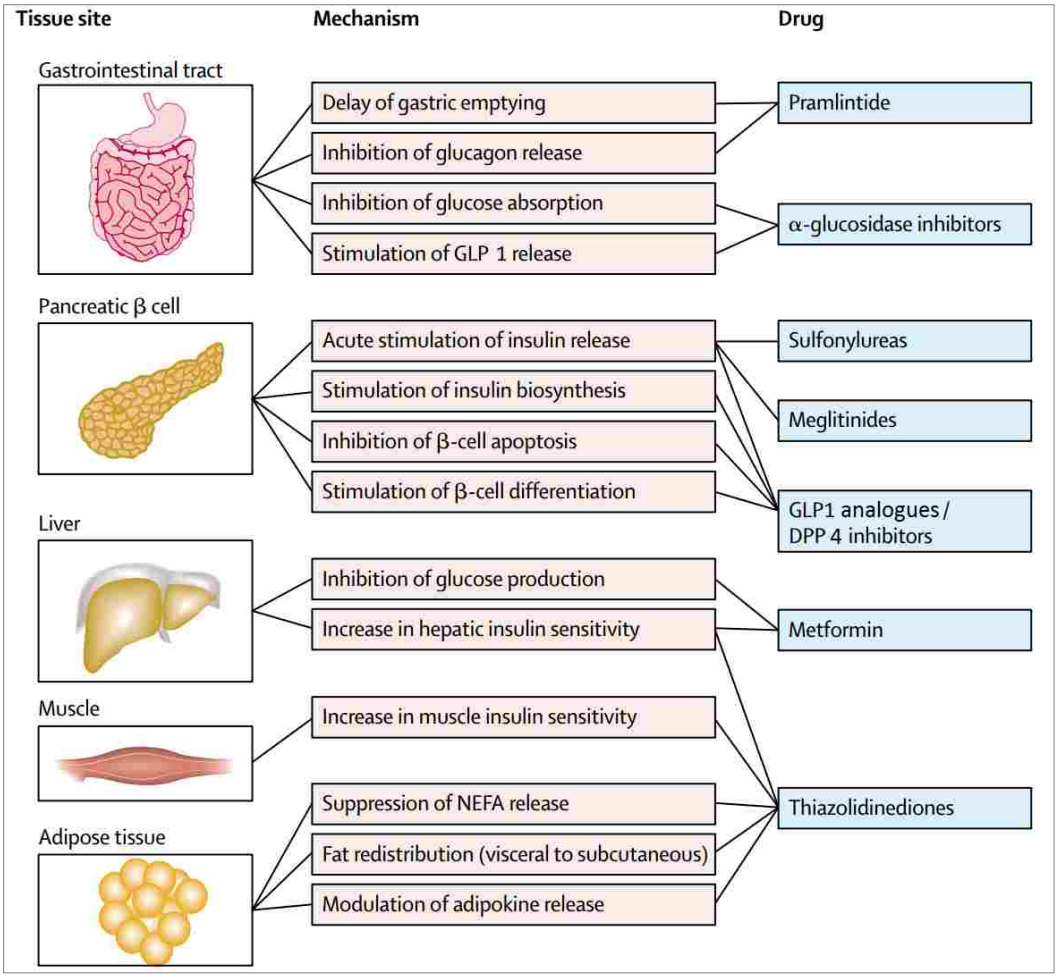

Figure 1-21: Mechanisms of pharmacological treatment of diabetes mellitus according to site of action

Adapted from [262]

GLP 1: glucagon-like peptide 1; **DPP 4:** dipeptidyl peptidase 4; **NEFA:** non-esterified fatty acid

1.4.2. Phlorizin

PHLOR (also known as phloretin 2′-O-glucoside, phloridzin, phlorrhizin, phlorhizin or phlorizoside [17]) is a competitive non-selective inhibitor of SGLT1 and 2 proteins [80]. It is a natural phloretin glycoside that belongs to the chalcone class [141]. Phloretin glycosides are found in several plants such as apples (leaves, bark, seeds and roots), strawberry fruits and sweet tea [141]. Although it was the first SGLT inhibitor discovered, it was not developed into a medication itself, due to its low oral bioavailability, rather it was used as a parent molecule for developing other SGLT inhibitors [280]. However, several animal studies showed that oral [272] and subcutaneous (s.c.) PHLOR improved hyperglycemia [35; 144; 156; 235; 236].

1.4.3. Quercetin-3-O-Glucoside

QUER-3-G (also known as Quercetin-3-O-β-D-glucopyranoside, Isoquercitrin [289] and Isoquercetin [174]) is a rare flavonol glycoside that is found in several plants such as apples, tea, onions, cratagus, pistachio nuts, Saint John’s wort in addition to many fruits, vegetables and cereals [228; 289; 294]. It has anti-diabetic abilities due to selective inhibition of SGLT1 and inhibition of alpha-glucosidase [2; 174; 219]. In addition to anti-diabetic activity, it also possesses anti-oxidant, anti-hypertensive, anti-cancer, anti-influenza, anti-proliferative, anti-inflammatory, cardioprotective, anti-allergic and diuretic properties [289; 294].

1.4.4. Dapagliflozin

DAPA (trade name: Farxiga® in the United States; Forxiga® in Europe, Australia and Japan) has been approved by the American Food and Drug Administration (FDA) [90], European Medicine Agency (EMA) [85], the Australian Therapeutic Goods Administration (TGA) [276] and the Japanese Ministry of Health, Labor and Welfare (MHLW) [13] for treatment of T2DM. It is the second FDA approved SGLT2 inhibitor after canagliflozin [282]. A new formulation combining DAPA and metformin has also been approved by EMA (trade name: XIGDUO®) for T2DM patients [15].

DAPA is the first selective SGLT 2 to be developed [195]. DAPA selectivity for SGLT2 protein exceeds that for SGLT1 protein by approximately 1200 times [88]. It is an orally administered medication that induces dose-proportional plasma concentration and dose-proportional glycosuria [164]. DAPA reaches its peak concentration after 2 hours [151]. The oral bioavailability and pharmacokinetic properties of DAPA are not affected by fat rich meals [88]. DAPA is extensively metabolized in the liver and kidney to its inactive metabolite dapagliflozin 3-O-glucuronide which is mainly eliminated by the kidneys [151]

Despite being the first member of its class to be developed, it was not the first to be approved by the FDA [282]. Clinical studies revealed some side effects such as mild or moderate genitourinary tract infections that were either self-limiting or respondent to treatment [158] and a 2-fold increase in genital infections that were also respondent to treatment [88]. There were also cases reported of urinary bladder and breast cancer [158].

There are still six post-marketing studies required by the FDA for evaluating DAPA effects on the CV outcomes, risk of bladder cancer, and pharmacokinetics, efficacy and safety in pediatric and pregnant patients [90]. The CV safety and outcomes of DAPA are being evaluated by a large clinical trial called 'DECLARE-TIMI58', which is expected to be completed in April 2019 [14].

Chapter 2: Hypothesis, Aims and Objectives

Owing to the progressive nature of DM which results in the development of serious complications, ongoing research is continuously working on finding new safe anti-diabetic therapies that would properly control DM and prevent the development of subsequent complications. One of the recently developed classes of anti-diabetic medications is SGLT inhibitors. In this study, the effects of PHLOR, a non-selective SGLT1 and 2 inhibitor, QUER-3-G, a selective SGLT1 inhibitor, and DAPA, a selective SGLT2 inhibitor, on contractility and intracellular Ca^{2+} were investigated in ventricular myocytes from streptozotocin (STZ)-induced diabetic rats.

It is important to study new therapeutic natural compounds that can be developed later, if proven to be safe. PHLOR was studied because it is the parent from which developing and commercially available SGLT inhibitors, such as DAPA, were derived. Non-selective SGLT1and 2 inhibitors are also being developed as potential anti-diabetic medications. Since there are studies in progress testing selective SGLT1 inhibitors including KGA-2727 and KGA-3235, this might pave the way for other naturally found selective SGLT1 inhibitors, like QUER-3-G, to be considered in the future as candidates for DM treatment. DAPA is the second FDA approved selective SGLT 2 inhibitor and was recently released onto the market. There is not enough data about the effects of DAPA on the CV system, and this evaluation is crucial for its safety profile characterization and benefit-risk assessment. Thus, this study contributes to the post-marketing evaluation of DAPA.

2.1. Hypothesis

Due to the lack of data available on the effects of SGLT inhibitors on the diabetic heart, we hypothesized that these anti-diabetic compounds may, in some way, affect the cardiac function, or may have side effects on the heart. Considering that SGLT proteins utilize Na^+, there is a strong possibility that SGLTs interact with NCX, which in turn interferes with Ca^{2+} signaling. Therefore, inhibiting SGLTs may directly or indirectly alter Ca^{2+} mobilization in cardiac myocytes.

2.2. Aims and Objectives

Generally, this project has two main objectives. One is studying the safety of natural anti-diabetic compounds such as PHLOR and QUER-3-G, and the other is studying a chemically manufactured and commercially available anti-diabetic medication such as DAPA. Studying three compounds each from a different subclass of SGLT inhibitors allows comparison of the common and different effects of the three subclasses.

The aim of this study was to investigate the following:

1) The effects of SGLT inhibitors PHLOR, QUER-3-G and DAPA on the amplitude and time course of ventricular myocyte shortening.

2) The effects of these SGLT inhibitors on the amplitude and time course of ventricular myocyte intracellular Ca^{2+}.

3) The effects of these SGLT inhibitors on ventricular myocyte myofilament sensitivity to Ca^{2+}.

4) The effects of these SGLT inhibitors on ventricular myocyte SR Ca^{2+} transport.

5) The long-term effects of DAPA on the amplitude and time course of ventricular myocyte shortening.

6) The effects of DAPA on ventricular myocyte L-type Ca^{2+} Current.

The experiments in this study provide an insight into the effects of SGLT inhibitors on cardiac contractility and some of the underlying Ca^{2+}-mediated mechanisms.

Chapter 3: Methodological Principles

3.1. Diabetes Mellitus Induction in Rats

Many aspects of DM would still be unexplained, if it was not for experimental models. Experimental models provide a convenient tool to understand DM pathogenesis and its complications, and to test new therapeutic strategies [169]. Animal models also develop the complications of DM faster than humans making them easier to study [53; 169]. Moreover, experimental models have a narrower range of variation regarding gender, age differences, ethnicity, diet, lifestyle and drug interactions compared to clinical studies [53; 169]. Most research uses rodent models as they are easier to handle and maintain, and are cost-effective [186]. Large animal models such as cats and dogs can also be used [186]. There are several ways to create experimental models of DM in animals including surgical pancreatectomy, chemical induction, dietary induction, hormone induction, virus induction, genetic induction and crossbreeding [169; 186; 259]. The first animal model for DM was the pancreatectomized dog in the experiments of Mehring and Minkowski [186]. Chemical induction of DM, sometimes called pharmacological induction, is another method of DM induction [186]. Intraveneous (i.v.), intraperitonial (i.p.) (Fig. 3-1) or s.c. injections of diabetogenic agents such as STZ, STZ-nicotinamide mixture, alloxan, vacor (vitamin B antagonist), dithizone, dehydro-ascorbic acid, pentamidine and 8-hydroxyquinoline, which destroy the insulin-producing pancreatic beta-cells (β-cells), are used in this method [96; 186; 229; 267].

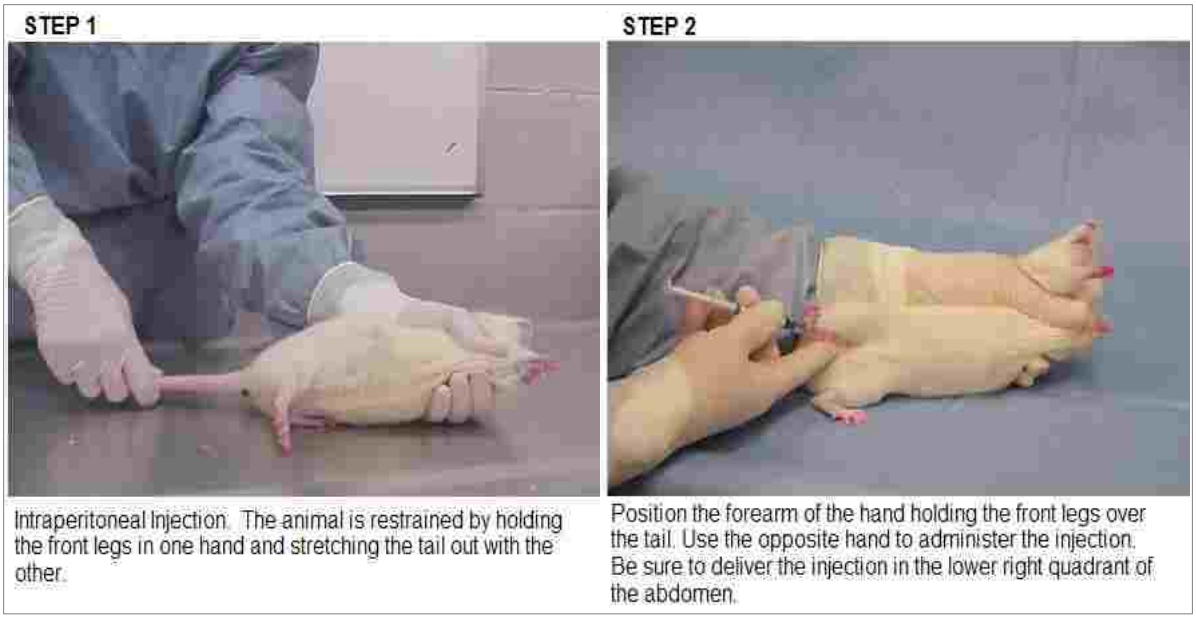

Figure 3-1: Intraperitonial injection in rats

Retrieved from [234]

The animal model produced by this method is suitable for screening natural products for their anti-diabetic properties (insulinomimetic, insulinotropic and anti-hyperglycemic) as well as studying the effect/response of anti-diabetic medications whose mechanism of action is β-cell-independent [159; 259]. However, this method has a disadvantage as the chemicals used might not be specific to the pancreas [159].

STZ and alloxan are the most commonly used diabetogenic chemicals. STZ has some advantages over alloxan, including a longer half-life (15 min) [259]. Thus, it takes longer to be metabolized and produces a more sustained hyperglycemia [259]. STZ also produces well-defined diabetic complications with a low chance of DKA and a low rate of mortality [259]. STZ (called Streptozotocin, Streptozocin, Izostazin or Zanosar) is isolated from *Streptomyces achromogenes* and was first discovered to

be diabetogenic in 1963 by Rakieten and his collegues from their experimetns on dogs and rats [5; 259]. It is also a broad-spectrum antibiotic, anti-neoplastic agent and alkylating agent with specific cytotoxic effects on the endocrine activity of pancreatic β-cells [206; 229]. It is used to induce both T1DM and T2DM [266]. Its structure is composed of two different moieties, a deoxyglucose and nitrosourea moieties (Fig. 3-2). The deoxyglucose moiety in the STZ structure interacts with GLUT2 protein which then allows STZ molecules to cross the cell membrane and enter the pancreatic cell [259; 266].

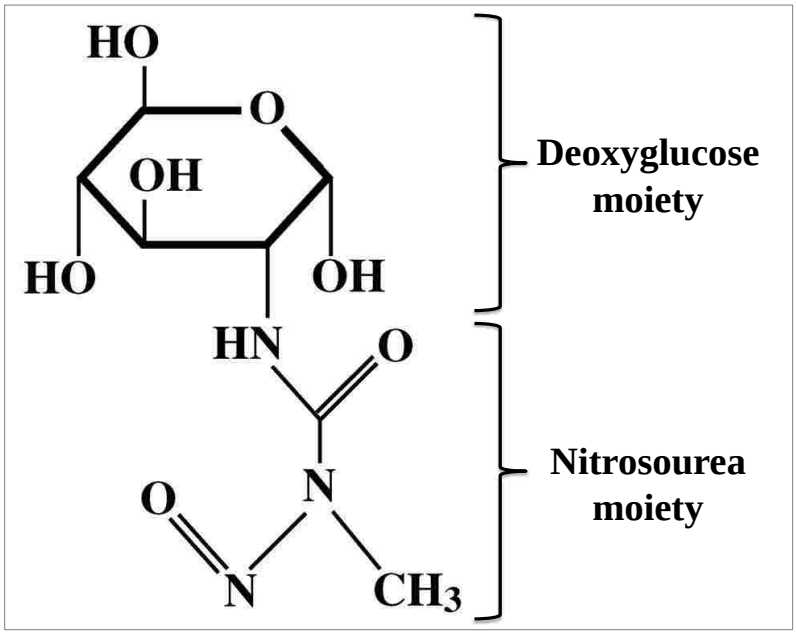

Figure 3-2: Chemical structure of streptozotocin

Destruction of β-cells by STZ takes place via both direct and indirect pathways (Fig. 3-3). The direct pathway is caused by the alkylating nitrosourea moiety of STZ which induces fragmentation of the DNA strands leading to activation

of poly-ADP-ribose synthase (PARS) which diminishes nicotinamide adenine dinucleotide (NAD^+) co-enzyme and eventually causes a reduction in cellular ATP and necrosis [259]. The indirect pathway involves the generation of nitric oxide (NO) and ROS, and an inhibition of the Krebs Cycle [266]. NO and inhibition of the Krebs Cycle cause a drop in cellular ATP production and ATP dephosphorylation by xanthine oxidase [266]. Xanthine oxidase then catalyzes the production of superoxide anion (O_2^-) followed by hydrogen peroxide (H_2O_2) and hydroxyl radical (OH^-) generation [266]. O_2^- can react with NO to generate peroxynitrate (ONOO) which is a highly toxic compound. NO and ROS cause DNA alkylation and cell necrosis [266]. Necrosis of β-cells causes reduced insulin production and DM.

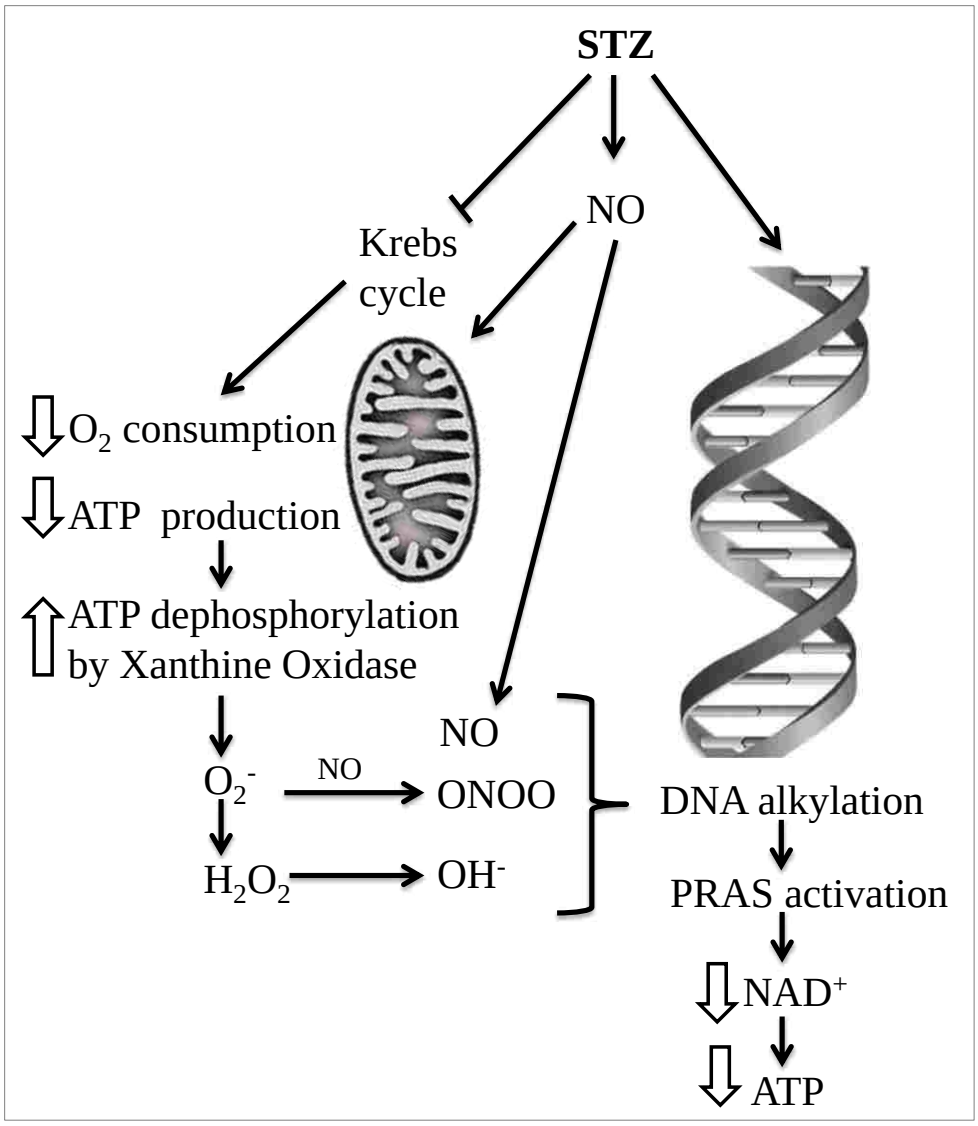

Figure 3-3: Mechanism of diabetes mellitus induction by streptozotocin

Adapted from [266]

STZ: streptozotocin**; DNA:** deoxyribonucleic acid; **PARS:** poly-ADP-ribose synthase; **NAD^+:** nicotinamide adenine dinucleotide; **ATP:** adenosine triphosphate; **NO:** nitric oxide; **ROS:** reactive oxygen species; **O_2^-:** superoxide anion; **H_2O_2:** hydrogen peroxide; **OH^-:** hydroxyl radicals; **ONOO:** peroxynitrate

STZ can produce DM in rodents by a single injection of a large dose or by multiple injections of small doses [229]. After STZ injection, fluctuations in β-cell

activity are observed causing subsequent changes in blood insulin and blood glucose [266]. Initially, the insulin-producing activity of β-cells is suppressed two hours after injection, which is reflected in low blood insulin and hyperglycemia [266]. Then after six hours, their activity is transiently restored causing high levels of blood insulin and hypoglycemia but eventually the cells lose their activity leading to a persistent rise in the BGL (Fig. 3-4) [266]. The STZ solution needs to be freshly prepared before injection due to its low stability, and experiments should take place at least 5–7 days after DM induction in order to attain stable hyperglycemia [159].

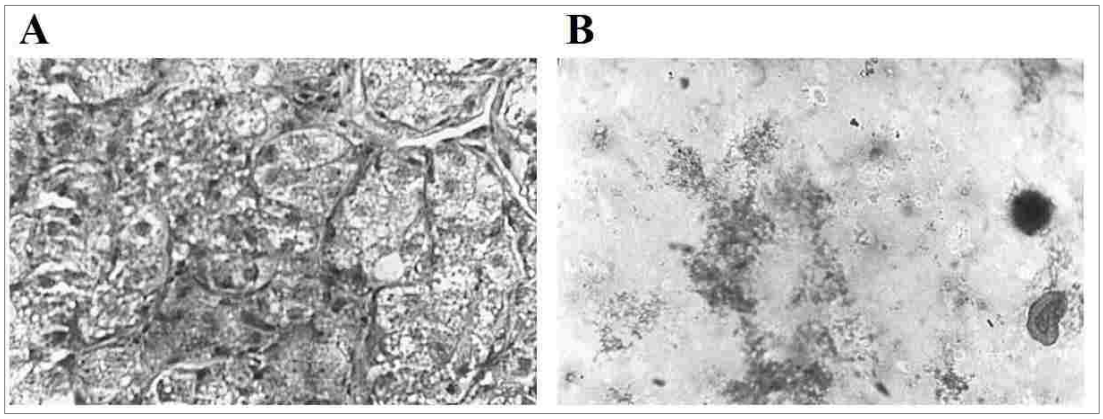

Figure 3-4: Effect of streptozotocin on rat pancreatic β-cells

Retrieved from [5]

(A) Biopsy of healthy pancreatic tissue before streptozotocin (STZ) injection
(B) Biopsy of pancreatic tissue after STZ injection showing destruction of β-cells

3.2. Isolation of Ventricular Myocytes

In 1846 at the University of Marburg, a student of the German Physiologist Carl Ludwig reported the development of experiments for studying isolated heart functions [328]. In 1866, Carl Ludwig and Elias Cyon published a paper describing

the first heart isolation experiment done with a frog's heart [175; 328]. Before 1880, experiments were done on frogs which are cold-blooded species because their hearts are simple having only one ventricle and not having a coronary circulation unlike warm-blooded mammalian hearts [253; 328]. The heart was mounted, cannulated and perfused with rabbit serum through the vena cava [253; 328]. The perfusate was discharged from the aorta to a glass tube then recirculated back to the vena cava [253; 328]. Different scientists were able to improve the procedure. Kronecker showed the importance of supplying the heart with oxygen and Ringer was the first to realize that isolated heart contraction can be maintained by perfusing it with electrolyte solutions containing Ca^{2+}, Na^{+} and K^{+} [175; 253]. He developed 'Ringer's solution', that was later modified to produce other physiological solutions including Tyrode and Krebs-Henseleit [175; 253]. In 1880, Henry Newell Martin tried to develop experiments to isolate mammalian hearts using heart-lung preparations from cats or dogs [328]. In 1895, the German physiologist Oscar Langendorff developed the Langendorff method, a method which is still widely used in many laboratories [175; 328]. In this method, the ascending aorta is cannulated and perfused in a 'retrograde manner' (opposite to the physiological circulation direction) (Fig. 3-5) [175]. In 1967, Howard Morgan and James Neely adapted the Langendorff retrograde method to develop the so-called 'working heart' model [175; 328].

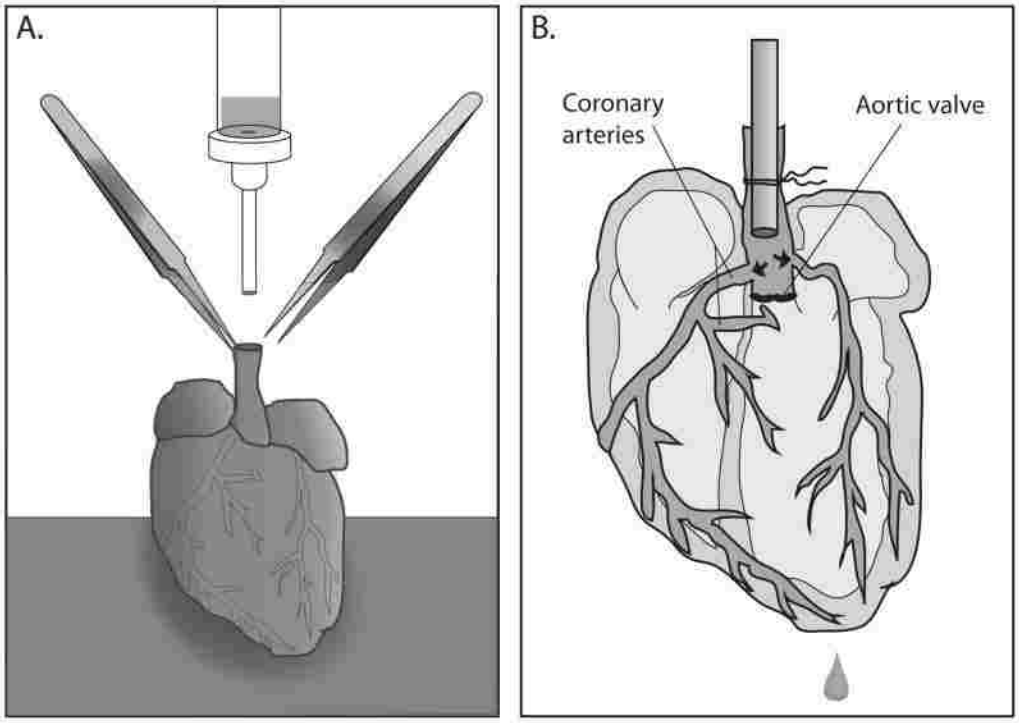

Figure 3-5: Cannulation of the heart through the aorta

Retrieved from [183]

(A) The aorta of the heart is mounted on the cannula of the Langendorff apparatus using fine-tipped forceps. A silk thread can be tied around the cannulated aorta to secure it in place.

(B) The Cannula should be inserted above the aortic valve to close it during perfusion allowing the perfusate to flow to the cornary arteries. If the cannula is inserted deep below the aortic valve, the perfusate flows to the heart chambers instead and the isolation process becomes unsuccessful.

After developing methods to study the intact isolated heart, the next step was to develop a method to study cardiac cells. This was made possible in 1969 when Kono used rat hearts to develop a technique for isolating adult mammalian ventricular myocytes [32; 86]. Generally in physiological studies, freshly isolated cells are closely related to cells *in vivo* and more reliable than immortalized cardiac cell lines in terms of structure and function [183]. Adult cardiac cells can be isolated by

mounting the heart on a cannula as mentioned previously. The cannula is connected to a perfusion system supplied with water-jacketed reservoirs and heat exchangers to maintain the temperature at 37°C throughout the whole perfusion process (Fig. 3-6) [23]. Perfusing solutions are delivered to the cannula by either gravity using constant pressure perfusion where a pressure transducer is connected above the cannula to monitor the coronary perfusion pressure or by using constant flow perfusion where a peristaltic pump is connected to a chamber to which the cannula is fixed (Fig. 3-6) to deliver the perfusate at a constant flow rate (flow rate range is 7-9 ml/min for rats) [23; 183; 253]. The cannula can be fabricated from glass, plastic or metal and its diameter size differs according to the species, and the age and sex of the same species ranging from 1.6 –3.2 mm for rats and 0.6–1.3 mm for mice according to the age and sex [183]. If it is too large, the cannula may not fit the aorta or may tear it and if it is too small, the cannula may hinder the flow of solutions to the heart [23].

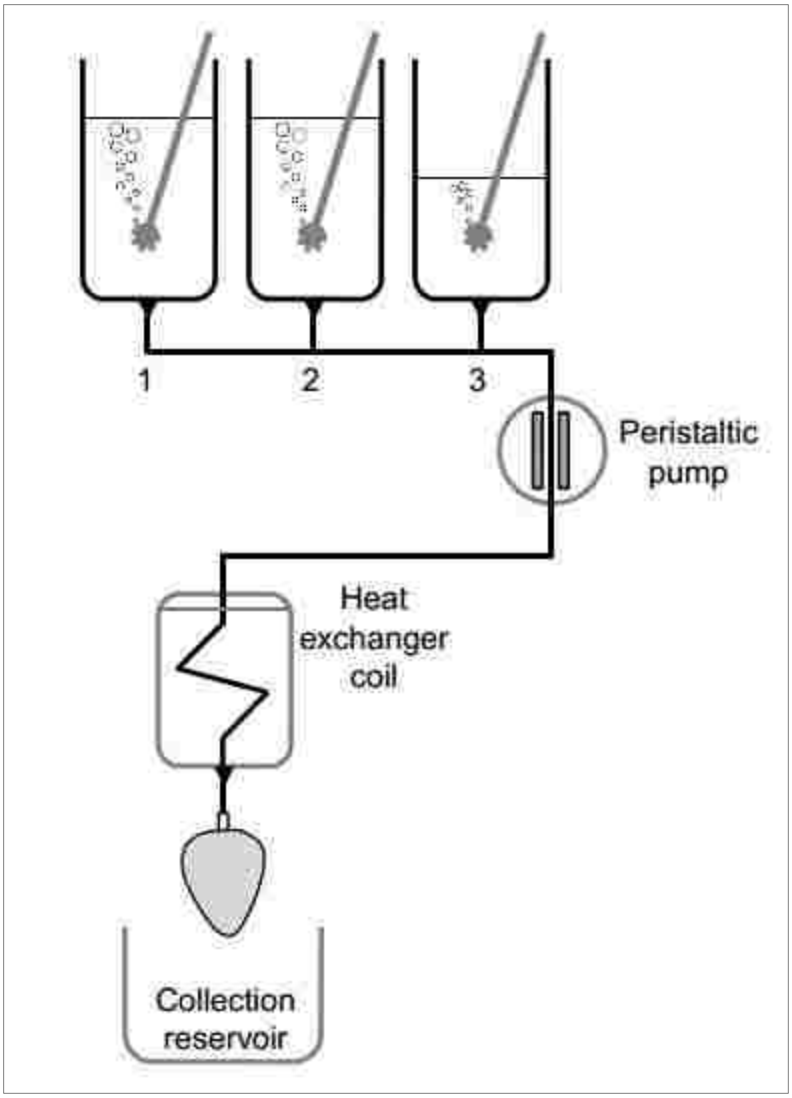

Figure 3-6: Ventricular myocyte isolation using retrograde perfusion

Retrieved from [187]

The cannulated heart is connected via tubes to three reservoirs and a peristaltic pump. The heart is perfused at a certain rate with **(1)** Ca^{2+}-containing, **(2)** Ca^{2+}-free ethylene glycol tetra-acetic acid-containing and **(3)** collagenase/protease isolation solutions.

Isolation of cardiomyocytes is done in several steps [32]. First, the cannulated heart is perfused with Ca^{2+}-containing isolation solution to wash out blood [32]. Heart contraction is allowed to stabilize. The heart contraction rate observed is bradycardiac

compared to that *in vivo* (250–320 compared to 350–400 beats/min in rats) due to the lack of neuro-humoral control and extra-cardiac vascular supply to the SA node [23]. Second, it is perfused with Ca^{2+}-free isolation solution to loosen the intracellular connections. Third, the heart is perfused with an enzyme-containing isolation solution [32]. Langendorff retrograde enzymatic digestion is commonly used to isolate ventricular myocytes [32; 183]. In some laboratories, Langendorff retrograde enzymatic digestion can be replaced or combined with another enzymatic digestion method called the 'immersion method' which involves incubation of tiny pieces of the tissue in different solutions and gentle agitation [32]. This method is used to isolate ventricular myocytes from bovine or canine hearts that cannot be perfused, and myocytes from certain heart tissues such as the SA node, Purkinjie fibers, and human heart biopsies [32]. Choosing the perfusing enzyme is a crucial step. Different types of collagenases, with collagenase type II from Worthington being the most common, can be used alone or with other enzymes including proteases or pancreatin for adult rats and mice cardiomyocyte isolation [183]. Hearts of older animals are bigger in size and have different extracellular matrices so, they usually need a higher concentration of enzymes, longer perfusion duration or both. After the heart is perfused with the three solutions, it becomes soft, swollen and pale [183]. Fourth, the heart tissue is shaken mechanically to release the myocytes from the tissue [32]. Scattered myocytes are allowed to sediment on a myocyte mesh collector (filter) (200-500 μm for adult myocytes) by means of gravity or gentle shaking [183]. Myocytes pass through the pores of the mesh collector whilst undigested cardiac tissue remains in the mesh [183]. Finally, the tissue is centrifuged to separate the

high-density rod-shaped viable myocytes from the low-density rounded dead myocytes [32; 183]. The supernatant is discarded and the pellets of myocytes are re-suspended in a physiological solution. The shaking, filtration and centrifugation processes are repeated several times as needed [183]. Myocyte viability can be assessed by measuring the ratio of rod-shaped (alive) myocytes to round-shaped (dead) myocytes using a Neubauer hemocytometer [34]. If the myocyte isolation process was performed properly, its final yield mainly consists of viable cardiomyocytes (Fig. 3-7).

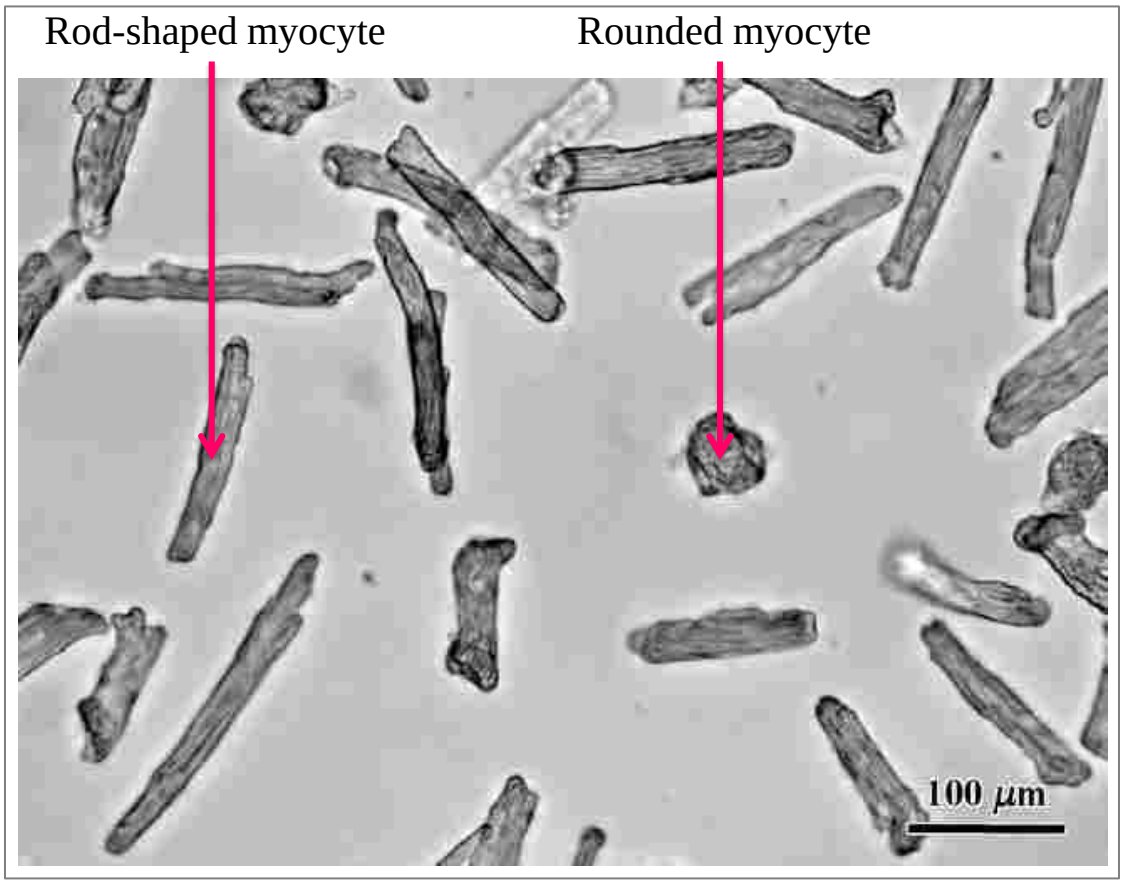

Figure 3-7: Isolated rat ventricular myocytes

Adapted from [326]

3.3. Video Edge Detection

The experiments previously mentioned developed to isolate heart myocytes paved the way to studying shortening and contractile functions within individual myocytes. Cardiomyocyte shortening has been studied by monitoring the movement of one or both ends of the myocyte [74]. Three popular methods are used including video edge detectors, photodiode arrays and laser diffraction techniques [260]. Video edge detection (VED) is widely used especially with adult cardiomyocytes [19]. Electrically-stimulated cardiomyocytes *in vitro* change their length along their longitudinal axis during contraction and relaxation; they shorten during contraction and return to their resting length during relaxation [260]. VED assesses changes in the length of the cardiomyocyte by using a raster-line at each of the left and the right edges of the myocyte to monitor its movement during shortening and relaxation [19]. VED can be done either by single-edge detection (SED), where the contraction of only one horizontal edge is monitored, or by double-edge detection (DED) (Fig. 3-8), where both horizontal edges of the myocyte are monitored [74]. DED is better because it avoids some problems that occur with the SED such as unequal contraction between both edges and inaccurate monitoring of myocytes moving non-longitudinally [74].

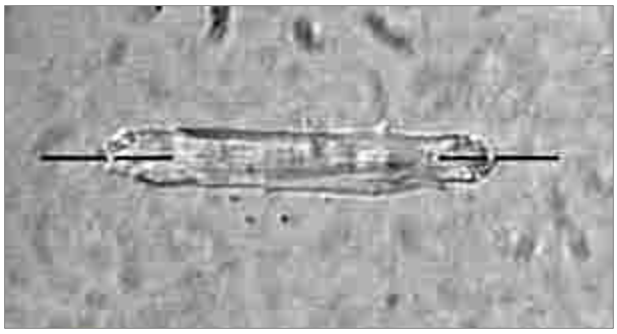

Figure 3-8: Double-edge detection video image of an isolated ventricular myocyte

Retrieved from [315]

The ventricular myocyte is anchored between two black raster-lines with white tracking dots to monitor the movement of the myocyte along its longitudinal axis.

The VED system is used along with an electrical stimulator, a television camera, an analogue-digital converter, a monitor screen, a computer and/or a chart recorder. To generate contractions, electrical stimuli are sent from the stimulator to the myocyte chamber (Fig. 3-9) via two platinum or silver wire electrodes, placed opposite to each other [163]. This causes a series of consecutive events in the chamber that eventually lead to myocyte contraction. First, an electric field is created around the myocytes which in turn generates a flow of current (charges movement) [283]. Subsequently, a gradient in potential is developed around the cell membrane leading to change of the outer membrane potential with respect to the inner membrane potential (transmembrane potential) which triggers voltage-gated ion channels of myocytes to produce transmembrane currents and then myocyte contraction [283].

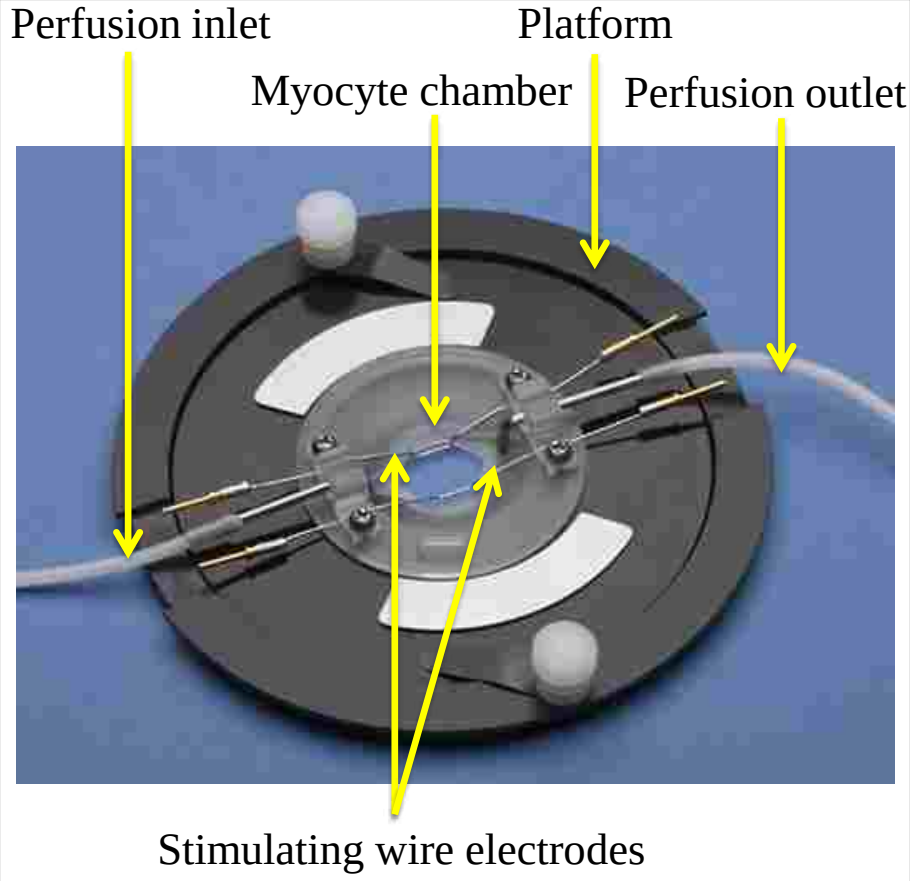

Figure 3-9: Myocyte perfusion chamber with field stimulation

Retrieved from [297]

Cardiomyocytes are characterised by having variable width, and having gap junctions and intercalated discs around their edges which make their edges irregular [19; 74]. Those chosen for shortening experiments should be viable rod-shaped with intact morphology and defined edges, they should contract consistently during the whole electrical stimulation process and they should not exhibit spontaneous contraction [19; 260; 315]. The two raster-lines are positioned at each end of the myocyte (Fig 3-8) from which light intensity-dependent voltages at myocyte edges can be measured [260]. The television camera focuses the image of the electrically-

stimulated myocyte allowing the image to be recorded [260]. The signal then passes from the camera to the VED system which analyzes the data and measures the distance between the two edges on a milli-second (ms) by ms basis [19; 260]. The analyzed data is then conveyed via an analogue-digital converter, which digitizes the signal, to the computer and/or chart recorder [260]. The analyzed data is also sent to the monitor screen to show the myocyte contraction. A series of contractions are recorded in each myocyte and their mean is used to evaluate the extent of shortening in the cell [260]. A summary of measuring shortening in electrically-stimulated myocytes is shown in Fig 3-10.

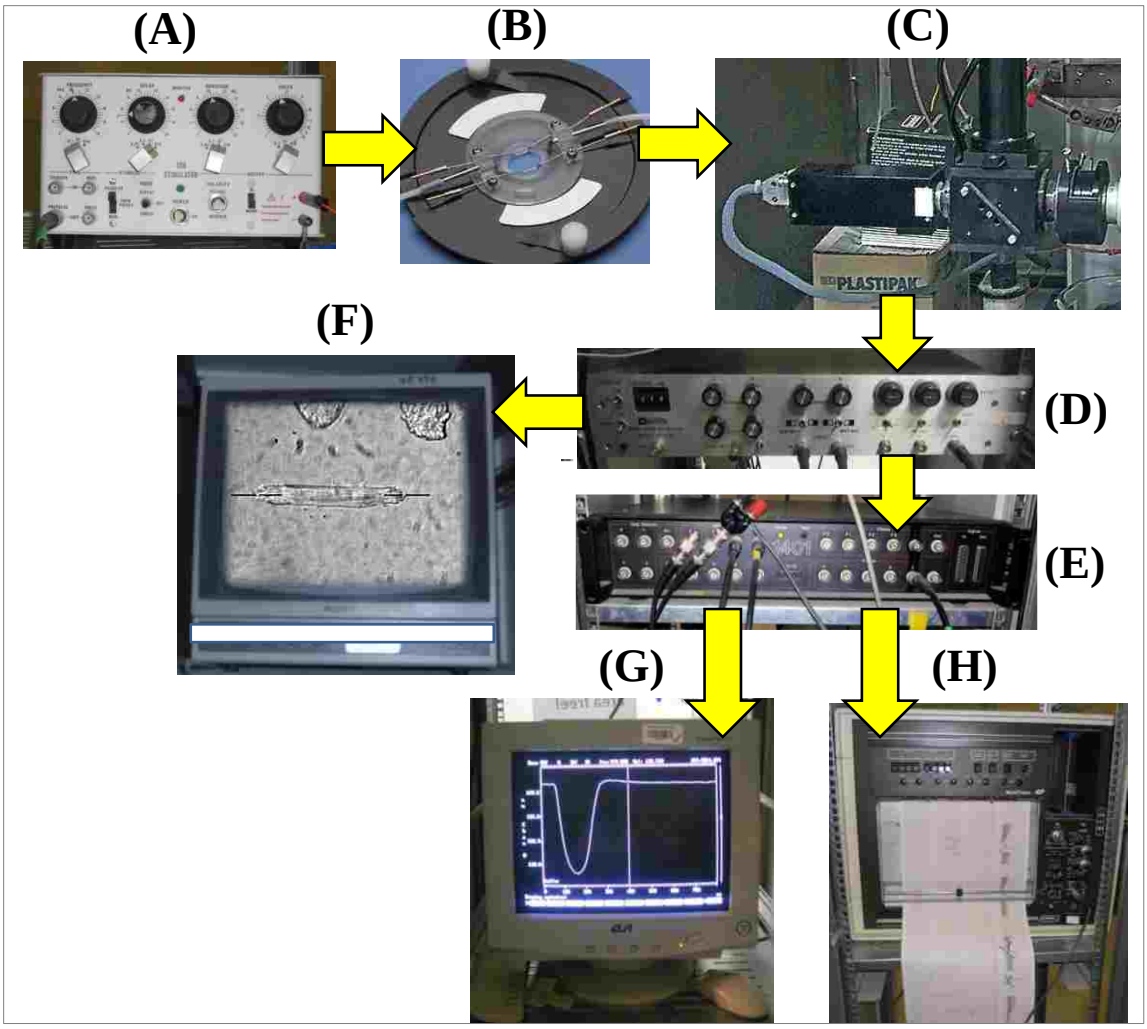

Figure 3-10: Measuring cardiomyocyte shortening

The stimulator **(A)** sends electrical signals to the cell chamber **(B)**. The camera **(C)** records the image of the myocyte. Movement is analyzed by the video edge detection system **(D)** and can be seen on the monitor **(F)**. The signal passes to the analogue-digital converter **(E)**. Data are captured, stored and analyzed on the computer **(G)** and/or chart recorder **(H)**.

3.4. Fluorescence Photometry

Fluorescence photometry is an optical technique that can be used to measure the concentration of intracellular ions and other parameters with fluorescent

indicators [45]. It is based on loading the cell with a fluorescent indicator by allowing it to pass passively into the cell across the membrane (diffusion), by injecting it into the cell via a microelectrode (microinjection) (used with relatively large cells) or by patch clamping in cell-attached configuration to introduce the indicator intracellularly (used with relatively small cells) [45; 65]. There are two forms of indicators available: potassium salt and acetoxy methyl (AM) ester forms [65]. Potassium salt indicators can be loaded by microinjection, with large cells, or patching, with small cells [45; 65]. On the other hand, AM ester indicators are often loaded by diffusion because it allows loading many cells together, but they can also be loaded with microinjection and patching [45]. AM ester renders the indicator molecule lipophilic so that it is able to cross the cell membrane passively [65]. The ester link is then degraded by cytosolic esterases releasing the free indicator [65]. The fluorescent indicator binds to the intracellular ion of interest causing a change in the indicator electronic configuration and a subsequent change in its fluorescence [45]. Photons are then bombarded at fluorescent indicator-loaded cells [45]. Photons react with the ion molecules bound to the fluorescent indicator (fluorescent molecules) in the cell that have absorbance within the photons wavelength range. The fluorescence molecules absorb the photons and they reach an excited state [45]. The excited molecules then emit the absorbed photon and return to the ground state (Fig. 3-11) [45]. Quantum efficiency is the ratio between photons emitted to photons absorbed [45]. Since the emitted photons are always less than those absorbed because they get reabsorbed or collide with other molecules and quench, quantum efficiency is always less than one [45]. The photons emitted have relatively low energy and long wavelengths, while

absorbed photons have relatively high energy and short wavelengths [45]. The emitted fluorescence is measured in which the indicator-photon interaction results in a change in the indicator fluorescence wavelength [45].

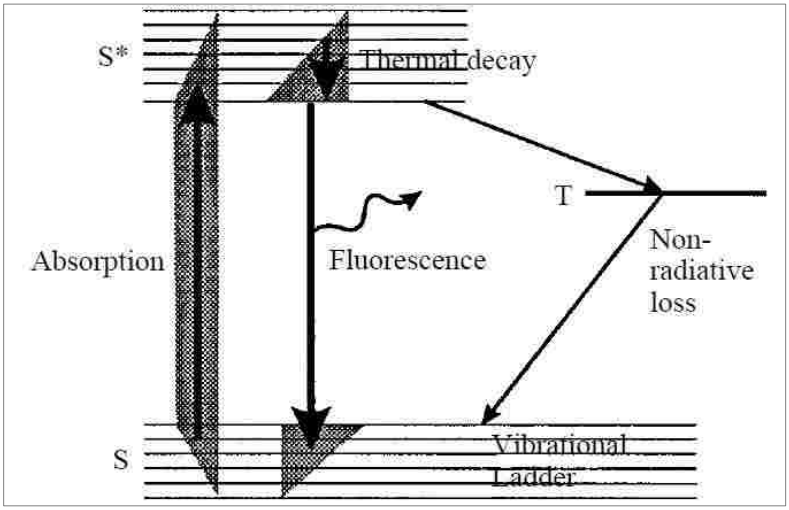

Figure 3-11: Effect of photons on the molecule of the fluorescence indicator

Retrieved from [45]

When the molecule absorbs the photons, the electron energy is increased and the electrons jump to the higher singlet level S* (excited state). Electrons then emit the absorbed photon and return from S* directly to their ground level (ground state) releasing fluorescence of a certain wavelength. If the indicator is bleached due to oxidation and thermal decay, the electron does not go directly to its ground level and non-radiative loss occurs where no fluorescence is emitted.

It should be noted when applying this method that some contamination errors might occur due to cell auto-fluorescence which occurs due to spontaneous fluorescence of some cellular components, or the presence of other molecules within the range of photons absorbance other than the molecules of interest [45; 271]. Energy associated with the photons can be very high, resulting in generation of large amounts of heat which might degrade the indicator by bleaching and destroy the cell

[45]. In addition, if the concentration of the ion measured, or that of the indicator, is too small to produce a signal, low signal to noise ratio is obtained [45].

There are two classes of fluorescence indicators: non-ratiometric and ratiometric [271]. Non-ratiometric indicators have one excitation and one emission wavelength and they do not show any shifts in any of their wavelengths on ion binding, but they increase their emission fluorescence yield [232; 271]. Ratiometeric indicators, on the other hand, either have two excitation and one emission wavelength such as Fura-2, or one excitation and two emission wavelengths such as Indo-1 and, on ion binding, they shift their excitation or emission wavelengths, respectively, increasing their emission fluorescence yield [232; 271]. Having a pivotal role in contraction regulation, Ca^{2+} is the first ion that comes to mind when studying muscle contraction in general and cardiac contraction in particular. In the early 1980s, Tsien and his colleagues developed several fluorescent Ca^{2+} chelators including Quin-2, Fura-2 and Indo-1 by adding fluorophores to 1, 2-bis-(2-aminophenoxy) ethane-NNN'N'-tetra-acetic acid (BAPTA) [65]. These indicators bind to Ca^{2+} with a stoichiometric ratio of 1:1 [65]. In some respects, Fura-2 is better than Quin-2 because it has a better absorption coefficient, quantum yield (30 times brighter), Ca^{2+} selectivity and bleaching resistance [65]. The high brightness of Fura-2 signals makes autofluorescence negligible [65]. These advantages make Fura-2 a popular indicator for studying intracellular Ca^{2+} [218]. Fura-2 has two excitation wavelengths at 340 and 380 nm and one emission wavelength that is usually measured at 510 nm [65]. Fura-2 produces a bluish-green glow that can be seen under the standard epifluorescence microscope [65]. On binding to Ca^{2+}, its electronic configuration

changes where the intensity of its 340 nm excitation fluorescence is increased 3 times while the intensity of its 380 nm excitation fluorescence is decreased 10 times (Fig. 3-12) [65].

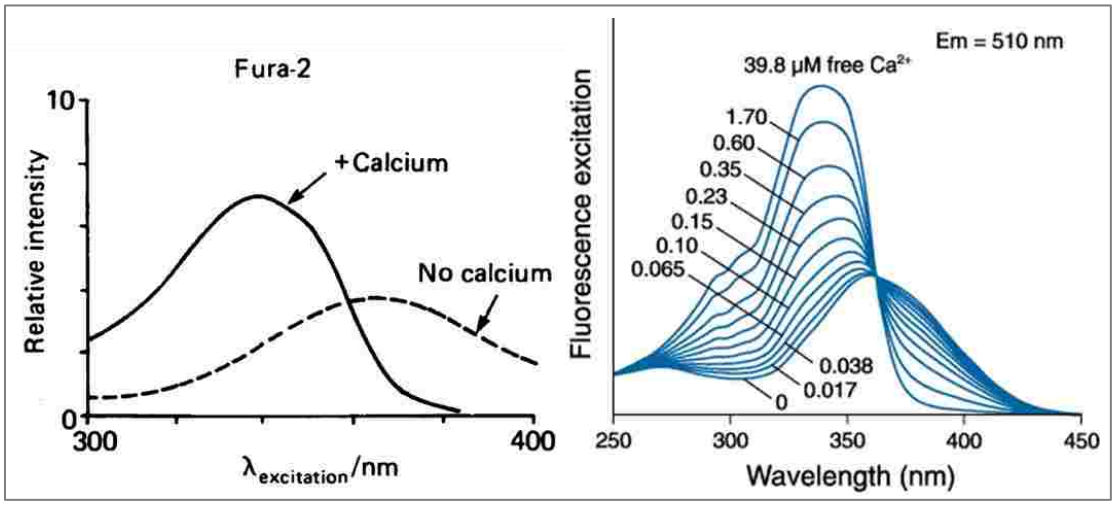

Figure 3-12: The shift in Fura-2 excitation fluorescence intensity on binding to Ca^{2+} Retrieved from [65; 176]

Left panel: the solid line represents the wavelength of Fura-2 saturated with Ca^{2+} and the dashed line represents the wavelength of free Fura-2. **Right panel:** gradual increase in concentration Ca^{2+} bound to Fura-2 causes gradual increase and decrease in the intensity of 340 and 380 nm excitation wavelengths, respectively.

To measure intracellular Ca^{2+} with Fura-2, a ratio method is applied where the ratio of bound to free indicator is calculated. This method removes any variations resulting from instrumental fluctuations as well as changes in the indicator concentration like leakage or bleaching, as it is independent of the indicator concentration [65; 218]. The following equation can be used to calculate this ratio:

$$[Ca^{2+}] = K_d \left(\frac{F\,0}{F\,s}\right) \left[\frac{R - R\min}{R\max - R}\right]$$

Where K_d is the dissociation constant, F_0 is 380 nm excitation fluorescence intensity at zero Ca^{2+} concentration, F_s is 380 nm excitation fluorescence intensity at saturated Ca^{2+} concentration, $\left(\frac{F\,0}{F\,s}\right)$ is the ratio of 380 nm excitation fluorescence intensity at zero to saturated Ca^{2+} concentrations, R is the ratio of fluorescence intensity induced by 340 nm to that induced by 380 nm, R_{min} is the ratio of excitation spectra (340/380) at zero Ca^{2+} concentration and R_{max} is ratio of excitation spectra (340/380) at saturated Ca^{2+} concentration [65; 218].

Despite the advantages of Fura-2 AM, it also has some problems. One of its major problems is compartmental leakage where it can bind to various cellular organelles including SR and mitochondria [65]. This problem can be overcome by storing the cells at 4°C before Fura-2 AM loading, by loading the cells at low temperatures or by dialyzing Fura-2 in its salt form into the cell using a pipette [233]. In addition to leaking into cellular organelles, Fura-2 can also leak outside some types of cells. This can be reduced by lowering the temperature of the experiments below the physiological temperature to 15-33°C [65; 233]. Some Fura-2 commercial preparations are contaminated with esterase resistant elements resulting in insufficient degradation of AM links in the cytosol [233]. This problem can be avoided by replacing AM links in Fura-2 molecules with pentapotassium salt [233]. Fura-2 is also susceptible to quenching with heavy metals, which can be avoided by adding heavy metal chelators such as N,N,N',N'-tetrakis (2-pyridylmethyl) ethylenediamine (TPEN) [233]. A summary of measuring intracellular Ca^{2+} concentration in Fura-2 loaded myocytes is shown in Fig 3-13.

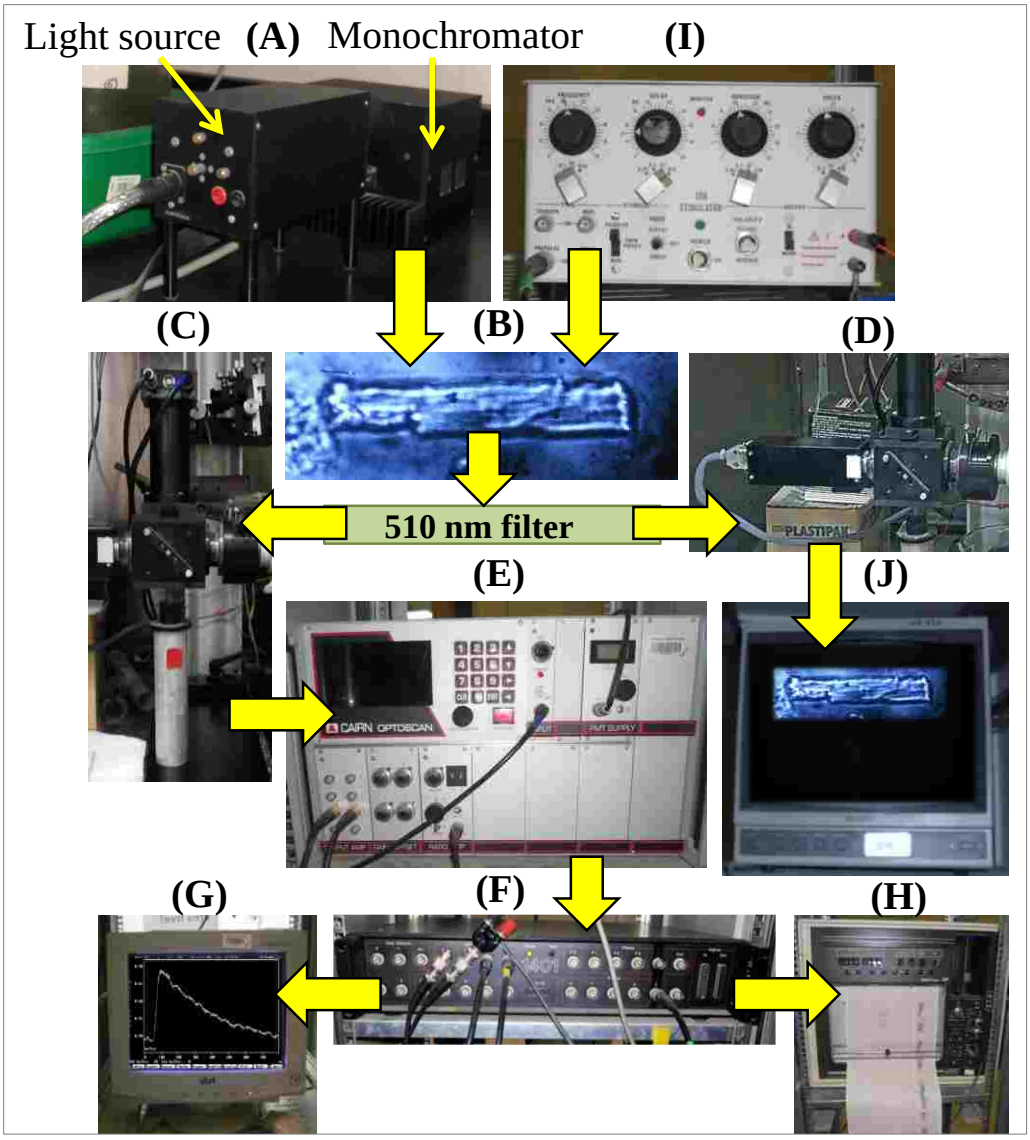

Figure 3-13: Measuring cardiac intracellular Ca^{2+} in Fura-2-loaded myocytes

Light is projected from the light source to the monochromator **(A)** which generates light of required wavelength (340/380 nm), bandwidth and millisecond time resolution. This light is then projected via a light guide through the microscope optics to the Fura-2 loaded myocytes **(B)**. Emitted fluorescence is passed through a 510 nm filter to the photomultiplier tube (PMT) **(C)** and collected by the camera **(D).** The PMT **(C)** converts light to electrical energy (volts), amplifies the signal and sends it to the fluorescence photometry system **(E)** which analyses the signal. The signal then passes to the analogue-digital converter **(F)**. Digitized signal is then sent to the computer **(G)** and/or chart recorder **(H)**. During experiments, the myocyte **(B)** is electrically stimulated by the stimulator **(I).** The camera **(D)** records the image and sends it to the monitor screen **(J)**.

3.5. Patch Clamp

Ion channels are transmembrane proteins which serve as passages for ions from and to the cell [302]. It is important to study their activity as they regulate the generation of cardiac and neural APs, through production of currents, because of their ion selective permeability and subsequent ionic movement [108; 302]. Electrical activity in muscles was first discovered by Luigi Galvani in 1791 [324]. Afterwards in 1939, Hodgkin and Huxley measured the intracellular AP for the first time in giant squid axon using glass capillaries [324]. In 1946, Graham and his colleagues developed micropipettes (less than 5 μm in outer diameter) to study APs in smaller structures [324]. In 1949, the voltage clamp technique was developed by Cole and Marmount to measure the voltage and current of the cell membrane using a micropipette [324]. The patch clamp technique was developed in the late 1970s by Neher and Sakman to allow recording of the membrane current in small cells with low noise where they replace the micropipette with a blunt-ended pipette (0.5-2.0 μm in diameter) [149; 324]. The technique involves positioning a glass pipette against the cell membrane till a seal, with 10-100 GΩ resistance, is formed [116]. This seal is called a 'giga-seal' and it improves the resolution of the currents recorded by reducing the background noise that might arise from the cell membrane, pipette and recording electronics [116]. This glass pipette injects current into the cell to stimulate it [89]. The depolarization of the cell causes ion channels to open [108]. Ion channels generally shift between three transitional conformations which are open, inactive and closed (resting) (Fig. 3-14) [166]. When the channel is open, it is activated and produces a current, while no current is produced when it is closed or inactivated

[166]. Gating is the process of opening and closing of the channel. Some channels (Ca^{2+} and Na^{+}) become inactivated after sustained activation (depolarization) or after closure [108]. Inactivation is observed as slow degradation of the current [149]. Inactivated channels cannot open directly, but should first recover by closure to become ready to re-open [149]. The inactivation process prevents premature activation and provides a refractory period before the following activation [108].

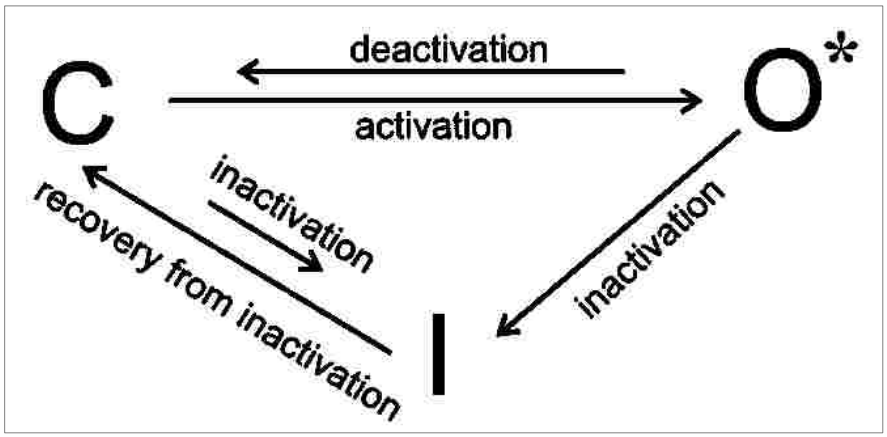

Figure 3-14: Behavior of voltage-gated channels

Retrieved from [149]

The ion channel goes through three transitional conformations; open (O), inactive (I) and closed (C). The asterisk indicates a conformation that passes current. Relative probability of transitions is indicated by size of arrows. Initially, a change in membrane voltage (depolarization) changes the closed transition to open (activation).The opened channel then becomes inactivated (inactivation). The channel eventually transitions from inactivated conformation to closed again (recovery).

The patch clamp technique can be used for the measurement of a single channel or whole cell channels electrical activity, gating, ion selectivity and ion permeability which makes it a useful tool for studying the molecular mechanisms underlying the electrical activity in cardiac cells as well as neurons [59; 166]. It is

also an ideal technique to study how ion channels are affected by different compounds [302]. Nevertheless, patch clamp is a challenging and complicated technique that demands well-controlled experimental conditions and a skillful, experienced researcher. It also has very low throughput [59].

Two modes of patch clamp can be applied which are voltage clamp, that involves holding membrane voltage at a certain value while measuring current generated as a result of ionic movement across the membrane, and current clamp that involves holding membrane current at a certain value while measuring voltage (action potential) [50; 149; 166].

There are two types of electrodes used in patch clamp recording: the reference (ground) and recording electrodes [50]. These electrodes are usually made of platinum or silver (Ag/AgCl) but Ag/AgCl is commonly used due to the high cost of platinum [324]. These metals have low junction potentials which minimizes the generation of a potential at the solid-liquid junction between the electrode and the solution in the chamber [324]. The AgCl layer at the surface of Ag electrodes is worn over time as it undergoes a reversible redox reaction, therefore, it needs to be replenished by either electrophoresis in a chloride solution or immersing it in sodium hypochlorite bleach [324]. The reference electrode is immersed in the bath solution for comparison with the recording electrode [50; 324]. A glass pipette is placed around the recording electrode with which the cell is approached [324]. The recording electrode translates the ionic current produced by the cell to an electrical current [324]. The glass pipette should have low resistance and capacitance transients in the range that can be compensated by the amplifier [324]. Glass pipettes are very

convenient as they can be filled with solutions, dyes or any compounds to be dialyzed into the cell during the experiment [50]. Before a glass pipette can be filled, it is fabricated by either pulling it once or more than once, in a horizontal or vertical puller [166; 215]. A metal filament or a laser is used to heat the glass pipette followed by drawing out the pipette using gravity or a mechanical system [36]. Figure 3-15 shows a pipette produced by double pulls. One of the techniques that can be used to estimate the diameter of the pipette tip is by measuring the pressure taken by the pipette to expel air bubbles from its tip in clean ethanol [215]. The tips of the pulled glass pipettes should be smooth and blunt to prevent damage to the cell membrane and to make better seals [324]. To avoid contamination of the pipettes and their tips with airborne particulates, pipettes are usually pulled shortly before use and kept in a sealed case [166]. After pulling, the pipette is fire polished using a heated platinum wire to smoothen and flatten the surface of its tip [215; 324]. Borosilicate glass (Pyrex) is the most commonly used glass because it softens at low temperatures facilitating its pulling, it seals easily with cell membranes during high resistant- and giga-seal formation and it has relatively low electrical noise during recordings [166; 215]. It has been reported that flint glass is better than borosilicate because it has a lower melting point and forms membrane seals with higher stability [116].

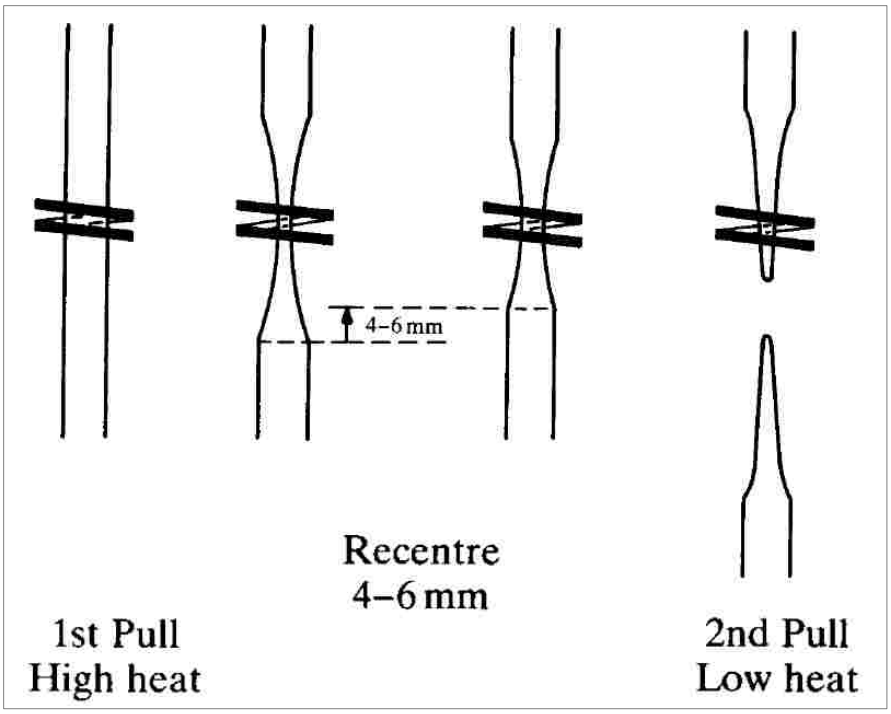

Figure 3-15: Heat double-pulling of patch pipette

Retrieved from [215]

The patch clamp set-up is composed of several components as shown in Figure 3-16. Cells are put in a bath chamber with volume usually ranging from 500 µl -1 ml, its bottom is made of glass to allow attachment of the cells when they settle [166]. The chamber is placed on an inverted microscope which is used to select suitable cells and adjust the patch pipette orientation as it approaches and makes contact with the cell [166]. There two main reasons for using an inverted microscope. The presence of the objective lens below the chamber facilitates the movement of the electrodes in the chamber, and it serves as a solid support and a large stage for the manipulator [50]. The location and movement of the patch pipette is controlled by a mechanical, electrical or hydraulic micromanipulator which allows three-dimensional

movement of the pipette in X, Y and Z axes [50; 166]. A headstage is mounted on the micromanipulator and is connected to the recording electrode (via an electrode holder), reference electrode, and a suction tube which is used to achieve a giga-seal [50; 166]. The headstage connects the cell chamber with an amplifier [166]. The main function of the amplifier is to amplify the signal (100-1000 x), coming from the two electrodes of the headstage, and compare them [50; 166]. In addition, the amplifier can be used to switch between voltage and current modes, compensate capacitance and assist in data acquisition [149; 166]. An analogue-digital converter converts the acquired analogue data, coming from the headstage, to digital and sends it to the computer to be analyzed and recorded [166]. The analogue-digital converter also converts the digital output data, coming from the computer, to analogue and sends it to the headstage [166]. Data is eventually acquired and analyzed using computer software [166]. An oscilloscope can either be used as the main source of data output where it displays the signal of the membrane voltage coming from the amplifier throughout the experiment, or instead, a computer with virtual oscilloscope software programs can perform this function [50]. The inverted microscope, micromanipulator and headstage are all placed on an anti-vibration table to provide a steady platform that eliminates vibrations during giga-seal formation and patch clamp experiments [166]. A Faraday cage, which is formed of a mesh made of a conductive material (usually copper), usually surrounds the entire patch clamp system and is connected to a ground source to insulate it from any ambient electromagnetic fields that may cause noise during recordings [50; 166].

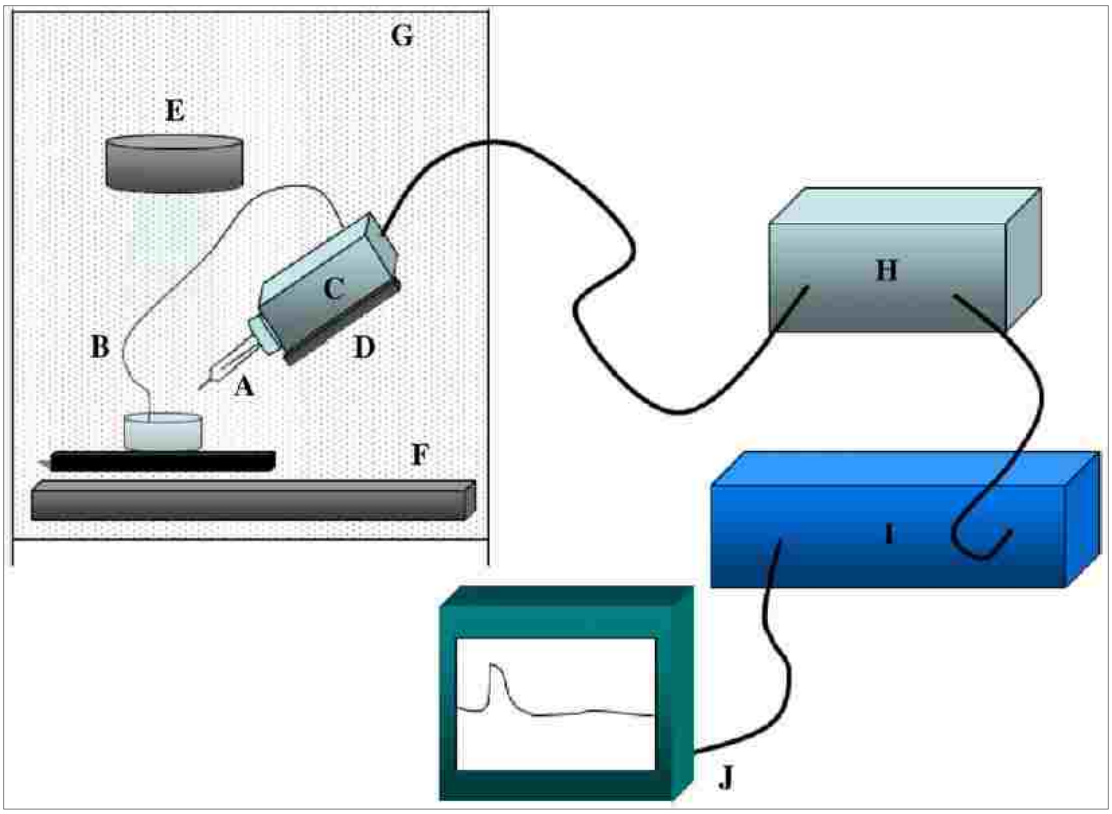

Figure 3-16: Main components of patch clamp set-up

Retrieved from [166]

The internal recording electrode **(A)**, in the patch pipette, and the reference electrode **(B)** are connected to the headstage **(C)** which is mounted on the micromanipulator **(D)**. The inverted light microscope **(E)** is used to visualize the isolated cells to select a suitable cell. The headstage **(C)**, the micromanipulator **(D)** and the inverted light microscope **(E)** are all placed on the anti-vibration table **(F)** to protect them from vibrations during giga-seal formation. The entire system is surrounded by Faraday cage **(G)** to insulate the system from ambient electrical noise. The headstage **(C)** sends the acquired analogue signal to the analog-digital converter **(H)**. The digitized signal is then sent to the computer **(I)** which is used to generate experimental protocols, and acquire and analyze the data. The experiment is monitored and data is displayed on the oscilloscope **(J)**.

The configurations that can be obtained with patch pipettes include cell-attached, whole-cell, inside-out, outside-out and perforated clamp configurations (Fig. 3-17). Cell-attached configuration is the non-invasive starting point for obtaining all

the other four configurations [324]. It involves approaching the cell with the glass pipette and then applying some negative pressure (suction) to the pipette, using the suction tube attached to the headstage, until a high resistance seal is obtained [166]. The tight attachment of the patch pipette with the patched cell membrane traps the ions in the patched area, which causes the ions to flow to the patch pipette reflecting the activity of ion channels in the patched area [50; 166]. Whole-cell configuration involves reaching cell-attached (giga-seal) configuration and applying more suction to disrupt the patched area of the membrane providing continuity of pipette with the cell membrane and continuity of the pipette solution with the intracellular fluid [324]. The electrical activity of the whole cell membrane can then be recorded [50]. Inside-out configuration can be obtained after cell-attached (giga-seal) configuration followed by withdrawing the pipette taking a patch of the membrane with it and thus, subjecting the intracellular environment to the chamber solution [324]. It is used to measure the electrical activity of single ion channels while changing the solution to which the intracellular environment is exposed [50; 324]. Outside-out configuration can be obtained by retracting the pipette after whole-cell configuration causing the removed membrane patch to invert its position with respect to the orientation of the cell membrane [50]. Thus, the exterior surface of the membrane comes in contact with the chamber solution [50]. It is used to study the effects of extracellular chemical signals on ion channel activity [50]. Both Inside-out and Outside-out configurations are called cell-excised configurations [324]. Perforated patch configuration is sometimes used instead of whole-cell configuration. It allows measuring the membrane activity without the risk of leakage of the intracellular contents that occurs

with whole-cell patching [50; 166]. It involves applying a chemical in the glass pipette such as amphothericin-B, nystatin or gramicidin, instead of suction, after cell-attached configuration which forms membrane perforations [50; 166].

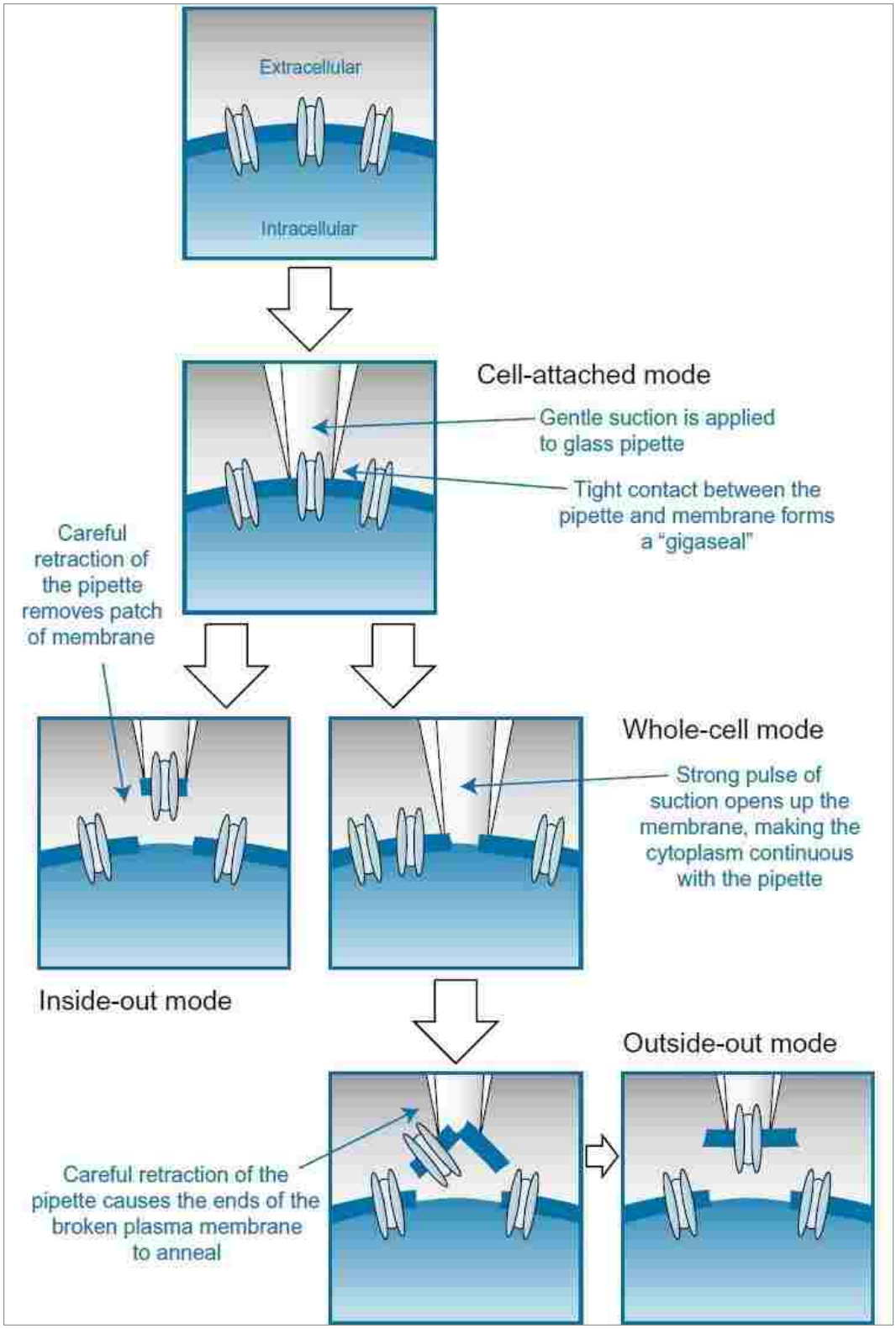

Figure 3-17: The four configurations of patch clamp technique

Retrieved from [50]

Chapter 4: Materials and Methods

4.1. Materials

4.1.1. Animal Model

Seventy male adult Wistar rats were used for these experiments and were bred in the animal house facility at the College of Medicine and Health Sciences, United Arab Emirates University. Rats (≈ 200-250 g) were divided into two subgroups. At the age of 2 months, DM was induced in one subgroup by a single i.p. injection of STZ (60mg/kg body weight) dissolved in a citrate buffer solution (0.1 mol/l citric acid and 0.1 mol/l sodium citrate, pH 4.5). The other subgroup received an equivalent volume of citrate buffer to form the Controls. To confirm DM, non-fasting BGL was measured in blood obtained from the rat tail vein, 3-5 days following the induction of DM. Each subgroup was caged separately, but both groups were kept under the same light and temperature conditions, and were supplied with standard rat chow diet and water *ad libitum*. Experiments were started 2 months (8-12 weeks) after DM induction. Prior to each experiment, rat body weight, heart weight and non-fasting blood glucose were measured. All the procedures implemented in this project were approved by the Animal Ethics Committee, College of Medicine and Health Sciences, United Arab Emirates University.

4.2. Methods

4.2.1. Isolation of Ventricular Myocytes

Fresh ventricular myocytes were isolated on a daily basis. Rats were euthanized using a guillotine and their hearts were rapidly removed. The heart was

mounted in Langendorff mode on the cell isolation apparatus. Hearts were perfused in a retrograde manner at a constant flow rate of 8 ml/g heart.min (Fig. 4-1). Initially, the heart was perfused with cell isolation solution containing in mmol/l: 130.0 NaCl, 5.4 KCl, 1.4 $MgCl_2$, 0.75 $CaCl_2$, 0.4 NaH_2PO_4, 5.0 4-(2-hydroxyethyl)-1-piperazine ethanesulfonic acid (HEPES), 10.0 glucose, 20.0 taurine and 10.0 creatine (pH 7.3). When contraction had stabilized, perfusion was switched to Ca^{2+}-free cell isolation solution containing 0.1 mmol/l ethylene glycol tetra-acetic acid (EGTA) for 4 minutes and then to cell isolation solution containing 0.05 mmol/l Ca^{2+}, 0.60 mg/ml type 1 collagenase (Worthington Biochemical Corp, Lakewood, NJ, USA) and 0.075 mg/ml type XIV protease (Sigma, Taufkirchen, Germany) for 6 minutes. The heart was then removed and ventricle tissue was excised and minced with scissors. The tissue was then shaken gently in collagenase and protease containing isolation solution supplemented with 1% bovine serum albumin (BSA). Ventricular myocytes were filtered from this solution at 4 minute intervals, using a nylon mesh (pore size ≈ 300 µm). The filtered myocytes were then centrifuged for 1 minute and the supernatant was discarded while the myocyte pellets were re-suspended in cell isolation solution containing 0.75 mmol/l Ca^{2+}. The shaking, filtration and centrifugation steps were repeated 4-5 times. Ventricular myocyte viability, indicated by the myocyte rod-shape, was checked after each shake under an upright compound microscope (Zeiss, Göttingen, Germany). Finally, isolated ventricular myocytes were stored in the refrigerator (4°C) in isolation solution containing 0.75 mmol/l Ca^{2+}, or in Kraft-Brühe (KB) solution for patch clamp experiments containing in mmol/l: 0.5 EGTA, 10.0 glucose, 10.0 HEPES, 40.0 KCl, 50.0 K glutamate, 20.0 KH_2PO_4 and 20.0 KOH (pH

7.4). It was reported that storing myocytes in KB solution increases the number of Ca^{2+} tolerant myocytes [135; 325]. Myocytes were used up to 8 hours after isolation.

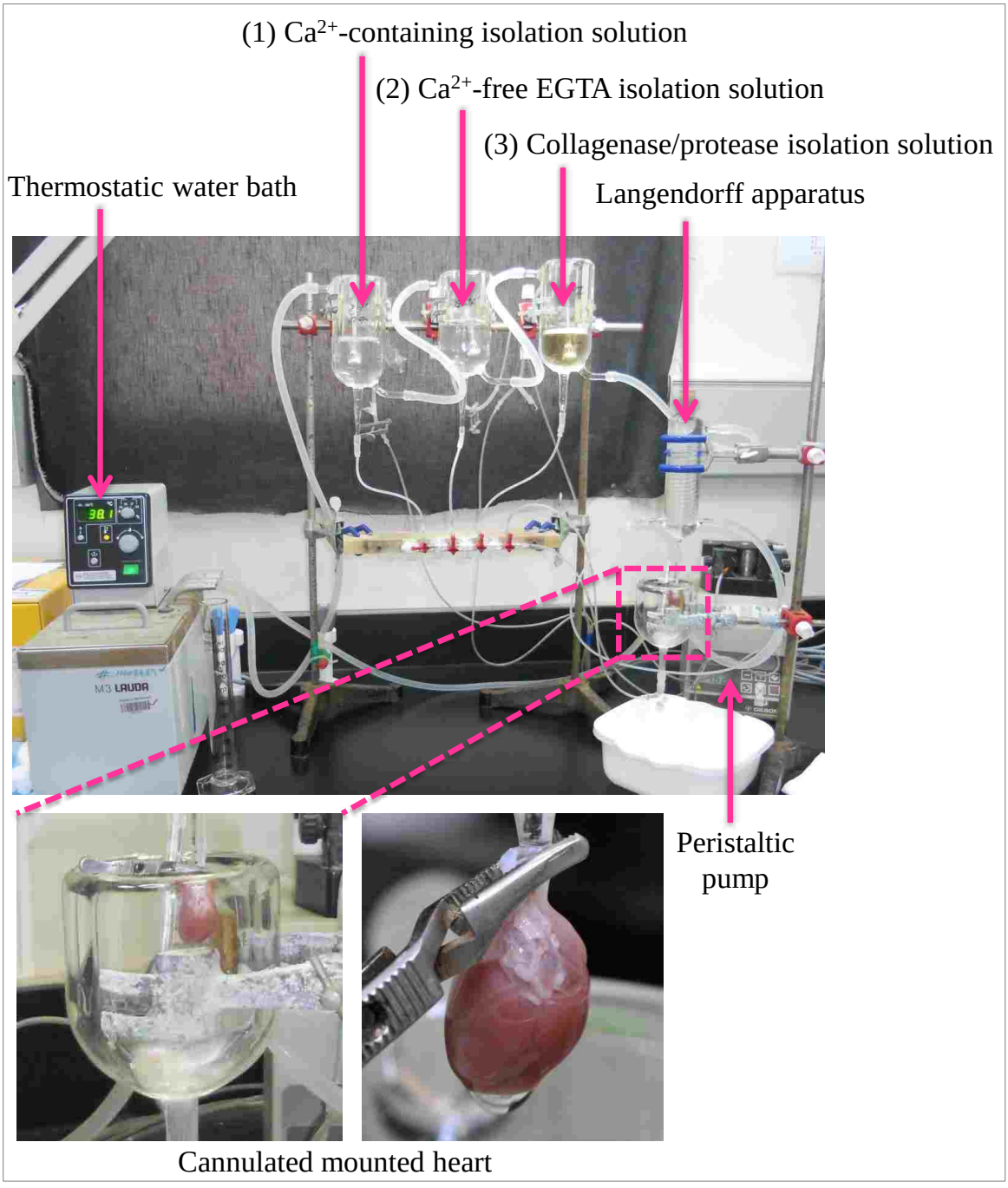

Figure 4-1: Ventricular myocyte isolation apparatus

4.2.2. Electrophysiological Measurements

4.2.2.1. Preparation of Sodium/Glucose Co-transporter Inhibitors and Normal Tyrode Working Solutions

Working solutions were freshly prepared prior to each experiment. In the experiments, two working solutions were used, one containing normal Tyrode (NT) (composed of in mmol/l: 140.0 NaCl, 5.0 KCl, 1.0 $MgCl_2$, 10.0 glucose, 5.0 HEPES, 1.8 $CaCl_2$ and pH 7.4) + 0.005% dimethyl sulfoxide (DMSO) (0.005 ml DMSO in each 100 ml NT) and the other containing 10^{-6} M of any sodium glucose co-transporter (SGLT) inhibitor tested + NT + 0.005% DMSO.

DMSO was used as an organic solvent for all SGLT inhibitors: PHLOR (CDS000104, Sigma-Aldrich, Saint Louis, Missouri, USA), QUER-3-G (17793, Sigma, Taufkirchen, Germany), and DAPA (S1548, Selleck Chemicals, Houston, Texas, USA), at a final concentration of 0.005%. At 0.01% concentration, DMSO has been reported to have no significant effects on contractile parameters and Ca^{2+} current [105; 263] and ≤0.1% DMSO showed no significant effects on myocyte morphology and contractile function [182] in rat myocytes. In this study, equivalent concentration of DMSO (0.005%) was dissolved in both NT and SGLT inhibitor working solutions to make sure that myocytes were exposed to the same concentration of DMSO in all experiments.

The electrophysiological set-up shown in Figure 4-2 was used to measure ventricular myocyte shortening, intracellular Ca^{2+} transient, myofilament sensitivity to Ca^{2+} and SR Ca^{2+} release.

Figure 4-2: Electrophysiological set-up

(1) Micropumps power supply, **(2)** Micropumps control, **(3)** Rapid solution switching device control, **(4)** Rapid solution switching device, **(5)** Inverted microscope, **(6)** Faraday cage, **(7)** Anti-vibration table, **(8)** Camera control **(9)** Video edge detection system, **(10)** Fluorescence photometry system, **(11)** Temperature control system, **(12)** TV monitor, **(13)** Computer, **(14)** Chart recorder and **(15)** Stimulator.

4.2.2.2. Measurement of Ventricular Myocyte Shortening

Ventricular myocyte shortening was recorded using a VED system (Fig. 4-3A). Unloaded myocytes (Fig. 4-3B) were allowed to settle on the glass bottom of a Perspex chamber mounted on the stage of an inverted microscope (Axiovert 35, Zeiss, Göttingen, Germany). Myocytes were continuously superfused with NT at a rate 3-5 ml/min. Shortening parameters including resting cell length (RCL), time to peak (TPK) shortening, time to half (THALF) relaxation and the amplitude (AMP) of shortening (expressed as a percentage of shortening in Control and STZ myocytes perfused with NT and expressed as a percentage of RCL) were measured in electrically stimulated (1 Hz) unloaded myocytes maintained at 35-36°C (Fig. 4-3B). Data were acquired and analyzed with Signal Averager software v 6.37 (Cambridge Electronic Design, Cambridge, UK) (Fig. 4-3C), statistically analyzed with SPSS statistics v 20.0 (IBM Software, Inc) and figures were plotted with Fig.P v 2.98 (Fig.P Software Corp., ON, Canada).

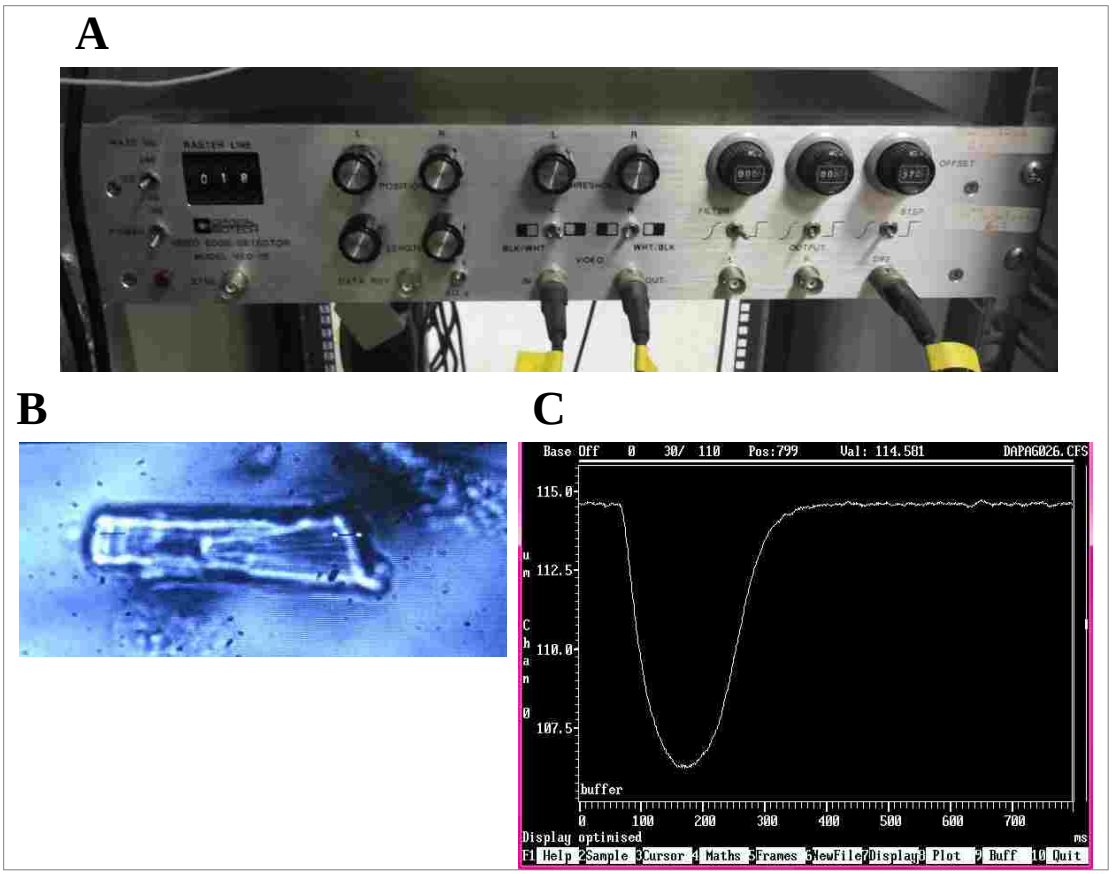

Figure 4-3: Measurement of ventricular myocyte shortening

(A) Video edge detection system
(B) Unloaded ventricular myocyte on the monitor
(C) Typical record of shortening

4.2.2.3. Measurement of Ventricular Myocyte Intracellular Ca^{2+} Transient

Fluorescent indicator Fura-2 AM ester (F-1221, Molecular Probes, Eugene, OR, USA) was used to assess intracellular Ca^{2+} in ventricular myocytes. Fura-2 AM was dissolved in DMSO to make a 1.0 mmol/l stock solution. Myocytes were loaded with Fura-2 AM by adding 6.25 µl of Fura-2 AM stock solution to 2.5 ml of isolated myocytes to give a final Fura-2 concentration of 2.5 µmol/l. Myocytes were then shaken gently (300 rpm) for 10 minutes at room temperature (24 °C). After loading with Fura-2 AM, the myocytes were centrifuged, washed with NT to remove extracellular Fura-2 and then left for 30 minutes to ensure complete hydrolysis of the intracellular ester. Intracellular Ca^{2+} concentration was measured in Fura-2 AM loaded myocytes with a fluorescence photometry system (Fig. 4-4; Cairn Research, Faversham, UK). The loaded myocytes were illuminated alternately by 340 nm and 380 nm lights using a monochromator which changed the excitation light every 2 ms. The resulting fluorescence emitted at 510 nm was recorded by a photomultiplier tube (PMT) and the ratio of the fluorescence emitted at the two excitation wavelengths (340/380 ratio) was calculated to provide an index of intracellular Ca^{2+} concentration (Fig. 4-4E). Resting Fura-2 ratio, time from stimulation to peak (TPK) Ca^{2+} transient, time from peak Ca^{2+} transient to half-decay (THALF) of the Ca^{2+} transient and the amplitude (AMP) of the Ca^{2+} transient (expressed as a percentage of Ca^{2+} transient in Control and STZ myocytes superfused with NT) were measured in electrically stimulated (1 Hz) myocytes maintained at 35-36°C (Fig. 4-4D). Data were acquired and analyzed with Signal Averager software v 6.37 (Cambridge Electronic Design,

Cambridge, UK), statistically analyzed with SPSS statistics v 20.0 (IBM Software, Inc) and figures were plotted with Fig.P v 2.98 (Fig.P Software Corp., ON, Canada).

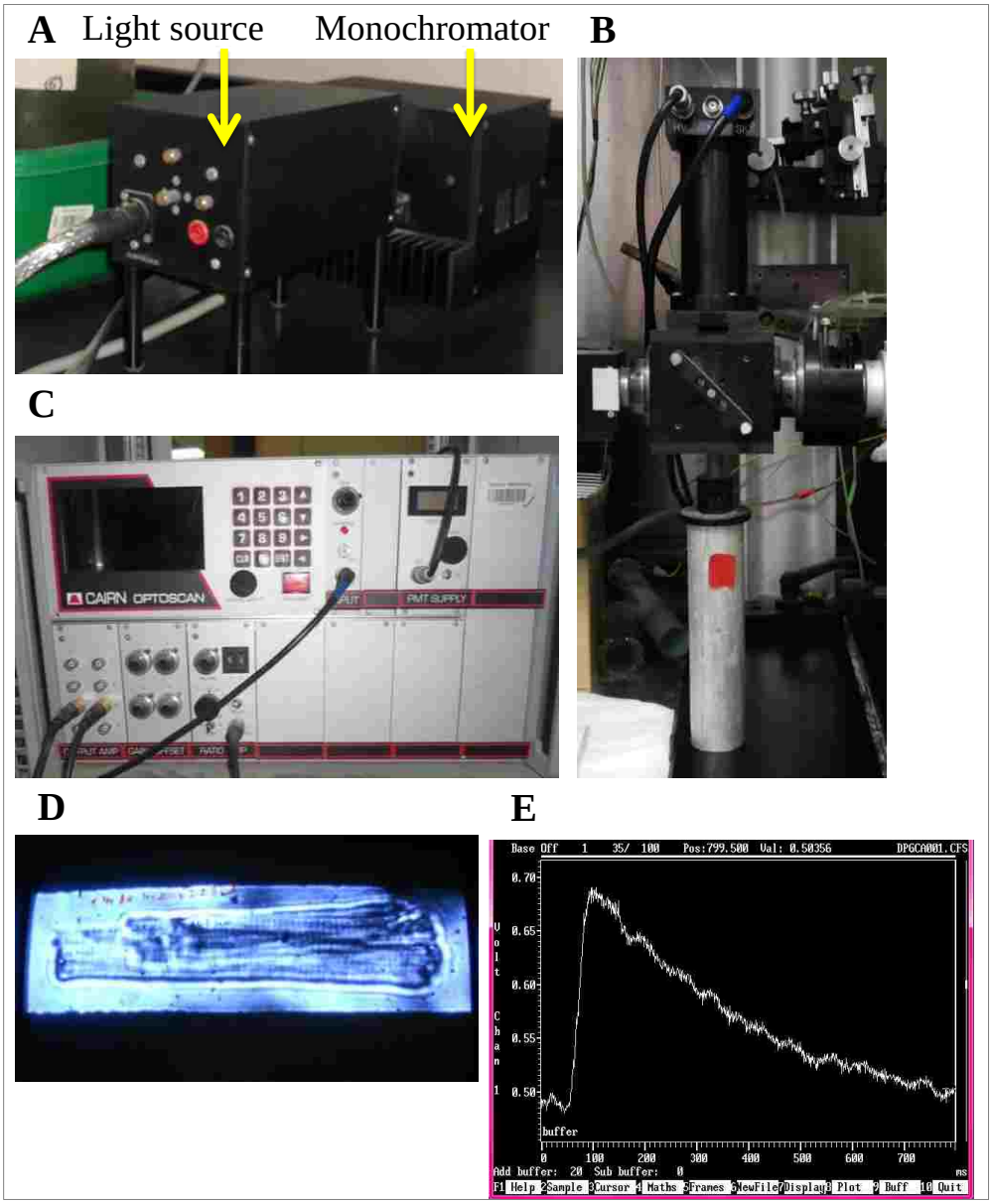

Figure 4-4: Measurement of ventricular myocyte intracellular Ca^{2+}

(A) Light source and monochromator
(B) Photomultiplier tube assembly
(C) Fluorescence photometry system
(D) Fura-2 AM loaded ventricular myocyte surrounded by iris diaphragm
(E) Typical record of a Ca^{2+} transient

4.2.2.4. Assessment of Ventricular Myocyte Myofilament Sensitivity to Ca^{2+}

Myofilament sensitivity to Ca^{2+} was assessed by recording shortening and Fura-2 ratio simultaneously (Fig. 4-5A), and analyzing phase-plane diagrams of Fura-2 ratio versus cell length by measuring the gradient of the Fura-2-cell length trajectory during late relaxation of the twitch contraction [126] (Fig. 4-5B). Previous studies have demonstrated that the position of the trajectory reflects the relative myofilament response to Ca^{2+} and thus, can be used as a measure of myofilament sensitivity to Ca^{2+} [124; 257]. Data were acquired and analyzed with Signal Averager software v 6.37 (Cambridge Electronic Design, Cambridge, UK), statistically analyzed with SPSS statistics v 20.0 (IBM Software, Inc) and figures were plotted with Fig.P v 2.98 (Fig.P Software Corp., ON, Canada).

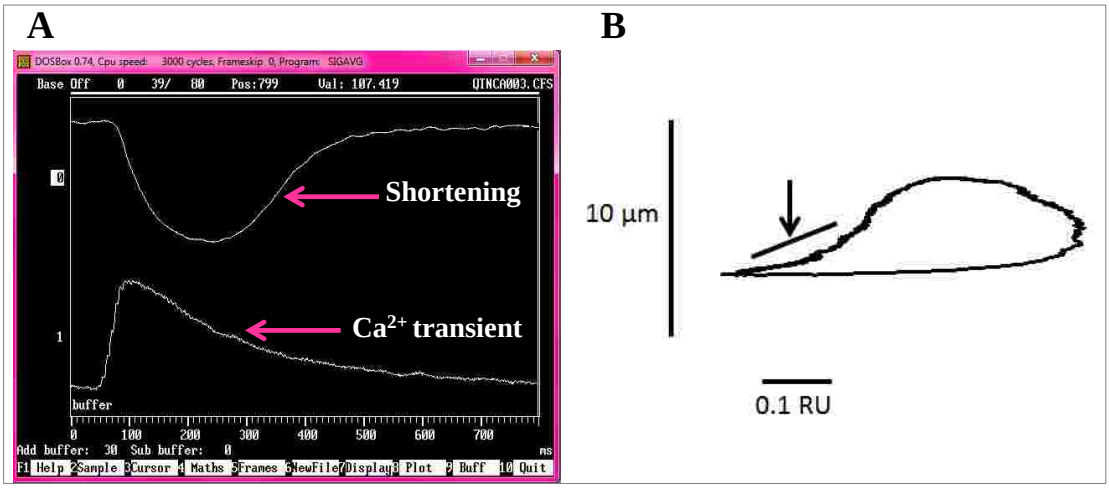

Figure 4-5: Assessment of myofilament sensitivity to Ca^{2+}

(A) Typical record of shortening and Ca^{2+} transient recorded simultaneously
(B) Typical phase plane diagram of Fura-2 ratio unit (RU) vs. cell length. The arrow indicates the region where the gradient was measured

4.2.2.5. Measurement of Ventricular Myocyte Sarcoplasmic Reticulum Ca^{2+} Transport

SR Ca^{2+} release was assessed using previously described techniques [125]. Myocytes maintained at 35-36°C and loaded with Fura-2 were electrically stimulated (1 Hz) until Ca^{2+} transients reached a steady state. Electrical stimulation was then paused for 5 seconds and caffeine (20 mmol) was rapidly applied using a solution switching device [173] (Fig. 4-6A,B). After 10 seconds of caffeine application, electrical stimulation was resumed and the Ca^{2+} transients were allowed to recover to a steady state (Fig. 4-6C). SR releasable Ca^{2+} was assessed by measuring the AMP of the caffeine-stimulated Ca^{2+} transient. By comparing the AMP of the electrically-stimulated steady state Ca^{2+} transients with that of the caffeine-stimulated Ca^{2+} transient, fractional release of SR Ca^{2+} was measured. Recovery of intracellular Ca^{2+} was assessed by measuring the gradient of recovery of electrically-stimulated Ca^{2+} transients after the application of caffeine. Data were acquired and analyzed with Signal v 1.82 (Cambridge Electronic Design, Cambridge, UK), statistically analyzed with SPSS statistics v 20.0 (IBM Software, Inc) and figures were plotted with Fig.P v 2.98 (Fig.P Software Corp., ON, Canada).

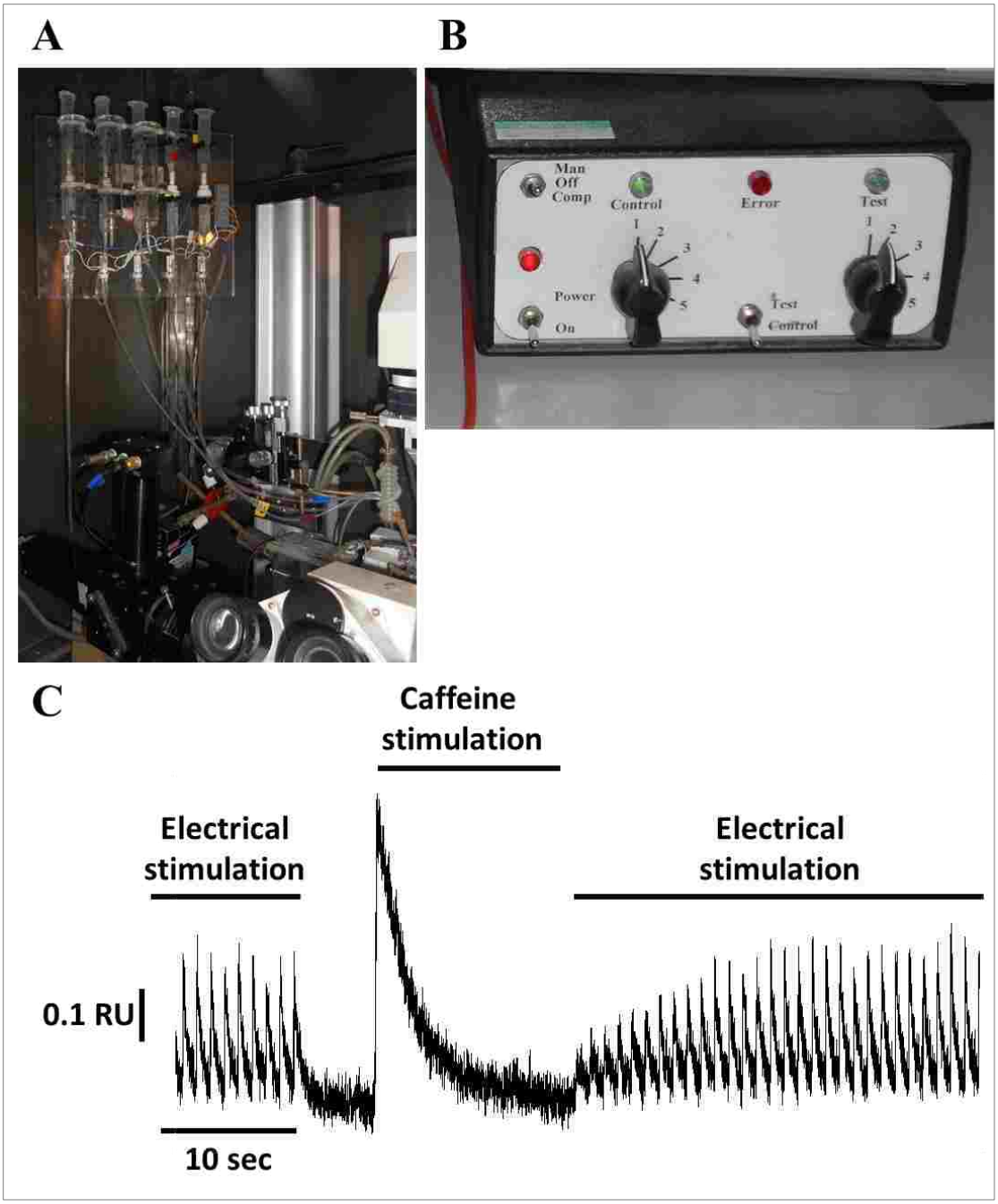

Figure 4-6: Measurement of ventricular myocyte sarcoplasmic reticulum Ca^{2+} transport

(A) Rapid solution switching device
(B) Rapid solution switching device control
(C) Typical record of the electrically-stimulated and caffeine-stimulated Ca^{2+} transient in a ventricular myocyte

4.2.2.6. Measurement of Ventricular Myocyte L-Type Ca^{2+} Current

After ventricular myocyte isolation, myocytes were stored in KB solution. Voltage-dependent L-type Ca^{2+} current was measured in ventricular myocytes with a whole-cell patch clamp system (Fig. 4-7). The current was recorded with an Axopatch 200B amplifier (Molecular Devices, Sunnyvale, CA, USA). The analog signal was filtered using an eight-pole Bessel filter with a bandwidth of 5 kHz and digitized at a sampling rate of 10 kHz under control of pCLAMP v 8.2 software (Molecular Devices, Sunnyvale, CA, USA) (Fig. 4-7A,B). Patch pipettes were fabricated from filamented BF150-86-10 borosilicate glass (Sutter Instrument, CA, USA). Experiments were performed at 34-36°C and myocytes in the chamber were superfused with Ca^{2+}-free extracellular solution containing in mmol/l: 150.0 NaCl, 2.0 $MgCl_2$, 10.0 HEPES and 10.0 glucose (pH 7.35) to facilitiate patching procedure. Once whole-cell mode had been achieved, the solution was switched to Ca^{2+}-containing extracellular solution containing in mmol/l: 145.0 NaCl, 2.0 $CaCl_2$, 2.0 $MgCl_2$, 10.0 HEPES and 10.0 glucose (pH 7.35). Recordings of L-type Ca^{2+} current were made after 5 minutes of superfusion with the Ca^{2+}-containing extracellular solution and after 5 minutes of superfusion with the tested SGLT inhibitor. The patch pipette was pulled (Sutter Instrument, CA, USA) and filled with intracellular solution containing in mmol/l: 140.0 CsCl, 2.0 $MgCl_2$, 10.0 N,N,N,N-tetramethylammonium (TEA Cl), 10.0 EGTA, 10.0 HEPES, 1.0 MgATP and 4.0 $CaCl_2$ (pH 7.25). The pipette solution contained Cs^+ and TEA^+ to supress K^+ currents [134; 155; 255] and fast Na^+ current was inactivated by holding myocytes at -40 mV [106] or -50 mV

[318]. Electrode resistances ranged from 3 to 5 MΩ, and seal resistances were 1–5 GΩ. Series resistances were compensated to > 75% of the uncompensated value.

The current-voltage relationship was used to measure the activation of Ca^{2+} current which was obtained by applying 300 ms test pulses in the range -60 mV to +70 mV in 10 mV steps from a holding potential of -50 mV. The steady-state inactivation of Ca^{2+} current was measured by stepping the membrane from various 1000 ms pre-pulses between -60 and +30 mV to a test pulse of 0 mV. Ca^{2+} current was measured as the relationship between the AMP of peak currents produced at each of the pre-pulses to those measured at the test pulse 0 mV. Time course of recovery from inactivation was measured using a two-pulse protocol. Two 100 ms membrane depolarizing pulses, from a holding potential of -40 mV to +10 mV, were separated by inter-pulse intervals with variable duration, which was increased gradually. Peak Ca^{2+} current AMP measured by the second pulse was normalized to that measured by the first pulse and their ratio was plotted against the durations of inter-pulse interval. Data were acquired and analyzed with pCLAMP v 8.2 (Molecular Devices, Sunnyvale, CA, USA) and OriginPro. v 8.5 (OriginLab Corporation, MA, USA).

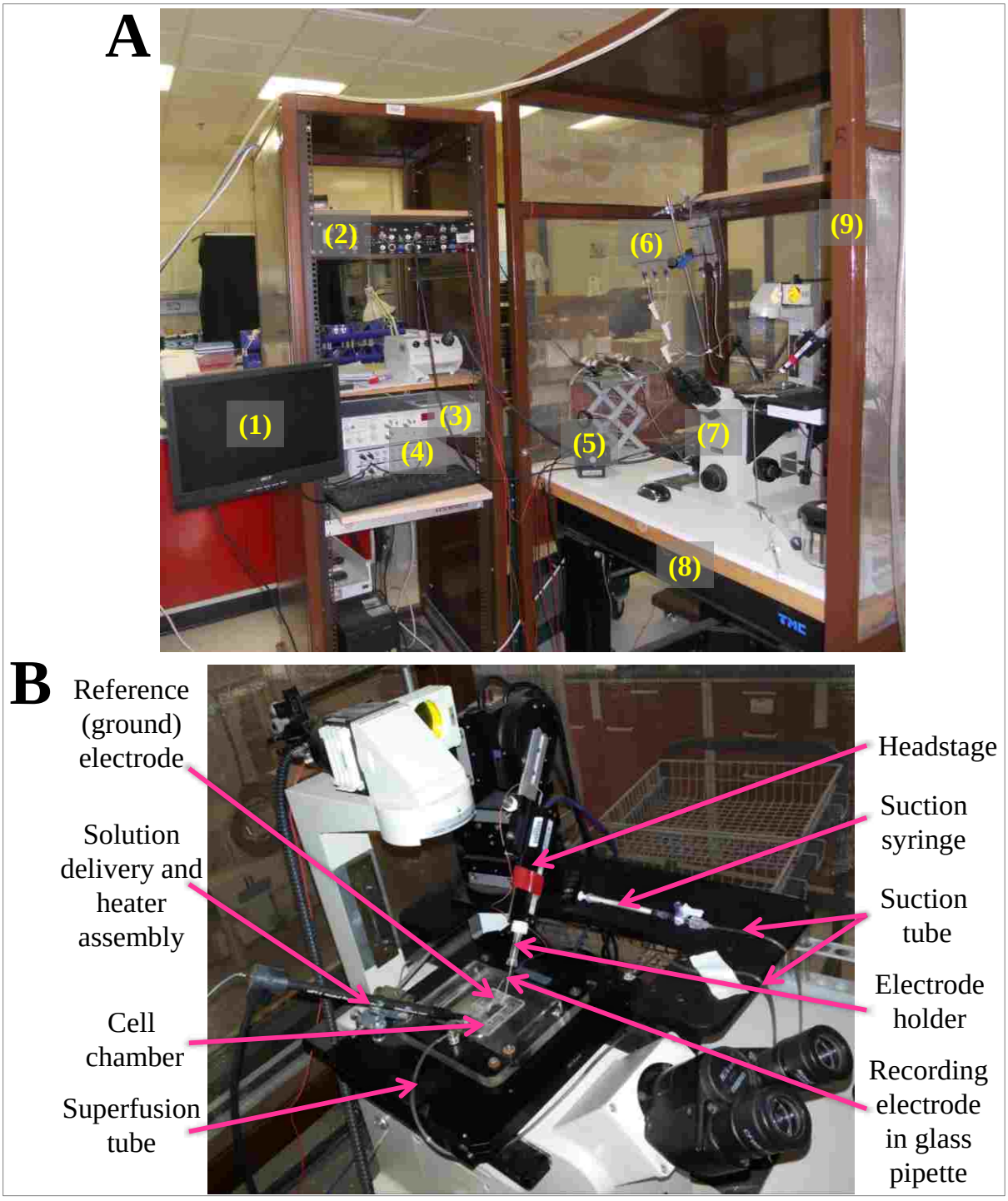

Figure 4-7: Patch clamp system

(1) Monitor, **(2)** Temperature control system, **(3)** Patch clamp amplifier, **(4)** Analogue-digital converter, **(5)** Micromanipulator control, **(6)** Rapid solution switching device, **(7)** Inverted microscope, **(8)** Anti-vibration table and **(9)** Faraday cage.

4.2.3. Statistical Analysis

Results are expressed as the mean ± standard error of the mean (SEM) of '*n*' observations. '*n*' refers to the number of animals or ventricular myocytes. Data were analyzed by either Paired Samples T-Test, Independent Samples T-Test, or one-way ANOVA with Bonferroni *post hoc* for multiple comparisons as appropriate using SPSS statistics v 20.0 (IBM Software, Inc). Statistical significance was set at $P < 0.05$.

Chapter 5: Results

5.1. Animal General Characteristics

Experiments were performed 2 months after STZ injection. DM was confirmed by measuring the non-fasting BGL in a blood sample taken from the tail vein, 3-5 days after STZ injection. Table 5-1 shows the general characteristics of STZ-induced diabetic and Control rats including BGL, body weight, heart weight and heart weight to body weight ratio. Non-fasting BGL was significantly ($P < 0.05$) elevated in STZ rats compared to Controls. The body weight and heart weight of STZ rats were significantly ($P < 0.05$) lower compared to Controls. There was a significant ($P < 0.05$) increase in heart weight to body weight ratio in STZ rats compared to Controls.

	Control	STZ
Blood glucose level (mg/dl)	100.77 ± 2.07 (35)	452.09 ± 17.16 (35)*
Body weight (g)	351.60 ± 6.11 (35)	262.46 ± 5.96 (35)*
Heart weight (g)	1.19 ± 0.01 (35)	1.05 ± 0.02 (35)*
Heart weight : Body weight (mg/g)	3.40 ± 0.04 (35)	4.07 ± 0.08 (35)*

Table 5-1: General characteristics of STZ-induced diabetic rats and age-matched Controls

Results were analyzed using Independent Samples T-Test. Data are mean ± SEM. Numbers of animals are shown in parentheses, *$P < 0.05$.

5.2. Streptozotocin-Induced Diabetes Results

5.2.1. Effects of Streptozotocin-Induced Diabetes on Ventricular Myocyte Shortening

The effects of STZ-induced diabetes on shortening were investigated in STZ-induced diabetic and Control ventricular myocytes, stimulated electrically (1 Hz) and superfused with NT at 35-36 °C.

RCL, TPK shortening, THALF relaxation and AMP of shortening (expressed as a percentage of RCL) are shown in Figures 5-1A-D. RCL was significantly (Independent Samples T-Test; $P < 0.05$) reduced in STZ (123.30 ± 1.71, $n = 136$) myocytes compared to Controls (129.24 ± 1.88, $n = 140$) (Fig. 5-1A).TPK shortening was significantly (Independent Samples T-Test; $P < 0.05$) prolonged in STZ (126.74 ± 1.74, $n = 136$) myocytes compared to Controls (114.55 ± 1.63, $n = 140$) (Fig. 5-1B). There was no significant (Independent Samples T-Test; $P < 0.05$) difference in THALF relaxation in STZ myocytes compared to Controls (Fig. 5-1C). The AMP of shortening was significantly (Independent Samples T-Test; $P < 0.05$) reduced in STZ (6.60 ± 0.16, $n = 136$) myocytes compared to Controls (7.35 ± 0.20, $n = 140$) (Fig. 5-1D).

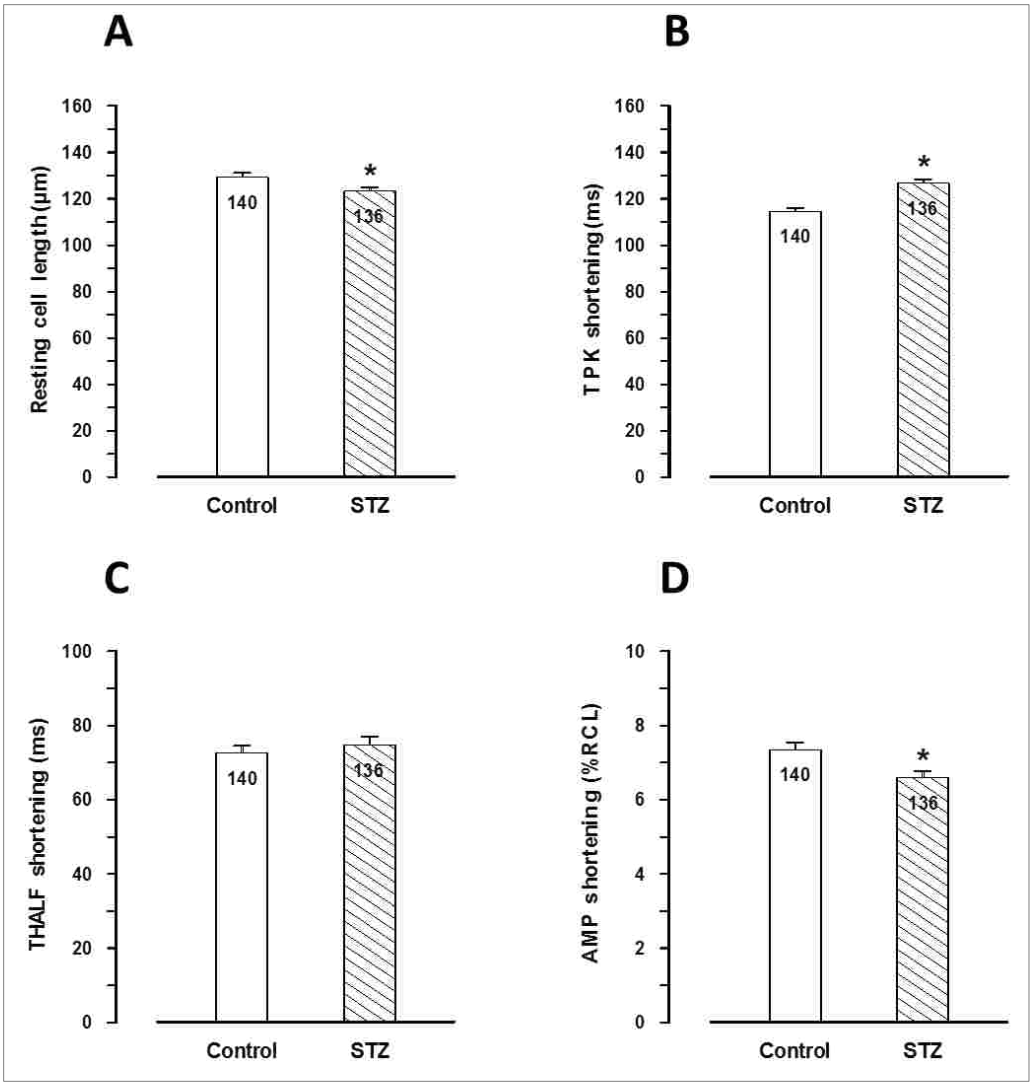

Figure 5-1: Effects of streptozotocin (STZ)-induced diabetes on the amplitude and time course of ventricular myocyte shortening

Graphs showing the mean:

(A) Resting cell length (RCL)
(B) Time to peak (TPK) shortening
(C) Time to half (THALF) relaxation of shortening
(D) Amplitude (AMP) of shortening

Results were analyzed using Independent Samples T-Test. Data are mean + S.E.M., *n* = 136-140 myocytes from 27-31 hearts. Asterisks above the bars represent significant differences at the level of $P < 0.05$.

5.2.2. Effects of Streptozotocin-Induced Diabetes on Ventricular Myocyte Intracellular Ca^{2+} Transient

The effects of STZ-induced diabetes on intracellular Ca^{2+} transient were investigated in Fura-2 AM-loaded STZ-induced diabetic and Control ventricular myocytes, stimulated electrically (1 Hz) and superfused with NT at 35-36 °C.

The resting Fura-2 ratio, TPK Ca^{2+} transient, THALF decay of the Ca^{2+} transient and AMP of the Ca^{2+} transient (expressed as a percentage of resting Fura-2 ratio) are shown in Figures 5-2A-D. The resting Fura-2 ratio was not significantly (Independent Samples T-Test; $P < 0.05$) altered in STZ myocytes compared to Controls (Fig. 5-2A). There was a significant (Independent Samples T-Test; $P < 0.05$) prolongation in TPK Ca^{2+} transient in STZ (63.87 ± 2.12, $n = 51$) myocytes compared to Controls (56.75 ± 1.24, $n = 83$) (Fig. 5-2B). THALF decay of the Ca^{2+} transient (Fig. 5-2C) and AMP of the Ca^{2+} transient (Fig. 5-2D) were not significantly (Independent Samples T-Test; $P < 0.05$) altered in STZ myocytes compared to Controls.

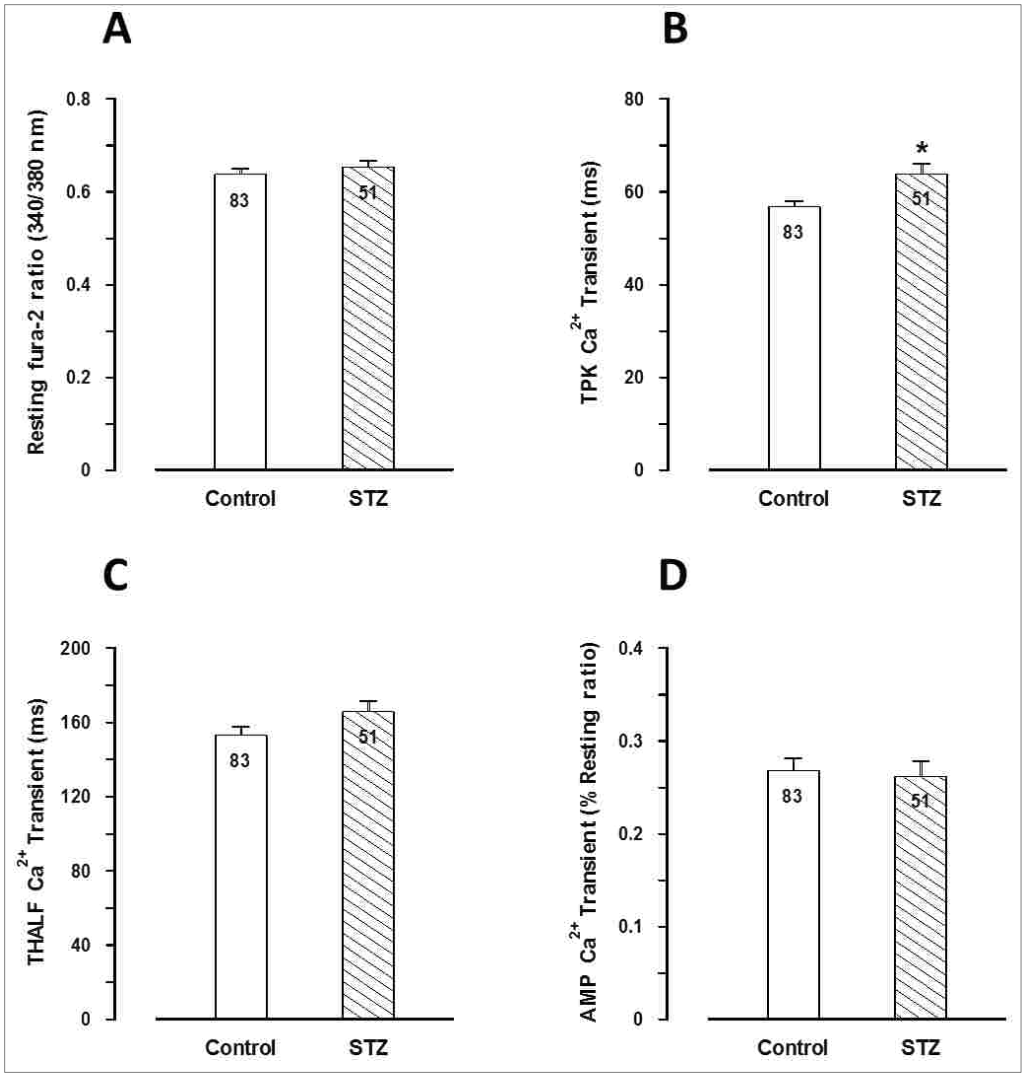

Figure 5-2: Effects of streptozotocin (STZ)-induced diabetes on the amplitude and time course of ventricular myocyte Ca^{2+} transient

Graphs showing the mean:

(A) Resting Fura-2 ratio
(B) Time to peak (TPK) Ca^{2+} transient
(C) Time to half (THALF) decay of the Ca^{2+} transient
(D) Amplitude (AMP) of the Ca^{2+} transient

Results were analyzed using Independent Samples T-Test. Data are mean + S.E.M., *n* = 51-83 myocytes from 16-24 hearts. Asterisks above the bars represent significant differences at the level of $P < 0.05$.

5.2.3. Effects of Streptozotocin-Induced Diabetes on Ventricular Myocyte Myofilament Sensitivity to Ca^{2+}

The effects of STZ-induced diabetes on myofilament response and sensitivity to Ca^{2+}, in STZ-induced diabetic and Control ventricular myocytes, were tested by recording myocyte shortening and intracellular Ca^{2+} transient simultaneously during superfusion with NT.

By measuring the gradient of the Fura-2-cell length trajectory, the relative myofilament response and sensitivity to Ca^{2+} were estimated during late relaxation of the twitch contraction during the period 500–800 ms. There was no significant (Independent Samples T-Test; $P < 0.05$) difference in the gradient of the trajectory in STZ myocytes compared to Controls (Fig. 5-3).

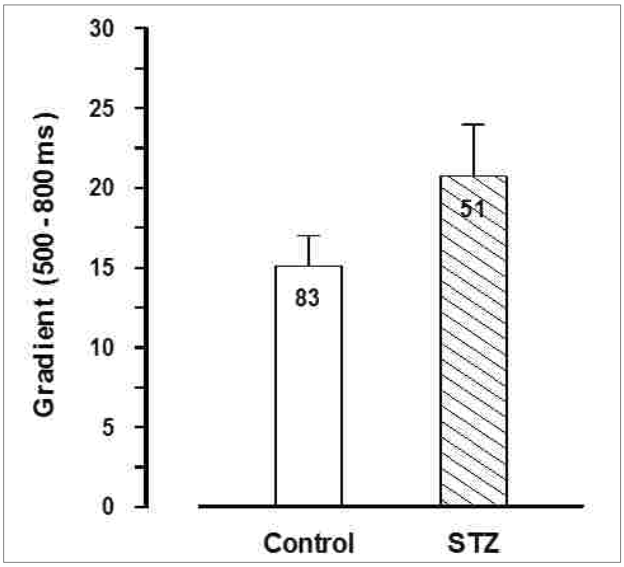

Figure 5-3: Effects of streptozotocin (STZ)-induced diabetes on ventricular myocyte myofilament sensitivity to Ca^{2+}

Graph showing mean gradient of the Fura-2-cell length trajectory during late relaxation of the twitch contraction during the period 500-800 ms. Results were analyzed using Independent Samples T-Test. Data are mean + S.E.M., n = 51-83 myocytes from 10-14 hearts.

5.2.4. Effects of Streptozotocin-Induced Diabetes on Ventricular Myocyte Sarcoplasmic Reticulum Ca^{2+} Transport

The effects of STZ-induced diabetes on SR Ca^{2+} transport were investigated in Fura-2 AM-loaded STZ-induced diabetic and Control ventricular myocytes after caffeine (20 mmol) application at 35-36 °C.

The protocol used in these experiments involved several steps starting with electrical stimulation of myocytes at 1 Hz. When the Ca^{2+} transients had stabilized, electrical stimulation was paused for 5 seconds. Caffeine was then applied using a rapid solution switching device for 10 seconds. Electrical stimulation was then resumed.

The SR Ca^{2+} was assessed by measuring the AMP of the caffeine-stimulated Ca^{2+} transient, fractional release of Ca^{2+} (measured as the relationship between the electrically-stimulated and caffeine-stimulated Ca^{2+} transients), and the gradient of myocyte recovery after caffeine application and following resumption of electrical stimulation (Fig. 5-4A-C). The AMP of caffeine-stimulated Ca^{2+} transient was significantly (Independent Samples T-Test; $P < 0.05$) reduced in STZ myocytes (0.489 ± 0.022, $n = 48$) compared to Controls (0.562 ± 0.024, $n = 62$) (Fig. 5-4A). Fractional release of Ca^{2+} did not show any significant (Independent Samples T-Test; $P < 0.05$) change in STZ myocytes compared to Controls (Fig. 5-4B). The gradient of myocyte recovery was also not significantly (Independent Samples T-Test; $P < 0.05$) altered in STZ myocytes compared to Controls (Fig. 5-4C).

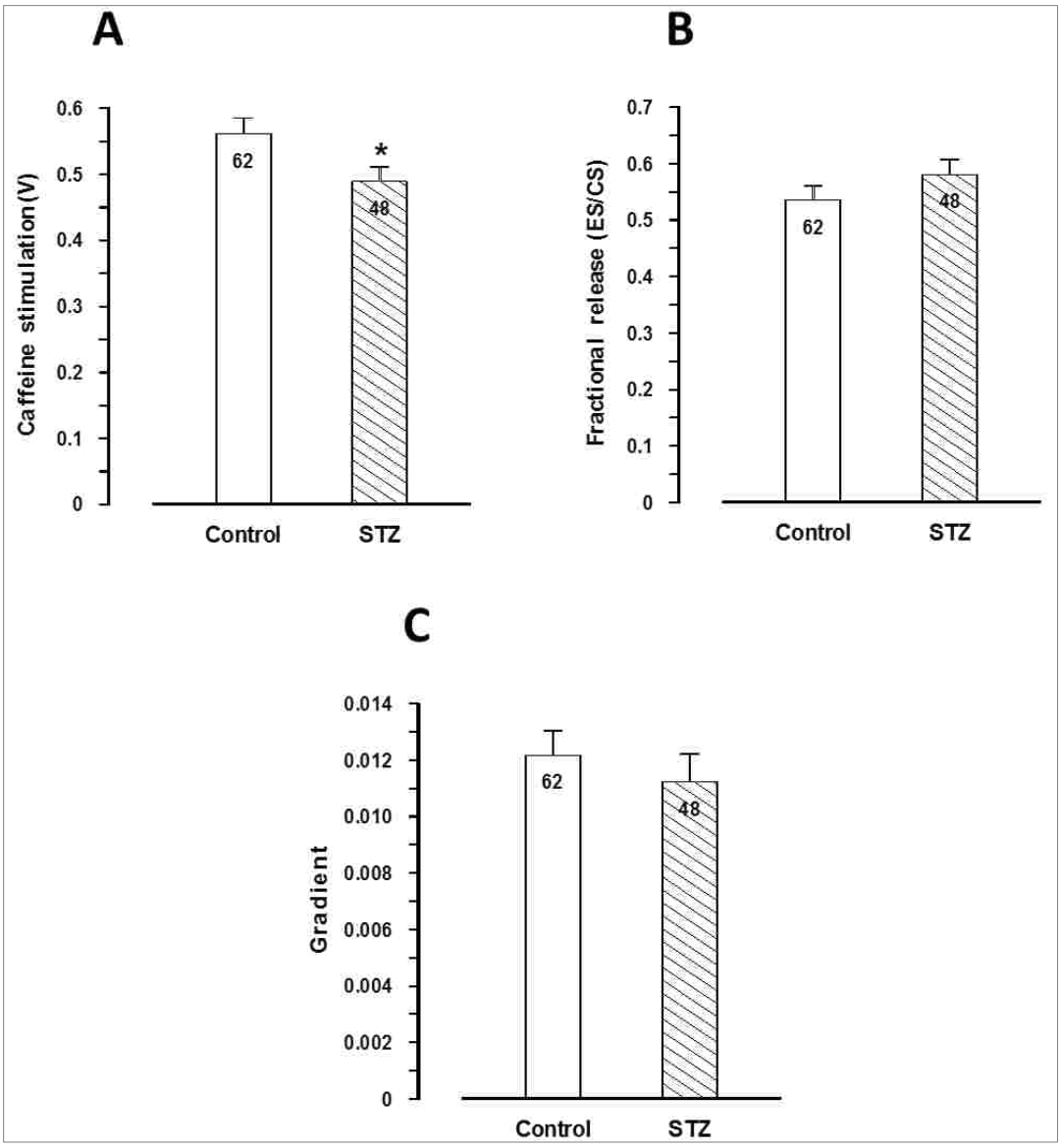

Figure 5-4: Effects of streptozotocin (STZ)-induced diabetes on ventricular myocyte sarcoplasmic reticulum Ca^{2+}

Graphs showing mean:

(A) Amplitude of caffeine-stimulated Ca^{2+} transient
(B) Fractional release of Ca^{2+} (Electrical stimulation/Caffeine stimulation)
(C) Recovery of the Ca^{2+} transients following rapid application of caffeine

Results were analyzed using Independent Samples T-Test. Data are mean + S.E.M., *n* = 48-62 myocytes from 10-13 hearts. Asterisks above the bars represent significant differences at the level of $P < 0.05$.

ES: electrical stimulation; **CS:** caffeine stimulation

5.3. Concentration-Response Experiments

In order to select a suitable concentration of the compound tested in the experiments, different concentrations of DAPA were tested on the AMP of shortening (expressed as a percentage of shortening in STZ and Control myocytes superfused with NT solution) in STZ-induced diabetic and Control ventricular myocytes during electrical stimulation (1 Hz) at 35-36°C (Fig. 5-5). Three concentrations (10^{-7} M, 10^{-6} M, and 10^{-5} M) of DAPA were tested. There were three stages in the protocol; myocytes were initially superfused with NT, then they were superfused with DAPA dissolved in NT for 5 minutes followed by NT washout for 5 minutes to assess reversibility, and the AMP of shortening was measured after each stage of the experiment.

Generally, the AMP of shortening was significantly (ANOVA; $P < 0.05$) reduced, to similar extents in STZ and Control myocytes, at concentrations 10^{-5} M and 10^{-6} M. No significant (ANOVA; $P < 0.05$) alteration was seen with 10^{-7} M DAPA in STZ and Control myocytes. As shown in Figure 5-5, there was a significant (ANOVA; $P < 0.05$) reduction in the AMP of shortening with 10^{-5} M DAPA in STZ/DAPA (78.59 ± 2.12%, $n = 26$) and Control/DAPA (73.42 ± 2.61%, $n = 25$) myocytes compared to STZ and Control (100%, $n = 87$-95) myocytes. Similarly, 10^{-6} M DAPA reduced the AMP of shortening significantly (ANOVA; $P < 0.05$) in STZ/DAPA (76.58 ± 1.89%, $n = 42$) and Control/DAPA (76.68 ± 2.28%, $n = 37$) myocytes compared to STZ and Control (100%, $n = 25$-95) myocytes, respectively (Fig. 5-5). However, there was no significant (ANOVA; $P < 0.05$) alteration in the AMP of shortening seen with 10^{-7} M DAPA in both STZ and Control myocytes (Fig.

5-5). It should be noted that although both DAPA concentrations 10^{-5} M and 10^{-6} M showed significant (ANOVA; $P < 0.05$) response, there was no significant (ANOVA; $P < 0.05$) difference between both concentrations in their effects (Fig. 5-5). Therefore, 10^{-6} M was used in all subsequent experiments.

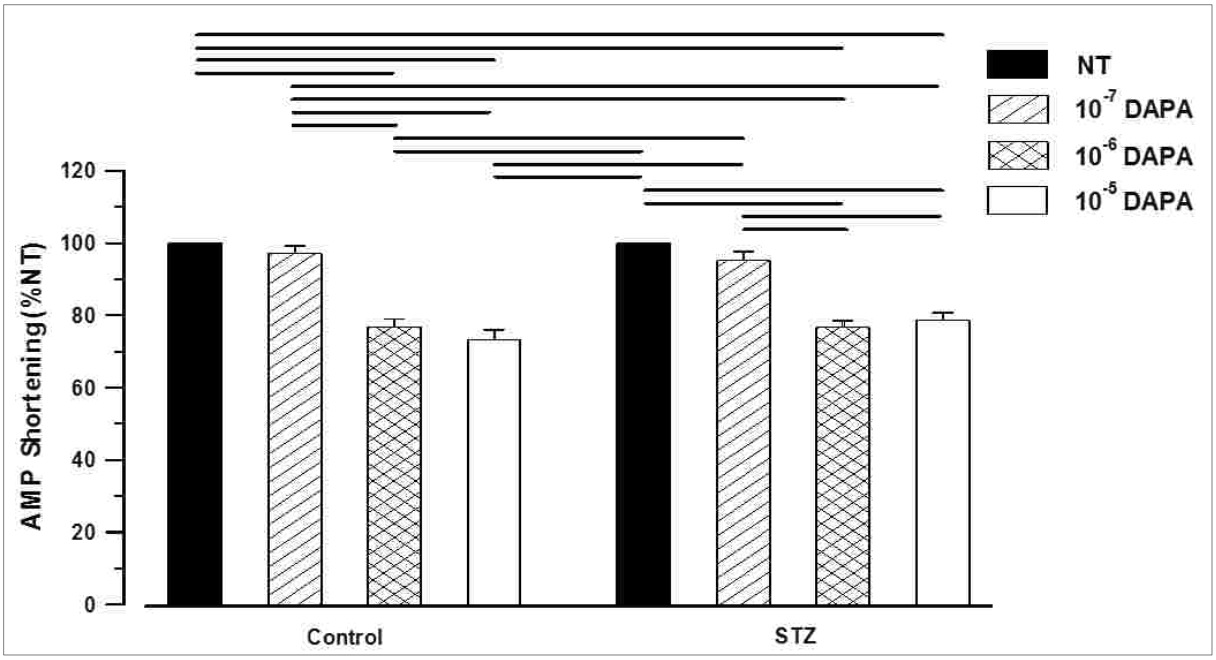

Figure 5-5: Effects of Dapagliflozin (DAPA) different concentrations on ventricular myocyte amplitude of shortening

Graph showing the mean amplitudes (AMP) of shortening, expressed as a percentage of shortening in STZ and Control myocytes superfused with normal Tyrode (NT) and in the presence of different concentrations of DAPA.

Results were analyzed using ANOVA and *post hoc* Bonferoni test. Data are means + S.E.M., n = 182 myocytes from 30 hearts. Horizontal lines above the bars represent significant differences at the level of $P < 0.05$.

5.4. Phlorizin Results

5.4.1. Effects of Phlorizin on Ventricular Myocyte Shortening

The effects of 10^{-6} M PHLOR on shortening were investigated in STZ-induced diabetic and Control ventricular myocytes during electrical stimulation (1 Hz) at 35-36 °C.

Figure 5-6A shows typical records of shortening in a Control myocyte. Myocytes were superfused with NT, then with 10^{-6} M PHLOR dissolved in NT for 5 minutes followed by NT washout for 5 minutes to assess reversibility. The effects of PHLOR, on RCL, TPK shortening, THALF relaxation and AMP of shortening (expressed as a percentage of shortening in STZ and Control myocytes superfused with NT) are shown in Figures 5-6B-E. There was no significant (ANOVA; $P < 0.05$) difference in RCL (Fig. 5-6B), TPK shortening (Fig. 5-6C) and THALF relaxation (Fig. 5-6D) by PHLOR in STZ and Control myocytes. However, PHLOR resulted in a significant (ANOVA; $P < 0.05$) reduction in the AMP of shortening in STZ/PHLOR (84.76 ± 2.91%, $n = 20$) and Control/PHLOR (83.72 ± 2.65%, $n = 23$) myocytes compared to STZ and Control (100%, $n = 21$-23) myocytes, respectively (Fig. 5-6E).

The AMP of shortening partially recovered in a few STZ myocytes from 72.58 ± 10.76% ($n = 2$) with PHLOR to 88.99 ± 21.72% ($n = 2$) after washout and in some Control myocytes from 80.77 ± 4.17% ($n = 10$) with PHLOR to 87.32 ± 3.73% ($n = 10$) after washout. Collectively, recovery was approximately 16% in STZ myocytes and 6% in Controls after washout. While it continued to decrease (no

recovery) in some STZ myocytes from 88.81 ± 1.81% (*n* = 9) with PHLOR to 82.85 ± 2.42% (*n* = 8) after washout and in some Control myocytes from 84.34 ± 4.33% (*n* = 5) with PHLOR to 80.10 ± 3.66% (*n* = 5) after washout.

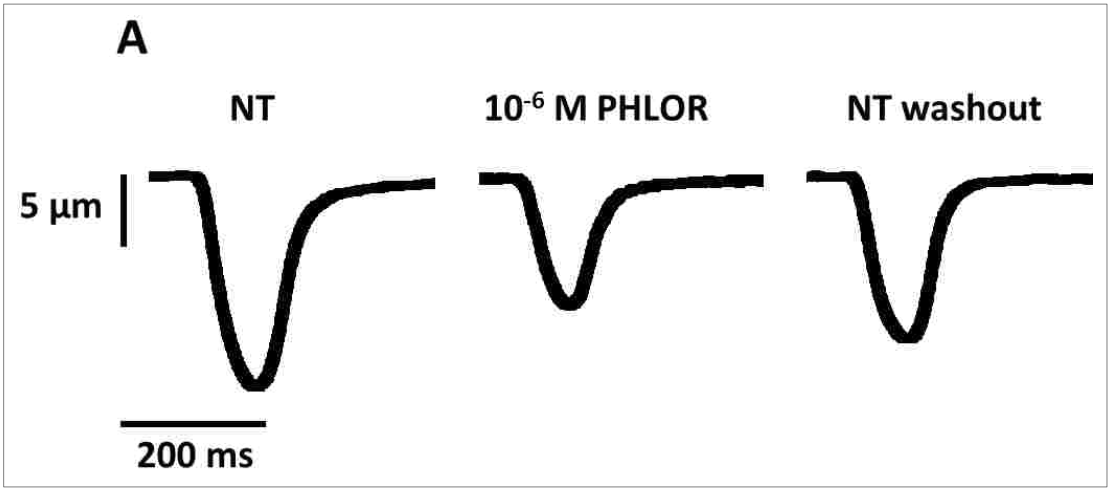

Figure 5-6: Effects of Phlorizin (PHLOR) on the amplitude and time course of ventricular myocyte shortening

(A) Typical records of shortening in a Control myocyte superfused with normal Tyrode (NT) (left panel), 10^{-6} M PHLOR + NT (middle panel) and during washout with NT (right panel)

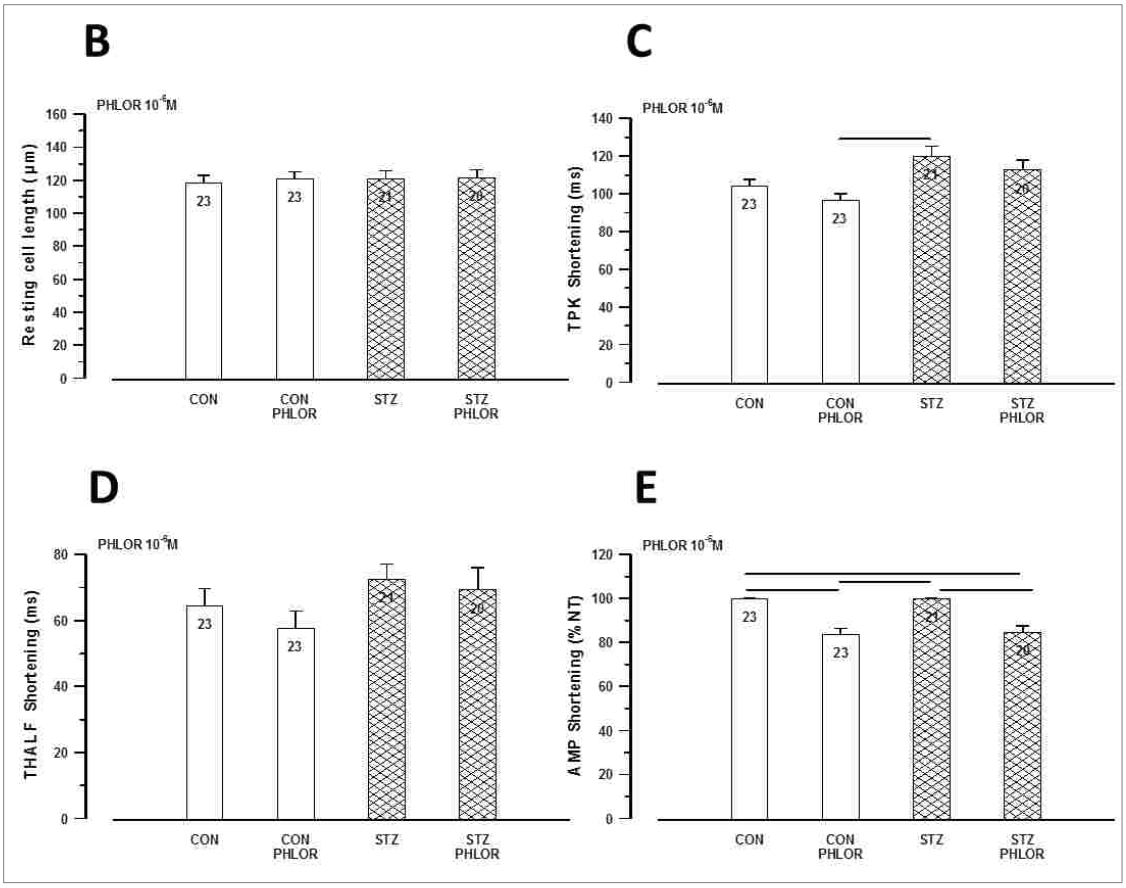

Figure 5-6 (continued): Effects of Phlorizin (PHLOR) on the amplitude and time course of ventricular myocyte shortening

Graphs showing the mean:

(B) Resting cell length
(C) Time to peak (TPK) shortening
(D) Time to half (THALF) relaxation of shortening
(E) Amplitude (AMP) of shortening

Results were analyzed using ANOVA and *post hoc* Bonferoni test. Data are mean + S.E.M., n = 23-20 myocytes from 7 hearts. Horizontal lines above the bars represent significant differences at the level of $P < 0.05$.

5.4.2. Effects of Phlorizin on Ventricular Myocyte Intracellular Ca^{2+} Transient

The effects of 10^{-6} M PHLOR on intracellular Ca^{2+} transient were investigated in Fura-2 AM-loaded STZ-induced diabetic and Control ventricular myocytes, stimulated electrically (1 Hz) at 35-36 °C.

Typical records of the Ca^{2+} transient in a Control myocyte, superfused with NT and then 10^{-6} M PHLOR dissolved in NT for 5 minutes, are shown in Figure 5-7A.

The resting Fura-2 ratio, TPK Ca^{2+} transient, THALF decay of the Ca^{2+} transient and AMP of the Ca^{2+} transient (expressed as a percentage of Ca^{2+} transient in STZ and Control myocytes superfused with NT) are shown in Figures 5-7B-E. There was no significant (ANOVA; $P < 0.05$) change in the resting Fura-2 ratio (Fig. 5-7B), TPK Ca^{2+} transient (Fig. 5-7C) and THALF decay of the Ca^{2+} transient (Fig. 5-7D) in both STZ and Control myocytes after exposure to PHLOR. The AMP of the Ca^{2+} transient was significantly (ANOVA; $P < 0.05$) reduced in STZ/PHLOR (82.37 ± 3.16%, n = 16) and Control/PHLOR (73.94 ± 5.22%, n = 21) myocytes compared to STZ and Control (100%, n = 16-23) myocytes, respectively (Fig. 5-7E).

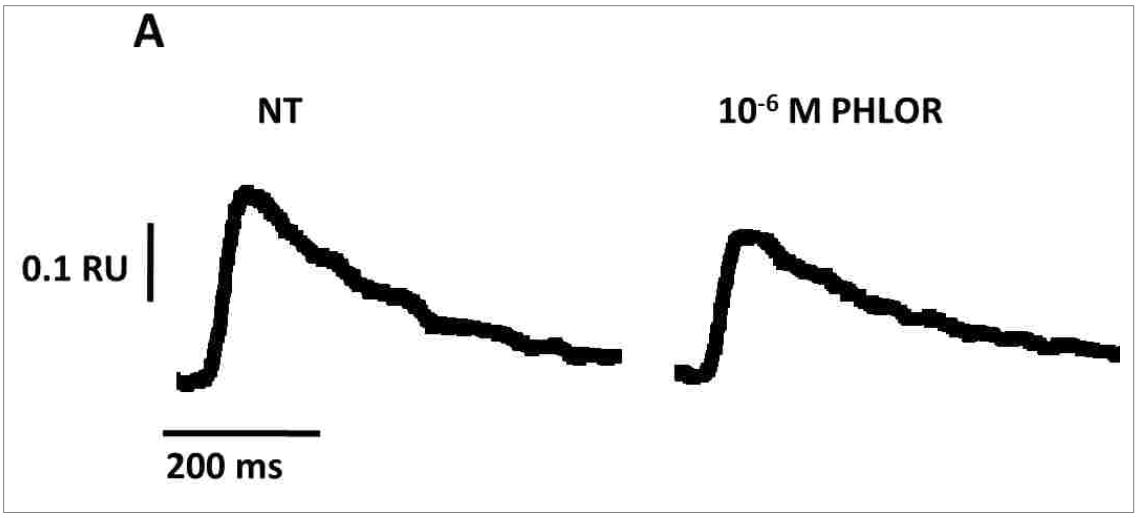

Figure 5-7: Effects of Phlorizin (PHLOR) on the amplitude and time course of ventricular myocyte Ca^{2+} transient

(A) Typical records of Ca^{2+}transient in a Control myocyte superfused with normal Tyrode (NT) (left panel) and 10^{-6} M PHLOR + NT (right panel)

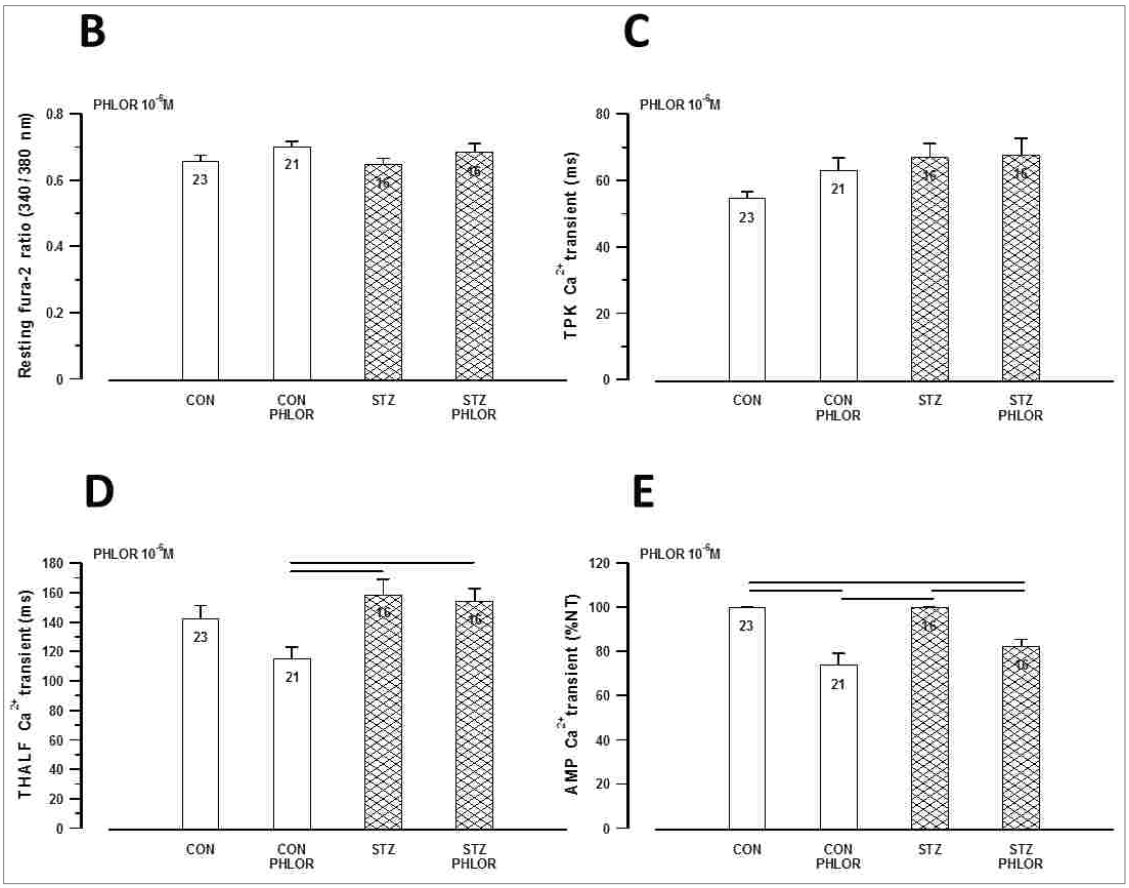

Figure 5-7 (continued): Effects of Phlorizin (PHLOR) on the amplitude and time course of ventricular myocyte Ca^{2+} transient

Graphs showing the mean:

(B) Resting Fura-2 ratio
(C) Time to peak (TPK) Ca^{2+} transient
(D) Time to half (THALF) decay of the Ca^{2+} transient
(E) Amplitude (AMP) of the Ca^{2+} transient

Results were analyzed using ANOVA and *post hoc* Bonferoni test. Data are mean + S.E.M., n = 16-23 myocytes from 3-4 hearts. Horizontal lines above the bars represent significant differences at the level of $P < 0.05$.

5.4.3. Effects of Phlorizin on Ventricular Myocyte Myofilament Sensitivity to Ca^{2+}

The effects of 10^{-6} M PHLOR were investigated on myofilament response and sensitivity to Ca^{2+} in STZ-induced diabetic and Control ventricular myocytes.

In these experiments, myocyte shortening and intracellular Ca^{2+} transient were recorded simultaneously after superfusion with NT and after 5 minutes of superfusion with 10^{-6} M PHLOR dissolved in NT. Figure 5-8A shows a typical record of myocyte shortening and Ca^{2+} transient, and Figure 5-8B shows a typical phase-plane diagram of Fura-2 ratio versus cell length recorded in a Control myocyte superfused with NT.

The relative myofilament response and sensitivity to Ca^{2+} were assessed by measuring the gradient of the Fura-2-cell length trajectory during late relaxation of the twitch contraction. The gradient of the trajectory was measured during the period 500–800 ms. As shown in Figure 5-8C, there were no significant (ANOVA; $P < 0.05$) differences in myofilament sensitivity in STZ and Control myocytes with PHLOR.

Therefore, myofilament sensitivity to Ca^{2+} is unlikely to underlie the effects of PHLOR on myocyte contraction.

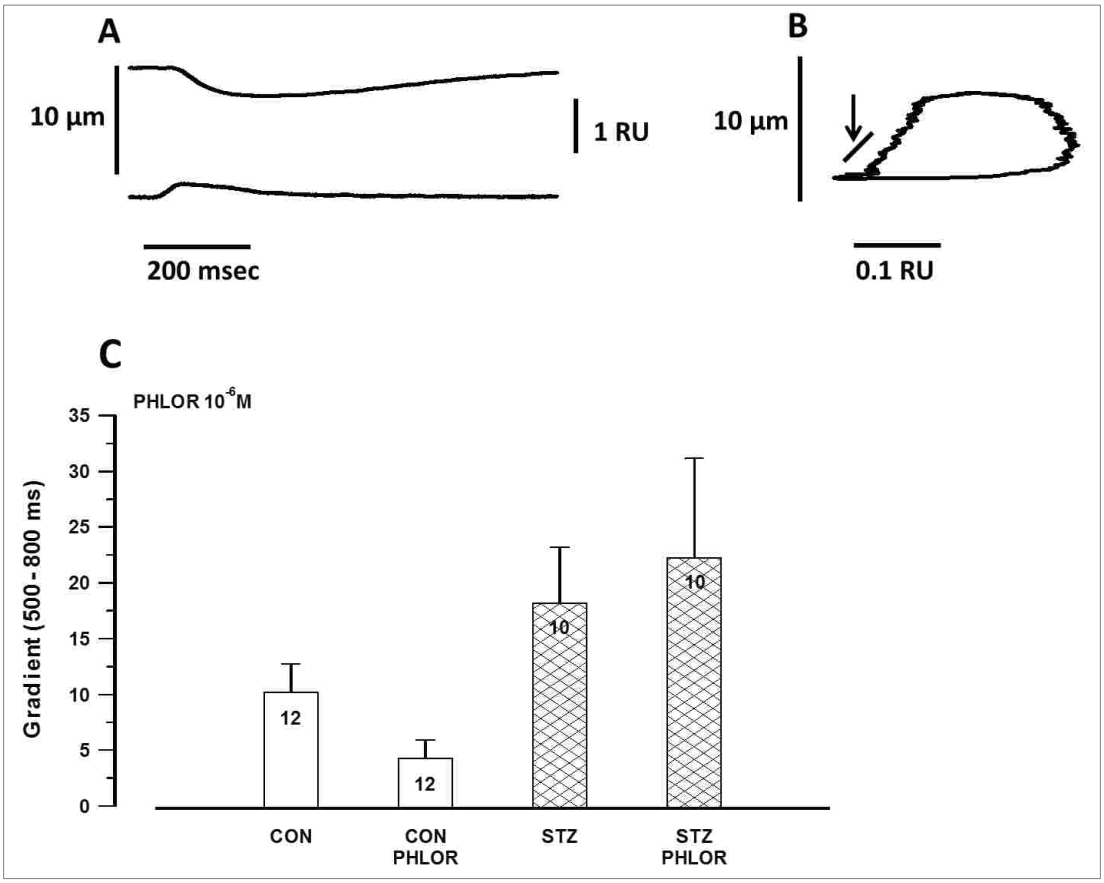

Figure 5-8: Effects of Phlorizin (PHLOR) on ventricular myocyte myofilament sensitivity to Ca^{2+}

(A) Typical record of shortening and Ca^{2+} transient recorded simultaneously in an electrically stimulated myocyte from a Control heart

(B) Typical phase plane diagram of Fura-2 ratio unit (RU) versus cell length in a myocyte from a Control heart. The arrow indicates the region where the gradient was measured

(C) Graph showing mean gradient of the Fura-2-cell length trajectory during late relaxation of the twitch contraction during the period 500-800 ms

Results were analyzed using ANOVA and *post hoc* Bonferoni test. Data are mean + S.E.M., *n* = 10-12 myocytes from 3-4 hearts.

5.4.4. Effects of Phlorizin on Ventricular Myocyte Sarcoplasmic Reticulum Ca^{2+} Transport

The effects of 10^{-6} M PHLOR on SR Ca^{2+} transport were investigated in Fura-2 AM-loaded STZ-induced diabetic and Control ventricular myocytes, when exposed to 20 mmol of caffeine at 35-36 °C.

A typical record of the protocol used in these experiments is shown in a Control myocyte superfused with NT in Figure 5-9A. Initially, myocytes were electrically stimulated at 1 Hz. When the Ca^{2+} transients had stabilized, electrical stimulation was paused for 5 seconds. Caffeine was then applied using a rapid solution switching device for 10 seconds. Electrical stimulation was then resumed. This protocol was repeated after the cell was superfused with NT and again after 5 minute superfusion of 10^{-6} M PHLOR dissolved in NT.

The AMP of the caffeine-stimulated Ca^{2+} transient was not significantly (ANOVA; $P < 0.05$) altered by PHLOR in STZ and Control myocytes (Fig. 5-9B). Fractional release of Ca^{2+}, measured as the relationship between the electrically-stimulated and caffeine-stimulated Ca^{2+} transients, did not show any significant (ANOVA; $P < 0.05$) change in STZ and Control myocytes with PHLOR (Fig. 5-9C). The gradient of myocyte recovery, after caffeine application and following resumption of electrical stimulation, was also not significantly (ANOVA; $P < 0.05$) altered by PHLOR in STZ and Control myocytes (Fig. 5-9D).

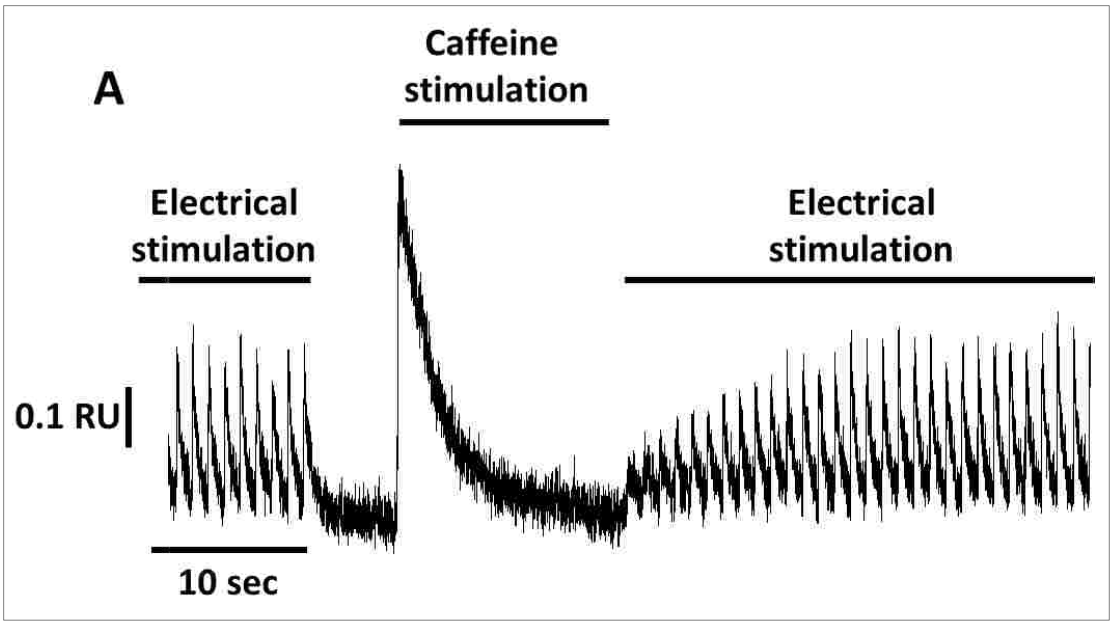

Figure 5-9: Effects of Phlorizin (PHLOR) on ventricular myocyte sarcoplasmic reticulum Ca^{2+}

(A) Typical record showing the protocol employed in a Control myocyte during SR Ca^{2+} experiments. Initially, myocytes were electrically stimulated at 1 Hz. When the Ca^{2+} transients had stabilized, electrical stimulation was paused for 5 seconds (sec). Caffeine was rapidly applied for 10 sec. Electrical stimulation was then resumed.

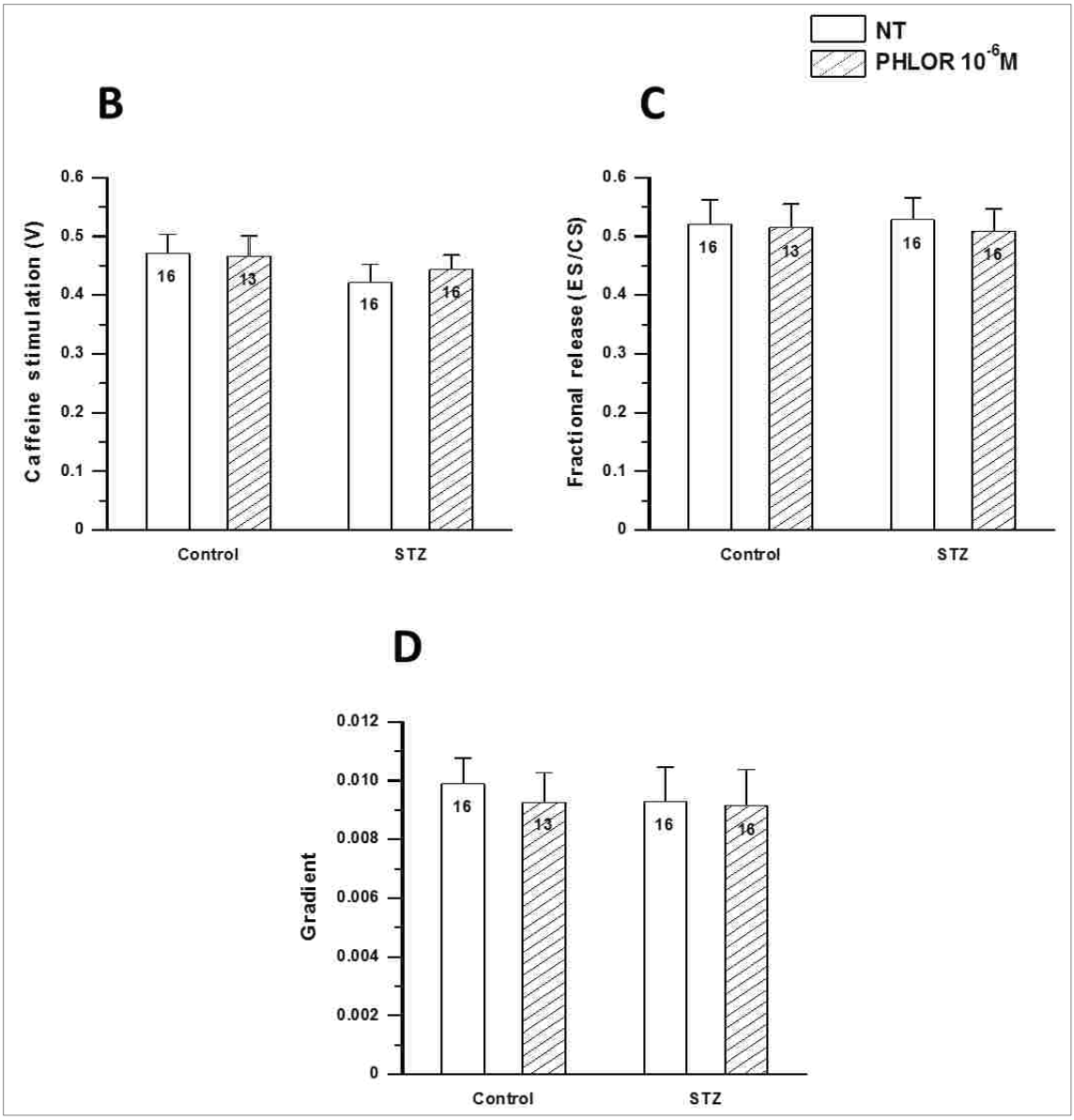

Figure 5-9 (continued): Effects of Phlorizin (PHLOR) on ventricular myocyte sarcoplasmic reticulum Ca^{2+}

Graphs showing mean:

(B) Amplitude of caffeine-stimulated Ca^{2+} transient
(C) Fractional release of Ca^{2+} (Electrical stimulation/Caffeine stimulation)
(D) Recovery of the Ca^{2+} transients following rapid application of caffeine

Results were analyzed using ANOVA and *post hoc* Bonferoni test. Data are mean + S.E.M., *n* = 13-16 myocytes from 3-4 hearts.

ES: electrical stimulation; **CS:** caffeine stimulation

5.5. Quercetin-3-O-Glucoside Results

5.5.1. Effects of Quercetin-3-O-Glucoside on Ventricular Myocyte Shortening

The effects of 10^{-6} M QUER-3-G on shortening, in electrically stimulated (1 Hz) STZ-induced diabetic and Control ventricular myocytes at 35-36°C, were investigated.

Typical records of shortening, in a Control myocyte superfused with NT followed by NT + 10^{-6} M QUER-3-G for 5 minutes and then NT washout for 5 minutes to assess recovery, are shown in Figure 5-10A. The effects of QUER-3-G on RCL, TPK shortening, THALF relaxation and AMP of shortening (expressed as a percentage of shortening in Control and STZ myocytes superfused with NT) are shown in Figures 5-10B-E. RCL was not significantly (ANOVA; $P < 0.05$) altered by QUER-3-G in STZ and Control myocytes (Fig. 5-10B). TPK shortening was significantly (ANOVA; $P < 0.05$) reduced on exposure to QUER-3-G from 129.65 ± 3.91 ms (n = 20) in STZ myocytes to 109.80 ± 3.34 (n = 20) in STZ/QUER-3-G myocytes, and from 114.37 ± 3.34 ms (n = 30) in Controls to 98.40 ± 3.18 (n = 30) in Control/QUER-3-G myocytes (Fig. 5-10C). THALF relaxation did not show any significant (ANOVA; $P < 0.05$) change in STZ and Control myocytes with QUER-3-G (Fig. 5-10D). The AMP of shortening was significantly (ANOVA; $P < 0.05$) decreased in STZ/QUER-3-G (79.12 ± 2.28%, n = 20) and Control/QUER-3-G (76.69 ± 1.92%, n = 30) myocytes compared to STZ and Control (100%, n = 20-30) myocytes, respectively (Fig. 5-10E).

The AMP of shortening partially recovered in some STZ myocytes from 76.78 ± 3.11% (*n* = 7) with QUER-3-G to 91.82 ± 9.49% (*n* = 7) after washout and in some Control myocytes from 75.04 ± 4.47% (*n* = 5) with QUER-3-G to 94.87 ± 6.87% (*n* = 5) after washout. Collectively, recovery was approximately 15% in STZ myocytes and 10% in Controls after washout. While it continued to decrease (no recovery) in some STZ myocytes from 79.56 ± 3.86% (*n* = 10) with QUER-3-G to 73.32 ± 3.35% (*n* = 9) after washout and in some Control myocytes from 76 ± 3.12% (*n* = 14) with QUER-3-G to 67.86 ± 4.38% (*n* = 12) after washout.

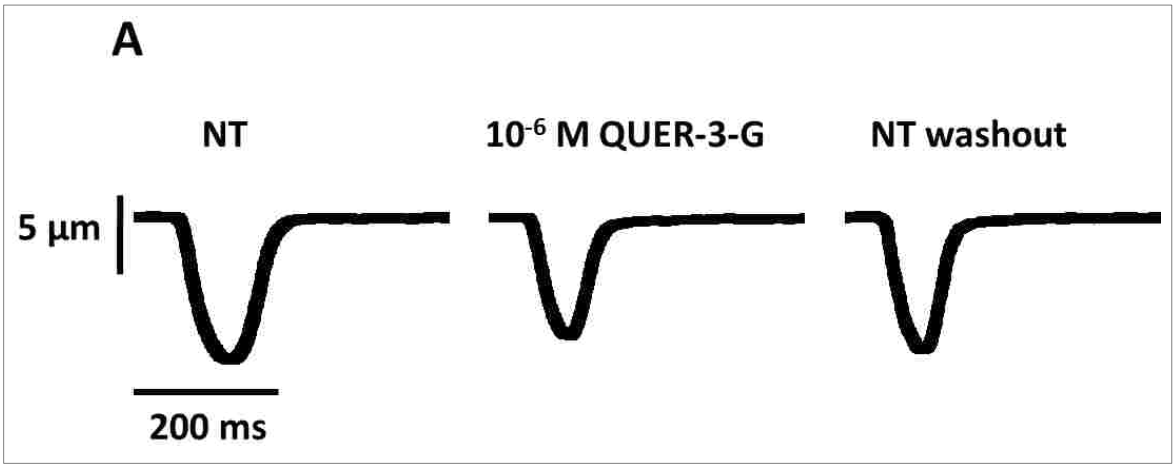

Figure 5-10: Effects of Quercetin-3-O-glucoside (QUER-3-G) on the amplitude and time course of ventricular myocyte shortening

(A) Typical records of shortening in a Control myocyte superfused with normal Tyrode (NT) (left panel), 10^{-6} M QUER-3-G + NT (middle panel) and during washout with NT (right panel)

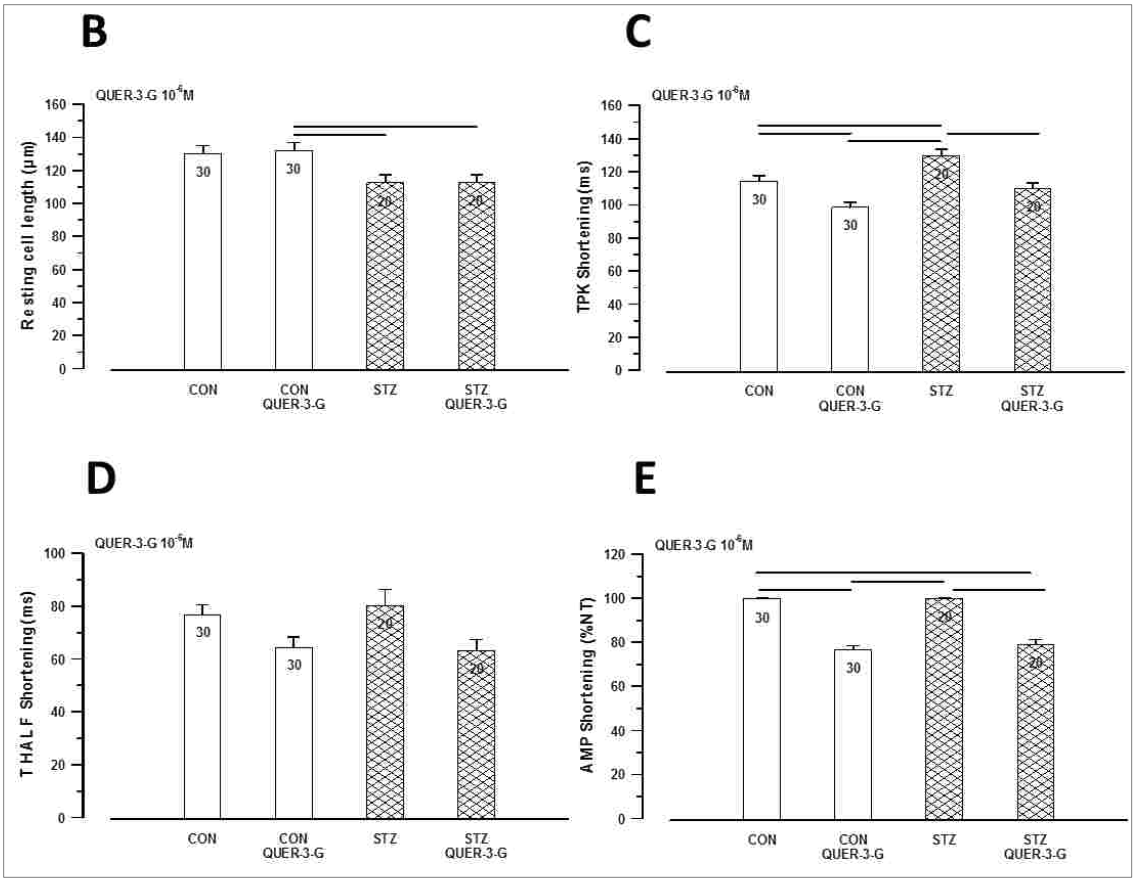

Figure 5-10 (continued): Effects of Quercetin-3-O-glucoside (QUER-3-G) on the amplitude and time course of ventricular myocyte shortening

Graphs showing the mean:

(B) Resting cell length
(C) Time to peak (TPK) shortening
(D) Time to half (THALF) relaxation of shortening
(E) Amplitude (AMP) of shortening

Results were analyzed using ANOVA and *post hoc* Bonferoni test. Data are mean + S.E.M., n = 20-30 myocytes from 6-9 hearts. Horizontal lines above the bars represent significant differences at the level of $P < 0.05$.

5.5.2. Effects of Quercetin-3-O-Glucoside on Ventricular Myocyte Intracellular Ca^{2+} Transient

The effects of 10^{-6} M QUER-3-G on intracellular Ca^{2+} transient were studied in electrically stimulated (1Hz) and Fura-2 AM-loaded STZ-induced diabetic and Control ventricular myocytes at 35-36 °C.

Typical records of the Ca^{2+} transient, in a Control myocyte exposed to NT and to 10^{-6} M QUER-3-G + NT for 5 minutes, are shown in Figure 5-11A.

The effects of QUER-3-G on the resting Fura-2 ratio, TPK Ca^{2+} transient, THALF decay of the Ca^{2+} transient and AMP of the Ca^{2+} transient (expressed as a percentage of Ca^{2+} transient in STZ and Control myocytes superfused with NT) are shown in Figure 5-11B-E. There was a significant (ANOVA; $P < 0.05$) increase in the resting Fura-2 ratio of Control/QUER-3-G (0.757 ± 0.025, n = 41) myocytes compared to Controls (0.661 ± 0.018, n = 41), while there was no significant (ANOVA; $P < 0.05$) difference between STZ/QUER-3-G and STZ myocytes (Fig. 5-11B). TPK Ca^{2+} transient was not significantly (ANOVA; $P < 0.05$) altered in STZ and Control myocytes after QUER-3-G (Fig. 5-11C). THALF decay of the Ca^{2+} transient showed significant (ANOVA; $P < 0.05$) reduction in STZ/QUER-3-G (130.94 ± 10.72 ms, n = 18) myocytes compared to STZ (182.06 ± 9.74 ms, n = 18) myocytes, and in Control/QUER-3-G (117.81±5.52 ms, n = 41) myocytes compared to Controls (155.83±6.02 ms, n = 41) (Fig. 5-11D). The AMP of the Ca^{2+} transient was also decreased significantly (ANOVA; $P < 0.05$) in STZ/QUER-3-G (73.62 ± 5.83%, n = 18) and Control/QUER-3-G (78.32 ± 3.54%, n = 41) myocytes compared to STZ and Control (100%, n = 41-18) myocytes, respectively (Fig. 5-11E).

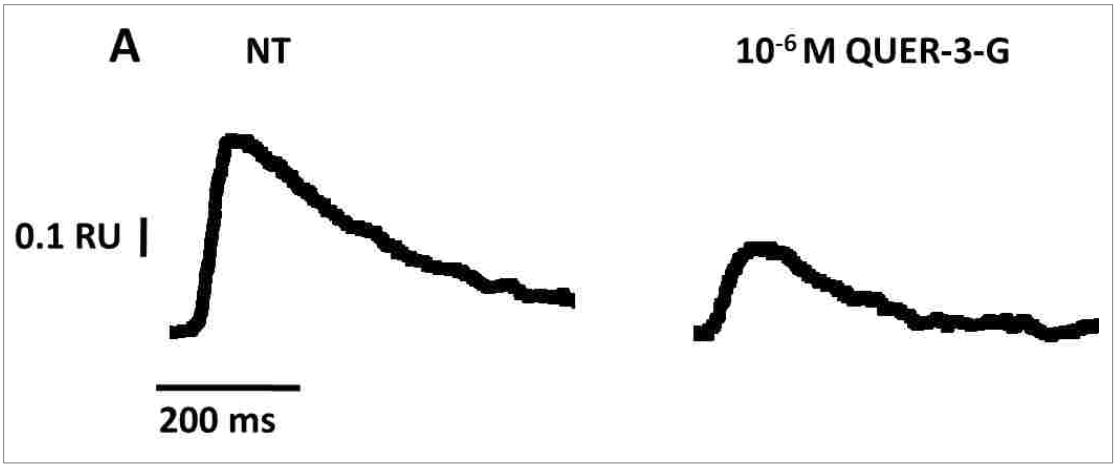

Figure 5-11: Effects of Quercetin-3-O-glucoside (QUER-3-G) on the amplitude and time course of ventricular myocyte Ca^{2+} transient

(A) Typical records of Ca^{2+}transient in a Control myocyte superfused with normal Tyrode (NT) (left panel) and 10^{-6} M QUER-3-G + NT (right panel)

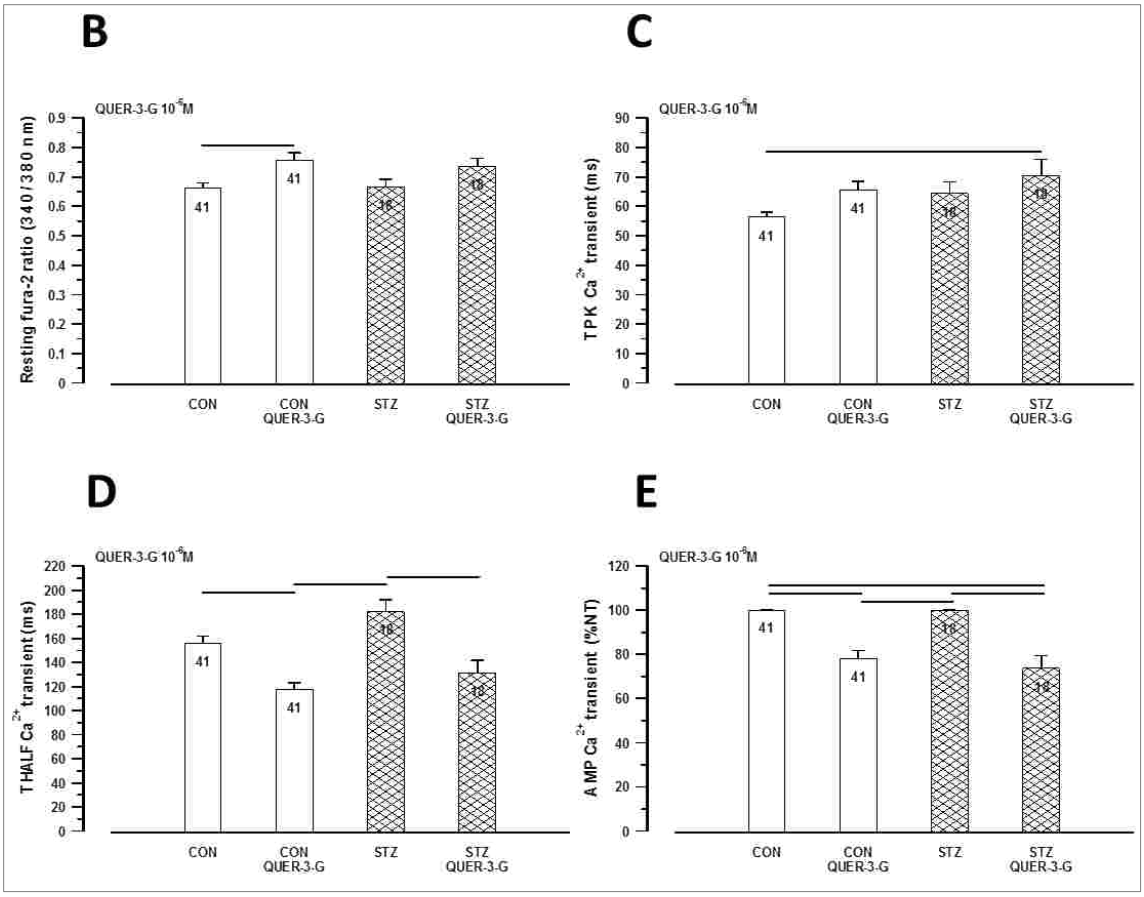

Figure 5-11 (continued): Effects of Quercetin-3-O-glucoside (QUER-3-G) on the amplitude and time course of ventricular myocyte Ca^{2+} transient

Graphs showing the mean:

(B) Resting Fura-2 ratio
(C) Time to peak (TPK) Ca^{2+} transient
(D) Time to half (THALF) decay of the Ca^{2+} transient
(E) Amplitude (AMP) of the Ca^{2+} transient

Results were analyzed using ANOVA and *post hoc* Bonferoni test. Data are mean + S.E.M., n = 18-41 myocytes from 3-6 hearts. Horizontal lines above the bars represent significant differences at the level of $P < 0.05$.

5.5.3. Effects of Quercetin-3-O-Glucoside on Ventricular Myocyte Myofilament Sensitivity to Ca^{2+}

The effects of 10^{-6} M QUER-3-G on myofilament response and sensitivity to Ca^{2+}, in STZ-induced diabetic and Control ventricular myocytes, were tested by recording myocyte shortening and intracellular Ca^{2+} transient simultaneously during superfusion with NT and with 10^{-6} M QUER-3-G + NT.

Figure 5-12A shows a typical record of myocyte shortening and Ca^{2+} transient, and Figure 5-12B shows a typical phase-plane diagram of Fura-2 ratio versus cell length recorded in a Control myocyte superfused with NT.

By measuring the gradient of the Fura-2-cell length trajectory, the relative myofilament response and sensitivity to Ca^{2+} were estimated during late relaxation of the twitch contraction during the period 500–800 ms. The gradient of the trajectory was modestly decreased in STZ/QUER-3-G (2.23 ± 2.05 ms, n = 12) myocytes compared to STZ (12.81 ± 5.30 ms, n = 12) myocytes, and it was significantly (ANOVA; $P < 0.05$) decreased in Control/QUER-3-G (4.19 ± 1.24 ms, n = 29) myocytes compared to Controls (12.69 ± 2.57 ms, n = 29) (Fig. 5-12C).

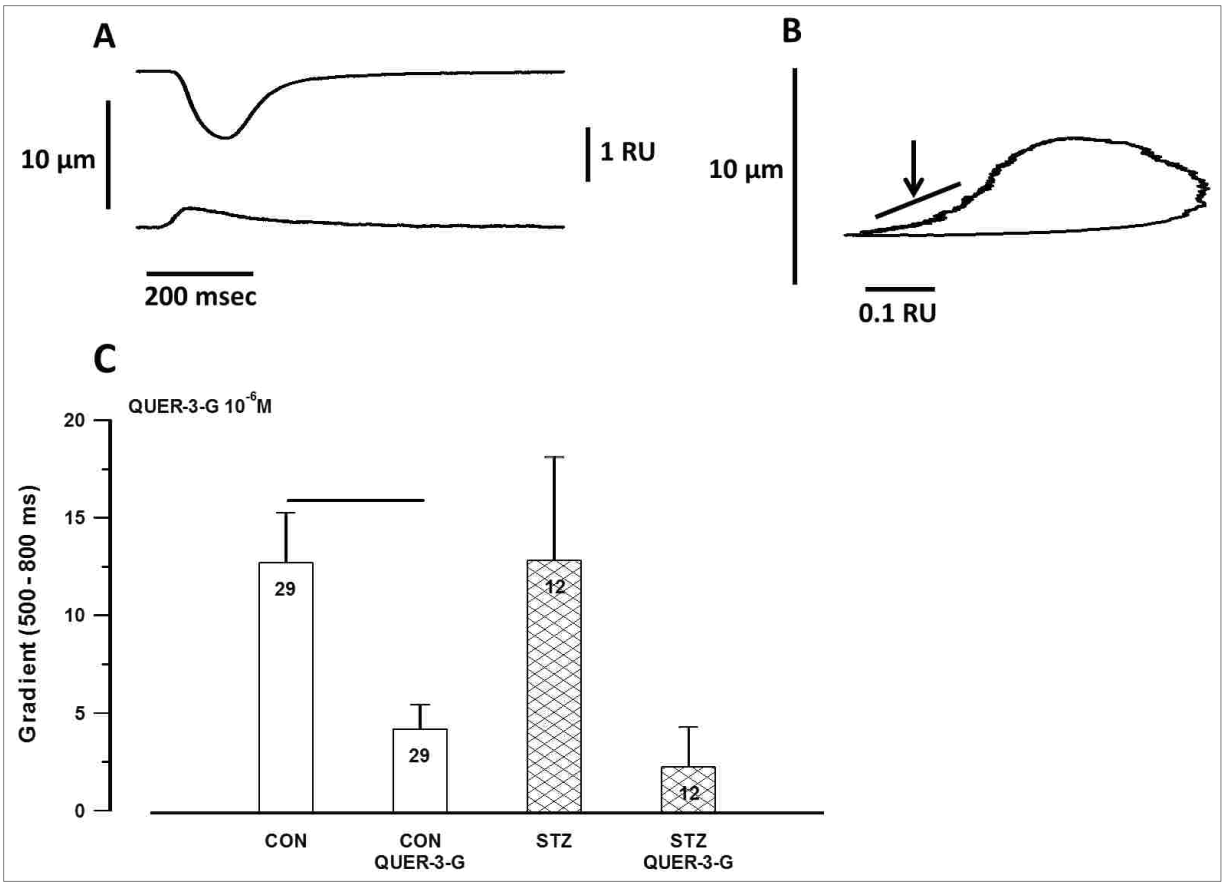

Figure 5-12: Effects of Quercetin-3-O-glucoside (QUER-3-G) on ventricular myocyte myofilament sensitivity to Ca^{2+}

(A) Typical record of shortening and Ca^{2+} transient recorded simultaneously in an electrically stimulated myocyte from a Control heart

(B) Typical phase plane diagram of Fura-2 ratio unit (RU) versus cell length in a myocyte from a Control heart. The arrow indicates the region where the gradient was measured

(C) Graph showing mean gradient of the Fura-2-cell length trajectory during late relaxation of the twitch contraction during the period 500-800 ms

Results were analyzed using ANOVA and *post hoc* Bonferoni test. Data are mean + S.E.M., n = 12-29 myocytes from 3-6 hearts. Horizontal lines above the bars represent significant differences at the level of $P < 0.05$.

5.5.4. Effects of Quercetin-3-O-Glucoside on Ventricular Myocyte Sarcoplasmic Reticulum Ca^{2+} Transport

The effects of 10^{-6} M QUER-3-G on SR Ca^{2+} transport were investigated in Fura-2 AM-loaded STZ-induced diabetic and Control ventricular myocytes after caffeine (20 mmol) application at 35-36 °C.

A typical record of the protocol used in these experiments is shown in a Control myocyte superfused with NT in Figure 5-13A. Initially, myocytes were electrically stimulated at 1 Hz. When the Ca^{2+} transients had stabilized, electrical stimulation was paused for 5 seconds. Caffeine was then applied using a rapid solution switching device for 10 seconds. Electrical stimulation was then resumed. This protocol was repeated after the cell was superfused with NT and again after 5 minute superfusion of 10^{-6} M QUER-3-G dissolved in NT.

The AMP of the caffeine-stimulated Ca^{2+} transient was not significantly (ANOVA; $P < 0.05$) altered by QUER-3-G in STZ and Controls myocytes (Fig. 5-13B). Fractional release of Ca^{2+}, measured as the relationship between the electrically-stimulated and caffeine-stimulated Ca^{2+} transients, did not show any significant (ANOVA; $P < 0.05$) change in STZ and Control myocytes with QUER-3-G (Fig. 5-13C). The gradient of myocyte recovery, after caffeine application and following resumption of electrical stimulation, was also not significantly (ANOVA; $P < 0.05$) changed by QUER-3-G in STZ and Control myocytes (Fig. 5-13D).

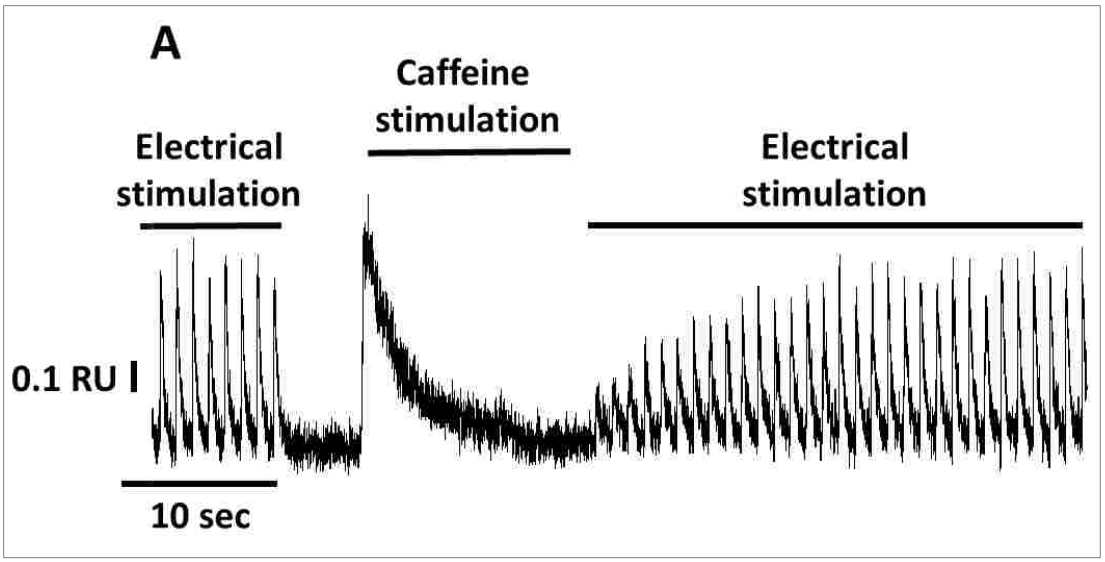

Figure 5-13: Effects of Quercetin-3-O-glucoside (QUER-3-G) on ventricular myocyte sarcoplasmic reticulum Ca^{2+}

(A) Typical record showing the protocol employed in a Control myocyte during SR Ca^{2+} experiments. Initially, myocytes were electrically stimulated at 1 Hz. When the Ca^{2+} transients had stabilized, electrical stimulation was paused for 5 seconds (sec). Caffeine was rapidly applied for 10 sec. Electrical stimulation was then resumed.

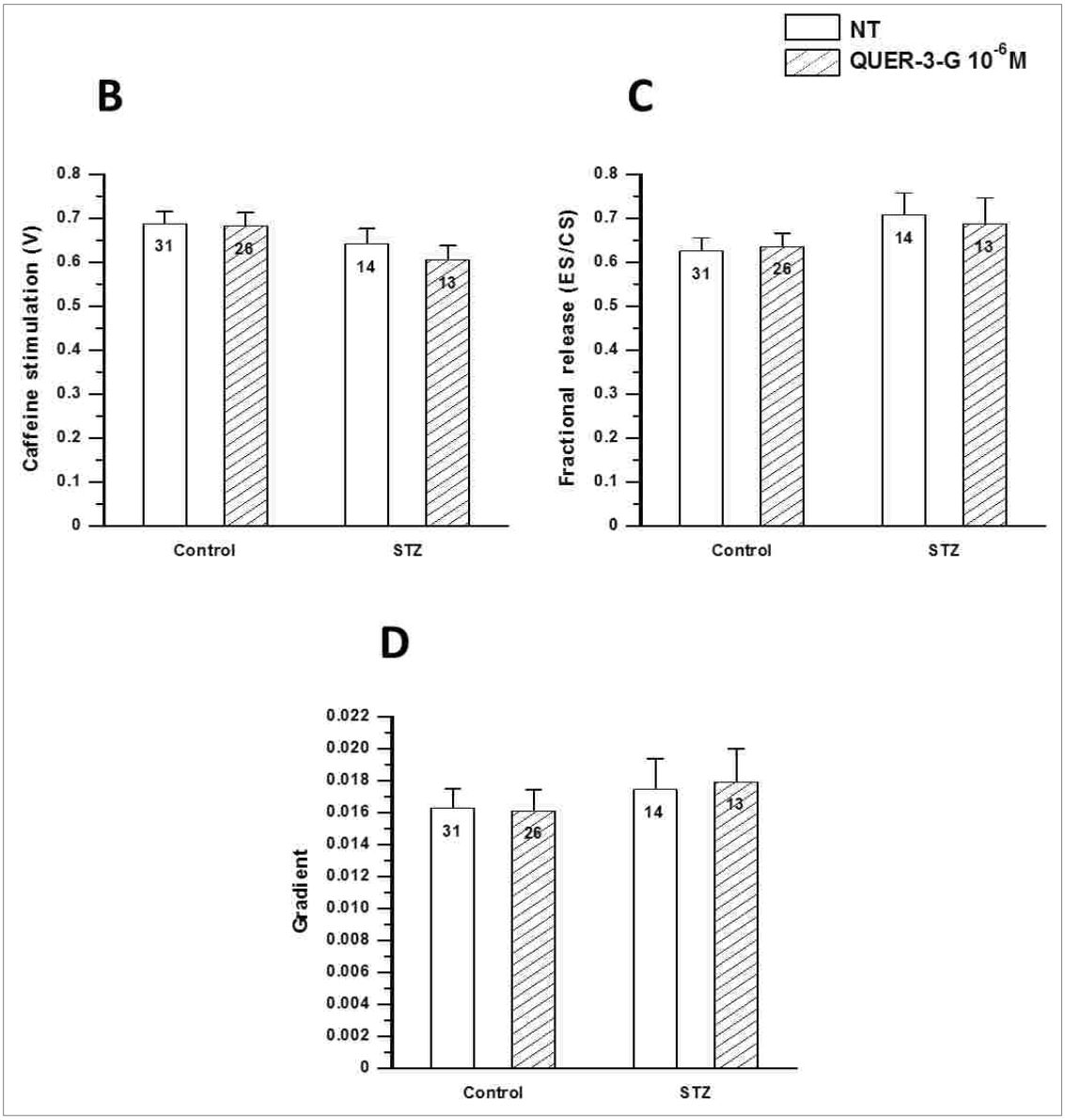

Figure 5-13 (continued): Effects of Quercetin-3-O-glucoside (QUER-3-G) on ventricular myocyte sarcoplasmic reticulum Ca^{2+}

Graphs showing mean:

(B) Amplitude of caffeine-stimulated Ca^{2+} transient
(C) Fractional release of Ca^{2+} (Electrical stimulation/Caffeine stimulation)
(D) Recovery of the Ca^{2+} transients following rapid application of caffeine

Results were analyzed using ANOVA and *post hoc* Bonferoni test. Data are mean + S.E.M., *n* = 13-31 myocytes from 3-6 hearts.

ES: electrical stimulation; **CS:** caffeine stimulation

5.6. Dapagliflozin Results

5.6.1. Effects of Short-Term Exposure to Dapagliflozin on Ventricular Myocyte Shortening

The effects of 10^{-6} M DAPA on shortening, in electrically stimulated (1Hz) STZ-induced diabetic and Control ventricular myocytes at 35-36°C were investigated.

Figure 5-14A shows typical records of shortening in a Control myocyte superfused with NT, 10^{-6} M DAPA + NT (5 min) and NT washout (5 min) to assess reversibility. The effects of DAPA on RCL, TPK shortening, THALF relaxation and AMP of shortening (expressed as a percentage of shortening in STZ and Control myocytes superfused with NT) are shown in Figure 5-14B-E. There were no significant (ANOVA; $P < 0.05$) changes observed in RCL (Fig. 5-14B), TPK shortening (Fig. 5-14C) and THALF relaxation (Fig. 5-14D) in STZ and Control myocytes with DAPA. DAPA significantly (ANOVA; $P < 0.05$) reduced the AMP of shortening in STZ/DAPA (76.58 ± 1.89%, n = 42) and Control/DAPA (76.68 ± 2.28%, n = 37) myocytes compared to STZ and Control (100%, n = 37-42) myocytes, respectively (Fig. 5-14E).

The AMP of shortening partially recovered in some STZ myocytes from 80.82 ± 5.39% (n = 9) with DAPA to 89.80 ± 5.45% (n = 9) after washout and in some Control myocytes from 79.28 ± 5.18% (n = 9) with DAPA to 89.34 ± 5.24% (n = 9) after washout. Collectively, recovery was approximately 10% in both STZ and Control myocytes after washout. While it continued to decrease (no recovery) in some STZ myocytes from 75.72 ± 2.28% (n = 25) with DAPA to 68.22 ± 2.84% (n =

23) after washout and in some Control myocytes from 76.83 ± 3.00% (*n* = 17) with DAPA to 63.85 ± 3.69% (*n* = 16) after washout.

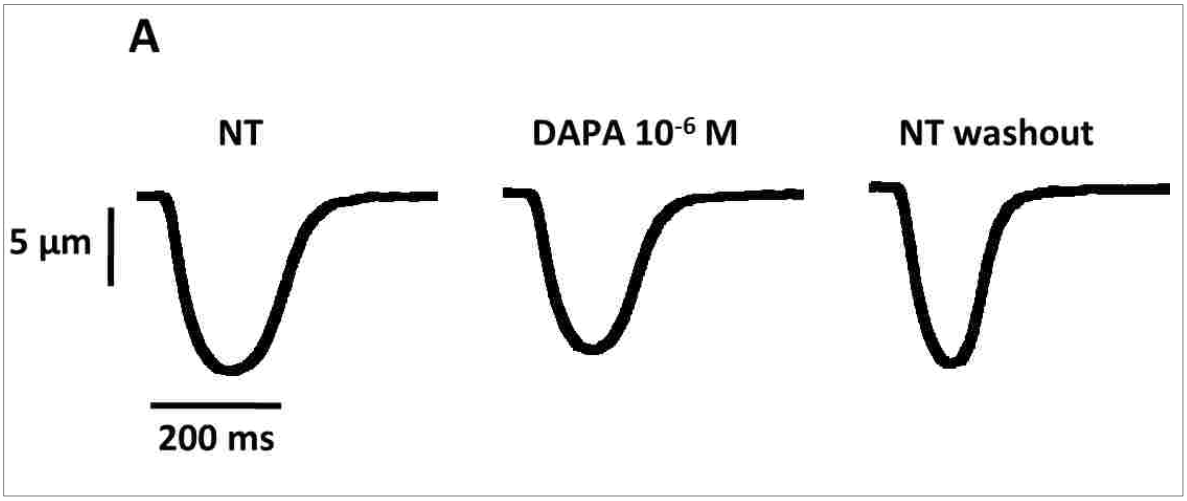

Figure 5-14: Effects of short-term exposure to Dapagliflozin (DAPA) on the amplitude and time course of ventricular myocyte shortening

(A) Typical records of shortening in a Control myocyte superfused with normal Tyrode (NT) (left panel), 10^{-6} M DAPA + NT (middle panel) and during washout with NT (right panel)

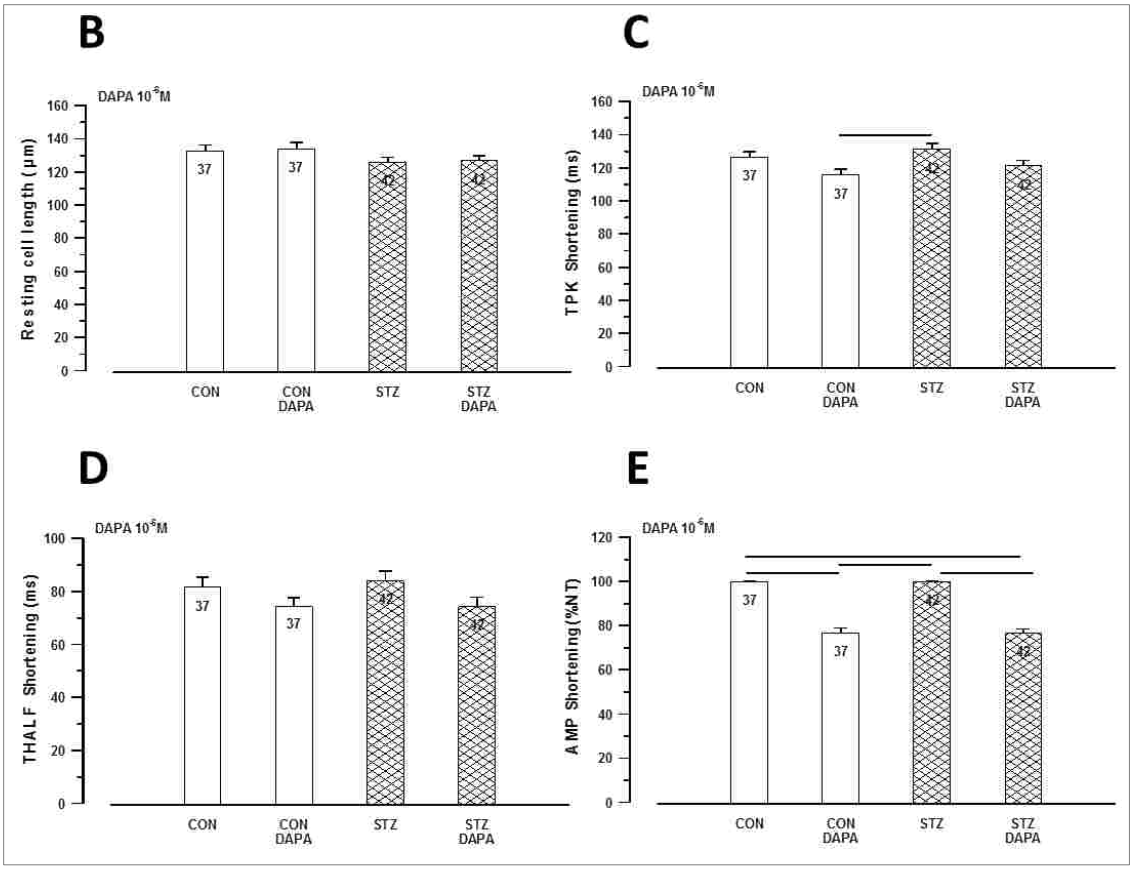

Figure 5-14 (continued): Effects of short-term exposure to Dapagliflozin (DAPA) on the amplitude and time course of ventricular myocyte shortening

Graphs showing the mean:

(B) Resting cell length
(C) Time to peak (TPK) shortening
(D) Time to half (THALF) relaxation of shortening
(E) Amplitude (AMP) of shortening

Results were analyzed using ANOVA and *post hoc* Bonferoni test. Data are mean + S.E.M., n = 37-42 myocytes from 18 hearts. Horizontal lines above the bars represent significant differences at the level of $P < 0.05$.

5.6.2. Comparing Short-Term versus Long-Term Effects of Dapagliflozin on Ventricular Myocyte Shortening

The effects of 10^{-6} M DAPA on myocyte shortening were tested by exposing myocytes to DAPA for a longer time to compare if this would exacerbate its effects.

STZ-induced diabetic and Control ventricular myocytes were split into 2 subgroups each. One subgroup of myocytes was incubated with NT and the other subgroup was incubated with 10^{-6} M DAPA + NT, and both were shaken in an oxygenated shaker (150 oscillations per minute) at 37° C for 1-3 hours. After the incubation period, RCL, TPK shortening, THALF relaxation and AMP of shortening (expressed as a percentage of shortening of RCL) were measured (Fig. 5-15B,D,F,H).

On Comparing myocyte shortening after short- and long-term exposure, the following was observed:

RCL was not significantly (ANOVA; $P < 0.05$) altered in STZ and Control myocytes after short and long-term exposure to DAPA (Fig.5-15A,B). Significant (ANOVA; $P < 0.05$) prolongation of TPK shortening was observed after long-term exposure to NT in STZ (118.88 ± 2.73 ms, $n = 32$) myocytes compared to Controls (88.47 ± 2.58 ms, $n = 30$) (Fig. 5-15C,D). THALF relaxation was not significantly (ANOVA; $P < 0.05$) altered in STZ and Control myocytes after short- and long-term exposure to DAPA (Fig. 5-15E,F). Short-term exposure of 10^{-6} DAPA significantly (ANOVA; $P < 0.05$) reduced the AMP of shortening (expressed as a percentage of RCL) in STZ/DAPA (5.15 ± 0.31%, $n = 42$) compared to STZ (6.63 ± 0.33%, $n = 42$) myocytes and in Control/DAPA (6.02 ± 0.41%, $n = 37$) compared to Control (7.86 ±

0.47%, n = 37) myocytes (Fig. 5-15G). However, long-term exposure to 10^{-6} DAPA did not cause any significant (ANOVA; $P < 0.05$) change in STZ/DAPA and Control/DAPA myocytes compared to STZ and Control myocytes, respectively. A significant (ANOVA; $P < 0.05$) increase in the AMP of shortening was observed when comparing STZ (8.53 ± 0.57%, n = 32) myocytes to Controls (6.84 ± 0.35%, n = 30) (Fig. 5-15H).

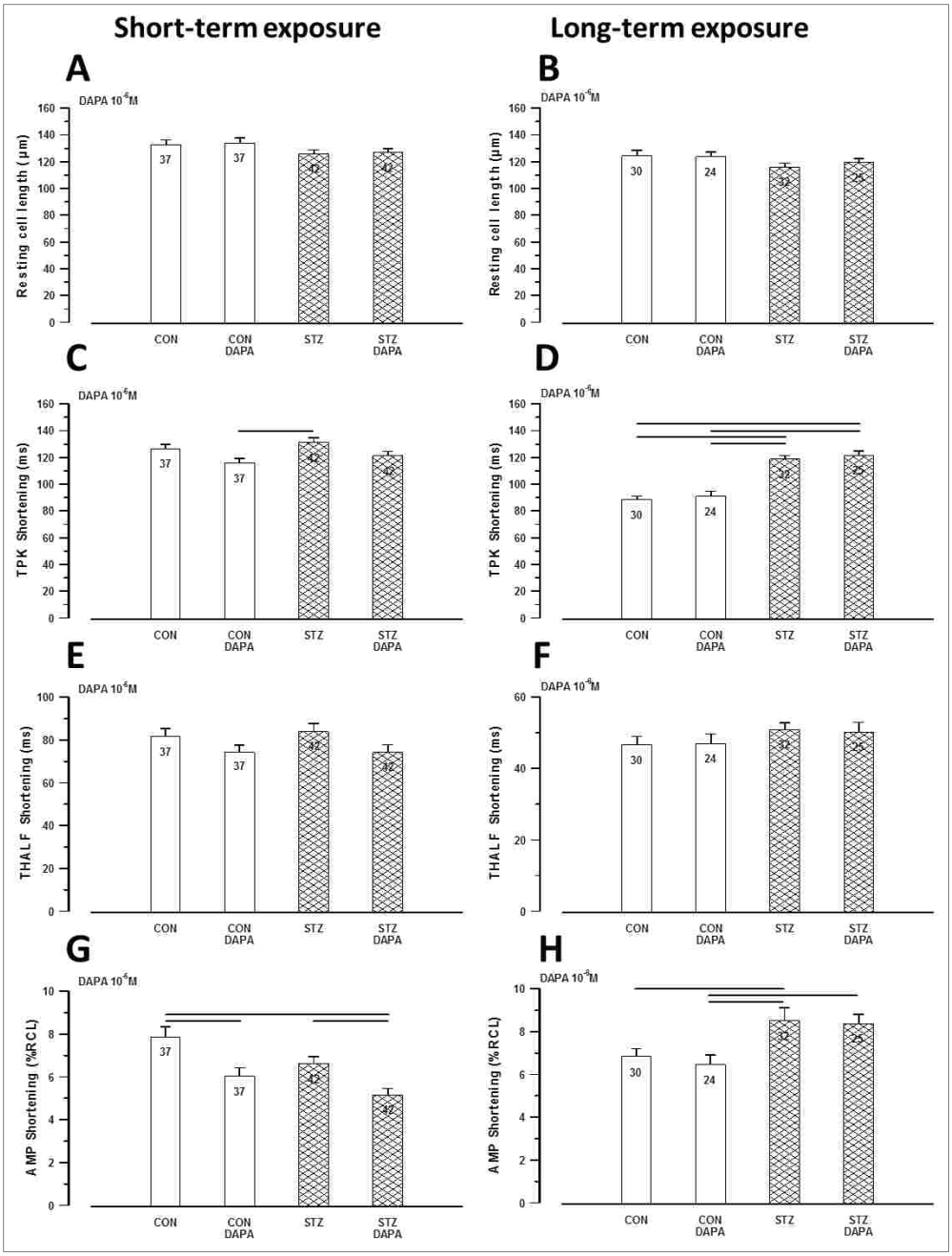

Figure 5-15: Short-term versus long-term effects of Dapagliflozin (DAPA) on ventricular myocyte shortening.

Graphs showing the mean: RCL after **(A)** short-term and **(B)** long-term exposure
TPK shortening after **(C)** short-term and **(D)** long-term exposure
THALF relaxation after **(E)** short-term and **(F)** long-term exposure
AMP of shortening after **(G)** short-term and **(H)** long-term exposure
Results were analyzed using ANOVA and *post hoc* Bonferoni test. Data are mean + S.E.M., n = 24-42 myocytes. Horizontal lines above the bars represent significant differences at the level of $P < 0.05$.

5.6.3. Effects of Dapagliflozin on Ventricular Myocyte Intracellular Ca^{2+} Transient

The effects of 10^{-6} M DAPA on intracellular Ca^{2+} transient were investigated in Fura-2 AM-loaded STZ-induced diabetic and Control ventricular myocytes, stimulated electrically (1 Hz) at 35-36 °C.

Typical records of the Ca^{2+} transient, in a Control myocyte exposed to NT and 10^{-6} M DAPA + NT for 5 minutes, are shown in Figure 5-16A. The resting Fura-2 ratio, TPK Ca^{2+} transient, THALF decay of the Ca^{2+} transient and AMP of the Ca^{2+} transient (expressed as a percentage of Ca^{2+} transient in STZ and Control myocytes superfused with NT) were measured (Fig. 5-16B-E). The resting Fura-2 ratio was not significantly (ANOVA; $P < 0.05$) altered in STZ and Control myocytes with DAPA (Fig. 5-16B). TPK Ca^{2+} transient was significantly (ANOVA; $P < 0.05$) prolonged in STZ/DAPA (82.38 ± 7.85 ms, $n = 16$) myocytes compared to STZ myocytes (60.56 ± 2.71 ms, $n = 17$), and modestly prolonged in Control/DAPA (67.62 ± 3.68 ms, $n = 17$) myocytes compared to Controls (60.55 ± 2.79 ms, $n = 19$) (Fig. 5-16C). There was no significant (ANOVA; $P < 0.05$) change in THALF decay of the Ca^{2+} transient by DAPA in STZ and Control myocytes (Fig. 5-16D). The AMP of the Ca^{2+} transient was significantly (ANOVA; $P < 0.05$) reduced in STZ/DAPA (71.45 ± 5.35%, $n = 16$) myocytes compared to STZ (100%, $n = 17$) and was modestly reduced in Control/DAPA (92.01 ± 2.72%, $n = 17$) myocytes compared to Controls (100%, $n = 19$) (Fig. 5-16E).

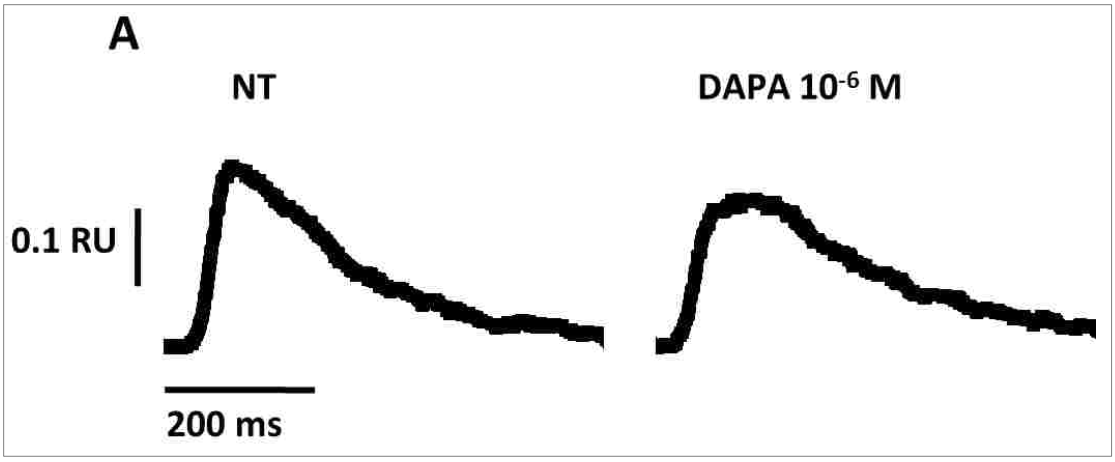

Figure 5-16: Effects of Dapagliflozin (DAPA) on the amplitude and time course of ventricular myocyte Ca^{2+} transient

(A) Typical records of the Ca^{2+} transient in a Control myocyte superfused with normal Tyrode (NT) (left panel) and 10^{-6} M DAPA + NT (right panel)

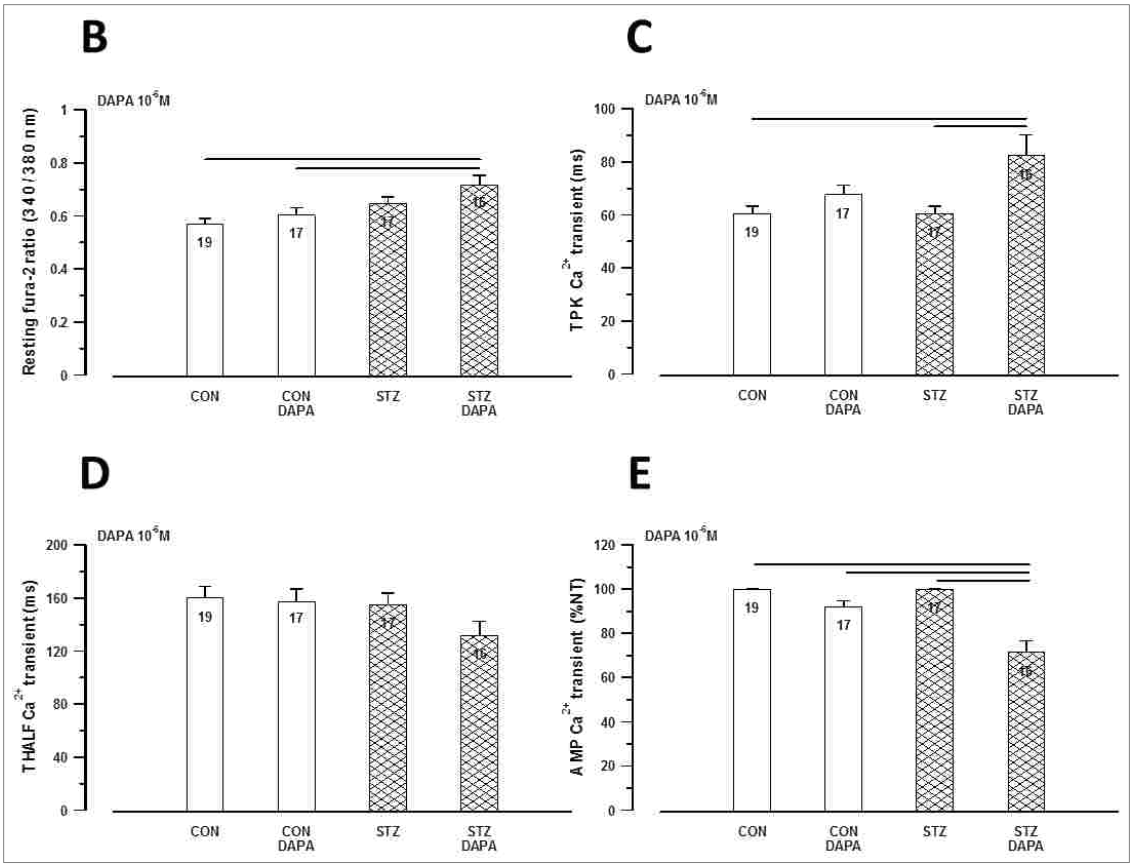

Figure 5-16 (continued): Effects of Dapagliflozin (DAPA) on the amplitude and time course of ventricular myocyte Ca^{2+} transient

Graphs showing the mean:

(B) Resting Fura-2 ratio
(C) Time to peak (TPK) Ca^{2+} transient
(D) Time to half (THALF) decay of the Ca^{2+} transient
(E) Amplitude (AMP) of the Ca^{2+} transient

Results were analyzed using ANOVA and *post hoc* Bonferoni test. Data are mean + S.E.M., n = 16-19 myocytes from 4 hearts. Horizontal lines above the bars represent significant differences at the level of $P < 0.05$.

5.5.4. Effects of Dapagliflozin on Ventricular Myocyte Myofilament Sensitivity to Ca^{2+}

The effects of 10^{-6} M DAPA on myofilament response and sensitivity to Ca^{2+} were tested.

Myocyte shortening and intracellular Ca^{2+} transient were recorded simultaneously after superfusion with NT and after 5 minutes of superfusion with 10^{-6} M DAPA + NT. Figure 5-17A shows a typical record of myocyte shortening and Ca^{2+} transient, and Figure 5-17B shows a typical phase-plane diagram of Fura-2 ratio versus cell length recorded in a Control myocyte superfused with NT.

The relative myofilament response and sensitivity to Ca^{2+} were assessed by measuring the gradient of the Fura-2-cell length trajectory during late relaxation of the twitch contraction. During the period 500–800 ms, there was no significant (ANOVA; $P < 0.05$) change in the gradient of the trajectory by DAPA in STZ and Control myocytes (Fig. 5-17C).

Therefore, myofilament sensitivity to Ca^{2+} is unlikely to be the cause for the effects of DAPA on myocyte contraction.

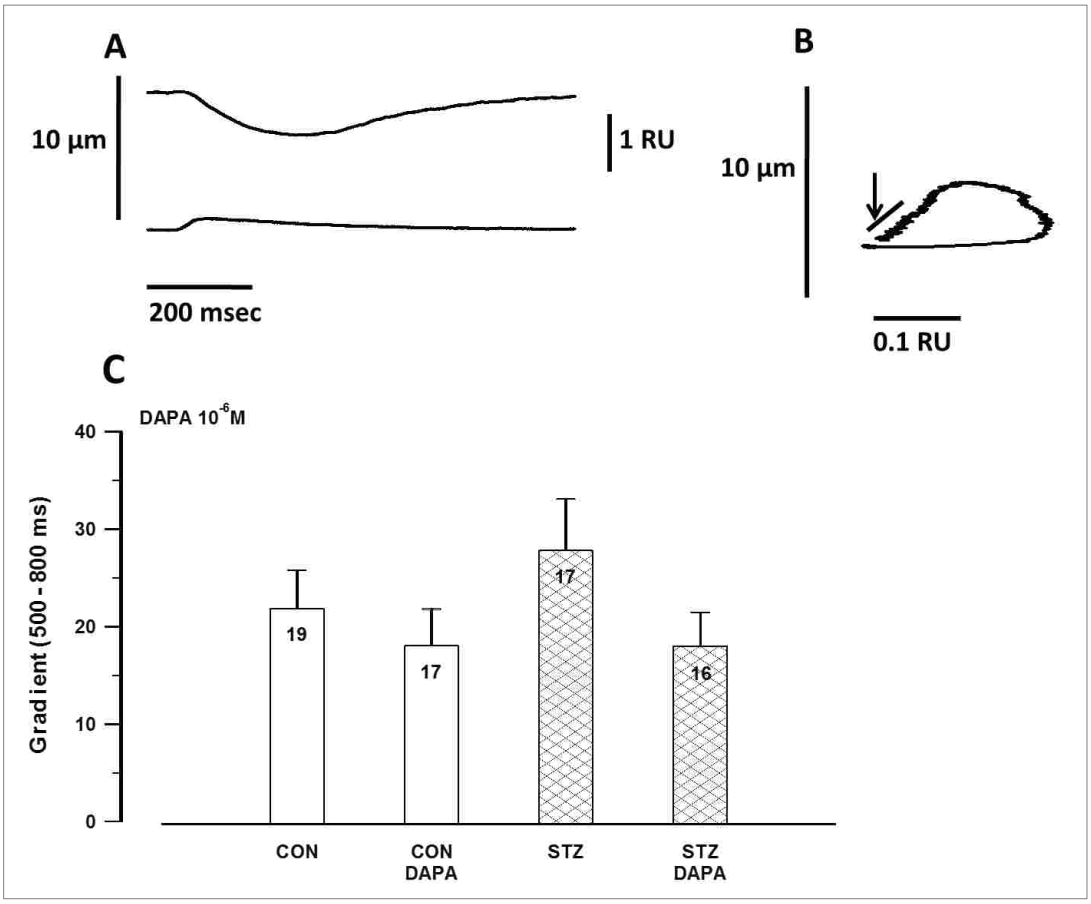

Figure 5-17: Effects of Dapagliflozin (DAPA) on ventricular myocyte myofilament sensitivity to Ca^{2+}

(A) Typical record of shortening and Ca^{2+} transient recorded simultaneously in an electrically stimulated myocyte from a Control heart

(B) Typical phase plane diagram of Fura-2 ratio unit (RU) versus cell length in a myocyte from a Control heart. The arrow indicates the region where the gradient was measured

(C) Graph showing mean gradient of the Fura-2-cell length trajectory during late relaxation of the twitch contraction during the period 500-800 ms

Results were analyzed using ANOVA and *post hoc* Bonferoni test. Data are mean + S.E.M., *n* = 16-19 myocytes from 4 hearts.

5.5.5. Effects of Dapagliflozin on Ventricular Myocyte Sarcoplasmic Reticulum Ca^{2+} Transport

The effects of 10^{-6} M DAPA on SR Ca^{2+} transport, in Fura-2 AM-loaded STZ-induced diabetic and Control ventricular myocytes, were investigated.

A typical record of the protocol used in these experiments is shown in Control myocyte superfused with NT in Figure 5-18A. Initially, myocytes were electrically stimulated at 1 Hz. When the Ca^{2+} transients had stabilized, electrical stimulation was paused for 5 seconds. Caffeine was then applied using a rapid solution switching device for 10 seconds. Electrical stimulation was then resumed. This protocol was repeated after the cell was superfused with NT and again after 5 minute superfusion of 10^{-6} M DAPA dissolved in NT.

The AMP of the caffeine-stimulated Ca^{2+} transient was not significantly (ANOVA; $P < 0.05$) altered in STZ and Control myocytes with DAPA (Fig. 5-18B). Fractional release of Ca^{2+} (measured as the relationship between the electrically-stimulated and caffeine-stimulated Ca^{2+} transients) did not show any significant (ANOVA; $P < 0.05$) change by DAPA in STZ and Control myocytes (Fig. 5-18C). The gradient of myocyte recovery after caffeine application was also not significantly (ANOVA; $P < 0.05$) altered in STZ and Control myocytes with DAPA (Fig. 5-18D).

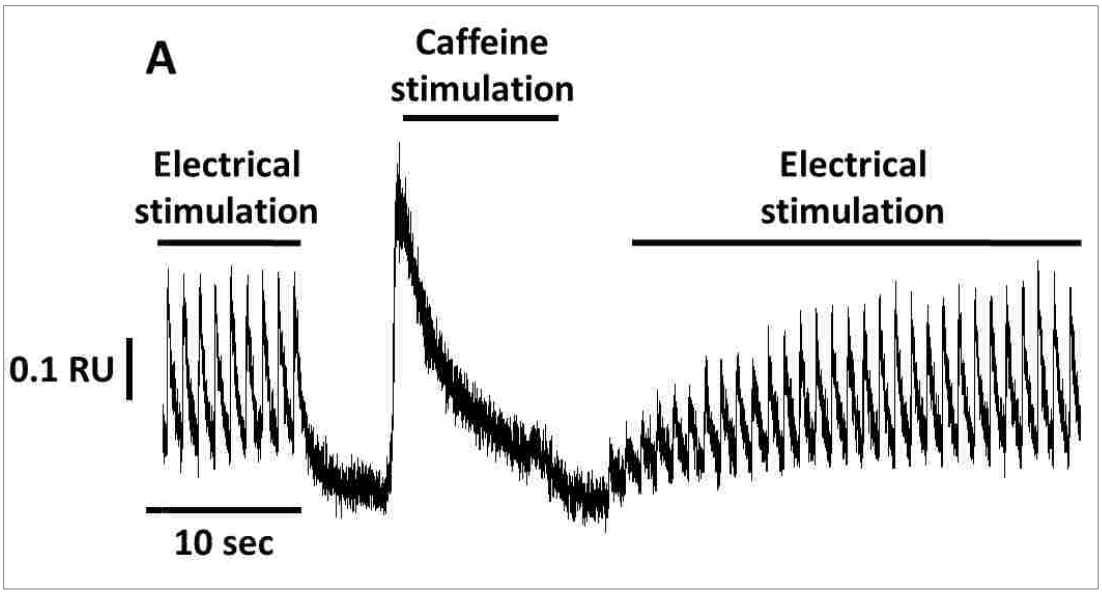

Figure 5-18: Effects of Dapagliflozin (DAPA) on ventricular myocyte sarcoplasmic reticulum Ca^{2+}

(A) Typical record showing the protocol employed in a Control myocyte during SR Ca^{2+} experiments. Initially, myocytes were electrically stimulated at 1 Hz. When the Ca^{2+} transients had stabilized, electrical stimulation was paused for 5 seconds (sec). Caffeine was rapidly applied for 10 sec. Electrical stimulation was then resumed.

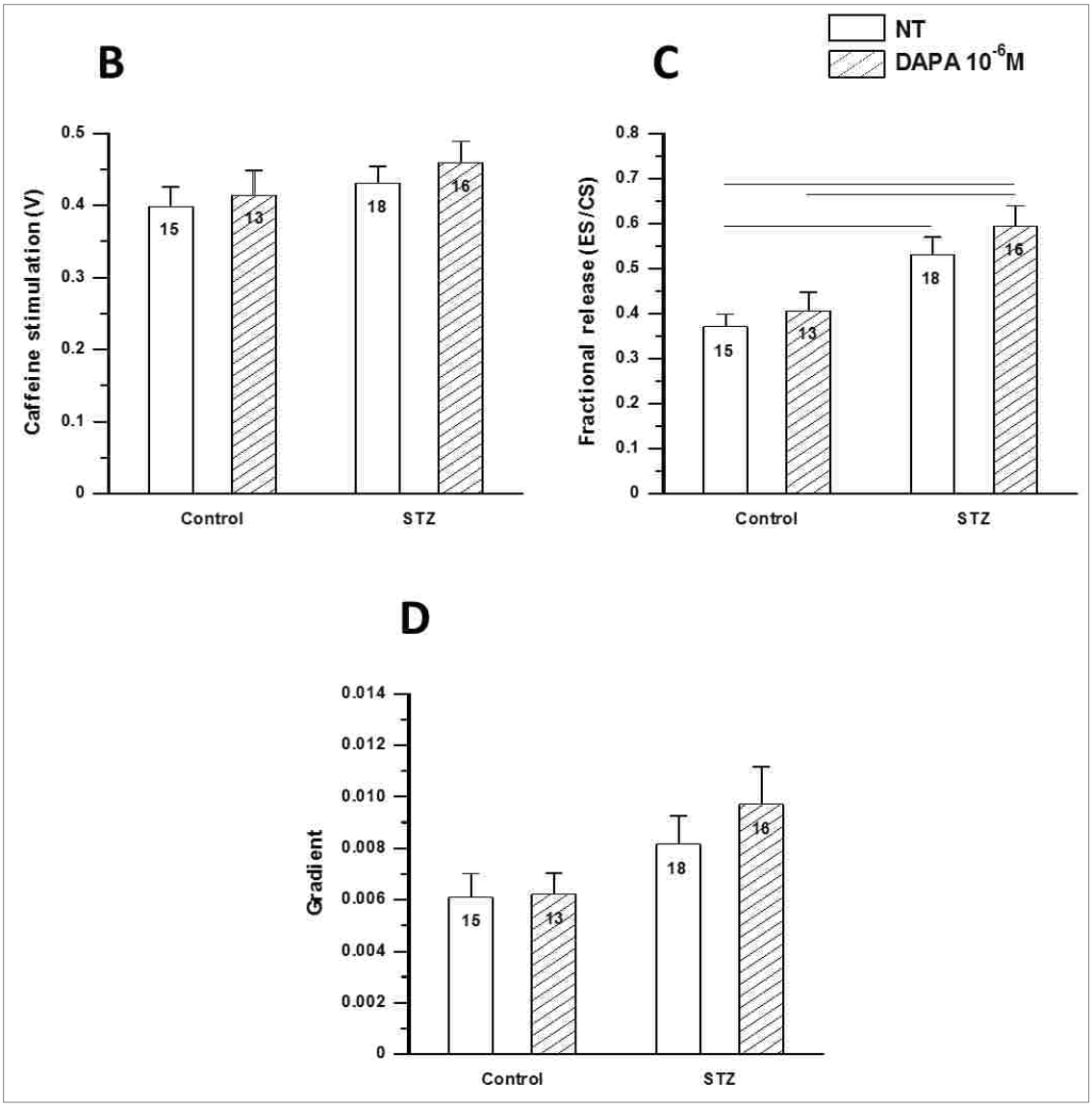

Figure 5-18 (continued): Effects of Dapagliflozin (DAPA) on ventricular myocyte sarcoplasmic reticulum Ca^{2+}

Graphs showing mean:

(B) Amplitude of caffeine-stimulated Ca^{2+} transient
(C) Fractional release of Ca^{2+} (Electrical stimulation/Caffeine stimulation)
(D) Recovery of the Ca^{2+} transients following rapid application of caffeine

Results were analyzed using ANOVA and *post hoc* Bonferoni test. Data are mean + S.E.M., n = 13-18 myocytes from 3-4 hearts. Horizontal lines above the bars represent significant differences at the level of $P < 0.05$.

ES: electrical stimulation; **CS:** caffeine stimulation

5.5.6. Effects of Dapagliflozin on Ventricular Myocyte L-Type Ca^{2+} Current

Since the effects of 10^{-6} M DAPA observed could neither be attributed to myofilament sensitivity to Ca^{2+} nor to SR Ca^{2+} release, its effects on L-type Ca^{2+} current were investigated.

L-type Ca^{2+} current was recorded at 34-36°C in ventricular myocytes superfused with Ca^{2+}-containing (2.0 mmol/l) extracellular solution for 5 minutes followed by superfusion with 10^{-6} M DAPA + Ca^{2+}-containing extracellular solution for 5 minutes. Whole-cell configuration was employed and L-type Ca^{2+} current activation, steady state inactivation and restitution were recorded.

Figure 5-19A shows the activation protocol (upper panel) and typical records of L-type Ca^{2+} current (pico-ampere/pico-farad; pA/pF) from a holding potential of -50 mV to different potentials, from -60mV to + 70 mV, in 10 mV steps each of 200 ms duration (lower panel). In general L-type Ca^{2+} current, over the test potential range -40 to +40 mV, was largest in myocytes from Control, followed by Control/DAPA, followed by STZ and smallest in STZ/DAPA (Fig. 5-19B). The results at each voltage from Control, Control/DAPA, STZ and STZ/DAPA myocytes are shown in Table 5-2.

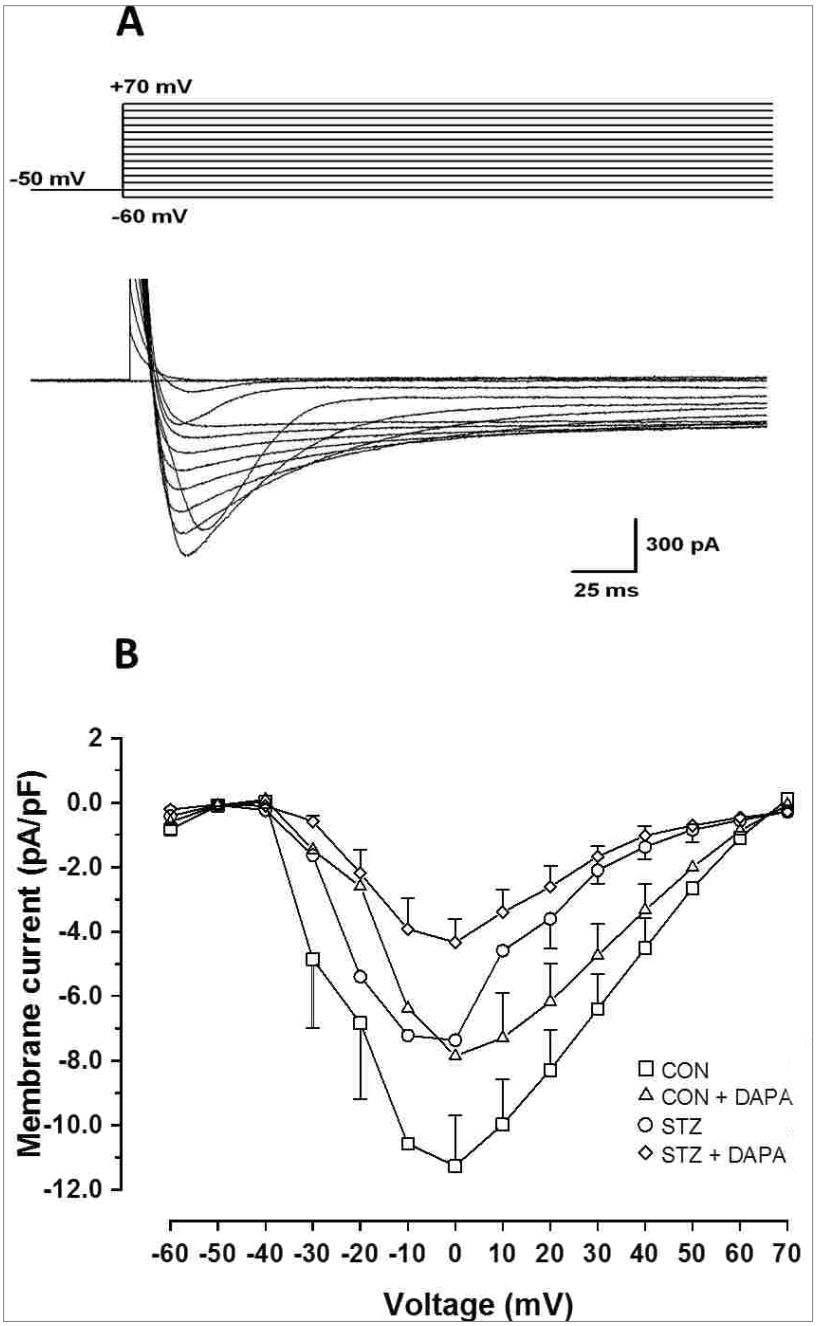

Figure 5-19: Effects of Dapagliflozin on activation of L-type Ca^{2+} current in ventricular myocytes from STZ and Control rats

(A) Voltage protocol (upper panel) and typical records of L-type Ca^{2+} current (lower panel) in a ventricular myocyte from a Control heart.

(B) Graph showing the amplitude of membrane currents evoked at different test potentials in the range -60 to + 70 mV in ventricular myocytes from STZ- induced diabetic and Control rats superfused with normal Tyrode (NT) or NT + 10^{-6} DAPA.

Voltage (mV)	Control (pA/pF)	Control/DAPA (pA/pF)	STZ (pA/pF)	STZ/DAPA (pA/pF)
-60	-0.826 ± 0.164	-0.599 ± 0.109[d]	-0.414 ± 0.159	-0.202 ± 0.076
-50	-0.087 ± 0.017	-0.080 ± 0.016	-0.068 ± 0.019	-0.058 ± 0.018
-40	0.028 ± 0.088	0.096 ± 0.052	-0.230 ± 0.056[a,b]	-0.095 ± 0.024[c]
-30	-4.857 ± 2.124	-1.459 ± 0.878	-1.632 ± 0.677	-0.578 ± 0.166
-20	-6.832 ± 2.362	-2.598 ± 0.901[d]	-5.392 ± 0.840	-2.184 ± 0.735[c]
-10	-10.573 ± 1.918	-6.370 ± 1.522[d]	-7.214 ± 0.758	-3.920 ± 0.949[c]
0	-11.269 ± 1.570	-7.856 ± 1.558[d]	-7.362 ± 0.881[b]	-4.334 ± 0.729[c]
+10	-9.977 ± 1.402	-7.294 ± 1.396[d]	-4.585 ± 0.931[a,b]	-3.391 ± 0.687[c]
+20	-8.287 ± 1.246	-6.167 ± 1.187[d]	-3.597 ± 0.933[a,b]	-2.607 ± 0.650[c]
+30	-6.395 ± 1.083	-4.739 ± 0.974	-2.094 ± 0.410[a,b]	-1.666 ± 0.327
+40	-4.509 ± 0.928	-3.329 ± 0.804	-1.369 ± 0.383[a,b]	-1.018 ± 0.302
+50	-2.652 ± 0.745	-2.007 ± 0.644	-0.835 ± 0.397[b]	-0.705 ± 0.289
+60	-1.089 ± 0.621	-0.868 ± 0.506	-0.543 ± 0.457	-0.459 ± 0.263
+70	0.117 ± 0.630	-0.063 ± 0.417	-0.276 ± 0.495	-0.282 ± 0.240

Table 5-2: Effects of Dapagliflozin on activation of L-type Ca^{2+} current in ventricular myocytes from STZ and Control rats

Table showing the mean membrane current (pA/pF) at each test voltage in the range from -60 mV to +70 mV. Results were analyzed using ANOVA and *post hoc* Bonferoni test and Independent Samples T-Test. Data are mean ± S.E.M., n = 10-14 myocytes from 4-7 hearts. Differences between groups, [a] (ANOVA; $P < 0.05$) versus Control myocytes, [b] (Independent Samples T-Test; $P < 0.05$) versus Control myocytes, [c] (Paired Samples T-Test; $P < 0.05$) versus STZ myocytes, [d] (Paired Samples T-Test; $P < 0.05$) versus Control myocytes

The protocol studying steady-state inactivation involved stepping the membrane from various 1000 ms pre-pulses between -60 and +30 mV to a test pulse of 0 mV, as illustrated in Figure 5-20A (upper panel). Ca^{2+} current was measured as the relationship between the AMP of peak currents produced at each of the pre-pulses to those measured at the test pulse 0 mV. Typical records of steady-state inactivation

Ca^{2+} current are shown in Figure 5-20A (lower panel). Figure 5-20B shows normalized peak currents measured after the pre-pulses at 0 mV plotted against the respective pre-pulse voltage/potential. Steady-state inactivation was not significantly (ANOVA; $P < 0.05$) altered in STZ compared to Control myocytes or by DAPA.

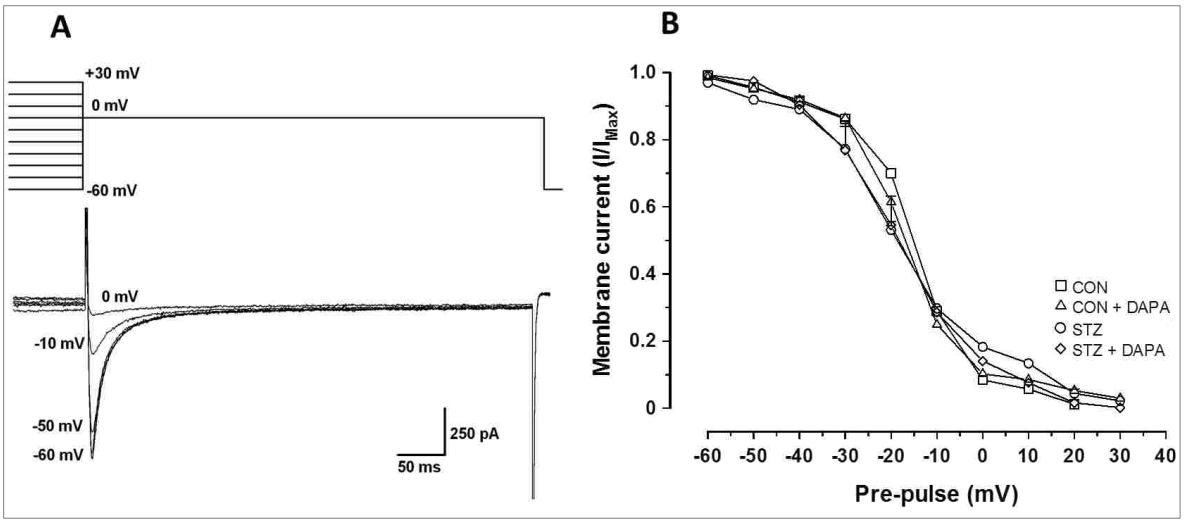

Figure 5-20: Effects of Dapagliflozin on steady state inactivation of L-type Ca^{2+} current in ventricular myocytes from STZ and Control rats

(A) Voltage protocol (upper panel) and typical records of inactivation currents (lower panel) in a ventricular myocyte from a Control heart

(B) A graph showing membrane currents following different pre-pulse potentials in the range -60 to +30 mV

Results were analyzed using ANOVA and *post hoc* Bonferoni test. Data are mean + S.E.M., *n* = 10-14 myocytes from 4-7 hearts.

I_{max}: amplitude of peak current at each pre-pulse; **I:** amplitude of peak current at the test pulse 0 mV

A two-pulse protocol was used to investigate the time course of recovery from inactivation (Fig. 5-21A, upper panel). These pulses were consecutively separated by inter-pulse intervals and each pulse was 100 ms in duration causing depolarization of

the membrane potential to +10 mV. The inter-pulse intervals were variable and increased gradually every time the protocol was applied. Typical records of Ca^{2+} current recovery after different inter-pulse intervals are shown in Figure 5-21A (lower panel). Measurement of the time course of recovery from inactivation was done by normalizing the AMP of peak Ca^{2+} current of the second pulse to that of the first pulse and their ratio was plotted against the durations of the inter-pulse interval (Fig. 5-21B). No significant alterations were obtained with the time course of recovery from inactivation in STZ compared to Control myocytes or by DAPA.

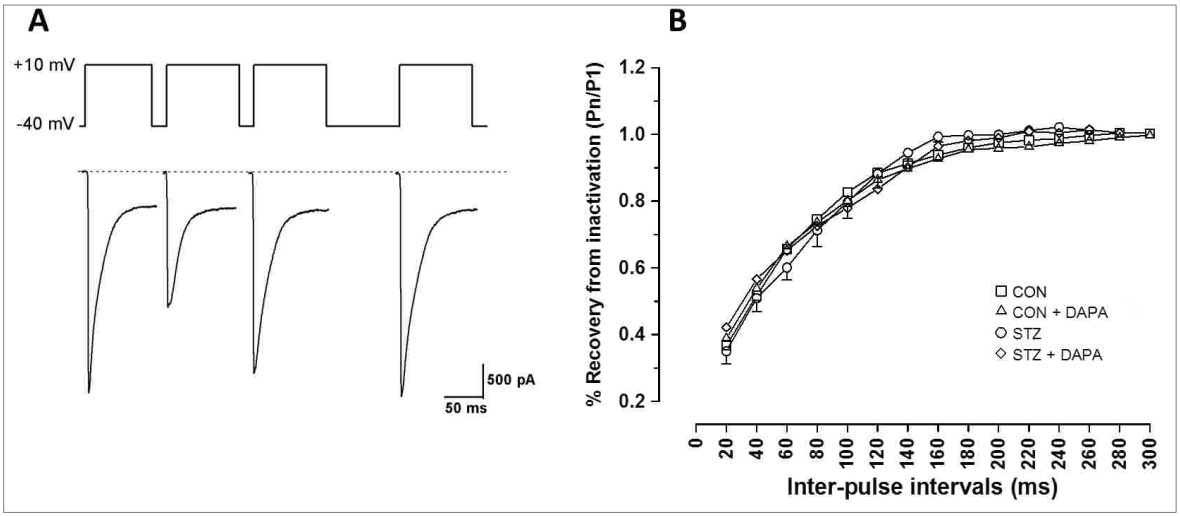

Figure 5-21: Effects of DAPA on restitution of L-type Ca^{2+} current in ventricular myocytes from STZ and Control rats

(A) Voltage protocol (upper panel) and typical records of membrane current during recovery from inactivation (lower panel) in a ventricular myocyte from a Control heart

(B) A graph showing recovery from inactivation at various inter-pulse intervals with variable duration

Results were analyzed using ANOVA and *post hoc* Bonferoni test. Data are mean + S.E.M., *n* = 10-14 myocytes from 4-7 hearts.

P_n: amplitude of peak current of the second pulse; **P_1:** amplitude of peak current of the first pulse

Chapter 6: Discussion

This study investigated the effects of the non-selective SGLT1 and 2 inhibitor PHLOR, selective SGLT1 inhibitor QUER-3-G and selective SGLT2 inhibitor DAPA on shortening and intracellular Ca^{2+} in ventricular myocytes from STZ-induced diabetic and Control rats. The major findings of the study were as follows:

1) PHLOR, QUER-3-G and DAPA significantly reduced the AMP of shortening in STZ and Control myocytes,

2) PHLOR and QUER-3-G significantly reduced the AMP of the intracellular Ca^{2+} transient in STZ and Control myocytes,

3) DAPA significantly reduced the AMP of the intracellular Ca^{2+} transient in STZ myocytes,

4) PHLOR and DAPA did not significantly alter myofilament sensitivity to Ca^{2+} in STZ and Control myocytes,

5) QUER-3-G significantly decreased myofilament sensitivity to Ca^{2+} in Control myocytes and modestly in STZ myocytes,

6) PHLOR, QUER-3-G and DAPA did not significantly alter fractional release of SR Ca^{2+} in STZ or Control myocytes, and

7) The AMP of L-type Ca^{2+} current was reduced in STZ compared to Control myocytes and was further reduced by DAPA.

6.1. Diabetes Mellitus Induction in Animals

Choosing an animal model for any study relies on the nature of the study and the variables to be investigated. Being a study that focuses on investigating the diabetic heart after a pharmacological intervention, the appropriate animal model should exhibit features of the diabetic heart. Rodents are a preferred option in research studies as they are easily handled and maintained at low cost and in relatively small spaces [186]. Among the different experimental methods used to obtain diabetic animal models including surgically-induced, diet-induced and genetically-derived, the chemically-induced STZ model has several advantages including cost-effectiveness and the ease of inducing DM regardless of the genetic background or the age of the animal [38; 72]. STZ-induced DM is a widely used animal model for human diseases, ranking second after the spontaneously hypertensive rat [298]. The STZ rat model resembles DM in humans in various ways. It exhibits diabetic signs such as hyperglycemia, reduced body weight, polyphagia and polydipsia [298], as well as diabetic symptoms/complications such as retinopathy and cataract [12; 136; 170; 298], cardiomyopathy [287], neuropathy [42; 199; 298] and nephropathy [49; 139; 161; 299] (for a detailed review see [279]).

Different cardiac dysfunctions have been reported in STZ rats at the whole animal (*in vivo*) and isolated heart/cardiac tissue (*in vitro*) levels. Some effects at the whole animal level include reduced resting HR [30; 31; 46; 64; 244], decreased cardiac contractility and relaxation, increased stroke volume, increased cardiac output [46], decreased myocardial blood flow reserve [66], reduced mean arterial pressure [31; 244] and reduced left ventricular function [64; 66; 67]. Effects at the isolated

heart/cardiac tissue level include structural and functional effects. Structural effects may involve reduced heart weight, reduced atrial, right and left ventricular weights [252], increased lipid deposition, loss of contractile proteins, myocytolysis [137], decreased diameter and surface area of capillaries in the myocardium [66], increase in the number of sarcolemmal Ca^{2+} channels [107], decreased thickness and increased internal diameter of the left ventricle [298] and increased collagen content in left ventricular tissues [30]. Functional effects may involve depressed cardiac performance [137; 287], reduced HR [64; 121; 298], prolonged AP duration in the SA node, right atrium and right ventricle [121; 298], diastolic stiffness [298], impaired relaxation (diastole) and contraction (systole) [64], reduced depolarization of the resting membrane potential [298], decreased ATPase activity of cardiac contractile proteins [189], increased ventricular sensitivity to Ca^{2+}, depressed atrial activity, enhanced right ventricular activity [227], elevated Fe^{2+} levels in the right ventricle, elevated Na^{+} levels in the atria and right ventricle, lower Ca^{2+} levels in the atria, right and left ventricles, increased Cu^{2+} levels in the atria and decreased Cu^{2+} levels in the left ventricle [252].

To induce DM, STZ (60 mg/kg body weight) dissolved in citrate buffer was injected i.p. in male adult Wistar rats. It would have been preferable to inject STZ via the i.v. route because the i.p. route involves the additional step of absorption of STZ into the bloodstream before its effects can take place. This decreases its bioavailability compared to that injected by the i.v. route [160]. The commonly used doses of STZ to induce DM in rats include 40 mg/kg [258], 45 mg/kg [66; 67; 249], 50 mg/kg [31; 140; 313], 60 mg/kg [60; 252; 264; 287], 65 mg/kg [30; 46; 137; 148;

226; 292; 317]. Also, some studies use STZ doses as high as 90 mg/kg [29; 122] and 100 mg/kg [214]. STZ at doses 50-65 mg/kg induces hyperglycemia without DKA. However, DKA or even death can occur at higher doses of STZ (≥75 mg/kg) [196; 298] and can be prevented by the administration of insulin [298]. Since DKA is a characteristic of T1DM [10], some studies generally describe models induced by doses that do not induce DKA as T2DM models [140].

DM induced by a single injection of 60 mg/kg STZ can be characterized as T1DM [60; 217], T2DM [113; 220] or unspecified [3; 121]. Like T1DM, after a single STZ injection, the insulin-producing pancreatic β-cells are destroyed and hypoinsulinemia rapidly develops [10; 70; 84]. However, unlike T1DM, a single dose of STZ destroys the cells due to toxicity (as a chemical insult) rather than an autoimmune response [5; 206]. An autoimmune response can be induced by multiple injections [194; 237]. On the other hand, several studies reported that damaged pancreatic β-cells can spontaneously regenerate with time after STZ injection in rats [203; 295; 296] and mice [314]. In addition, considering that STZ rat models produced by this dose (60 mg/kg) do not exhibit DKA [143; 196; 298] and show significant glycemic improvement with anti-diabetic medications, other than insulin, such as metformin [61], tolbutamide [171], glibenclamide [4; 156], vanadyl sulphate [224], pioglitazone [98], rosiglitazone [82; 184] and empagliflzoin [185], it also resembles T2DM. Collectively, it can be concluded that the rat model produced by 60 mg/kg STZ cannot be strictly described as neither T1DM nor T2DM, but rather an unspecified model of hyperglycemia.

DM characteristics take some time to develop in STZ-induced diabetic rats. Body weight becomes significantly lower, compared to controls, only after 2 weeks following STZ injection. Diabetic CV complications begin 5-7 days after STZ injection and continue to worsen with time. The earliest complication is reduced HR occurring after 5-7 days, followed by reduced mean arterial pressure after 14 days and eventually reduced variability of HR and mean arterial pressure after 30-45 days [244]. In order to allow these complications to develop, the experiments started 2 months after STZ injection. Since it is well known that the key element of DM is hyperglycemia, DM was confirmed in the rats by measuring their BGL, using a glucometer, in blood taken from the tail vein 3-5 days after STZ injection. To ensure that the injected rats were still diabetic and regeneration of β-cells had not occurred, measuring the BGL of the tested rat prior to the experiment was essential. Rats that exhibited recovery from DM, indicated by normoglycemia, were excluded from the study. Only rats with a BGL of ≈ 200 mg/dl and above were included in the diabetic group. Control rats were injected with an equivalent volume of citrate buffer only and their BGL ranged from ≈ 75-130 mg/dl. Differences in STZ rats compared to Controls, aside from the hyperglycemia, included reduced body weight, reduced heart weight and increased heart weight to body weight ratio. These results have been shown repeatedly in previous studies using this model [34; 121; 123; 125; 148]. Three batches of rats were used and each batch was used for a period of approximately 12 weeks after DM induction. No cases of death were reported whether in STZ-induced diabetic or Control rats in any of the batches.

6.2. The Reason for Choosing to Study the Effects of Sodium/Glucose Co-transporter Inhibitors on the Heart

SGLT inhibitors have been receiving more attention recently as a novel anti-diabetic therapy. Before it was known that PHLOR mechanism of action involves inhibiting SGLT proteins, its glycosuric effect had been first observed in 1886 [80]. Studies in the late 1980s and early 1990s showed that s.c. injections of PHLOR significantly improved both fasting and fed BGL in partially pancreatectomized rats [144; 235; 236], normalized their tissue insulin sensitivity and increased glycosuria compared to the untreated diabetic rats [236]. This was also confirmed by later studies on STZ-induced diabetic rats which showed that PHLOR significantly improved fasting BGL and restored diabetic insulin sensitivity [157]. Glycemic improvement with glycosuria was also observed after s.c. injection of PHLOR in cattle [35]. Despite its observed anti-diabetic effects via the s.c. route, no studies have been done, or at least published, on the effects of s.c. PHLOR in humans. Previous studies showed that PHLOR can be safely administered i.v. in human subjects [80; 172].

PHLOR was reported to have a low oral bioavailability because it is metabolized in the intestine by β-glucosidase (β-glucuronidase) and/or sulfatase that splits it into phloretin and glucose [69; 280]. However, oral administration of PHLOR in mice reduced their BGL in a dose-dependent manner [272] and intragastric administration also reduced BGL in diabetic mice [40]. Phloretin, the metabolite of PHLOR, is an inhibitor of the GLUT transporters which are widely expressed throughout the body [280]. GLUTs are responsible for bidirectional passive transport

of glucose between the blood and the cell cytoplasm [204] and thus, chronic inhibition by phloretin can cause damage especially in glucose-dependent organs, like the brain, due to a lack of cellular glucose [280].

Since the oral route is the best method of administration in the clinical setting, PHLOR was used as the parent molecule to produce other oral bioavailable SGLT inhibitors [280]. SGLT inhibitors that are being developed include non-selective SGLT1 and 2 inhibitors such as LX4211 [319], selective SGLT1 inhibitors such as KGA-2727 [250] and KGA-3235 [162], and the majority are selective SGLT2 inhibitors such as DAPA [195], canagliflozin [213], empagliflozin [109], ipragliflozin [246], topogliflozin [265], remogliflozin etabonate [97] and lesugliflozin [146]. Several studies on STZ rat showed improved glycemic control after treatment with SGLT inhibitors such as PHLOR [60], DAPA [195], empagliflozin [185], ipragliflozin [269] and topogliflozin [265].

In this study, three compounds from the three subclasses of SGLT inhibitors were tested. This allows evaluation of the differences and similarities between representatives from each subclass. By having the parent compound of SGLT inhibitors PHLOR, it is also more likely that the other SGLT inhibitors derived from PHLOR would act in a similar manner. QUER-3-G was shown to have anti-diabetic effects [219] due to its selective SGLT1 inhibiting [2; 54] and α-glucosidase inhibiting properties [174]. DAPA is now a commercially available anti-diabetic medication in various countries [282]. It is the first selective SGLT2 inhibitor developed in its class and it is the second SGLT2 inhibitor approved by the FDA [90; 282].

Since PHLOR, QUER-3-G and DAPA all have anti-diabetic properties, their effects should be tested on diabetic organs, especially those susceptible to diabetic complications. There appeared to be no data available about the effects of PHLOR, QUER-3-G and DAPA on ventricular myocytes from diabetic heart.

6.3. Effects of Sodium/Glucose Co-transporter Inhibitors on the Cardiovascular System

Previous studies done with PHLOR, QUER-3-G and DAPA showed that they can affect the CV system.

PHLOR treatment was shown to have protective effects against the development of diabetic cardiomyopathy in *db/db* mice by downregulating the expression of cardiac damaging proteins and upregulating the cardiac proteins responsible for cardiac lipid metabolism, causing a reduction in cardiac lipid accumulation [40]. Isoproterenol-induced myocardial necrosis was partially prevented in mice by PHLOR [114]. PHLOR suppressed the production of ROS in rat cardiomyocytes by inhibiting SGLT1 [18]. Hypotension, elevated baroreflex sensitivity and increased expression of cardiac M_2-muscurinic receptors were reversed by PHLOR treatment in STZ-diabetic rats [180]. Restoration of glucose utilization in heart muscle to the normal level was seen after PHLOR treatment in STZ-diabetic rats [178].

QUER-3-G was reported to have several anti-hypertensive mechanisms including diuresis and potassium-sparing activity [100; 101], reduction of angiotensin converting enzyme activity and reduction of plasma aldosterone in spontaneously

hypertensive rats [101]. QUER-3-G was also shown to have a protective effect against ROS-induced injury in cultured human endothelial cells in a dose-dependent manner, which provides an additional benefit to diabetic patients [291]. In addition, studies showed that QUER-3-G-containing plants exhibited various beneficial effects against the development of atherosclerosis in rats by lowering total cholesterol, triglycerides and LDL-C, increasing the beneficial high-density lipoprotein-cholesterol (HDL-C) levels and decreasing inflammatory responses [321].

Little is known about the effects of DAPA on the CV system. A large clinical trial 'DECLARE-TIMI58', to be completed in April 2019, is progressing to evaluate DAPA safety and effects on CV outcomes [14]. Several studies showed that DAPA monotherapy reduces the systolic blood pressure [16; 147; 179]. Small and inconsistent decreases of HR [179] and less pronounced reductions of diastolic blood pressure have been reported in DAPA-treated diabetic subjects [147; 179]. A slight increase of HDL-C was seen in diabetic subjects treated with DAPA [16; 87]. DAPA add-on therapy to metformin, sulphonylureas or thiazolidinediones produced a significant reduction in various CV outcomes including MI incidence, stroke incidence, coronary heart disease death, stroke death and all-cause death compared to metformin, sulphonylureas and thiazolidinediones monotherapies [79]. Supratherapeutic doses of DAPA (150 mg compared to 5-10 mg as the therapeutic dose) did not significantly prolong QT interval in healthy individuals [47].

6.4. Concentration of Sodium/Glucose Co-transporters and their Solvent

In the preliminary experiments, the effects of DAPA on shortening were tested at three concentrations (10^{-5} M, 10^{-6} M and 10^{-7}). DAPA was only significantly effective at 10^{-5} M and 10^{-6} M to similar extents. Therefore, 10^{-6} M DAPA was used in all experiments. PHLOR and QUER-3-G were also used at the same concentration (10^{-6} M) to facilitate comparison of results.

Certainly it is preferable to use milli-Q water to dissolve any compounds tested because it has a neutral effect on whichever parameter is being investigated, which ensures that any effects observed are from the compound tested rather than the solvent. However, according to the information supplied by the manufacturer, DAPA is most soluble in DMSO (82 mg/ml) for *in vitro* use [247]. DMSO is a widely used solvent and vehicle in research and is soluble in aqueous and organic media because of its amphiphillic structure, which is composed of one highly polar (hydrophilic) and two apolar (lipophilic) groups [243]. The solubilities of PHLOR and QUER-3-G were also tested in DMSO and they were found to be soluble in this organic solvent. Using one solvent for all the tested compounds eliminated the chance for any variability that could have occurred if different solvents were used for each compound. All the working solutions in the experiments contained 0.005% DMSO which does not have any detectable effects on any of the parameters measured in this research. Previous studies in rat myocytes have shown that 0.01% DMSO does not have significant effects on contractile parameters and Ca^{2+} current [105; 263]. Also, $\leq$0.1% DMSO does not significantly alter myocyte morphology and contractile function [182].

In vitro superfusion of PHLOR, QUER-3-G and DAPA was employed. *In vitro* treatment allows more straightforward evaluation of the SGLT inhibitors effects as it ensures that the effects seen are from the compounds themselves and not from their metabolites, while *in vivo* treatment is subjected to various pharmacokinetic influences.

6.5. Phlorizin, Quercetin-3-O-Glucoside and Dapagliflozin Reduce the Amplitude of Shortening in Ventricular Myocytes from Streptozotocin-Induced Diabetic and Control Rats

Ventricular myocytes were freshly isolated on each experimental day. Freshly isolated cells are generally preferable to cell lines in physiological studies as they closely resemble the *in vivo* cell in both structure and function [183]. In addition, cell lines do not exhibit the features required for ECC experiments, including rod-shaped morphology and complement of proteins [241].

A VED system was used to measure myocyte shortening. This technique overcomes some disadvantages of *in vivo* experiments, including the interference of autonomic nerve endings, gap junctions and neurotransmitter uptake systems, and *in vitro* systems such as Langendorff-perfused heart preparation, including the interference of coronary perfusion status [6]. VED also measures shortening in a single-cell rather than in the whole heart [6].

The effects of PHLOR, QUER-3-G and DAPA on shortening were evaluated after exposing the myocytes to the tested SGLT inhibitor for 5 minutes, while being electrically-stimulated at 1 Hz. Although, the HR of adult Wistar rat under normal conditions ranges from about 300-400 beats/min (314.1 ± 4.7 beat/min in light to

380.8 ± 4.6 beat/min in dark) [320], which is approximately equivalent to 5-7 Hz, the myocytes were stimulated at a lower frequency because high frequencies (5-9 Hz) were shown to have a reducing effect on rat myocyte shortening *in vitro* [210]. In addition, many studies use this frequency (1 Hz) for ventricular myocyte electrical stimulation [48; 222; 231; 322]. This enables comparisons between studies. All experiments were performed at physiological temperature (34-36 °C) to mimic the physiological conditions of the ventricular myocytes as much as possible.

RCL, TPK shortening, THALF relaxation and AMP of shortening (expressed as a percentage of shortening of RCL and as a percentage of shortening in STZ and Control myocytes superfused with NT) were measured. There was a significant decrease in RCL in STZ myocytes compared to Controls indicating reduced myocyte size in STZ rats, which is consistent with the significantly reduced heart weights in STZ rats. Reduced RCL may also suggest elevated resting intracellular Ca^{2+} levels which could be attributed to impaired uptake of Ca^{2+} by the SR or impaired exit of Ca^{2+} by NCX. Consistent with previous studies, TPK shortening was significantly prolonged in STZ myocytes compared to Controls [168; 252], which may suggest slow Ca^{2+} entry form the L-type Ca^{2+} channels, slow CICR or reduced myofilament sensitivity. THALF relaxation was not significantly altered between STZ and Control myocytes as shown in previous studies [181; 252]. The AMP of shortening (expressed as a percentage of shortening of RCL) was significantly reduced in STZ myocytes compared to Controls. Figure 6-1 shows the effects of PHLOR, QUER-3-G and DAPA on ventricular myocyte shortening.

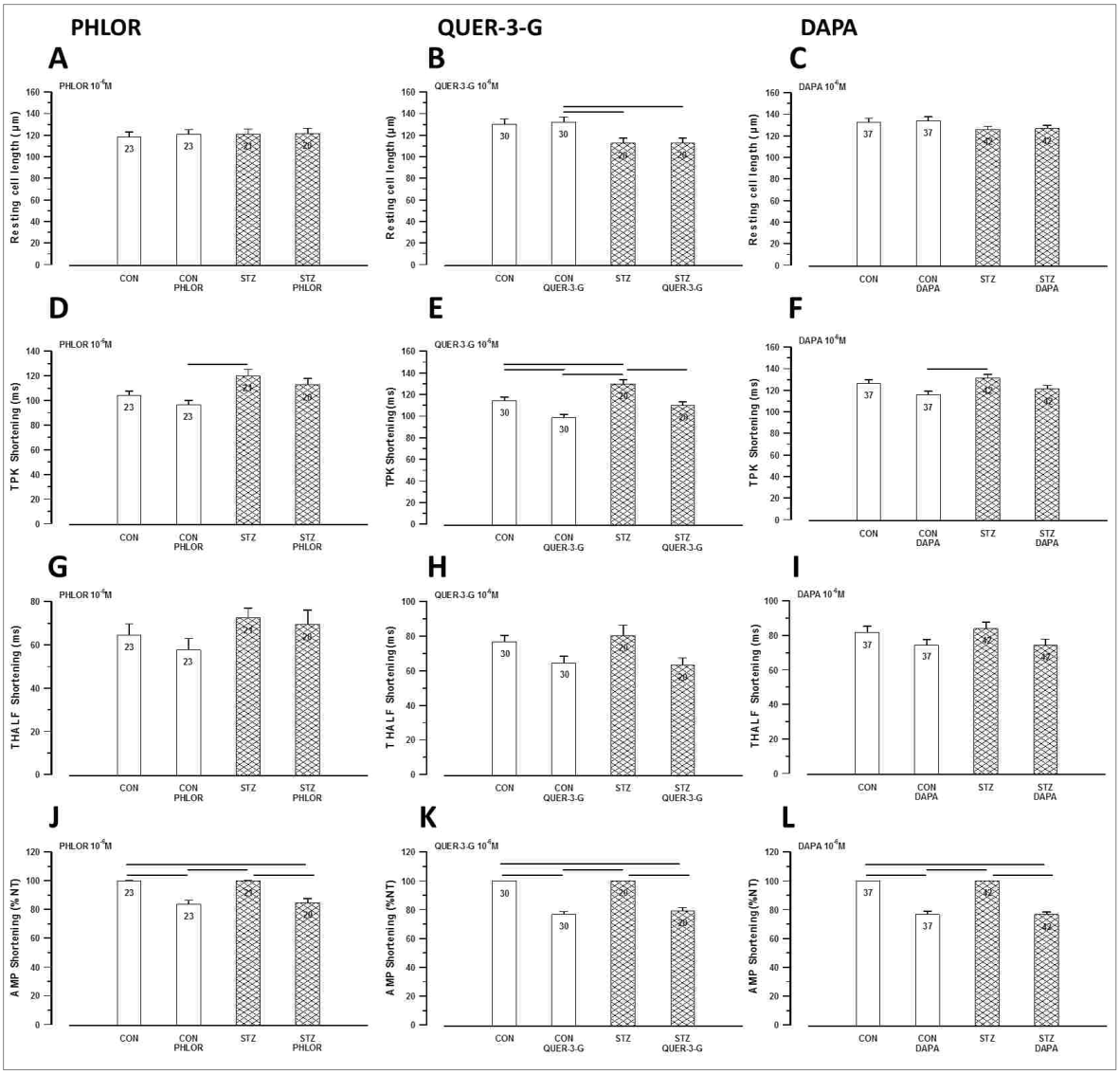

Figure 6-1: Effects of Phlorizin (PHLOR), Quercetin-3-O-glucoside (QUER-3-G) and Dapagliflozin (DAPA) on the amplitude and time course of ventricular myocyte shortening

Graphs showing the mean:

- Resting cell length with PHLOR **(A)**, QUER-3-G **(B)** and DAPA **(C)**
- Time to peak (TPK) shortening with PHLOR **(D)**, QUER-3-G **(E)** and DAPA **(F)**
- Time to half (THALF) with PHLOR **(G)**, QUER-3-G **(H)** and DAPA **(I)**
- Amplitude (AMP) of shortening with PHLOR **(J)**, QUER-3-G **(K)** and DAPA **(L)**

PHLOR, QUER-3-G and DAPA had no significant effects on RCL in STZ and Control myocytes (Fig. 6-1A-C). These results may indicate that SGLT inhibitors do not affect the resting intracellular Ca^{2+} levels. PHLOR and DAPA did not significantly affect TPK shortening in STZ and Control myocytes (Fig. 6-1A,C), whereas QUER-3-G significantly reduced TPK shortening in STZ and Control myocytes (Fig. 6-1B). PHLOR, QUER-3-G and DAPA did not have significant effects on THALF relaxation (Fig. 6-1G-I). This indicates that PHLOR and DAPA, in particular, have no significant effects on the durations of myocyte contraction (indicated by TPK shortening) and relaxation (indicated by THALF relaxation), while QUER-3-G has a reducing effect on the duration of myocyte contraction and no significant effect on the duration of relaxation. There were significant and consistent reductions of the AMP of shortening (expressed as a percentage of shortening in STZ and Control myocytes superfused with NT) to similar extents in both STZ and Control myocytes with PHLOR, QUER-3-G and DAPA (Fig. 6-1J-L) indicating that they exert negative inotropic effects. It was then speculated that these SGLT inhibitors might have effects on the intracellular Ca^{2+} transient.

It was unexpected to observe that long-term exposure (1-3 hrs) to DAPA did not show any significant difference in the AMP of shortening in both Control and STZ myocytes. It seems that DAPA effects were only pronounced after short-term exposure, which might suggest the development of a tolerance towards DAPA effects after long-term exposure.

6.6. Phlorizin, Quercetin-3-O-Glucoside and Dapagliflozin Reduce the Amplitude of Intracellular Ca^{2+} Transient in Ventricular Myocytes from Streptozotocin-Induced Diabetic Rats

The second set of experiments investigated whether PHLOR, QUER-3-G and DAPA have any effect on myocyte intracellular Ca^{2+} transient. Ventricular myocytes were loaded with the fluorescent Ca^{2+}-binding indicator Fura-2 AM. Fura-2AM is widely used to image intracellular Ca^{2+} owing to its better absorption coefficient, quantum yield, Ca^{2+} selectivity, bleaching resistance and the high brightness of its signal compared to other indicators [65; 218].

Fura-2 loaded myocytes, maintained at 35-36°C, were electrically stimulated (1 Hz) and exposed to the tested SGLT inhibitor for 5 minutes. Resting Fura-2 ratio, TPK Ca^{2+} transient, THALF decay of the Ca^{2+} transient and AMP of the Ca^{2+} transient (expressed as a percentage of resting Fura-2 ratio and as a percentage of Ca^{2+} transient in Control and STZ myocytes superfused with NT) were measured. As in previous studies, STZ myocytes did not show any significant alteration in resting Fura-2 ratio compared to Controls [123; 252]. This indicates that the reduction in RCL in STZ myocytes is not attributed to increased resting intracellular Ca^{2+} levels. TPK Ca^{2+} transient was significantly prolonged in STZ myocytes compared to Controls which explains the prolonged TPK shortening in STZ myocytes. THALF decay of the Ca^{2+} transient was not significantly changed in STZ myocytes compared to Controls. As shown in previous studies, the AMP of the Ca^{2+} transient (expressed as a percentage of resting Fura-2 ratio) was not significantly altered in STZ myocytes compared to Controls [34; 123; 181; 252]. Figure 6-2 shows the effects of PHLOR, QUER-3-G and DAPA on ventricular myocyte intracellular Ca^{2+} transient.

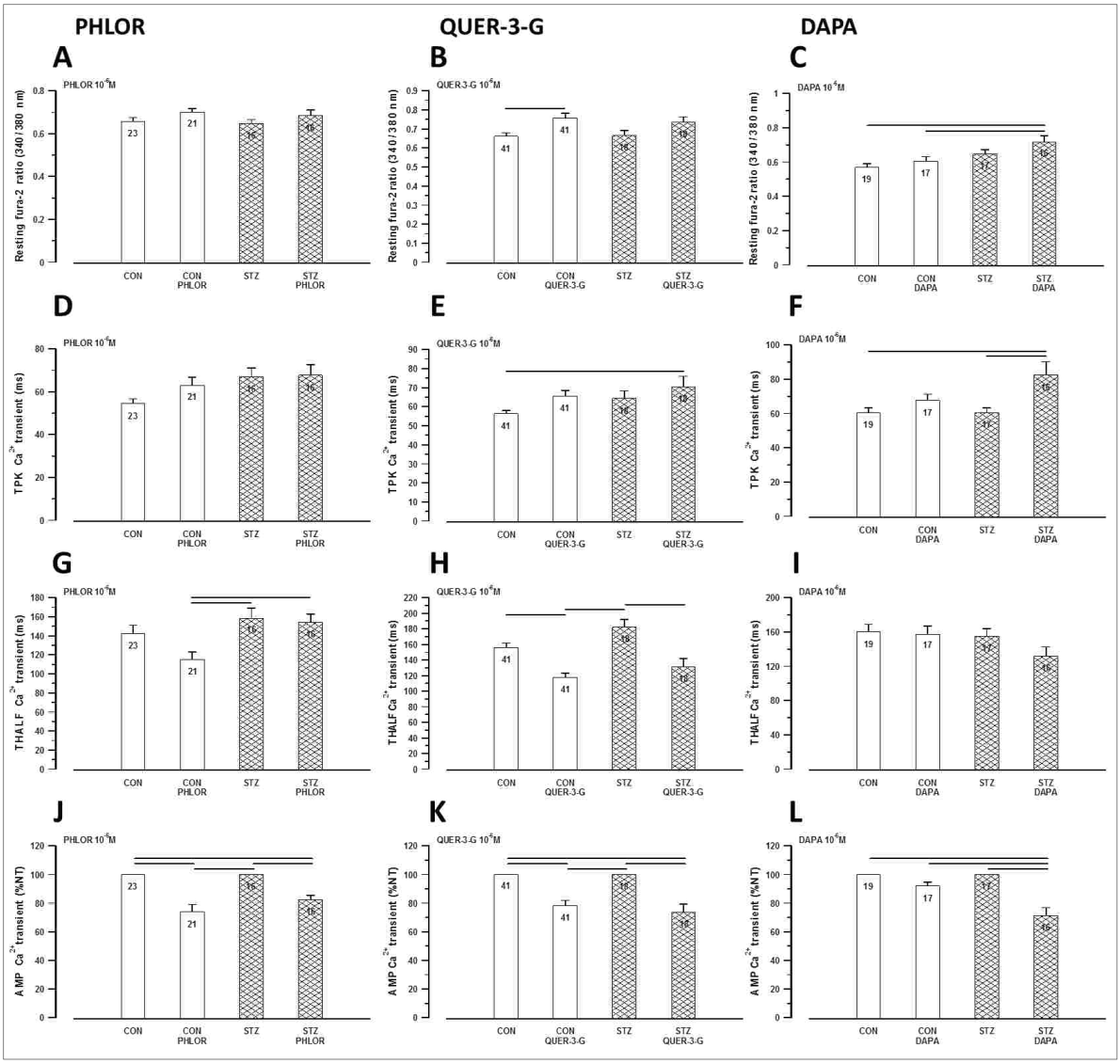

Figure 6-2: Effects of Phlorizin (PHLOR), Quercetin-3-O-glucoside (QUER-3-G) and Dapagliflozin (DAPA) on the amplitude and time course of ventricular myocyte intracellular Ca^{2+} transient

Graphs showing the mean:

- Resting Fura-2 ratio with PHLOR **(A)**, QUER-3-G **(B)** and DAPA **(C)**
- Time to peak (TPK) Ca^{2+} transient with PHLOR **(D)**, QUER-3-G **(E)** and DAPA **(F)**
- Time to half (THALF) decay of the Ca^{2+} transient with PHLOR **(G)**, QUER-3-G **(H)** and DAPA **(I)**
- Amplitude (AMP) of the Ca^{2+} transient with PHLOR **(J)**, QUER-3-G **(K)** and DAPA **(L)**

PHLOR (Fig. 6-2A) and DAPA (Fig. 6-2C) had no significant effects on resting Fura-2 ratio in STZ or Control myocytes (Fig. 6-2A-C) which is consistent with their effects on RCL. However, QUER-3-G significantly increased resting Fura-2 ratio in Control myocytes which might suggest that QUER-3-G affects one of the elements responsible for the removal of intracellular Ca^{2+} during relaxation, such as NCX or SERCA. PHLOR (Fig. 6-2D) and QUER-3-G (Fig. 6-2E) did not significantly alter TPK Ca^{2+} transient in both STZ and Control myocytes. This was expected for PHLOR but not for QUER-3-G owing to its effects on TPK shortening. This may suggest that the observed effects of QUER-3-G on TPK shortening were mediated by a factor other than Ca^{2+}. On the other hand, DAPA (Fig. 6-2F) significantly prolonged TPK Ca^{2+} transient in STZ myocytes without significantly affecting TPK shortening. STZ myocytes appeared to be more susceptible than Controls to the effects of DAPA on the Ca^{2+} transient. PHLOR (Fig. 6-2G) and DAPA (Fig. 6-2I) did not significantly affect THALF decay of the Ca^{2+} transient in either STZ or Control myocytes. On the other hand, QUER-3-G (Fig. 6-2H) significantly reduced THALF decay of the Ca^{2+} transient in both STZ and Control myocytes. PHLOR, QUER-3-G significantly reduced the AMP of the Ca^{2+} transient (expressed as a percentage of shortening in Control and STZ myocytes superfused with NT) in both STZ and Control myocytes, and DAPA significantly reduced it in STZ myocytes which again might suggest a higher susceptibility of STZ myocytes to the effects of DAPA. Olson and colleagues have previously reported that PHLOR modestly decreases the AMP of the Ca^{2+} transient in healthy rat ventricular myocytes

[216]. Lack of significance in their results might be attributed to the smaller sample size used in their study (n = 6) compared to this study (n = 21-23).

6.7. Phlorizin, Quercetin-3-O-Glucoside and Dapagliflozin Do Not Alter Myofilament Sensitivity to Ca^{2+} in Ventricular Myocytes from Streptozotocin-Induced Diabetic and Control Rats

Shortening and Fura-2 ratio were recorded simultaneously to assess myofilament sensitivity to Ca^{2+}. Measuring the gradient of the Fura-2-cell length trajectory during late relaxation of the twitch contraction indicates myofilament response to Ca^{2+} as reported by previous studies [124; 257].

Consistent with previous studies, there was no significant difference in myofilament sensitivity between STZ and Control myocytes [231]. Figure 6-3 shows the effects of PHLOR, QUER-3-G and DAPA on ventricular myocyte myofilament sensitivity to Ca^{2+}.

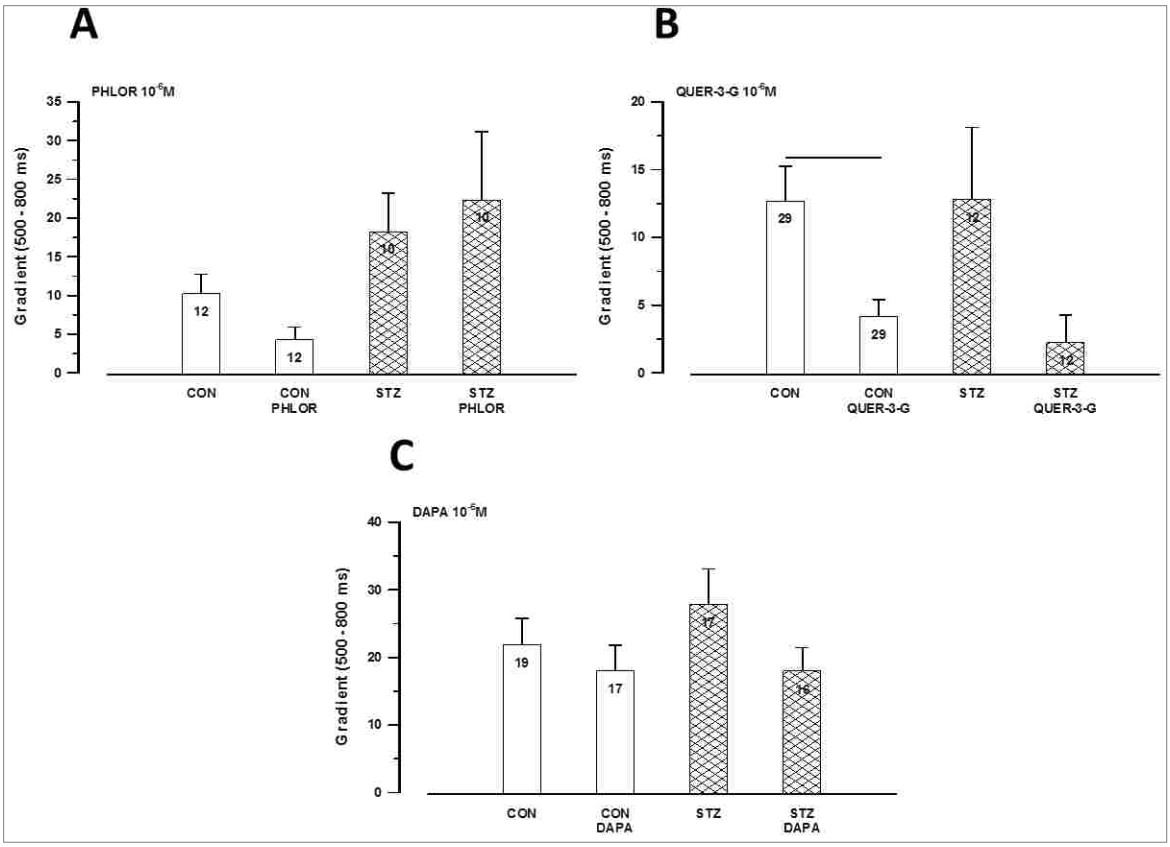

Figure 6-3: Effects of Phlorizin (PHLOR), Quercetin-3-O-glucoside (QUER-3-G) and Dapagliflozin (DAPA) on ventricular myocyte myofilament sensitivity to Ca^{2+}

Graphs showing mean gradient of the Fura-2-cell length trajectory during late relaxation of the twitch contraction during the period 500-800 ms with PHLOR **(A)**, QUER-3-G **(B)** and DAPA **(C)**.

Although PHLOR effects were not significant, it showed a modest decreasing effect on myofilament sensitivity in Control myocytes and an increasing effect in STZ myocytes (Fig. 6-3A). Unlike PHLOR, both QUER-3-G (Fig. 6-3B) and DAPA (Fig. 6-3C) showed the same pattern of effects in both STZ and Control myocytes. QUER-3-G tended to reduce myofilament sensitivity in STZ and Control myocytes, however, its effects were only significant in Control myocytes. DAPA also tended to reduce myofilament sensitivity in STZ and Control myocytes, but none of the effects were

significant. Collectively, these results may suggest that the negative inotropic effects of PHLOR, QUER-3G and DAPA were not mediated by alterations in myofilament sensitivity to Ca^{2+}. Increasing the sample size might reduce the variability of the data and bring some of the changes reported to significance.

6.8. Phlorizin, Quercetin-3-O-Glucoside and Dapagliflozin Do Not Alter Sarcoplasmic Reticulum Ca^{2+} Transport in Ventricular Myocytes from Streptozotocin-Induced Diabetic and Control Rats

SR Ca^{2+} transport was measured in ventricular myocytes maintained at 35-36°C. The experiment protocol involved electrically stimulating the myocytes at 1 Hz, then pausing it for 5 seconds, applying caffeine (20 mmol) for 10 seconds and then resuming the electrical stimulation. Caffeine is a RyR agonist that has been widely used to trigger CICR from the SR by lowering the threshold of RyR for Ca^{2+} activation [165]. During this protocol, the AMP of the caffeine-stimulated Ca^{2+} transient, fractional release of Ca^{2+} (electrical stimulation/caffeine stimulation), and the gradient of myocyte recovery after caffeine application and following resumption of electrical stimulation, were measured once during NT superfusion and repeated during the superfusion of the tested SGLT inhibitor.

The AMP of the caffeine-stimulated Ca^{2+} transient was significantly reduced in STZ myocytes compared to Controls indicating an impaired release of Ca^{2+} form the SR. Fractional release was not significantly altered in STZ myocytes compared to Controls. Recovery of the Ca^{2+} transients was also not significantly altered in STZ myocytes compared to Controls indicating that STZ-induced diabetes does not interfere with the recovery of intracellular Ca^{2+} transient and the refill of SR with

Ca^{2+} during relaxation. Figure 6-4 shows the effects of PHLOR, QUER-3-G and DAPA on ventricular myocyte sarcoplasmic reticulum Ca^{2+}.

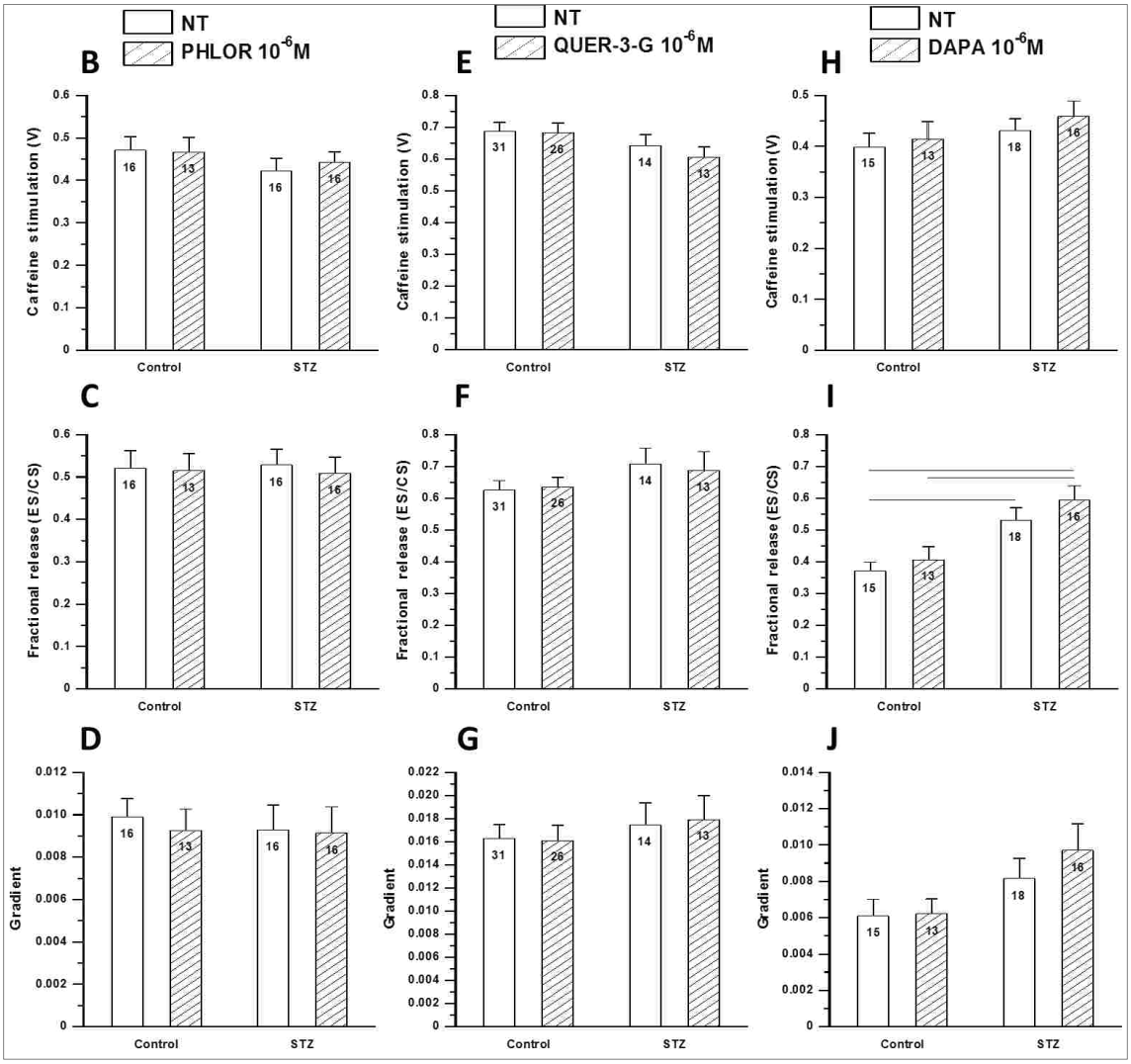

Figure 6-4: Effects of Phlorizin (PHLOR), Quercetin-3-O-glucoside (QUER-3-G) and Dapagliflozin (DAPA) on ventricular myocyte sarcoplasmic reticulum Ca^{2+}

Graphs showing mean:

- Amplitude of the caffeine-stimulated Ca^{2+} transient with PHLOR **(A)**, QUER-3-G **(B)** and DAPA **(C)**
- Fractional release of Ca^{2+} (Electrical stimulation/Caffeine stimulation) with PHLOR **(D)**, QUER-3-G **(E)** and DAPA **(F)**
- Recovery of the Ca^{2+} transients following rapid application of caffeine with PHLOR **(G)**, QUER-3-G **(H)** and DAPA **(I)**

No significant effects for PHLOR, QUER-3-G and DAPA were observed on the AMP of the caffeine-stimulated Ca^{2+} transient (Fig.6-4B,E,H), fractional release of Ca^{2+} (Fig.6-4C,F,I) and the recovery of the Ca^{2+} transients (Fig.6-4D,G,J) in STZ and Control myocytes. PHLOR was previously reported to have no effect on the caffeine-stimulated SR Ca^{2+} load in healthy rat ventricular myocytes [216]. These findings collectively indicate that the negative inotropic effect produced by PHLOR, QUER-3-G and DAPA is independent of SR Ca^{2+} content and transport.

6.9. Dapagliflozin Reduces the Amplitude of L-type Ca^{2+} Current in Ventricular Myocytes from Streptozotocin-Induced Diabetic and Control Rats

As a voltage-gated channel, the Ca^{2+} channel passes through three transitions including closed, activated (open) and inactivated [149; 166] depending on the electrical membrane potential of the myocyte [24]. Using the patch clamp technique, the effects of DAPA on each of the three transitions were studied. The patch pipette was made from borosilicate glass which is widely used and has several advantages such as the ease of pulling at low temperature, ease of sealing with the cell and lower electrical noise during recordings [166; 215]. Interference of other cardiac ion channel currents was prevented by blocking K^+ current with TEA^+ to suppress ATP-sensitive K^+ currents and residual delayed rectifier K^+ currents [155; 255] and by using Cs^+, in the intracellular patch pipette solution, instead of K^+ to suppress outward K^+ currents [134; 255]. Na^+ current was blocked by holding myocytes at -40 mV [106] or at -50 mV [318].

As reported in previous studies, L-type Ca^{2+} current was smaller in myocytes from STZ-induced diabetic rats compared to Controls [34; 292]. DAPA further significantly decreased the AMP of L-type Ca^{2+} current in STZ/DAPA myocytes compared to STZ myocytes at -40 mV and from -20 mV to +20 mV, and in Control/DAPA myocytes compared to Controls at -60 mV and from -20 mV to +20 mV. Both STZ/DAPA and Control/DAPA myocytes showed significant reductions of L-type Ca^{2+} current between -20 mV to +20 mV compared to STZ myocytes and Controls, respectively. Since the L-type Ca^{2+} channel is the main pathway for entry of extracellular Ca^{2+} during contraction, decreasing Ca^{2+} channel activation by DAPA reduces the levels of Ca^{2+} entering the myocyte. This in turn reduces myocyte contractility suggesting that the effects of DAPA on L-type Ca^{2+} current may partly underlie the negative inotropic effects of DAPA.

DAPA did not significantly alter the inactivation and recovery of L-type Ca^{2+} current which indicates that DAPA only affects the channel when activated/open. Voltage-gated ion channels can act as allosteric receptors allowing a drug to bind to them during a certain transition. By switching to another transition, this alters the conformation of the drug binding site and thus, the drug would not recognize its binding site unless the channel goes back to the previous transition [24]. This phenomenon is called ‘use-dependence’ [24] and can be applied to interpret the behavior of DAPA on the L-type Ca^{2+} channel. During activation, DAPA may have bound to an allosteric site of the L-type Ca^{2+} channel and resulted in the reduction of Ca^{2+} current. However, when the channel switched from the activated state to the inactivated or closed state, the conformation of the allosteric site, to which DAPA

binds, changed preventing DAPA from recognizing and binding to it during closed and inactivated states. The binding of DAPA to the opened channel prevented the influx of Ca^{2+} through the channel and decreased myocyte shortening as a result of the reduced levels of intracellular Ca^{2+}. Calcium channel blockers inhibit Ca^{2+} entry through the channel into the cell [153]. They are most effective during the inactivated transition [20; 119; 120]. This suggests that DAPA is an L-type Ca^{2+} channel blocker that, unlike the traditional Ca^{2+} channel blockers, is selective for channels during the activated transition.

6.10. Clinical Significance of Sodium/Glucose Co-transporter Inhibitors on Shortening and Intracellular Ca^{2+}

During heart contraction, Ca^{2+}, which is the main regulator of this process, enters the cardiomyocyte mainly through the L-type Ca^{2+} channels, which then triggers Ca^{2+} release from the SR [26]. The concentration of Ca^{2+} rises transiently and initiates the process of myocyte contraction [52].

PHLOR and QUER-3-G decreased the level of intracellular Ca^{2+} levels by one or more mechanism(s) which need further investigation. This resulted in a reduction of ventricular myocyte shortening. DAPA blocked the activated L-type Ca^{2+} channel at voltages ranging from -20 mv to +20 mV in both STZ and Control myocytes, which lead to a reduction of intracellular Ca^{2+} levels and consequent reduction of myocyte shortening.

The negative inotropic effects of all the tested SGLT inhibitors were produced in diabetic (STZ) myocytes. Since these negative inotropic effects are suggested to be

mediated by blocking the activity of the L-type Ca^{2+} channel (as in case of DAPA), it is necessary to know the outcome of these effects on the diabetic heart. L-type Ca^{2+} channel blockers are widely used to treat CV disorders such as hypertension, angina and arrhythmias [110]. They also have anti-inflammatory [71] and immunosuppressive [112] effects. Considering that DM patients are usually hypertensive, it was reported previously in clinical trials that calcium channel blockers have been beneficial in hypertension treatment in diabetic patients [285; 286; 293]. The activity of the L-type Ca^{2+} channel is also modulated by several factors such as voltage, enzymes and the activity of receptors [193]. The negative inotropic effects of SGLT inhibitors in this study can be indirectly mediated by one or more of these factors. Therefore, the direct mechanism underlying the observed effect requires further studies.

This study is also considered as a toxicological study owing to the relatively high concentration of DAPA used compared to that in the clinical setting. A clinical pharmacokinetic study has shown that oral administration of 10 mg DAPA produces maximum plasma concentration (C_{max}) that reaches ≈ 0.333 x 10^{-6} M, which is less than DAPA concentration (10^{-6} M) in this study by approximately 3 times [152].

6.11. Limitations of Study

There were some technical and time limitations in this study including the following:

1) Induction of DM in rats using STZ employed the i.p. route that, unlike the i.v. route, requires absorption of STZ to the bloodstream before initiating its action.

2) Evaluation of myofilament sensitivity to Ca^{2+}, which involves measuring myocyte shortening and Ca^{2+} transient simultaneously, was performed in the presence of the Ca^{2+} chelator and indicator Fura-2 AM which slightly hinders shortening. Thus, Fura-2 AM does not allow accurate assessment for the actual myocyte shortening, however, it is essential for Ca^{2+} transient measurements. That is why separate experiments were performed for measuring shortening in the absence of Fura-2 AM.

3) Experiments on myofilament sensitivity to Ca^{2+} still need a bigger sample size to provide more conclusive results with PHLOR, QUER-3-G and DAPA.

4) Due to shortage of time, patch clamp experiments testing the effects on L-type Ca^{2+} current were only conducted with DAPA rather than including PHLOR and QUER-3-G as well. Future experiments should include testing PHLOR and QUER-3-G on L-type Ca^{2+} current.

Chapter 7: Conclusions and Future Directions

7.1. Conclusions

Collectively, all the tested SGLT inhibitors: PHLOR, QUER-3-G and DAPA, produced negative inotropic effects.

For PHLOR, QUER-3-G and DAPA, it can be concluded that the negative inotropism produced was not related to changes in SR Ca^{2+} transport of STZ and Control myocytes. However, more evidence is needed to conclude whether they significantly affect myofilament sensitivity to Ca^{2+}, which can be provided by increasing the sample size of the myocytes tested.

PHLOR and QUER-3-G are suggested to produce negative inotropic effects by reducing the AMP of the intracellular Ca^{2+} transient. However, the exact mechanism(s) behind reducing intracellular Ca^{2+} transient is yet to be investigated. DAPA is suggested to produce its negative inotropic effects by blocking the L-type Ca^{2+} channel, which consequently decreases the intracellular levels of Ca^{2+} and reduces myocyte shortening.

A summary for the main findings of the study and some future directions are shown in Figure 7-1.

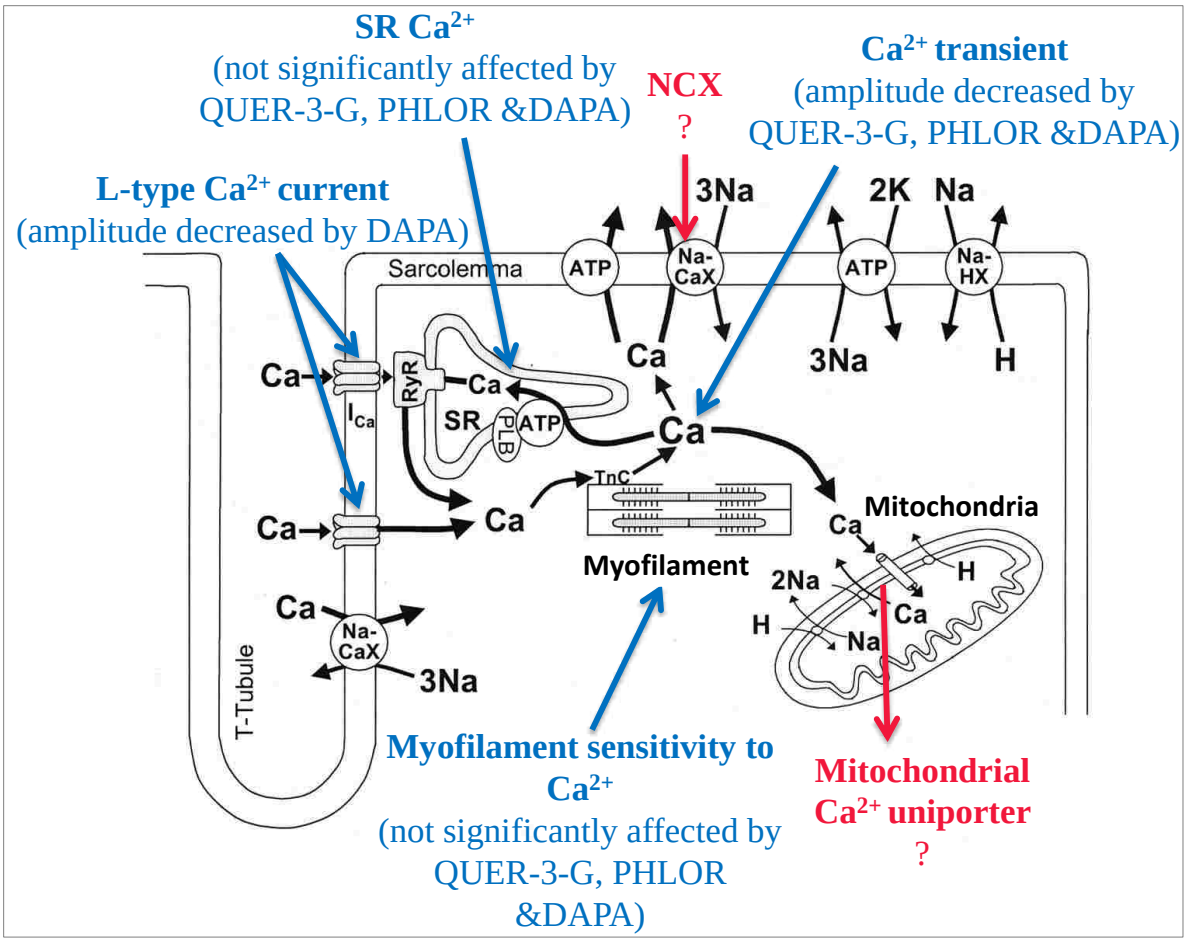

Figure 7-1: Summary of the main findings of the study and some future directions

Adapted from [26]

SR: sarcoplasmic reticulum; **NCX:** Na^+/Ca^{2+} exchanger; **PHLOR:** Phlorizin; **QUER-3-G:** Quercetin-3-O-glucoside; **DAPA:** Dapagliflozin. Future directions are denoted by a question mark (**?**).

7.2. Future Directions

Data generated in this study has set the stage for several future studies. These might include the following:

1) The sample size for the experiments of myofilament sensitivity to Ca^{2+} should be increased with PHLOR, QUER-3-G and DAPA.

2) The effects of PHLOR and QUER-3-G on L-type Ca^{2+} current should be investigated as a possible mechanism for their observed negative inotropic effects.

3) DAPA was tested on shortening at three concentrations after a 5 minute application. Further studies could be conducted over different drug application times on myocyte shortening, and at different concentrations and application times on intracellular Ca^{2+} and L-type Ca^{2+} current.

4) Similarly, PHLOR and QUER-3-G can be further studied on myocyte shortening, intracellular Ca^{2+} and L-type Ca^{2+} current at different concentrations and over different application times.

5) Patch clamp experiments can be performed at different concentrations of extracellular Ca^{2+}.

6) The activity of the L-type Ca^{2+} channel is known to be modulated by several factors such as β- and α-adrenergic receptors. The effects of DAPA on these receptors can be further studied to investigate whether it affects the L-type Ca^{2+} channel directly or indirectly.

7) Other factors involved in controlling intracellular Ca^{2+} signaling such as the mitochondria and NCX can be tested with PHLOR, QUER-3-G and DAPA (Fig. 7-1).

8) Expression of messenger ribonucleic acid (mRNA) and protein of SGLTs and GLUTs can be studied in control and diabetic hearts using polymerase chain reaction (PCR) and western blot techniques.

9) Expression of mRNA and protein of the L-type Ca^{2+} channel, and SGLT1 and 2 can be studied in control and diabetic hearts, after *in vivo* treatment of PHLOR, QUER-3-G and DAPA.

10) As more SGLT inhibitors with greater selectivity are developed, they can also be used to further characterize the effects of these medications on contraction and intracellular Ca^{2+} in control and diabetic hearts.

11) In the long-term, the effects of SGLT inhibitors might also be investigated in SGLT knockout myocytes and knockout animals.

Chapter 8: References

1. Abel, E. D., Kaulbach, H. C., Tian, R., Hopkins, J. C. A., Duffy, J., Doetschman, T., Minnemann, T., Boers, M. E., Hadro, E., Oberste-Berghaus, C., Quist, W., Lowell, B. B., Ingwall, J. S., & Kahn, B. B. (1999). Cardiac hypertrophy with preserved contractile function after selective deletion of GLUT4 from the heart. *The Journal of Clinical Investigation, 104,* 1703-1714.

2. Ader, P., Blöck, M., Pietzsch, S., & Wolffram, S. (2001). Interaction of quercetin glucosides with the intestinal sodium/glucose co-transporter (SGLT-1). *Cancer Letters, 162,* 175-180.

3. Ahmed, D., Kumar, V., Verma, A., Gupta, P., Kumar, H., Dhingra, V., Mishra, V., & Sharma, M. (2014). Antidiabetic, renal/hepatic/pancreas/cardiac protective and antioxidant potential of methanol/dichloromethane extract of Albizzia Lebbeck Benth. stem bark (ALEx) on streptozotocin induced diabetic rats. *BMC Complementary and Alternative Medicine, 14,* 243.

4. Akbar, D. H., Hagras, M. M., Amin, H. A., & Khorshid, O. A. (2013). Comparison between the effect of glibenclamide and captopril on experimentally induced diabetic nephropathy in rats. *Journal of Renin-Angiotensin-Aldosterone System, 14,* 103-115.

5. Akbarzadeh, A., Norouzian, D., Mehrabi, M. R., Jamshidi, S., Farhangi, A., Verdi, A. A., Mofidian, S. M. A., & Rad, B. L. (2007). Induction of diabetes by Streptozotocin in rats. *Indian J Clin Biochem, 22,* 60-64.

6. Al Kury, L. T., Voitychuk, O. I., Ali, R. M., Galadari, S., Yang, K. H. S., Howarth, F. C., Shuba, Y. M., & Oz, M. (2014). Effects of endogenous cannabinoid anandamide on excitation–contraction coupling in rat ventricular myocytes. *Cell Calcium, 55,* 104-118.

7. Alberts, B., Bray, D., Hopkin, K., Johnson, A., Lewis, J., Raff, M., Roberts, K., & Walter, P. (2013). Transport Across Cell Membranes. In *Essential Cell Biology* (4 ed., pp. 383-418). Taylor & Francis Group.

8. American Diabetes Association (2000). Type 2 diabetes in children and adolescents. American Diabetes Association. *Diabetes Care, 23,* 381-389.

9. American Diabetes Association (2003). Peripheral Arterial Disease in People With Diabetes. *Diabetes Care, 26,* 3333-3341.

10. American Diabetes Association (2013). Diagnosis and Classification of Diabetes Mellitus. *Diabetes Care, 36,* S67-S74.

11. American Diabetes Association (2013). Standards of Medical Care in Diabetes–2013. *Diabetes Care, 36,* S11-S66.

12. Armstrong, D. & Al-Awadi, F. (1991). Lipid peroxidation and retinopathy in streptozotocin-induced diabetes. *Free Radical Biology and Medicine, 11,* 433-436.

13. AstraZeneca (3-24-2014). Forxiga® receives regulatory approval in Japan for the treatment of type 2 diabetes. http://www.astrazeneca.com/Media/Press-releases/Article/20140324--forxiga-japan-approval

14. AstraZeneca (8-11-2014). Multicenter Trial to Evaluate the Effect of Dapagliflozin on the Incidence of Cardiovascular Events (DECLARE-TIMI58). http://clinicaltrials.gov/show/NCT01730534

15. AstraZeneca (1-22-2014). XIGDUO™ (dapagliflozin and metformin hydrochloride) approved in the European Union for type 2 diabetes. http://www.astrazeneca.com/Media/Press-releases/Article/20142101--xigduo-dapagliflozin-and-metformin-hydrochloride

16. Bailey, C. J., Iqbal, N., T'joen, C., & List, J. F. (2012). Dapagliflozin monotherapy in drug-naïve patients with diabetes: a randomized-controlled trial of low-dose range. *Diabetes, Obesity and Metabolism, 14,* 951-959.

17. Baldisserotto, A., Malisardi, G., Scalambra, E., Andreotti, E., Romagnoli, C., Vicentini, C. B., Manfredini, S., & Vertuani, S. (2012). Synthesis, antioxidant and antimicrobial activity of a new phloridzin derivative for dermo-cosmetic applications. *Molecules., 17,* 13275-13289.

18. Balteau, M., Tajeddine, N., de Meester, C., Ginion, A., Des Rosiers, C., Brady, N. R., Sommereyns, C., Horman, S., Vanoverschelde, J. L., Gailly, P., Hue, L., Bertrand, L., & Beauloye, C. (2011). NADPH oxidase activation by hyperglycaemia in cardiomyocytes is independent of glucose metabolism but requires SGLT1. *Cardiovascular Research, 92,* 237-246.

19. Bazan, C., Barba, D. T., Blomgren, P., & Paolini, P. (2009). Image Processing Techniques for Assessing Contractility in Isolated Adult Cardiac Myocytes. *International Journal of Biomedical Imaging*.

20. Bean, B. P. (1984). Nitrendipine block of cardiac calcium channels: high-affinity binding to the inactivated state. *Proceedings of the National Academy of Sciences, 81,* 6388-6392.

21. Behme, M., Dupre, J., Harris, S., Hramiak, I., & Mahon, J. (2003). Insulin Resistance in Latent Autoimmune Diabetes of Adulthood. *Annals of the New York Academy of Sciences, 1005,* 374-377.

22. Bell, G. I., Kayano, T., Buse, J. B., Burant, C. F., Takeda, J., Lin, D., Fukumoto, H., & Seino, S. (1990). Molecular biology of mammalian glucose transporters. *Diabetes Care, 13,* 198-208.

23. Bell, R. M., Mocanu, M. M., & Yellon, D. M. (2011). Retrograde heart perfusion: The Langendorff technique of isolated heart perfusion. *Journal of Molecular and Cellular Cardiology, 50,* 940-950.

24. Bennett, P. B. (2006). Ion-channel drug screening galvanized. *Nat Biotech, 24,* 415-416.

25. Berry, G. T., Mallee, J. J., Kwon, H. M., Rim, J. S., Mulla, W. R., Muenke, M., & Spinner, N. B. (1995). The human osmoregulatory Na+/myo-inositol cotransporter gene (SLC5A3): molecular cloning and localization to chromosome 21. *Genomics, 25,* 507-513.

26. Bers, D. M. (2000). Calcium Fluxes Involved in Control of Cardiac Myocyte Contraction. *Circulation Research, 87,* 275-281.

27. Bers, D. M. (2002). Cardiac excitation-contraction coupling. *Nature, 415,* 198-205.

28. Bertrand, L., Horman, S., Beauloye, C., & Vanoverschelde, J. L. (2008). Insulin signalling in the heart. *Cardiovascular Research, 79,* 238-248.

29. Bnouham, M., Merhfour, F. Z., Ziyyat, A., Aziz, M., Legssyer, A., & Mekhfi, H. (2010). Antidiabetic effect of some medicinal plants of Oriental Morocco in neonatal non-insulin-dependent diabetes mellitus rats. *Human & Experimental Toxicology, 29,* 865-871.

30. Bollano, E., Omerovic, E., Svensson, H., Waagstein, F., & Fu, M. (2007). Cardiac remodeling rather than disturbed myocardial energy metabolism is associated with cardiac dysfunction in diabetic rats. *International Journal of Cardiology, 114,* 195-201.

31. Borges, G., de Oliveira, M., Salgado, H., & Fazan, R. (2006). Myocardial performance in conscious streptozotocin diabetic rats. *Cardiovascular Diabetology, 5,* 26.

32. Bouron, A., Potreau, D., Besse, C., & Raymond, G. (1990). An efficient isolation procedure of Ca-tolerant ventricular myocytes from ferret heart for applications in electrophysiological studies. *Biology of the Cell, 70,* 121-127.

33. Boyett, M. R. (2009). 'And the beat goes on' The cardiac conduction system: the wiring system of the heart. *Experimental physiology, 94,* 1035-1049.

34. Bracken, N., Howarth, F. C., & Singh, J. (2006). Effects of Streptozotocin-Induced Diabetes on Contraction and Calcium Transport in Rat Ventricular Cardiomyocytes. *Annals of the New York Academy of Sciences, 1084,* 208-222.

35. Bradford, B. J. & Allen, M. S. (2007). Phlorizin Administration Does Not Attenuate Hypophagia Induced by Intraruminal Propionate Infusion in Lactating Dairy Cattle. *The Journal of Nutrition, 137,* 326-330.

36. Brown, L., Johnson, E., & Goodman, B. (2008). Making Patch-pipettes and Sharp Electrodes with a Programmable Puller. e939.

37. Brownie, S., Hunter, L., Rossiter, R., Hills, A. P., Robb, W., & Hag-Ali, M. (2014). Diabetes in the United Arab Emirates: the need for valid datasets for health service planning. *The Lancet Diabetes & Endocrinology, 2,* 535-537.

38. Bugger, H. & Abel, E. D. (2009). Rodent models of diabetic cardiomyopathy. *Disease Models & Mechanisms, 2,* 454-466.

39. Cade, W. T. (2008). Diabetes-Related Microvascular and Macrovascular Diseases in the Physical Therapy Setting. *Physical Therapy, 88,* 1322-1335.

40. Cai, Q., Li, B., Yu, F., Lu, W., Zhang, Z., Yin, M., & Gao, H. (2013). Investigation of the Protective Effects of Phlorizin on Diabetic Cardiomyopathy in db/db Mice by Quantitative Proteomics. *Journal of Diabetes Research, 2013*.

41. Callaghan, B. C., Cheng, H. T., Stables, C. L., Smith, A. L., & Feldman, E. L. (2012). Diabetic neuropathy: clinical manifestations and current treatments. *The Lancet Neurology, 11,* 521-534.

42. Cameron, N. E. & Cotter, M. A. (2001). Diabetes causes an early reduction in autonomic ganglion blood flow in rats. *Journal of Diabetes and its Complications, 15,* 198-202.

43. Canivell, S. & Gomis, R. (2014). Diagnosis and classification of autoimmune diabetes mellitus. *Autoimmunity Reviews, 13*.

44. Cannell, M. B., Cheng, H., & Lederer, W. J. Spatial non-uniformities in [Ca2+]i during excitation-contraction coupling in cardiac myocytes. *Biophysical Journal, 67,* 1942-1956.

45. Cannell, M. & Thomas, M. (1994). Intracellular ion measurement with fluorescent indicators. In D.C.Ogden (Ed.), *Microelectrode techniques, The Plymouth workshop handbook.* (2 ed., pp. 317-359). Cambridge, UK.

46. Carbonell, L. F. S. (1987). Hemodynamic alterations in chronically conscious unrestrained diabetic rats. *American Journal of Physiology - Heart and Circulatory Physiology, 252,* H900-H905.

47. Carlson, G., Tou, C., Parikh, S., Birmingham, B., & Butler, K. (2011). Evaluation of the effect of dapagliflozin on cardiac repolarization: a thorough QT/QTc study. *Diabetes Ther, 2,* 123-132.

48. Carneiro-Júnior, M. A., Pelúzio, M. C. G., Silva, C. H. O., Amorim, P. R. S., Silva, K. A., Souza, M. O., Castro, C. A., Roman-Campos, D., Prímola-Gomes, T. N., & Natali, A. J. (2010). Exercise training and detraining modify the morphological and mechanical properties of single cardiac myocytes obtained from spontaneously hypertensive rats. *Brazilian Journal of Medical and Biological Research, 43,* 1042-1046.

49. Carney, S. L., Wong, N. L., & Dirks, J. H. (1979). Acute effects of streptozotocin diabetes on rat renal function. *The Journal of laboratory and clinical medicine, 93,* 950-961.

50. Carter, M. & Shieh, J. C. (2010). Chapter 4 - Electrophysiology. In M.Carter & J. C. Shieh (Eds.), *Guide to Research Techniques in Neuroscience* (pp. 91-118). New York: Academic Press.

51. Castaneda-Sceppa, C. & Castaneda, F. (2011). Sodium–dependent glucose transporter protein as a potential therapeutic target for improving glycemic control in diabetes. *Nutrition reviews, 69,* 720-729.

52. Catterall, W. A. (2011). Voltage-Gated Calcium Channels. *Cold Spring Harbor Perspectives in Biology, 3*.

53. Cefalu, W. T. (2006). Animal Models of Type 2 Diabetes: Clinical Presentation and Pathophysiological Relevance to the Human Condition. *ILAR Journal, 47,* 186-198.

54. Cermak, R., Landgraf, S., & Wolffram, S. (2004). Quercetin glucosides inhibit glucose uptake into brush-border-membrane vesicles of porcine jejunum. *British Journal of Nutrition, 91,* 849-855.

55. Chandar, N. & Viselli, S. (2012). Glucose Transport. In *Cell and Molecular Biology-Lippincott's Illustrated Reviews Series* (Wolters Kluwer Health.

56. Chao, E. C. & Henry, R. R. (2010). SGLT2 inhibition –a novel strategy for diabetes treatment. *Nat Rev Drug Discov, 9,* 551-559.

57. Chen, L. Q., Hou, B. H., Lalonde, S., Takanaga, H., Hartung, M. L., Qu, X. Q., Guo, W. J., Kim, J. G., Underwood, W., & Chaudhuri, B. (2010). Sugar transporters for intercellular exchange and nutrition of pathogens. *Nature, 468*, 527-532.

58. Chen, L. Q., Qu, X. Q., Hou, B. H., Sosso, D., Osorio, S., Fernie, A. R., & Frommer, W. B. (2012). Sucrose efflux mediated by SWEET proteins as a key step for phloem transport. *Science, 335*, 207-211.

59. Chen, P., Zhang, W., Zhou, J., Wang, P., Xiao, L., & Yang, M. (2009). Development of planar patch clamp technology and its application in the analysis of cellular electrophysiology. *Progress in Natural Science, 19*, 153-160.

60. Chen, Z. C., Cheng, Y. Z., Chen, L. J., Cheng, K. C., Li, Y., & Cheng, J. (2012). Increase of ATP-sensitive potassium (KATP) channels in the heart of type-1 diabetic rats. *Cardiovascular Diabetology, 11*, 8.

61. Cheng, J. T., Huang, C. C., Liu, I. M., Tzeng, T. F., & Chang, C. J. (2006). Novel Mechanism for Plasma Glucose–Lowering Action of Metformin in Streptozotocin-Induced Diabetic Rats. *Diabetes, 55*, 819-825.

62. Cheung, N., Mitchell, P., & Wong, T. Y. (2010). Diabetic retinopathy. *The Lancet, 376*, 124-136.

63. Chiu, H. K., Tsai, E. C., Juneja, R., Stoever, J., Brooks-Worrell, B., Goel, A., & Palmer, J. P. (2007). Equivalent insulin resistance in latent autoimmune diabetes in adults (LADA) and type 2 diabetic patients. *Diabetes Research and Clinical Practice, 77*, 237-244.

64. Choi, K. M., Zhong, Y., Hoit, B. D., Grupp, I. L., Hahn, H., Dilly, K. W., Guatimosim, S., Ledere, W. J., & Matlib, M. A. (2002). Defective intracellular Ca2+ signaling contributes to cardiomyopathy in Type 1 diabetic rats. *American Journal of Physiology - Heart and Circulatory Physiology, 283*, H1398-H1408.

65. Cobbold, P. H. & Rink, T. J. (1987). Fluorescence and bioluminescence measurement of cytoplasmic free calcium. *Biochemical Journal, 248*, 313.

66. Cosyns, B., Droogmans, S., Hernot, S., Degaillier, C., Garbar, C., Weytjens, C., Roosens, B., Schoors, D., Lahoutte, T., Franken, P., & Van Camp, G. (2008). Effect of streptozotocin-induced diabetes on myocardial blood flow reserve assessed by myocardial contrast echocardiography in rats. *Cardiovascular Diabetology, 7,* 26.

67. Cosyns, B., Droogmans, S., Weytjens, C., Lahoutte, T., Van Camp, G., Schoors, D., & Franken, P. (2007). Effect of streptozotocin-induced diabetes on left ventricular function in adult rats: an in vivo Pinhole Gated SPECT study. *Cardiovascular Diabetology, 6,* 30.

68. Craig, M. E., Hattersley, A., & Donaghue, K. C. (2009). Definition, epidemiology and classification of diabetes in children and adolescents. *Pediatric diabetes, 10,* 3-12.

69. Crespy, V., Aprikian, O., Morand, C., Besson, C., Manach, C., Demigné, C., & Rémésy, C. (2001). Bioavailability of Phloretin and Phloridzin in Rats. *The Journal of Nutrition, 131,* 3227-3230.

70. Dai, S., Fraser, H., Yuen, V. G., & McNeill, J. H. (1994). Improvement in cardiac function in streptozotocin-diabetic rats by salt loading. *Can.J Physiol Pharmacol, 72,* 1288-1293.

71. Das, R., Burke, T., Van Wagoner, D. R., & Plow, E. F. (2009). L-Type Calcium Channel Blockers Exert an Antiinflammatory Effect by Suppressing Expression of Plasminogen Receptors on Macrophages. *Circulation Research, 105,* 167-175.

72. Deeds, M. C., Anderson, J. M., Armstrong, A. S., Gastineau, D. A., Hiddinga, H. J., Jahangir, A., Eberhardt, N. L., & Kudva, Y. C. (2011). Single dose streptozotocin-induced diabetes: considerations for study design in islet transplantation models. *Laboratory Animals, 45,* 131-140.

73. DeFronzo, R. A. (2004). Pathogenesis of type 2 diabetes mellitus. *Med Clin N Am, 88,* 787-835.

74. Delbridge, L. M. D. & Roos, K. P. (1997). Optical Methods to Evaluate the Contractile Function of Unloaded Isolated Cardiac Myocytes. *Journal of Molecular and Cellular Cardiology, 29,* 11-25.

75. Dokken, B. B. (2008). The Pathophysiology of Cardiovascular Disease and Diabetes: Beyond Blood Pressure and Lipids. *Diabetes Spectrum, 21,* 160-165.

76. Donaghue, K. C., Chiarelli, F., Trotta, D., Allgrove, J., & Dahl-Jorgensen, K. (2009). Microvascular and macrovascular complications associated with diabetes in children and adolescents. *Pediatric diabetes, 10,* 195-203.

77. Donnan, G. A., Fisher, M., Macleod, M., & Davis, S. M. (2010). Stroke. *The Lancet, 371,* 1612-1623.

78. Donnelly, R., Emslie-Smith, A. M., Gardner, I. D., & Morris, A. D. (2000). ABC of arterial and venous disease: vascular complications of diabetes. *BMJ: British Medical Journal, 320,* 1062.

79. Dziuba, J., Alperin, P., Racketa, J., Iloeje, U., Goswami, D., Hardy, E., Perlstein, I., Grossman, H. L., & Cohen, M. (2014). Modeling effects of SGLT-2 inhibitor dapagliflozin treatment versus standard diabetes therapy on cardiovascular and microvascular outcomes. *Diabetes, Obesity and Metabolism, 16,* 628-635.

80. Ehrenkranz, J. R. L., Lewis, N. G., Ronald Kahn, C., & Roth, J. (2005). Phlorizin: a review. *Diabetes/Metabolism Research and Reviews, 21,* 31-38.

81. Eisenbarth, G. S. (2010). Banting Lecture 2009: An Unfinished Journey: Molecular Pathogenesis to Prevention of Type 1A Diabetes. *Diabetes, 59,* 759-774.

82. Elçioglu, H. K., Kabasakal, L., Özkan, N., Çelikel, Ç., & Aanoglu-Dülger, G. (2011). A study comparing the effects of rosiglitazone and/or insulin treatments on streptozotocin induced diabetic (type I diabetes) rat aorta and cavernous tissues. *European Journal of Pharmacology, 660,* 476-484.

83. Ellis, H. (2009). The anatomy of the heart. *Anaesthesia & Intensive Care Medicine, 10,* 357-359.

84. Erejuwa, O. O., Sulaiman, S. A., Wahab, M. S., Sirajudeen, K. N., Salleh, M. S., & Gurtu, S. (2011). Glibenclamide or metformin combined with honey improves glycemic control in streptozotocin-induced diabetic rats. *Int J Biol.Sci, 7,* 244-252.

85. European Medicines Agency (2012). *Forxiga-dapagliflozin*.

86. Farmer, B. B., Mancina, M., Williams, E. S., & Watanabe, A. M. (1983). Isolation of calcium tolerant myocytes from adult rat hearts: review of the literature and description of a method. *Life Sci., 33,* 1-18.

87. Ferrannini, E., Ramos, S. J., Salsali, A., Tang, W., & List, J. F. (2010). Dapagliflozin Monotherapy in Type 2 Diabetic Patients With Inadequate Glycemic Control by Diet and Exercise: A randomized, double-blind, placebo-controlled, phase 3 trial. *Diabetes Care, 33,* 2217-2224.

88. Ferrannini, E. & Solini, A. (2012). SGLT2 inhibition in diabetes mellitus: rationale and clinical prospects. *Nature Reviews Endocrinology, 8,* 495-502.

89. Fishler, M. G., Sobie, E. A., Thakor, N. V., & Tung, L. (1996). Mechanisms of cardiac cell excitation with premature monophasic and biphasic field stimuli: a model study. *Biophysical Journal, 70,* 1347-1362.

90. Food and Drug Administration (1-8-2014). FDA approves Farxiga to treat type 2 diabetes. http://www.fda.gov/NewsEvents/Newsroom/PressAnnouncements/ucm380829.htm

91. Forbes, J. M. C. & Cooper, M. E. (2013). Mechanisms of Diabetic Complications. *Physiological reviews, 93,* 137-188.

92. Fourlanos, S., Dotta, F., Greenbaum, C. J., Palmer, J. P., Rolandsson, O., Colman, P. G., & Harrison, L. C. (2005). Latent autoimmune diabetes in adults (LADA) should be less latent. *Diabetologia, 48,* 2206-2212.

93. Fowler, M. J. (2008). Microvascular and Macrovascular Complications of Diabetes. *Clinical Diabetes, 26,* 77-82.

94. Fox, K., Garcia, M. A. A., Ardissino, D., Buszman, P., Camici, P. G., Crea, F., Daly, C., De Backer, G., Hjemdahl, P., Lopez-Sendon, J., Marco, J., Morais, J., Pepper, J., Sechtem, U., Simoons, M., Thygesen, K., Priori, S. G., Blanc, J. J., Budaj, A., Camm, J., Dean, V., Deckers, J., Dickstein, K., Lekakis, J., McGregor, K., Metra, M., Morais, J., Osterspey, A., Tamargo, J., Zamorano, J. L., Zamorano, J. L., Andreotti, F., Becher, H., Dietz, R., Fraser, A., Gray, H., Antolin, R. A. H., Huber, K., Kremastinos, D. T., Maseri, A., Nesser, H. J., Pasierski, T., Sigwart, U., Tubaro, M., & Weis, M. (2006). Guidelines on the management of stable angina pectoris: executive summary: The Task Force on the Management of Stable Angina Pectoris of the European Society of Cardiology. *European Heart Journal, 27,* 1341-1381.

95. Freeman, R. (2002). Autonomic peripheral neuropathy. *The Lancet, 365,* 1259-1270.

96. Fröde, T. S. & Medeiros, Y. S. (2008). Animal models to test drugs with potential antidiabetic activity. *Journal of Ethnopharmacology, 115,* 173-183.

97. Fujimori, Y., Katsuno, K., Nakashima, I., Ishikawa-Takemura, Y., Fujikura, H., & Isaji, M. (2008). Remogliflozin Etabonate, in a Novel Category of Selective Low-Affinity Sodium Glucose Cotransporter (SGLT2) Inhibitors, Exhibits Antidiabetic Efficacy in Rodent Models. *Journal of Pharmacology and Experimental Therapeutics, 327,* 268-276.

98. Gales, C., Zamfir, C., Stoica, B., & Nechifor, M. (2013). The effect of pioglitazone on non-pregnant female genital tract in experimental diabetes mellitus. *Revista medico-chirurgicala a Societatii de Medici si Naturalisti din Iasi, 117,* 954-958.

99. Gardner, D. S. & Tai, E. S. (2012). Clinical features and treatment of maturity onset diabetes of the young (MODY). *Diabetes, Metabolic Syndrome and Obesity, 5,* 101-108.

100. Gasparotto Junior, A., Gasparotto, F. M., Boffo, M. A., Lourenço, E. L. B., Stefanello, M. É. A., Salvado, M. J., Da Silva-Santos, J. E., Marques, M. C. A., & Kassuya, C. A. L. (2011). Diuretic and potassium-sparing effect of isoquercitrin–An active flavonoid of Tropaeolum majus L. *Journal of Ethnopharmacology, 134,* 210-215.

101. Gasparotto Junior, A., Prando, T. B. L., Leme, T. d. S. V., Gasparotto, F. M., Lourenço, E. L. B., Rattmann, Y. D., Da Silva-Santos, J. E., Kassuya, C. A. L., & Marques, M. C. A. (2012). Mechanisms underlying the diuretic effects of Tropaeolum majus L. extracts and its main component isoquercitrin. *Journal of Ethnopharmacology, 141,* 501-509.

102. Gianani, R. & Eisenbarth, G. S. (2005). The stages of type 1A diabetes: 2005. *Immunological Reviews, 204,* 232-249.

103. Gilliam, L. K., Brooks-Worrell, B. M., Palmer, J. P., Greenbaum, C. J., & Pihoker, C. (2005). Autoimmunity and clinical course in children with type 1, type 2, and type 1.5 diabetes. *Journal of Autoimmunity, 25,* 244-250.

104. Glatz, J. F. C. L., Luiken, J. J. F. P., & Bonen, A. (2010). Membrane Fatty Acid Transporters as Regulators of Lipid Metabolism: Implications for Metabolic Disease. *Physiological reviews, 90,* 367-417.

105. Gomez, A. M., Kerfant, B. G., & Vassort, G. (2000). Microtubule Disruption Modulates Ca2+ Signaling in Rat Cardiac Myocytes. *Circulation Research, 86,* 30-36.

106. Goonasekera, S. A., Hammer, K., Auger-Messier, M., Bodi, I., Chen, X., Zhang, H., Reiken, S., Elrod, J. W., Correll, R. N., York, A. J., Sargent, M. A., Hofmann, F., Moosmang, S., Marks, A. R., Houser, S. R., Bers, D. M., & Molkentin, J. D. (2012). Decreased cardiac L-type Ca2+ channel activity induces hypertrophy and heart failure in mice. *The Journal of Clinical Investigation, 122,* 280-290.

107. Gotzsche, L. B., Rosenqvist, N., Gronbaek, H., Flyvbjerg, A., & Gotzsche, O. (1996). Increased number of myocardial voltage-gated Ca2+ channels and unchanged total beta-receptor number in long-term streptozotocin-diabetic rats. *Eur J Endocrinol, 134,* 107-113.

108. Grant, A. O. (2009). Cardiac Ion Channels. *Circulation: Arrhythmia and Electrophysiology, 2,* 185-194.

109. Grempler, R., Thomas, L., Eckhardt, M., Himmelsbach, F., Sauer, A., Sharp, D. E., Bakker, R. A., Mark, M., Klein, T., & Eickelmann, P. (2012). Empagliflozin, a novel selective sodium glucose cotransporter-2 (SGLT-2) inhibitor: characterisation and comparison with other SGLT-2 inhibitors. *Diabetes, Obesity and Metabolism, 14,* 83-90.

110. Grossman, E. & Messerli, F. H. (2004). Calcium antagonists. *Progress in Cardiovascular Diseases, 47,* 34-57.

111. Grundy, S. M., Benjamin, I. J., Burke, G. L., Chait, A., Eckel, R. H., Howard, B. V., Mitch, W., Smith, S. C., & Sowers, J. R. (1999). Diabetes and Cardiovascular Disease: A Statement for Healthcare Professionals From the American Heart Association. *Circulation, 100,* 1134-1146.

112. Guillen, C., Prieto, A., De Buergo, M. A., Villa, L., Rico, H., Zea, A., Hernandez, M. P., & Alvarez-Mon, M. (1995). Isradipine, a calcium-channel antagonist, has immunosuppressor activity on T lymphocytes from peripheral blood and synovial fluid from patients with autoimmune arthritis. *Journal of Immunotherapy, 18,* 66-74.

113. Gupta, A., Brahmbhatt, S., & Sharma, A. C. (2004). Left ventricular mitogen activated protein kinase signaling following polymicrobial sepsis during streptozotocin-induced hyperglycemia. *Biochimica et Biophysica Acta (BBA) - Molecular Basis of Disease, 1690,* 42-53.

114. Gupta, P., Kanwal, A., Putcha, U. K., Bulani, Y., Sojitra, B., Khatua, T. N., Kuncha, M., & Banerjee, S. K. (2013). Cardioprotective effect of ritonavir, an antiviral drug, in isoproterenol induced myocardial necrosis: a new therapeutic implication. *Journal of Translational Medicine, 11,* 80.

115. Halban, P. A., Polonsky, K. S., Bowden, D. W., Hawkins, M. A., Ling, C., Mather, K. J., Powers, A. C., Rhodes, C. J., Sussel, L., & Weir, G. C. (2014). B-Cell Failure in Type 2 Diabetes: Postulated Mechanisms and Prospects for Prevention and Treatment. *Diabetes Care, 37,* 1751-1758.

116. Hamill, O. P., Marty, A., Neher, E., Sakmann, B., & Sigworth, F. J. (1981). Improved patch-clamp techniques for high-resolution current recording from cells and cell-free membrane patches. *Pflugers Arch, 391,* 85-100.

117. Hanafusa, T. & Imagawa, A. (2007). Fulminant type 1 diabetes: a novel clinical entity requiring special attention by all medical practitioners. *Nat Clin Pract End Met, 3,* 36-45.

118. Henzen, C. (2012). Monogenic diabetes mellitus due to defects in insulin secretion. *Swiss Med Wkly, 142,* w13690.

119. Hering, S., Acz_Ñl, S., Kraus, R. L., Berjukow, S., Striessnig, J., & Timin, E. N. (1997). Molecular mechanism of use-dependent calcium channel block by phenylalkylamines: role of inactivation. *Proceedings of the National Academy of Sciences, 94,* 13323-13328.

120. Hess, P., Lansman, J. B., & Tsien, R. W. (1984). Different modes of Ca channel gating behaviour favoured by dihydropyridine Ca agonists and antagonists. *Nature, 311,* 538-544.

121. Howarth, F. C., Al-Sharhan, R., Al-Hammadi, A., & Qureshi, M. A. (2007). Effects of streptozotocin-induced diabetes on action potentials in the sinoatrial node compared with other regions of the rat heart. *Mol Cell Biochem, 300,* 39-46.

122. Howarth, F. C. & Qureshi, M. A. (2001). Characterisation of Ventricular Myocyte Shortening after Administration of Streptozotocin (STZ) to Neonatal Rats. *Archives of Physiology and Biochemistry, 109,* 200-205.

123. Howarth, F. C. & Qureshi, M. A. (2001). Myofilament Ca 2+ sensitivity in ventricular myocytes from streptozotocin-induced diabetic rat. *Int J Diabetes Metab, 9,* 67-74.

124. Howarth, F. C. & Qureshi, M. A. (2008). Myofilament sensitivity to Ca2+ in ventricular myocytes from the Goto-Kakizaki diabetic rat. *Mol.Cell Biochem., 315,* 69-74.

125. Howarth, F. C., Qureshi, M. A., & White, E. (2002). Effects of hyperosmotic shrinking on ventricular myocyte shortening and intracellular Ca(2+) in streptozotocin-induced diabetic rats. *Pflügers Arch, 444,* 446-451.

126. Howarth, F. C., Qureshi, M. A., Sobhy, Z. H. H., Parekh, K., Yammahi, S. R. R. K., Adrian, T. E., & Adeghate, E. (2011). Structural lesions and changing pattern of expression of genes encoding cardiac muscle proteins are associated with ventricular myocyte dysfunction in type 2 diabetic Goto-Kakizaki rats fed a high-fat diet. *Experimental physiology, 96*, 765-777.

127. Imagawa, A., Hanafusa, T., Makino, H., Miyagawa, J. I., & Juto, P. (2005). High titres of IgA antibodies to enterovirus in fulminant type-1 diabetes. *Diabetologia, 48*, 290-293.

128. Imagawa, A., Hanafusa, T., Uchigata, Y., Kanatsuka, A., Kawasaki, E., Kobayashi, T., Shimada, A., Shimizu, I., Maruyama, T., & Makino, H. (2005). Different contribution of class II HLA in fulminant and typical autoimmune type 1 diabetes mellitus. *Diabetologia, 48*, 294-300.

129. Imagawa, A. & Hanafusa, T. (2006). Pathogenesis of fulminant type 1 diabetes. *The Review of Diabetic Studies, 3*, 169.

130. Imagawa, A., Hanafusa, T., Miyagawa, J. i., & Matsuzawa, Y. (2000). A novel subtype of type 1 diabetes mellitus characterized by a rapid onset and an absence of diabetes-related antibodies. *New England Journal of Medicine, 342*, 301-307.

131. Imagawa, A., Hanafusa, T., Uchigata, Y., Kanatsuka, A., Kawasaki, E., Kobayashi, T., Shimada, A., Shimizu, I., Toyoda, T., & Maruyama, T. (2003). Fulminant type 1 diabetes a nationwide survey in Japan. *Diabetes Care, 26*, 2345-2352.

132. International Diabetes Federation (2013). *International Diabetes Federation ATLAS, 6th edn*. Brussels, Belgium: International Diabetes Federation.

133. International Diabetes Federation (2014). Signs and symptoms of diabetes. http://www.idf.org/signs-and-symptoms-diabetes

134. Isenberg, G. (1976). Cardiac Purkinje fibers: cesium as a tool to block inward rectifying potassium currents. *Pflügers Arch, 365*, 99-106.

135. Isenberg, G. & Klockner, U. (1982). Calcium tolerant ventricular myocytes prepared by preincubation in a KB medium. *Pflügers Arch, 395*, 6-18.

136. Ishibashi, T., Tanaka, K., & Taniguchi, Y. (1981). Platelet Aggregation and Coagulation in the Pathogenesis of Diabetic Retinopathy in Rats. *Diabetes, 30,* 601-606.

137. Jackson, C. V., McGrath, G. M., Tahiliani, A. G., Vadlamudi, R. V., & McNeill, J. H. (1985). A Functional and Ultrastructural Analysis of Experimental Diabetic Rat Myocardium: Manifestation of a Cardiomyopathy. *Diabetes, 34,* 876-883.

138. Jasinski, J. M. & Eisenbarth, G. S. (2005). Insulin as a primary autoantigen for type 1A diabetes. *Clinical and developmental immunology, 12,* 181-186.

139. Jensen, P. K., Christiansen, J. S., Steven, K., & Parving, H. H. (1981). Renal function in streptozotocin-diabetic rats. *Diabetologia, 21,* 409-414.

140. Joffe, I. I., Travers, K. E., Perreault-Micale, C. L., Hampton, T., Katz, S. E., Morgan, J. P., & Douglas, P. S. (1999). Abnormal cardiac function in the streptozotocin-induced, non–insulin-dependent diabetic rat: Noninvasive assessment with Doppler echocardiography and contribution of the nitric oxide pathway. *Journal of the American College of Cardiology, 34,* 2111-2119.

141. Jugdé, H., Nguy, D., Moller, I., Cooney, J. M., & Atkinson, R. G. (2008). Isolation and characterization of a novel glycosyltransferase that converts phloretin to phlorizin, a potent antioxidant in apple. *FEBS journal, 275,* 3804-3814.

142. Jung, H. (2002). The sodium/substrate symporter family: structural and functional features. *FEBS Letters, 529,* 73-77.

143. Junod, A., Lambert, A., Stauffacher, W., & Renold, A. E. (1969). Diabetogenic action of streptozotocin: relationship of dose to metabolic response. *The Journal of Clinical Investigation, 48,* 2129-2139.

144. Kahn, B. B., Shulman, G. I., DeFronzo, R. A., Cushman, S. W., & Rossetti, L. (1991). Normalization of blood glucose in diabetic rats with phlorizin treatment reverses insulin-resistant glucose transport in adipose cells without restoring glucose transporter gene expression. *The Journal of Clinical Investigation, 87,* 561-570.

145. Kahn, S. E., Cooper, M. E., & Del Prato, S. (2014). Pathophysiology and treatment of type 2 diabetes: perspectives on the past, present, and future. *The Lancet, 383,* 1068-1083.

146. Kakinuma, H., Oi, T., Hashimoto-Tsuchiya, Y., Arai, M., Kawakita, Y., Fukasawa, Y., Iida, I., Hagima, N., Takeuchi, H., Chino, Y., Asami, J., Okumura-Kitajima, L., Io, F., Yamamoto, D., Miyata, N., Takahashi, T., Uchida, S., & Yamamoto, K. (2010). (1S)-1,5-Anhydro-1-[5-(4-ethoxybenzyl)-2-methoxy-4-methylphenyl]-1-thio-d-glucitol (TS-071) is a Potent, Selective Sodium-Dependent Glucose Cotransporter 2 (SGLT2) Inhibitor for Type 2 Diabetes Treatment. *Journal of Medicinal Chemistry, 53*, 3247-3261.

147. Kaku, K., Inoue, S., Matsuoka, O., Kiyosue, A., Azuma, H., Hayashi, N., Tokudome, T., Langkilde, A. M., & Parikh, S. (2013). Efficacy and safety of dapagliflozin as a monotherapy for type 2 diabetes mellitus in Japanese patients with inadequate glycaemic control: a phase II multicentre, randomized, double-blind, placebo-controlled trial. *Diabetes, Obesity and Metabolism, 15*, 432-440.

148. Kamata, K., Ozawa, Y., Kobayashi, T., & Matsumoto, T. (2008). Effect of long-term streptozotocin-induced diabetes on coronary vasoconstriction in isolated perfused rat heart. *Journal of Smooth Muscle Research, 44,* 177-188.

149. Karmažínová, M. & Lacinová, L. (2010). Measurement of cellular excitability by whole cell patch clamp technique. *Physiol Res, 59 Suppl 1,* S1-S7.

150. Karvonen, M., Pitkäniemi, M., Pitkäniemi, J., Kohtamäki, K., Tajima, N., & Tuomilehto, J. (1997). Sex difference in the incidence of insulin-dependent diabetes mellitus: an analysis of the recent epidemiological data. *Diabetes/Metabolism Reviews, 13,* 275-291.

151. Kasichayanula, S., Liu, X., LaCreta, F., Griffen, S. C., & Boulton, D. W. (2014). Clinical pharmacokinetics and pharmacodynamics of dapagliflozin, a selective inhibitor of sodium-glucose co-transporter type 2. *Clinical pharmacokinetics, 53,* 17-27.

152. Kasichayanula, S., Liu, X., Zhang, W., Pfister, M., LaCreta, F. P., & Boulton, D. W. (2011). Influence of Hepatic Impairment on the Pharmacokinetics and Safety Profile of Dapagliflozin: An Open-Label, Parallel-Group, Single-Dose Study. *Clinical Therapeutics, 33*, 1798-1808.

153. Katz, A. M. (1986). Pharmacology and mechanisms of action of calcium-channel blockers. *Journal of clinical hypertension, 2*, 28S.

154. Kawasaki, E., Imagawa, A., Makino, H., Uga, M., Abiru, N., Hanafusa, T., Uchigata, Y., & Eguchi, K. (2008). Differences in the Contribution of the CTLA4 Gene to Susceptibility to Fulminant and Type 1A Diabetes in Japanese Patients. *Diabetes Care, 31*, 1608-1610.

155. Kenyon, J. L. & Gibbons, W. R. (1979). Influence of chloride, potassium, and tetraethylammonium on the early outward current of sheep cardiac Purkinje fibers. *The Journal of General Physiology, 73*, 117-138.

156. Kim, J. D., Kang, S. M., Seo, B. I., Choi, H. Y., Choi, H. S., & Ku, S. K. (2006). Anti-diabetic Activity of SMK001, a Poly Herbal Formula in Streptozotocin Induced Diabetic Rats: Therapeutic Study. *Biological and Pharmaceutical Bulletin, 29*, 477-482.

157. Kim, Y. W., Kim, J. Y., & Lee, S. K. (1995). Effects of phlorizin and acipimox on insulin resistance in STZ-diabetic rats. *Journal of Korean medical science, 10*, 24.

158. Kim, Y. & Babu, A. R. (2012). Clinical potential of sodium-glucose cotransporter 2 inhibitors in the management of type 2 diabetes. *Diabetes, metabolic syndrome and obesity: targets and therapy, 5*, 313.

159. King, A. J. (2012). The use of animal models in diabetes research. *British Journal of Pharmacology, 166*, 877-894.

160. Kintoko, K., Wen, Q., Lin, X., Zheng, N., Xu, X., & Huang, R. (2014). Diabetogenic Activity of Streptozotocin on Kunming Strain Mice as Animal Model of Diabetes Mellitus. *IOSR Journal of Pharmacy and Biological Sciences*.

161. Kiran, G., Nandini, C. D., Ramesh, H. P., & Salimath, P. V. (2012). Progression of early phase diabetic nephropathy in streptozotocin-induced diabetic rats: Evaluation of various kidney-related parameters. *Indian Journal of Experimental Biology, 50,* 133-140.

162. Kissei Pharmaceuticals (7-3-2009). Discontinuation of the development of "Remogliflozin" by GlaxoSmithKline. http://www.kissei.co.jp/e_contents/relation/2009/20090703.html.

163. Klauke, N., Smith, G. L., & Cooper, J. (2003). Stimulation of Single Isolated Adult Ventricular Myocytes within a Low Volume Using a Planar Microelectrode Array. *Biophysical Journal, 85,* 1766-1774.

164. Komoroski, B., Vachharajani, N., Boulton, D., Kornhauser, D., Geraldes, M., Li, L., & Pfister, M. (2009). Dapagliflozin, a Novel SGLT2 Inhibitor, Induces Dose-Dependent Glucosuria in Healthy Subjects. *Clin Pharmacol Ther, 85,* 520-526.

165. Kong, H., Jones, P., Koop, A., Zhang, L., Duff, H., & Chen, S. (2008). Caffeine induces Ca2+ release by reducing the threshold for luminal Ca2+ activation of the ryanodine receptor. *Biochem.J, 414,* 441-452.

166. Kornreich, B. G. (2007). The patch clamp technique: Principles and technical considerations. *Journal of Veterinary Cardiology, 9,* 25-37.

167. Kotani, R., Nagata, M., Imagawa, A., Moriyama, H., Yasuda, H., Miyagawa, J., Hanafusa, T., & Yokono, K. (2004). T lymphocyte response against pancreatic beta cell antigens in fulminant type 1 diabetes. *Diabetologia, 47,* 1285-1291.

168. Kotsanas, G., Delbridge, L. M., & Wendt, I. R. (2000). Stimulus interval-dependent differences in Ca2+ transients and contractile responses of diabetic rat cardiomyocytes. *Cardiovascular Research, 46,* 450-462.

169. Kumar, S., Singh, R., Vasudeva, N., & Sharma, S. (2012). Acute and chronic animal models for the evaluation of anti-diabetic agents. *Cardiovascular Diabetology, 11,* 9.

170. Kyselova, Z., Garcia, S. J., Gajdosikova, A., Gajdosik, A., & Stefek, M. (2005). Temporal relationship between lens protein oxidation and cataract development in streptozotocin-induced diabetic rats. *Physiol Res, 54,* 49-56.

171. Lee, C. W., Lee, H. S., Cha, Y. J., Joo, W. H., Kang, D. O., & Moon, J. Y. (2013). In vivo Investigation of anti-diabetic properties of ripe onion juice in normal and streptozotocin-induced diabetic rats. *Preventive nutrition and food science, 18,* 169.

172. Leveen, H. H., Leveen, R. F., & LeVeen, E. G. (8-4-1987). Treatment of cancer with phlorizin and its derivatives. Google Patents.

173. Levi, A. J., Hancox, J. C., Howarth, F. C., Croker, J., & Vinnicombe, J. (1996). A method for making rapid changes of superfusate whilst maintaining temperature at 37 degrees C. *Pflugers Arch, 432,* 930-937.

174. Li, Y. Q., Zhou, F. C., Gao, F., Bian, J. S., & Shan, F. (2009). Comparative Evaluation of Quercetin, Isoquercetin and Rutin as Inhibitors of a-Glucosidase. *Journal of Agricultural and Food Chemistry, 57,* 11463-11468.

175. Liao, R., Podesser, B. K., & Lim, C. C. (2012). The continuing evolution of the Langendorff and ejecting murine heart: new advances in cardiac phenotyping. *American Journal of Physiology - Heart and Circulatory Physiology, 303,* H156-H167.

176. Life Technologies (2011). Fluorescent Ca{2+} Indicators Excited with UV Light - Section 19.2. Retrieved from: http://www.b2b.invitrogen.com/site/us/en/home/References/Molecular-Probes-The-Handbook/Indicators-for-Ca2-Mg2-Zn2-and-Other-Metal-Ions/Fluorescent-Ca2-Indicators-Excited-with-UV-Light.html#head1

177. Lin, I. W., Sosso, D., Chen, L. Q., Gase, K., Kim, S. G., Kessler, D., Klinkenberg, P. M., Gorder, M. K., Hou, B. H., Qu, X. Q., Carter, C. J., Baldwin, I. T., & Frommer, W. B. (2014). Nectar secretion requires sucrose phosphate synthases and the sugar transporter SWEET9. *Nature, 508,* 546-549.

178. Lisato, G., Cusin, I., Tiengo, A., Del Prato, S., & Jeanrenaud, B. (1992). The contribution of hyperglycaemia and hypoinsulinaemia to the insulin resistance of streptozotocin-diabetic rats. *Diabetologia, 35,* 310-315.

179. List, J. F., Woo, V., Morales, E., Tang, W., & Fiedorek, F. T. (2009). Sodium-Glucose Cotransport Inhibition With Dapagliflozin in Type 2 Diabetes. *Diabetes Care, 32,* 650-657.

180. Liu, I. M., Chang, C. K., Juang, S. W., Kou, D. H., Tong, Y. C., Cheng, K. C., & Cheng, J. T. (2008). Role of hyperglycaemia in the pathogenesis of hypotension observed in type-1 diabetic rats. *International Journal of Experimental Pathology, 89,* 292-300.

181. Ljubisavijevic, M. (2007). Effects of voluntary exercise on heart function in streptozotocin (STZ)–induced diabetic rat. *Int J Diabetes & Metabolism, 15,* 32-37.

182. Ljubojevic, S., Walther, S., Asgarzoei, M., Sedej, S., Pieske, B., & Kockskämper, J. (2011). In Situ Calibration of Nucleoplasmic versus Cytoplasmic Ca2+ Concentration in Adult Cardiomyocytes. *Biophysical Journal, 100,* 2356-2366.

183. Louch, W. E., Sheehan, K. A., & Wolska, B. M. (2011). Methods in cardiomyocyte isolation, culture, and gene transfer. *Journal of Molecular and Cellular Cardiology, 51,* 288-298.

184. Lu, H. J., Tzeng, T. F., Liou, S. S., Da Lin, S., Wu, M. C., & Liu, I. M. (2014). Ruscogenin ameliorates diabetic nephropathy by its anti-inflammatory and anti-fibrotic effects in streptozotocin-induced diabetic rat. *BMC Complementary and Alternative Medicine, 14,* 110.

185. Luippold, G., Klein, T., Mark, M., & Grempler, R. (2012). Empagliflozin, a novel potent and selective SGLT-2 inhibitor, improves glycaemic control alone and in combination with insulin in streptozotocin-induced diabetic rats, a model of type 1 diabetes mellitus. *Diabetes, Obesity and Metabolism, 14,* 601-607.

186. Lukaèínová, A., Hubková, B., Rácz, O., & Ništiar, F. (2013). Animal Models for Study of Diabetes Mellitus. In (pp. 229-254).

187. MacDougall, D. A. & Calaghan, S. (2013). A novel approach to the Langendorff technique: preparation of isolated cardiomyocytes and myocardial samples from the same rat heart. *Experimental physiology, 98,* 1295-1300.

188. Mahadevan, V. (2012). Anatomy of the heart. *Surgery (Oxford), 30,* 5-8.

189. Malhotra, A., Penpargkul, S., Fein, F. S., Sonnenblick, E. H., & Scheuer, J. (1981). The effect of streptozotocin-induced diabetes in rats on cardiac contractile proteins. *Circulation Research, 49,* 1243-1250.

190. Malik, M., Bakir, A., Saab, B. A., Roglic, G., & King, H. (2005). Glucose intolerance and associated factors in the multi-ethnic population of the United Arab Emirates: results of a national survey. *Diabetes Research and Clinical Practice, 69,* 188-195.

191. Mather, A. & Pollock, C. (2010). Renal glucose transporters: novel targets for hyperglycemia management. *Nat Rev Nephrol, 6,* 307-311.

192. McCauley, R. A. & Wang, X. (2011). Fulminant type 1 diabetes mellitus-like presentation in a Hispanic woman in the United States. *Diabetes & Metabolism, 37,* 356-358.

193. McDonald, T. F., Pelzer, S., Trautwein, W., & Pelzer, D. J. (1994). Regulation and modulation of calcium channels in cardiac, skeletal, and smooth muscle cells. *Physiological reviews, 74,* 365-507.

194. McEvoy, R. C., Andersson, J., Sandler, S., & Hellerström, C. (1984). Multiple low-dose streptozotocin-induced diabetes in the mouse. Evidence for stimulation of a cytotoxic cellular immune response against an insulin-producing beta cell line. *The Journal of Clinical Investigation, 74,* 715-722.

195. Meng, W., Ellsworth, B. A., Nirschl, A. A., McCann, P. J., Patel, M., Girotra, R. N., Wu, G., Sher, P. M., Morrison, E. P., Biller, S. A., Zahler, R., Deshpande, P. P., Pullockaran, A., Hagan, D. L., Morgan, N., Taylor, J. R., Obermeier, M. T., Humphreys, W. G., Khanna, A., Discenza, L., Robertson, J. G., Wang, A., Han, S., Wetterau, J. R., Janovitz, E. B., Flint, O. P., Whaley, J. M., & Washburn, W. N. (2008). Discovery of Dapagliflozin: A Potent, Selective Renal Sodium-Dependent Glucose Cotransporter 2 (SGLT2) Inhibitor for the Treatment of Type 2 Diabetes. *Journal of Medicinal Chemistry, 51,* 1145-1149.

196. Miethke, H., Wittig, B., Nath, A., & Jungermann, K. (1986). Gluconeogenic-glycolytic capacities and metabolic zonation in liver of rats with streptozotocin, non-ketotic as compared to alloxan, ketotic diabetes. *Histochemistry, 85,* 483-489.

197. Miki, T., Itoh, T., Sunaga, D., & Miura, T. (2012). Effects of diabetes on myocardial infarct size and cardioprotection by preconditioning and postconditioning. *Cardiovascular Diabetology, 11,* 67.

198. Mittendorfer, B. & Klein, S. (2014). Absence of leptin triggers type 1 diabetes. *Nat Med, 20,* 705-706.

199. Monckton, G. & Pehowich, E. (1980). Autonomic neuropathy in the streptozotocin diabetic rat. *The Canadian journal of neurological sciences.Le journal canadien des sciences neurologiques, 7,* 135-142.

200. Montessuit, C. & Lerch, R. Ñ. (2013). Regulation and dysregulation of glucose transport in cardiomyocytes. *Biochimica et Biophysica Acta (BBA) - Molecular Cell Research, 1833,* 848-856.

201. Montessuit, C., Rosenblatt-Velin, N., Papageorgiou, I. Đ., Campos, L., Pellieux, C., Palma, T., & Lerch, R. Ñ. (2004). Regulation of glucose transporter expression in cardiac myocytes: p38 MAPK is a strong inducer of GLUT4. *Cardiovascular Research, 64,* 94-104.

202. Moreau, C., Drui, D., Arnault-Ouary, G., Charbonnel, B., Chaillous, L., & Cariou, B. (2008). Fulminant type 1 diabetes in Caucasians: A report of three cases. *Diabetes & Metabolism, 34,* 529-532.

203. Movassat, J. & Portha, B. (1999). Beta-cell growth in the neonatal Goto-Kakisaki rat and regeneration after treatment with streptozotocin at birth. *Diabetologia, 42,* 1098-1106.

204. Mueckler, M. (1994). Facilitative glucose transporters. *European Journal of Biochemistry, 219,* 713-725.

205. Mueckler, M. & Thorens, B. (2013). The SLC2 (GLUT) family of membrane transporters. *Molecular aspects of medicine, 34,* 121-138.

206. Mythili, M. D., Vyas, R., Akila, G., & Gunasekaran, S. (2004). Effect of streptozotocin on the ultrastructure of rat pancreatic islets. *Microscopy Research and Technique, 63,* 274-281.

207. Nabeebaccus, A. & Shah, A. M. (2014). Biochemistry and physiology of cardiac muscle. *Medicine, 42,* 413-417.

208. Nagata, M., Moriyama, H., Kotani, R., Yasuda, H., Kishi, M., Kurohara, M., Hara, K., & Yokono, K. (2007). Immunological aspects of 'fulminant type 1 diabetes'. *Diabetes Research and Clinical Practice, 77,* S99-S103.

209. Naik, R. G., Brooks-Worrell, B. M., & Palmer, J. P. (2009). Latent Autoimmune Diabetes in Adults. *The Journal of Clinical Endocrinology & Metabolism, 94,* 4635-4644.

210. Natali, A. J., Turner, D. L., Harrison, S. M., & White, E. (2001). Regional effects of voluntary exercise on cell size and contraction-frequency responses in rat cardiac myocytes. *Journal of Experimental Biology, 204,* 1191-1199.

211. Nerbonne, J. M. K. & Kass, R. S. (2005). Molecular Physiology of Cardiac Repolarization. *Physiological reviews, 85,* 1205-1253.

212. Nolan, C. J., Damm, P., & Prentki, M. (2009). Type 2 diabetes across generations: from pathophysiology to prevention and management. *The Lancet, 378,* 169-181.

213. Nomura, S., Sakamaki, S., Hongu, M., Kawanishi, E., Koga, Y., Sakamoto, T., Yamamoto, Y., Ueta, K., Kimata, H., Nakayama, K., & Tsuda-Tsukimoto, M. (2010). Discovery of Canagliflozin, a Novel C-Glucoside with Thiophene Ring, as Sodium-Dependent Glucose Cotransporter 2 Inhibitor for the Treatment of Type 2 Diabetes Mellitus(1). *Journal of Medicinal Chemistry, 53,* 6355-6360.

214. Nygren, A., Olson, M. L., Chen, K. Y., Emmett, T., Kargacin, G., & Shimoni, Y. (2007). Propagation of the cardiac impulse in the diabetic rat heart: reduced conduction reserve. *The Journal of Physiology, 580,* 543-560.

215. Ogden, D. & Stanfield, P. (1994). Patch clamp techniques for single channel and whole-cell recording. In *In Microelectrode techniques: the Plymouth workshop handbook* (2 ed., pp. 53-78).

216. Olson, M. L., Kargacin, M. E., Ward, C. A., & Kargacin, G. J. (2007). Effects of Phloretin and Phloridzin on Ca2+ Handling, the Action Potential, and Ion Currents in Rat Ventricular Myocytes. *Journal of Pharmacology and Experimental Therapeutics, 321,* 921-929.

217. Oshiro, K., Murakami, K., Sunagawa, R., & Mimura, G. (1991). Chronic effects of tolbutamide on myocardial tension during ischemia and reperfusion in perfused hearts isolated from insulin dependent and non insulin dependent diabetic rats. *Jpn.Heart J, 32,* 347-361.

218. Palmer, B. M. & Moore, R. L. (2000). Excitation wavelengths for fura 2 provide a linear relationship between [Ca2+] and fluorescence ratio. *American Journal of Physiology - Cell Physiology, 279,* C1278-C1284.

219. Panda, S. & Kar, A. (2007). Antidiabetic and antioxidative effects of Annona squamosa leaves are possibly mediated through quercetin-3-O-glucoside. *BioFactors, 31,* 201-210.

220. Pandya, K. G., Patel, M. R., & Lau-Cam, C. A. (2010). Comparative study of the binding characteristics to and inhibitory potencies towards PARP and in vivo antidiabetogenic potencies of taurine, 3-aminobenzamide and nicotinamide. *J Biomed.Sci, 17 Suppl 1,* S16.

221. Papa, G., Degano, C., Iurato, M., Licciardello, C., Maiorana, R., & Finocchiaro, C. (2013). Macrovascular complication phenotypes in type 2 diabetic patients. *Cardiovascular Diabetology, 12,* 20.

222. Pavlovic, D., McLatchie, L. M., & Shattock, M. J. (2010). The rate of loss of T-tubules in cultured adult ventricular myocytes is species dependent. *Experimental physiology, 95,* 518-527.

223. Pinnell, J., Turner, S., & Howell, S. (2007). Cardiac muscle physiology. *Continuing Education in Anaesthesia, Critical Care & Pain, 7,* 85-88.

224. Poucheret, P., Gross, R., Cadène, A., Mantéguetti, M., Serrano, J. J., Ribes, G., & Cros, G. (1995). Long-term correction of STZ-diabetic rats after short-term i.p. VOSO4 treatment: Persistence of insulin secreting capacities assessed by isolated pancreas studies. *Mol Cell Biochem, 153,* 197-204.

225. Pozzilli, P. & Buzzetti, R. (2007). A new expression of diabetes: double diabetes. *Trends in Endocrinology & Metabolism, 18,* 52-57.

226. Ramanadham, S., Decker, P., & Tenner, T. E., Jr. (1983). Effect of insulin replacement on streptozotocin-induced effects in the rat heart. *Life Sci, 33,* 289-296.

227. Ramanadham, S. & Tenner, J. (1983). Alterations in Cardiac Performance in Experimentally-Induced Diabetes. *Pharmacology, 27,* 130-139.

228. Razavi, S., Zahri, S., Zarrini, G., Nazemiyeh, H., & Mohammadi, S. (2009). Biological activity of quercetin-3-O-glucoside, a known plant flavonoid. *Russ J Bioorg Chem, 35,* 376-378.

229. Rees, D. A. & Alcolado, J. C. (2005). Animal models of diabetes mellitus. *Diabetic Medicine, 22,* 359-370.

230. Reinehr, T., Schober, E., Wiegand, S., Thon, A., & Holl, R. (2006). B-cell autoantibodies in children with type 2 diabetes mellitus: subgroup or misclassification? *Archives of Disease in Childhood, 91,* 473-477.

231. Rithalia, A., Qureshi, M. A., Howarth, F. C., & Harrison, S. M. (2004). Effects of halothane on contraction and intracellular calcium in ventricular myocytes from streptozotocin–induced diabetic rats. *British journal of anaesthesia, 92*, 246-253.

232. Robinson, J. A., Jenkins, N. S., Holman, N. A., Roberts-Thomson, S. J., & Monteith, G. R. (2004). Ratiometric and nonratiometric Ca2+ indicators for the assessment of intracellular free Ca2+ in a breast cancer cell line using a fluorescence microplate reader. *Journal of Biochemical and Biophysical Methods, 58*, 227-237.

233. Roe, M. W., Lemasters, J. J., & Herman, B. (1990). Assessment of Fura-2 for measurements of cytosolic free calcium. *Cell Calcium, 11*, 63-73.

234. Roese, John H. (2013). Laboratory rats: injection sites. Retrieved from: http://www.lssu.edu/faculty/jroese/AnimalCare/rat_injections.htm

235. Rossetti, L. & Lauglin, M. R. (1989). Correction of chronic hyperglycemia with vanadate, but not with phlorizin, normalizes in vivo glycogen repletion and in vitro glycogen synthase activity in diabetic skeletal muscle. *The Journal of Clinical Investigation, 84*, 892-899.

236. Rossetti, L., Smith, D., Shulman, G. I., Papachristou, D., & DeFronzo, R. A. (1987). Correction of hyperglycemia with phlorizin normalizes tissue sensitivity to insulin in diabetic rats. *Journal of Clinical Investigation, 79*, 1510.

237. Rossini, A. A., Like, A. A., Chick, W. L., Appel, M. C., & Cahill, G. F. (1977). Studies of streptozotocin-induced insulitis and diabetes. *Proceedings of the National Academy of Sciences, 74*, 2485-2489.

238. Rubio-Cabezas, O. & Ellard, S. (2013). Diabetes Mellitus in Neonates and Infants: Genetic Heterogeneity, Clinical Approach to Diagnosis, and Therapeutic Options. *Hormone Research in Paediatrics, 80*, 137-146.

239. Saadi, H., Carruthers, S. G., Nagelkerke, N., Al-Maskari, F., Afandi, B., Reed, R., Lukic, M., Nicholls, M. G., Kazam, E., Algawi, K., Al-Kaabi, J., Leduc, C., Sabri, S., El-Sadig, M., Elkhumaidi, S., Agarwal, M., & Benedict, S. (2007). Prevalence of diabetes mellitus and its complications in a population-based sample in Al Ain, United Arab Emirates. *Diabetes Research and Clinical Practice, 78,* 369-377.

240. Sabino-Silva, R., Mori, R. C., David-Silva, A., Okamoto, M. M., Freitas, H. S., & Machado, U. F. (2010). The Na+/glucose cotransporters: from genes to therapy. *Brazilian Journal of Medical and Biological Research, 43,* 1019-1026.

241. Sambrano, G. R., Fraser, I., Han, H., Ni, Y., O'Connell, T., Yan, Z., & Stull, J. T. (2002). Navigating the signalling network in mouse cardiac myocytes. *Nature, 420,* 712-714.

242. Santer, R., Schneppenheim, R., Dombrowski, A., Gotze, H., Steinmann, B., & Schaub, J. (1997). Mutations in GLUT2, the gene for the liver-type glucose transporter, in patients with Fanconi-Bickel syndrome. *Nat Genet, 17,* 324-326.

243. Santos, N. C., Figueira-Coelho, J., Martins-Silva, J., & Saldanha, C. (2003). Multidisciplinary utilization of dimethyl sulfoxide: pharmacological, cellular, and molecular aspects. *Biochemical Pharmacology, 65,* 1035-1041.

244. Schaan, B. D., Dall'Ago, P., Maeda, C. Y., Ferlin, E., Fernandes, T. G., Schmid, H., & Irigoyen, M. C. (2004). Relationship between cardiovascular dysfunction and hyperglycemia in streptozotocin-induced diabetes in rats. *Brazilian Journal of Medical and Biological Research, 37,* 1895-1902.

245. Scheepers, A., Joost, H. G., & Schurmann, A. (2004). The glucose transporter families SGLT and GLUT: molecular basis of normal and aberrant function. *Journal of Parenteral and Enteral Nutrition, 28,* 364-371.

246. Schwartz, S. L., Akinlade, B., Klasen, S., Kowalski, D., Zhang, W., & Wilpshaar, W. (2011). Safety, pharmacokinetic, and pharmacodynamic profiles of ipragliflozin (ASP1941), a novel and selective inhibitor of sodium-dependent glucose co-transporter 2, in patients with type 2 diabetes mellitus. *Diabetes Technol.Ther, 13,* 1219-1227.

247. Selleck Chemicals (2013). Dapagliflozin: Catalog No.S1548. http://www.selleckchem.com/products/Dapagliflozin.html

248. Severs, N. J. (2000). The cardiac muscle cell. *Bioessays, 22*, 188-199.

249. Shao, C. H., Capek, H. L., Patel, K. P., Wang, M., Tang, K., DeSouza, C., Nagai, R., Mayhan, W., Periasamy, M., & Bidasee, K. R. (2011). Carbonylation Contributes to SERCA2a Activity Loss and Diastolic Dysfunction in a Rat Model of Type 1 Diabetes. *Diabetes, 60*, 947-959.

250. Shibazaki, T., Tomae, M., Ishikawa-Takemura, Y., Fushimi, N., Itoh, F., Yamada, M., & Isaji, M. (2012). KGA-2727, a Novel Selective Inhibitor of a High-Affinity Sodium Glucose Cotransporter (SGLT1), Exhibits Antidiabetic Efficacy in Rodent Models. *Journal of Pharmacology and Experimental Therapeutics, 342*, 288-296.

251. Silverthorn, D. U., Johnson, B. R., Ober, W. C., Garrison, C. W., & Silverthorn, A. C. (2013). Human Physiology: An Integrated Approach. In (6 ed., pp. 462-507). Pearson Education.

252. Singh, J., Chonkar, A., Bracken, N., Adeghate, E., Latt, Z., & Hussain, M. (2006). Effect of Streptozotocin-Induced Type 1 Diabetes Mellitus on Contraction, Calcium Transient, and Cation Contents in the Isolated Rat Heart. *Annals of the New York Academy of Sciences, 1084*, 178-190.

253. Skrzypiec-Spring, M., Grotthus, B., Szelag, A., & chulz, R. (2007). Isolated heart perfusion according to Langendorff – Still viable in the new millennium. *Journal of Pharmacological and Toxicological Methods, 55*, 113-126.

254. Slingerland, A. S. (2006). Monogenic diabetes in children and young adults: Challenges for researcher, clinician and patient. *Rev Endocr Metab Disord, 7*, 171-185.

255. Smith, P. A., Aschroft, F. M., & Fewtrell, C. M. (1993). Permeation and gating properties of the L-type calcium channel in mouse pancreatic beta cells. *The Journal of General Physiology, 101*, 767-797.

256. Sobel, B. E. & Schneider, D. J. (2005). Cardiovascular complications in diabetes mellitus. *Current Opinion in Pharmacology, 5,* 143-148.

257. Spurgeon, H. A., duBell, W. H., Stern, M. D., Sollott, S. J., Ziman, B. D., Silverman, H. S., Capogrossi, M. C., Talo, A., & Lakatta, E. G. (1992). Cytosolic calcium and myofilaments in single rat cardiac myocytes achieve a dynamic equilibrium during twitch relaxation. *The Journal of Physiology, 447,* 83-102.

258. Squadrito, F., Trimarchi, G. R., Lupica, S., Magri, V., Costa, G., Brezenoff, H. E., & Caputi, A. P. (1986). Cerebral cholinergic control of rat arterial blood pressure in streptozotocin-induced diabetes. *Pharmacol Res Commun., 18,* 951-965.

259. Srinivasan, K. & Ramarao, P. (2007). Animal models in type 2 diabetes research: an overview. *Indian J Med Res, 125,* 451-472.

260. Steadman, B. W., Moore, K. B., Spitzer, K. W., & Bridge, J. H. B. (1988). A video system for measuring motion in contracting heart cells. *Biomedical Engineering, IEEE Transactions on, 35,* 264-272.

261. Stümpel, F., Burcelin, R., Jungermann, K., & Thorens, B. (2001). Normal kinetics of intestinal glucose absorption in the absence of GLUT2: Evidence for a transport pathway requiring glucose phosphorylation and transfer into the endoplasmic reticulum. *Proceedings of the National Academy of Sciences, 98,* 11330-11335.

262. Stumvoll, M., Goldstein, B. J., & van Haeften, T. W. (2009). Type 2 diabetes: principles of pathogenesis and therapy. *The Lancet, 365,* 1333-1346.

263. Sun, Q., Ma, Y., Zhang, L., Zhao, Y. F., Zang, W. J., & Chen, C. (2010). Effects of GH secretagogues on contractility and Ca2+ homeostasis of isolated adult rat ventricular myocytes. *Endocrinology, 151,* 4446-4454.

264. Sunagawa, R., Nagamine, F., Murakami, K., Mimura, G., & Sakanashi, M. (1989). Effects of dobutamine and acetylcholine on perfused hearts isolated from streptozocin-induced diabetic rats. *Arzneimittelforschung., 39,* 470-474.

265. Suzuki, M., Honda, K., Fukazawa, M., Ozawa, K., Hagita, H., Kawai, T., Takeda, M., Yata, T., Kawai, M., Fukuzawa, T., Kobayashi, T., Sato, T., Kawabe, Y., & Ikeda, S. (2012). Tofogliflozin, a Potent and Highly Specific Sodium/Glucose Cotransporter 2 Inhibitor, Improves Glycemic Control in Diabetic Rats and Mice. *Journal of Pharmacology and Experimental Therapeutics, 341,* 692-701.

266. Szkudelski, T. (2001). The mechanism of alloxan and streptozotocin action in B cells of the rat pancreas. *Physiol Res, 50,* 537-546.

267. Szkudelski, T. (2012). Streptozotocin–nicotinamide-induced diabetes in the rat. Characteristics of the experimental model. *Experimental Biology and Medicine, 237,* 481-490.

268. Tabibiazar, R. & Edelman, S. V. (2003). Silent Ischemia in People With Diabetes: A Condition That Must Be Heard. *Clinical Diabetes, 21,* 5-9.

269. Tahara, A., Kurosaki, E., Yokono, M., Yamajuku, D., Kihara, R., Hayashizaki, Y., Takasu, T., Imamura, M., Li, Q., Tomiyama, H., Kobayashi, Y., Noda, A., Sasamata, M., & Shibasaki, M. (2014). Effects of sodium-glucose cotransporter 2 selective inhibitor ipragliflozin on hyperglycaemia, oxidative stress, inflammation and liver injury in streptozotocin-induced type 1 diabetic rats. *Journal of Pharmacy and Pharmacology, 66,* 975-987.

270. Tahrani, A. A., Barnett, A. H., & Bailey, C. J. (2013). SGLT inhibitors in management of diabetes. *The Lancet Diabetes & Endocrinology, 1,* 140-151.

271. Takahashi, A., Camacho, P., Lechleiter, J. D., & Herman, B. (1999). Measurement of intracellular calcium. *Physiological reviews, 79*.

272. TAKII, H., MATSUMOTO, K., KOMETANI, T., OKADA, S., & FUSHIKI, T. (1997). Lowering Effect of Phenolic Glycosides on the Rise in Postprandial Glucose in Mice. *Bioscience, Biotechnology, and Biochemistry, 61,* 1531-1535.

273. the DECODA Study Group (2003). Age- and Sex-Specific Prevalence of Diabetes and Impaired Glucose Regulation in 11 Asian Cohorts. *Diabetes Care, 26,* 1770-1780.

274. The DECODE Study Group (2003). Age- and Sex-Specific Prevalences of Diabetes and Impaired Glucose Regulation in 13 European Cohorts1. *Diabetes Care, 26,* 61-69.

275. The DIAMOND Project Group (2006). Incidence and trends of childhood Type-1 diabetes worldwide 1990–1999. *Diabetic Medicine, 23,* 857-866.

276. Therapeutic Goods Administration (2013). *Australian Public Assessment Report for Dapagliflozin propanediol monohydrate*.

277. Thorens, B. & Mueckler, M. (2010). Glucose transporters in the 21st Century. *American Journal of Physiology-Endocrinology and Metabolism, 298,* E141-E145.

278. Thygesen, K., Alpert, J. S., Jaffe, A. S., Simoons, M. L., Chaitman, B. R., & White, H. D. (2012). Third Universal Definition of Myocardial Infarction. *Circulation, 126,* 2020-2035.

279. Tomlinson, K. C., Gardiner, S. M., Hebden, R. A., & Bennett, T. (1992). Functional consequences of streptozotocin-induced diabetes mellitus, with particular reference to the cardiovascular system. *Pharmacological Reviews, 44,* 103-150.

280. Tsujihara, K., Hongu, M., Saito, K., Inamasu, M., Arakawa, K., Oku, A., & Matsumoto, M. (1996). Na (+)-glucose cotransporter inhibitors as antidiabetics. I. Synthesis and pharmacological properties of 4'-dehydroxyphlorizin derivatives based on a new concept. *Chemical & pharmaceutical bulletin, 44,* 1174-1180.

281. Tsutsumi, C., Imagawa, A., Ikegami, H., Makino, H., Kobayashi, T., Hanafusa, T., & on behalf of the Japan Diabetes Society Committee on Type (2012). Class II HLA genotype in fulminant type 1 diabetes: A nationwide survey with reference to glutamic acid decarboxylase antibodies. *Journal of Diabetes Investigation, 3,* 62-69.

282. Tucker, Miriam E. (1-8-2014). FDA Approves Dapagliflozin (Farxiga) for Type 2 Diabetes Treatment. http://www.medscape.com/viewarticle/818858

283. Tung, L. & Borderies, J. R. (1992). Analysis of electric field stimulation of single cardiac muscle cells. *Biophysical Journal, 63,* 371-386.

284. Tuomi, T., Santoro, N., Caprio, S., Cai, M., Weng, J., & Groop, L. (2013). The many faces of diabetes: a disease with increasing heterogeneity. *The Lancet*.

285. Tuomilehto, J., Rastenyte, D., Birkenh_Ìger, W. H., Thijs, L., Antikainen, R., Bulpitt, C. J., Fletcher, A. E., Forette, F. Ï., Goldhaber, A., Palatini, P., Sarti, C., Staessen, J. A., & Fagard, R. (1999). Effects of Calcium-Channel Blockade in Older Patients with Diabetes and Systolic Hypertension. *New England Journal of Medicine, 340,* 677-684.

286. Ushigome, E., Fukui, M., Hamaguchi, M., Tanaka, T., Atsuta, H., Ohnishi, M., Oda, Y., Yamazaki, M., Hasegawa, G., & Nakamura, N. (2013). Beneficial effect of calcium channel blockers on home blood pressure variability in the morning in patients with type_È2 diabetes. *Journal of Diabetes Investigation, 4,* 399-404.

287. Vadlamudi, R. V., Rodgers, R. L., & McNeill, J. H. (1982). The effect of chronic alloxan- and streptozotocin-induced diabetes on isolated rat heart performance. *Can J Physiol Pharmacol, 60,* 902-911.

288. Valentine, V. (2012). The Role of the Kidney and Sodium-Glucose Cotransporter-2 Inhibition in Diabetes Management. *Clinical Diabetes, 30,* 151-155.

289. Valentová, K., Vrba, J., Bancírová, M., lrichová, J., Kr, & , V. (2014). Isoquercitrin: Pharmacology, toxicology, and metabolism. *Food and Chemical Toxicology, 68,* 267-282.

290. Viglietta, V., Kent, S. C., Orban, T., & Hafler, D. A. (2002). GAD65-reactive T cells are activated in patients with autoimmune type 1a diabetes. *The Journal of Clinical Investigation, 109,* 895-903.

291. Vitor, R. F., Mota-Filipe, H., Teixeira, G., Borges, C., Rodrigues, A. I., Teixeira, A., & Paulo, A. (2004). Flavonoids of an extract of Pterospartum tridentatum showing endothelial protection against oxidative injury. *Journal of Ethnopharmacology, 93,* 363-370.

292. Wang, D. W. K. (1995). Abnormalities of K+ and Ca2+ currents in ventricular myocytes from rats with chronic diabetes. *American Journal of Physiology - Heart and Circulatory Physiology, 269,* H1288-H1296.

293. Wang, J. G., Staessen, J. A., Gong, L., & Liu, L. (2000). Chinese trial on isolated systolic hypertension in the elderly. *Archives of internal medicine, 160,* 211-220.

294. Wang, J., Sun, G. X., Yu, L., Wu, F. A., & Guo, X. J. (2013). Enhancement of the selective enzymatic biotransformation of rutin to isoquercitrin using an ionic liquid as a co-solvent. *Bioresource Technology, 128,* 156-163.

295. Wang, R. N., Bouwens, L., & Klöppel, G. (1994). Beta-cell proliferation in normal and streptozotocin-treated newborn rats: site, dynamics and capacity. *Diabetologia, 37,* 1088-1096.

296. Wang, R. N., Bouwens, L., & Klöppel, G. (1996). Beta-cell growth in adolescent and adult rats treated with streptozotocin during the neonatal period. *Diabetologia, 39,* 548-557.

297. Warner Instruments (2014). Perfusion Chamber with Field Stimulation (RC-49MFS). https://www.warneronline.com/product_info.cfm?id=731

298. Wei, M., Ong, L., Smith, M. T., Ross, F. B., Schmid, K., Hoey, A. J., Burstow, D., & Brown, L. (2003). The streptozotocin-diabetic rat as a model of the chronic complications of human diabetes. *Heart, lung and circulation, 12,* 44-50.

299. Weil, R., Nozawa, M., Koss, M., Weber, C., Reemtsma, K., & McIntosh, R. (1976). The kidney in streptozotocin diabetic rats. Morphologic, ultrastructural, and function studies. *Archives of pathology & laboratory medicine, 100,* 37-49.

300. Whitaker, R. H. (2014). Anatomy of the heart. *Medicine, 42,* 406-408.

301. Wilcken, D. E. L. (2014). Physiology of the normal heart. *Medicine, 42,* 409-412.

302. Wood, C., Williams, C., & Waldron, G. J. (2004). Patch clamping by numbers. *Drug Discovery Today, 9*, 434-441.

303. Wood, I. S. & Trayhurn, P. (2003). Glucose transporters (GLUT and SGLT): expanded families of sugar transport proteins. *British Journal of Nutrition, 89*, 3-9.

304. Woodcock, E. A. & Matkovich, S. J. (2005). Cardiomyocytes structure, function and associated pathologies. *The International Journal of Biochemistry & Cell Biology, 37*, 1746-1751.

305. World Health Organization (1999). Definition, Diagnosis and Classification of Diabetes Mellitus and its Complications. Part 1: Diagnosis and Classification of Diabetes Mellitus. *Geneva: World Health Organization*.

306. World Health Organization (2006). Definition and diagnosis of diabetes mellitus and intermediate hyperglycemia: report of a WHO/IDF consultation. *Geneva: World Health Organization,* 1-50.

307. World Health Organization (2011). Use of glycated haemoglobin (HbA1c) in the diagnosis of diabetes mellitus: abbreviated report of a WHO consultation. *Geneva: World Health Organization*.

308. World Health Organization (2011). Global status report on noncommunicable diseases 2010. *Geneva: World Health Organization*.

309. Wright, E. M. (1998). I. Glucose Galactose Malabsorption. *American Journal of Physiology - Gastrointestinal and Liver Physiology, 275*, G879-G882.

310. Wright, E. M. (2013). Glucose transport families SLC5 and SLC50. *Molecular aspects of medicine, 34*, 183-196.

311. Xu, Y., Tao, Y., Cheung, L. S., Fan, C., Chen, L. Q., Xu, S., Perry, K., Frommer, W. B., & Feng, L. (2014). Structures of bacterial homologues of SWEET transporters in two distinct conformations. *Nature, advance online publication*.

312. Xuan, Y. H., Hu, Y. B., Chen, L. Q., Sosso, D., Ducat, D. C., Hou, B. H., & Frommer, W. B. (2013). Functional role of oligomerization for bacterial and plant SWEET sugar transporter family. *Proceedings of the National Academy of Sciences, 110,* E3685-E3694.

313. Yaras, N., Ugur, M., Ozdemir, S., Gurdal, H., Purali, N., Lacampagne, A., Vassort, G., & Turan, B. (2005). Effects of Diabetes on Ryanodine Receptor Ca Release Channel (RyR2) and Ca2+ Homeostasis in Rat Heart. *Diabetes, 54,* 3082-3088.

314. Yin, D., Tao, J., Lee, D. D., Shen, J., Hara, M., Lopez, J., Kuznetsov, A., Philipson, L. H., & Chong, A. S. (2006). Recovery of Islet B-Cell Function in Streptozotocin- Induced Diabetic Mice: An Indirect Role for the Spleen. *Diabetes, 55,* 3256-3263.

315. Yoo, K. H. (2006). MATERIALS AND METHODS. In *Contractile Behavior of Field Stimulated Left Ventricular Myocytes from Biopsy Samples of the Anterior and Remote Regions of the Swine Heart* (pp. 48-64). State University of New York at Buffalo.

316. Young, L., Coven, D., & Russell, R. (2000). Cellular and molecular regulation of cardiac glucose transport. *J Nucl Cardiol, 7,* 267-276.

317. Young, M. E., Wilson, C. R., Razeghi, P., Guthrie, P. H., & Taegtmeyer, H. (2002). Alterations of the Circadian Clock in the Heart by Streptozotocin-induced Diabetes. *Journal of Molecular and Cellular Cardiology, 34,* 223-231.

318. Zahradník, I., Minarovic, I., & Zahradníková, A. (2008). Inhibition of the Cardiac L-Type Calcium Channel Current by Antidepressant Drugs. *Journal of Pharmacology and Experimental Therapeutics, 324,* 977-984.

319. Zambrowicz, B., Freiman, J., Brown, P. M., Frazier, K. S., Turnage, A., Bronner, J., Ruff, D., Shadoan, M., Banks, P., Mseeh, F., Rawlins, D. B., Goodwin, N. C., Mabon, R., Harrison, B. A., Wilson, A., Sands, A., & Powell, D. R. (2012). LX4211, a Dual SGLT1/SGLT2 Inhibitor, Improved Glycemic Control in Patients With Type 2 Diabetes in a Randomized, Placebo-Controlled Trial. *Clin Pharmacol Ther, 92,* 158-169.

320. Zhang, B. l. & Sannajust, F. (2000). Diurnal rhythms of blood pressure, heart rate, and locomotor activity in adult and old male Wistar rats. *Physiology & Behavior, 70,* 375-380.

321. Zhang, J., Liang, R., Wang, L., Yan, R., Hou, R., Gao, S., & Yang, B. (2013). Effects of an aqueous extract of Crataegus pinnatifida Bge. var. major N.E.Br. fruit on experimental atherosclerosis in rats. *Journal of Ethnopharmacology, 148,* 563-569.

322. Zhang, X.-Q. S. & Jianliang Carl, L. (2002). Effects of sprint training on contractility and [Ca2+]i transients in adult rat myocytes. *Journal of Applied Physiology, 93,* 1310-1317.

323. Zhao, F. Q. & Keating, A. F. (2007). Functional properties and genomics of glucose transporters. *Current genomics, 8,* 113.

324. Zhao, Y., Inayat, S., Dikin, D. A., Singer, J. H., Ruoff, R. S., & Troy, J. B. (2008). Patch clamp technique: Review of the current state of the art and potential contributions from nanoengineering. *Proceedings of the Institution of Mechanical Engineers, Part N: Journal of Nanoengineering and Nanosystems, 222,* 1-11.

325. Zhao, Y., Xu, J., Gong, J., & Qian, L. (2009). L-type calcium channel current up-regulation by chronic stress is associated with increased *alpha*-1c subunit expression in rat ventricular myocytes. *Cell Stress and Chaperones, 14,* 33-41.

326. Zheng, M., Hou, R., & Xiao, R. P. (2004). Acidosis-induced p38 MAPK activation and its implication in regulation of cardiac contractility. *Acta Pharmacol.Sin., 25,* 1299-1305.

327. Zhou, L., Cryan, E. V., D'Andrea, M. R., Belkowski, S., Conway, B. R., & Demarest, K. T. (2003). Human cardiomyocytes express high level of Na+/glucose cotransporter 1 (SGLT1). *Journal of cellular biochemistry, 90,* 339-346.

328. Zimmer, H. G. (1998). The Isolated Perfused Heart and Its Pioneers. *Physiology, 13,* 203-210.

Chapter 9: Conference Presentations and Journal Publications

9.1. Conference Presentations

Hamouda N. N., Qureshi M. A., Sydorenko V., Howarth F. C. (2014). Sodium-glucose co-transporter inhibitor reduces the amplitude of shortening and Ca^{2+} transient in ventricular myocytes from streptozotocin-induced diabetic rat, Physiology 2014, London, England.

9.2. Journal Publications

Hamouda, N. N., Sydorenko, V., Qureshi, M. A., Alkaabi, J. M., Oz, M., & Howarth, F. C. (2014). Dapagliflozin reduces the amplitude of shortening and Ca^{2+} transient in ventricular myocytes from streptozotocin-induced diabetic rats. Molecular and Cellular Biochemistry, 1-12.

Hamouda, N. N.,Qureshi, M. A., Alkaabi, J. M., Oz, M., & Howarth, F. C. (2014). Reduction in the amplitude of shortening and Ca^{2+} transient by Phlorizin and Quercetin-3-O-Glucoside in ventricular myocytes from streptozotocin-induced diabetic rats [In process].